



**Y.C. YÜKSEKÖĞRETİM KURULU  
DOKÜMANTASYON MERKEZİ**

**AN EXPERIMENTAL INVESTIGATION ON  
HEAT AND MASS TRANSFER IN A  
DESICCANT COOLING SYSTEM**

**121742**

**A Ph.D. THESIS**

**In**

**Mechanical Engineering**

**UNIVERSITY OF GAZIANTEP**

**Y.C. YÜKSEKÖĞRETİM KURULU  
DOKÜMANTASYON MERKEZİ**

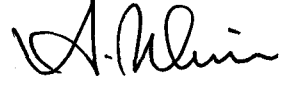
**By**

**Murtaza YILDIRIM**

**December 2002**

121742

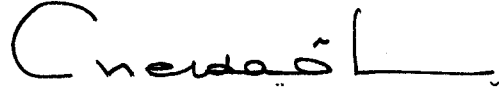
Approval of the Graduate School of Natural and Applied Science.



Prof Dr. Ali Rıza TEKİN

Director

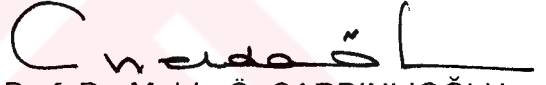
I certify that this thesis satisfies all the requirements as a thesis for the degree of Ph.D. of Science.



Assoc Prof. Dr. Melda Ö. ÇARPINLIOĞLU

Chairman of the Department

This is to certify that we have read this thesis and that in our opinion it is fully adequate in scope and quality, as a thesis for the degree of Ph.D. of Science.




Assoc Prof. Dr. Melda Ö. ÇARPINLIOĞLU

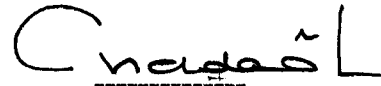
Supervisor

Examining Committee in Charge

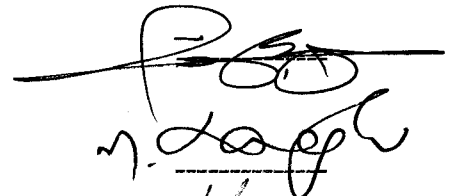
Prof. Dr. Ali Rıza TEKİN



Assoc. Prof. Dr. Melda Ö. ÇARPINLIOĞLU



Assoc. Prof. Dr. M. Sait SÖYLEMEZ



Assoc. Prof. Dr. Mehmet KANOĞLU



Assist. Prof. Dr. Hüseyin AKILLI

## ABSTRACT

### AN EXPERIMENTAL INVESTIGATION ON HEAT AND MASS TRANSFER IN A DESICCANT COOLING SYSTEM

YILDIRIM, Murtaza

Ph. D. in Mechanical Engineering

Supervisor: Assoc. Prof. Dr. Melda Ö. ÇARPINLIOĞLU

December 2002, 234 pages

In this study, the performance of an open cycle Desiccant Cooling System (DCS) in terms of heat and mass transfers was investigated. The primary components of the system including a Rotary Regenerator (RR) and a Desiccant Wheel (DW) were designed and constructed. Natural Zeolite of Balıkesir was used as a desiccant in DW. The design of the overall system and the collaborative measurement system was established considering the operation of the cooling system such that the system and operating parameters can be controlled to cover an extensive range of experimental task.

Tests were performed to investigate the effects of various system operating parameters including rotational speeds of DW and RR, air mass flow rate flowing through the process and regeneration lines, and regeneration temperature on the various system performance parameters including coefficient of performance (COP) and cooling capacity of DCS, moisture removal capacity of DW, and effectiveness of RR. A maximum COP of 1.3 is obtained for a mass flow rate of 0.083 kg/s, a regeneration temperature of 60C, and rotational speeds of 5 rpm for RR and 0.3 rpm for DW. However, a maximum cooling capacity of 17 kW/kg dry air is obtained for a mass flow rate of 0.139 kg/s, a regeneration temperature of 60C, and

rotational speeds of 5 rpm for RR and 0.1 rpm for DW. Both maximum COP and CC are obtained at 35C outside dry bulb temperature and 20% relative humidity.

**Keywords:** Desiccant Cooling System, Rotary Regenerator, Desiccant Wheel, Zeolite, COP, Cooling Capacity, Moisture Removal Capacity, Effectiveness.



## ÖZ

### DESİKANT SOĞUTMA SİSTEMLERİNDE ISI VE KÜTLE TRANSFERİ ÜZERİNE DENEYSEL BİR ARAŞTIRMA

YILDIRIM, Murtaza

Doktora Tezi: Mak. Müh. Böl.

Tez yöneticisi: Doç. Dr. Melda Ö. ÇARPINLIOĞLU

Aralık 2002, 234 sayfa

Bu çalışmanın amacı açık dolaşimli, desikant soğutma sistemlerinin, DCS ısı ve kütle transferi açısından verimliliğinin incelenmesidir. Orijinal tasarım ve üretimi yapılan döner rejeneratör RR, ve desikant teker, DW, sistemin temel parçalarını oluşturmaktadır. Desikant tekerinde, desikant madde olarak Balıkesir Biğadiç yöresinde bulunan doğal zeolit kullanıldı. Sistemin tamamı ve kullanılan ölçme yöntemleri, sistem tasarım ve çalışma şartları, deneysel çalışma aralığı da dikkate alınarak tasarlanmıştır.

Yapılan deneyler ile döner rejeneratörün ve desikant tekerin dönel hızı, proses ve rejenerasyon hatlarında hava kütle akımı, regenerasyon sıcaklığı gibi işletim değişkenlerinin, desikant soğutma sisteminin verimlilik katsayısı (COP), soğutma kapasitesi (CC), desikant tekerin kütle alma kapasitesi, döner rejeneratörün etkinliği üzerine etkisi incelenmiştir. Maximum COP, hava debisinin 0.083kg/s, rejenerasyon sıcaklığının 60C, dönel rejeneratörün dönel hızının 5 rpm, desikant tekerinin dönel hızının ise 0.3 rpm olduğu durumda 1.3 olarak elde edilmiştir. Oysa maximum CC, hava debisinin 0.139kg/s, rejenerasyon sıcaklığının 60C, dönel rejeneratörün dönel hızının 5 rpm, desikant tekerinin dönel hızının ise 0.1 rpm olduğu durumda 17kW/kg<sub>dryair</sub> olarak elde edilmiştir. Her iki durumda da dış havanın kuru termometre sıcaklığı 35C ve mutlak men oranı %20'dir.

**Anahtar Kelimeler:** Desikant Soğutma Sistemi, Döner Regeneratör, Desikant Teker, Zeolit, COP, Soğutma Kapasitesi, Nem Alma Kapasitesi, Etkinlik.



## ACKNOWLEDGEMENTS

I would like to express my gratitude to Assoc. Prof. Dr. Melda Ö. ÇARPINLIOĞLU for her valuable comments, supervision and suggestions and for a considerable amount of time she spent discussing and criticizing the manuscript.

This study would have never been completed without continuous moral support, encouragement, and patience of my wife Rabia Güler Ö. YILDIRIM, and therefore my very special thanks are due to her. I would like to thank Bedirhan and Aylin for their great understanding and patience during this study.

I would like to express my sincere thanks to Research Fund of the University of GAZIANTEP for the research project supported under the Grant no: MF 97-05.

Lastly, I wish to offer my thanks to the personnel of the mechanical Engineering department; especially Mr. Mehmet TAŞDEMİR, Mr. İbrahim KORKMAZ, and Mr. Seyit BOSTANCIERİ for their valuable help in the construction of the experimental set-up.



## TABLE OF CONTENTS

ABSTRACT.....	iii
ÖZ.....	v
ACKNOWLEDGEMENTS.....	vii
LIST OF TABLES.....	xi
LIST OF FIGURE.....	xii
LIST OF SYMBOLS.....	xxii
<b>1. INTRODUCTION.....</b>	<b>1</b>
<b>2. LITERATURE SURVEY.....</b>	<b>7</b>
2.1. Introduction.....	7
2.2. An Overall Analysis of Desiccant Cooling System.....	8
2.3. Studies on Desiccant wheels.....	14
2.4. Analysis on Performance of Desiccant Cooling System.....	18
2.5. Studies on Rotary Regenerators.....	24
2.6. Studies Regarding The Performance of Desiccant Cooling Systems In Terms of Heat and Mass Transfer.....	36
2.7. Conclusion.....	41
<b>3. EXPERIMENTAL SET-UP AND MEASUREMENTS.....</b>	<b>42</b>
3.1. Introduction.....	42
3.2. Design and Construction of Experimental Set-Up.....	42
3.1.1 Desiccant Wheel.....	46
3.2.1.1. Design–Construction and Modification of DW .....	50
3.2.1. Rotary Regenerator.....	52
3.2.2.1. Design–Construction and Modification of DW.....	53
3.2.2. Evaporative coolers.....	55
3.2.3. Pipe-Line.....	56
3.2.4. Pipe-Line Transition elements.....	57
3.2.5. Heaters.....	57
3.2.6. Centrifugal Fan.....	59
3.2.7. Driving Components of RR and DW.....	59
3.2.8. Speed Control Units.....	60

3.2.9. Test Set-up Insulation Materials.....	60
3.3. Measurement Methods and Utilized Devices.....	60
3.3.1. Temperature Measurement.....	60
3.3.1.1. Thermocouple Configuration.....	61
3.3.1.2. Dry Bulb Temperature Probe.....	62
3.3.1.3. Wet Bulb Temperature probe.....	62
3.3.2. Flow Rate Measurement.....	65
3.3.2.1. Orifice Plate; Design, Construction and Calibration....	65
3.3.3. Pressure Drop Measurements.....	69
3.3.4. Manometers.....	69
3.3.5. Hilton Data Logger.....	70
3.4. Test of Zeolite as a Desiccant .....	73
3.5. Conclusion.....	75
<b>4. EXPERIMENTAL STUDY AND EVALUATION OF DATA.....</b>	<b>77</b>
4.1. Introduction.....	77
4.2. Experimental Procedure.....	78
4.2.1. Setting of Air Flow Rates in Process and Regeneration Lines.....	78
4.2.2. Steps in Experiment.....	80
4.3. Evaluation of Measurements.....	82
4.4. Conclusion.....	88
<b>5. PERFORMANCE OF DCS IN TERMS OF OPERATING PARAMETERS FOR SELECTED SYSTEM CONSTRAINTS.....</b>	<b>93</b>
5.1. Introduction.....	93
5.2. Analysis of the DCS-Operation Through Psychrometric Charts.....	94
5.3. Effects of $N_{RR}$ and $N_{DW}$ .....	99
5.3.1 Effects of $N_{RR}$ and $N_{DW}$ on CC and COP.....	100
5.3.2. Effects of $N_{RR}$ and $N_{DW}$ on $\Delta w_p$ and $\Delta w_r$ .....	120
5.3.3. Effects of $N_{RR}$ and $N_{DW}$ on $\epsilon_{RR}$ and $\epsilon_{EC}$ .....	139
5.4. Analysis of the Pressure Losses Through RR and DW.....	157
5.5. Correlation Trials on Dominant Heat and Mass Transfer Parameter.....	158
5.6. Effects of Desiccant Material (Zeolite) Particle Size on DCS Performance.....	167

5.7. Effects of DW Thickness on DCS Performance.....	184
5.8. Comparison with Previous Works.....	199
5.9. Conclusion.....	202
<b>6. SUGGESTIONS FOR FURTHER WORK.....</b>	<b>204</b>
6.1. Suggestions for Development of the Experimental Set-Up.....	204
6.2. Suggestions for Future Study with Variation of System Parameters.....	204
APPENDIX 1. Technical Specifications of the Driving Units for the Fans...	207
APPENDIX 2. Technical Specifications of the Driving Units for the RR.....	208
APPENDIX 3. Technical Specifications of the Driving Units for the DW....	209
APPENDIX 4. Correction Cart for the Head of Alcohol.....	210
APPENDIX 5. Hilton Data Logger Interface Plan View.....	211
APPENDIX 6. Sample Outputs.....	212
APPENDIX 7. Psychrometric Chart.....	218
<b>REFERENCES.....</b>	<b>219</b>

## LIST OF TABLES

Table 4.1. System description.....	88
Table 4.2. Operating parameters of the DCS.....	89
Table 4.3. Ranges of the variables in the conducted experimental study.....	89
Table 4.4. Ranges of the variables in the conducted experimental study. for testing $\Delta X_{DW}$ and $d_z$ .....	91
Table 4.5. Ranges of the variables in the conducted experimental study. for testing $\Delta X_{DW}=10\text{cm}$ and $d_z=20\text{mm}$ .....	91
Table 4.6. Ranges of the variables in the conducted experimental study. for testing $\Delta X_{DW}=15\text{cm}$ and $d_z=20\text{mm}$ .....	92

## LIST OF FIGURES

Figure 1.1. Schematic of an open-cycle desiccant cooling system.....	4
Figure 3.1. A schematic Layout of the Experimental Test Set-Up.....	43
Figure 3.2.a) A Schematic of Ventilation Mode Open Cycle DCS.....	45
b) Psychrometric Diagram of Ventilation Mode.....	45
Figure 3.3. Schematic of a Parallel-Plate Rotary Dehumidifier.....	50
Figure 3.4. Preparation of the Zeolite as Desiccant.....	51
Figure 3.5. Development and Modifications of DW and Matrix Material Arrangements .....	52
Figure 3.6. Special Shape Cu Plate RR Matrix Material.....	54
Figure 3.7a) RR Cu Matrix Rounded on the Shaft.....	54
b) Modified RR Matrix Material Housing.....	54
Figure 3.8. Balanced Flow Housing for RR and DW.....	55
Figure 3.9. Evaporative Cooler and Filling Material.....	56
Figure 3.10. Pipe-Line Transition Elements.....	58
Figure 3.11. Auxiliary Heaters.....	58
Figure 3.12.a) Location of Dry and Wet Bulb Temperature Probes in the Pipe .....	63
b) Detail of the Temperature Probe.....	63
Figure 3.13. Orifice Plate.....	65
Figure 3.14.a) Set-up for Calibration of the Orifice Plate.....	66
b) Calibration Curve of the Orifice Plate.....	68
Figure 3.15.a) Pressure Drop Measurement.....	70
b) 4 point Average Pressure Measuring Device.....	70
c) Inclined Manometer.....	70

Figure 3.16.a) Zeolite Test Set-Up.....	73
b) Psychrometric Representation of the Processes.....	73
c) First Test Result on Zeolite.....	73
(Variation of zeolite moisture content with/without heat wrt time)	
Figure 3.17. Second Test Result on Zeolite.....	74
(Changes of Zeolite Weight Loss With Time)	
Figure 3.18. Adsorption Isotherms for Adsorbent-Water Pairs.....	75
Figure 4.1. Schematics of the DCS.....	82
Figure 4.2. Sensible Load Analysis of DCS.....	83
Figure 5.1. Predicted Psychrometric Representation of DCS Processes.....	96
Figure 5.2. Sensible Load Analysis of DCS.....	96
Figure 5.3. Psychrometric Representation of same Sample Test Result of DCS.....	99
Figure 5.4.a) Variation of Sensible Cooling Capacity of DCS with $N_{RR}$ and $N_{DW}$ for $m_a=0.056\text{kg/s}$ and $T_r=60\text{C}$ .....	104
b) Variation of Sensible COP of DCS with $N_{RR}$ and $N_{DW}$ for $m_a=0.056\text{kg/s}$ and $T_r=60\text{C}$ .....	104
Figure 5.5.a) Variation of Sensible Cooling Capacity of DCS with $N_{RR}$ and $N_{DW}$ for $m_a=0.083\text{kg/s}$ and $T_r=60\text{C}$ .....	105
b) Variation of Sensible COP of DCS with $N_{RR}$ and $N_{DW}$ for $m_a=0.083\text{kg/s}$ and $T_r=60\text{C}$ .....	105
Figure 5.6.a) Variation of Sensible Cooling Capacity of DCS with $N_{RR}$ and $N_{DW}$ for $m_a=0.111\text{kg/s}$ and $T_r=60\text{C}$ .....	106
b) Variation of Sensible COP of DCS with $N_{RR}$ and $N_{DW}$ for $m_a=0.111\text{kg/s}$ and $T_r=60\text{C}$ .....	106
Figure 5.7.a) Variation of Sensible Cooling Capacity of DCS with $N_{RR}$	

and $N_{DW}$ for $m_a=0.139\text{kg/s}$ and $T_r=60\text{C}$ .....	107
b) Variation of Sensible COP of DCS with $N_{RR}$ and $N_{DW}$ for $m_a=0.139\text{kg/s}$ and $T_r=60\text{C}$ .....	107
Figure 5.8.a) Variation of Sensible Cooling Capacity of DCS with $N_{RR}$ and $N_{DW}$ for $m_a=0.056\text{kg/s}$ and $T_r=70$ .....	108
b) Variation of Sensible COP of DCS with $N_{RR}$ and $N_{DW}$ for $m_a=0.056\text{kg/s}$ and $T_r=70\text{C}$ .....	108
Figure 5.9.a) Variation of Sensible Cooling Capacity of DCS with $N_{RR}$ and $N_{DW}$ for $m_a=0.083\text{kg/s}$ and $T_r=70\text{C}$ .....	109
b) Variation of Sensible COP of DCS with $N_{RR}$ and $N_{DW}$ for $m_a=0.083\text{kg/s}$ and $T_r=70\text{C}$ .....	109
Figure 5.10.a) Variation of Sensible Cooling Capacity of DCS with $N_{RR}$ and $N_{DW}$ for $m_a=0.111\text{kg/s}$ and $T_r=70\text{C}$ .....	110
b) Variation of Sensible COP of DCS with $N_{RR}$ and $N_{DW}$ for $m_a=0.111\text{kg/s}$ and $T_r=70\text{C}$ .....	110
Figure 5.11.a) Variation of Sensible Cooling Capacity of DCS with $N_{RR}$ and $N_{DW}$ for $m_a=0.139\text{kg/s}$ and $T_r=70\text{C}$ .....	111
b) Variation of Sensible COP of DCS with $N_{RR}$ and $N_{DW}$ for $m_a=0.139\text{kg/s}$ and $T_r=70\text{C}$ .....	111
Figure 5.12.a) Variation of Sensible Cooling Capacity of DCS with $N_{RR}$ and $N_{DW}$ for $m_a=0.056\text{kg/s}$ and $T_r=80\text{C}$ .....	112
b) Variation of Sensible COP of DCS with $N_{RR}$ and $N_{DW}$ for $m_a=0.056\text{kg/s}$ and $T_r=80\text{C}$ .....	112
Figure 5.13.a) Variation of Sensible Cooling Capacity of DCS with $N_{RR}$ and $N_{DW}$ for $m_a=0.083\text{kg/s}$ and $T_r=80\text{C}$ .....	113
b) Variation of Sensible COP of DCS with $N_{RR}$ and $N_{DW}$ for	

$m_a=0.083\text{kg/s}$ and $T_r=80\text{C}$ .....	113
Figure 5.14.a) Variation of Sensible Cooling Capacity of DCS with $N_{RR}$ and $N_{DW}$ for $m_a=0.111\text{kg/s}$ and $T_r=80\text{C}$ .....	114
b) Variation of Sensible COP of DCS with $N_{RR}$ and $N_{DW}$ for $m_a=0.111\text{kg/s}$ and $T_r=80\text{C}$ .....	114
Figure 5.15.a) Variation of Sensible Cooling Capacity of DCS with $N_{RR}$ and $N_{DW}$ for $m_a=0.139\text{kg/s}$ and $T_r=80\text{C}$ .....	115
b) Variation of Sensible COP of DCS with $N_{RR}$ and $N_{DW}$ for $m_a=0.139\text{kg/s}$ and $T_r=80\text{C}$ .....	115
Figure 5.16.a) Variation of Sensible Cooling Capacity of DCS with $N_{RR}$ and $N_{DW}$ for $m_a=0.056\text{kg/s}$ and $T_r=90\text{C}$ .....	116
b) Variation of Sensible COP of DCS with $N_{RR}$ and $N_{DW}$ for $m_a=0.056\text{kg/s}$ and $T_r=90\text{C}$ .....	116
Figure 5.17.a) Variation of Sensible Cooling Capacity of DCS with $N_{RR}$ and $N_{DW}$ for $m_a=0.083\text{kg/s}$ and $T_r=90\text{C}$ .....	117
b) Variation of Sensible COP of DCS with $N_{RR}$ and $N_{DW}$ for $m_a=0.083\text{kg/s}$ and $T_r=90\text{C}$ .....	117
Figure 5.18.a) Variation of Sensible Cooling Capacity of DCS with $N_{RR}$ and $N_{DW}$ for $m_a=0.111\text{kg/s}$ and $T_r=90\text{C}$ .....	118
b) Variation of Sensible COP of DCS with $N_{RR}$ and $N_{DW}$ for $m_a=0.111\text{kg/s}$ and $T_r=90\text{C}$ .....	118
Figure 5.19.a) Variation of Sensible Cooling Capacity of DCS with $N_{RR}$ and $N_{DW}$ for $m_a=0.139\text{kg/s}$ and $T_r=90\text{C}$ .....	119
b) Variation of Sensible COP of DCS with $N_{RR}$ and $N_{DW}$ for $m_a=0.139\text{kg/s}$ and $T_r=90\text{C}$ .....	119
Figure 5.20. Variation of moisture removal capacity of DW with $N_{RR}$ and	



$N_{DW}$ for $m_a=0.056\text{kg/s}$ and $T_r=60\text{C}$ .....	123
Figure 5.21. Variation of moisture removal capacity of DW with $N_{RR}$ and $N_{DW}$ for $m_a=0.083\text{kg/s}$ and $T_r=60\text{C}$ .....	124
Figure 5.22. Variation of moisture removal capacity of DW with $N_{RR}$ and $N_{DW}$ for $m_a=0.111\text{kg/s}$ and $T_r=60\text{C}$ .....	125
Figure 5.23. Variation of moisture removal capacity of DW with $N_{RR}$ and $N_{DW}$ for $m_a=0.139\text{kg/s}$ and $T_r=60\text{C}$ .....	126
Figure 5.24. Variation of moisture removal capacity of DW with $N_{RR}$ and $N_{DW}$ for $m_a=0.056\text{kg/s}$ and $T_r=70\text{C}$ .....	127
Figure 5.25. Variation of moisture removal capacity of DW with $N_{RR}$ and $N_{DW}$ for $m_a=0.083\text{kg/s}$ and $T_r=70\text{C}$ .....	128
Figure 5.26. Variation of moisture removal capacity of DW with $N_{RR}$ and for $m_a=0.111\text{kg/s}$ and $T_r=70\text{C}$ .....	129
Figure 5.27. Variation of moisture removal capacity of DW with $N_{RR}$ and $N_{DW}$ for $m_a=0.139\text{kg/s}$ and $T_r=70\text{C}$ .....	130
Figure 5.28. Variation of moisture removal capacity of DW with $N_{RR}$ and $N_{DW}$ for $m_a=0.056\text{kg/s}$ and $T_r=80\text{C}$ .....	131
Figure 5.29. Variation of moisture removal capacity of DW with $N_{RR}$ and $N_{DW}$ for $m_a=0.083\text{kg/s}$ and $T_r=80\text{C}$ .....	132
Figure 5.30. Variation of moisture removal capacity of DW with $N_{RR}$ and $N_{DW}$ for $m_a=0.111\text{kg/s}$ and $T_r=80\text{C}$ .....	133
Figure 5.31. Variation of moisture removal capacity of DW with $N_{RR}$ and $N_{DW}$ for $m_a=0.139\text{kg/s}$ and $T_r=80\text{C}$ .....	134
Figure 5.32. Variation of moisture removal capacity of DW with $N_{RR}$ and $N_{DW}$ for $m_a=0.056\text{kg/s}$ and $T_r=90\text{C}$ .....	135
Figure 5.33. Variation of moisture removal capacity of DW with $N_{RR}$ and	

$N_{DW}$ for $m_a=0.083\text{kg/s}$ and $T_r=90\text{C}$ .....	136
Figure 5.34. Variation of moisture removal capacity of DW with $N_{RR}$ and $N_{DW}$ for $m_a=0.111\text{kg/s}$ and $T_r=90\text{C}$ .....	137
Figure 5.35. Variation of moisture removal capacity of DW with $N_{RR}$ and $N_{DW}$ for $m_a=0.139\text{kg/s}$ and $T_r=90\text{C}$ .....	138
Figure 5.36. Effectiveness of RR as a function of $N_{RR}$ and $N_{DW}$ for $T_r=60\text{C}$ .....	142
Figure 5.37. Effectiveness of EC as a function of $N_{RR}$ and $N_{DW}$ for $T_r=60\text{C}$ .....	144
Figure 5.38. Effectiveness of RR as a function of $N_{RR}$ and $N_{DW}$ for $T_r=70\text{C}$ .....	146
Figure 5.39. Effectiveness of EC as a function of $N_{RR}$ and $N_{DW}$ for $T_r=70\text{C}$ .....	148
Figure 5.40. Effectiveness of RR as a function of $N_{RR}$ and $N_{DW}$ for $T_r=80\text{C}$ .....	150
Figure 5.41. Effectiveness of EC as a function of $N_{RR}$ and $N_{DW}$ for $T_r=80\text{C}$ .....	152
Figure 5.42. Effectiveness of RR as a function of $N_{RR}$ and $N_{DW}$ for $T_r=90\text{C}$ .....	154
Figure 5.43. Effectiveness of EC as a function of $N_{RR}$ and $N_{DW}$ for $T_r=90\text{C}$ .....	156
Figure 5.44. Effects of Air Flow Rate on Pressure loss trough RR and DW.....	157
Figure 5.45. Variation of CC at $N_{DW}=0.1\text{rpm}$ and $N_{RR} =5\text{rpm}$ .....	161
Figure 5.46. Variation of COP at $N_{DW}=0.1\text{rpm}$ and $N_{RR} =5\text{rpm}$ .....	162
Figure 5.47. Variation of $\Delta w_p$ at $N_{DW}=0.1\text{rpm}$ and $N_{RR} =5\text{rpm}$ .....	163

Figure 5.48. Variation of $\Delta w_r$ at $N_{DW}=0.1\text{rpm}$ and $N_{RR}=5\text{rpm}$ .....	164
Figure 5.49. Variation of $\varepsilon_{RR}$ at $N_{DW}=0.1\text{rpm}$ and $N_{RR}=5\text{rpm}$ .....	165
Figure 5.50. Variation of $\varepsilon_{EC}$ at $N_{DW}=0.1\text{rpm}$ and $N_{RR}=5\text{rpm}$ .....	166
Figure 5.51. Variation of CC with Zeolite Size at Constant $m_a=0.111\text{kg/s}$ , $T_r=60\text{C}$ , and $N_{DW}=0.1\text{rpm}$ .....	171
Figure 5.52. Variation of COP with Zeolite Size at Constant $m_a=0.111\text{kg/s}$ , $T_r=60\text{C}$ , and $N_{DW}=0.1\text{rpm}$ .....	171
Figure 5.53. Variation of CC with Zeolite Size at Constant $m_a=0.111\text{kg/s}$ , $T_r=60\text{C}$ , and $N_{RR}=10\text{rpm}$ .....	172
Figure 5.54. Variation of COP with Zeolite Size at Constant $m_a=0.111\text{kg/s}$ , $T_r=60\text{C}$ , and $N_{RR}=10\text{rpm}$ .....	172
Figure 5.55. Variation of $\Delta w_p$ with Zeolite Size at Constant $m_a=0.111\text{kg/s}$ , $T_r=60\text{C}$ , and $N_{DW}=0.1\text{rpm}$ .....	173
Figure 5.56. Variation of $\Delta w_r$ with Zeolite Size at Constant $m_a=0.111\text{kg/s}$ , $T_r=60\text{C}$ , and $N_{DW}=0.1\text{rpm}$ .....	173
Figure 5.57. Variation of $\Delta w_p$ with Zeolite Size at Constant $m_a=0.111\text{kg/s}$ , $T_r=60\text{C}$ , and $N_{RR}=10\text{rpm}$ .....	174
Figure 5.58. Variation of $\Delta w_r$ with Zeolite Size at Constant $m_a=0.111\text{kg/s}$ , $T_r=60\text{C}$ , and $N_{RR}=10\text{rpm}$ .....	174
Figure 5.59. Variation of $\varepsilon_{RR}$ with Zeolite Size at Constant $m_a=0.111\text{kg/s}$ , $T_r=60\text{C}$ , and $N_{DW}=0.1\text{rpm}$ .....	175
Figure 5.60. Variation of $\varepsilon_{EC}$ with Zeolite Size at Constant $m_a=0.111\text{kg/s}$ , $T_r=60\text{C}$ , and $N_{DW}=0.1\text{rpm}$ .....	175
Figure 5.61. Variation of $\varepsilon_{RR}$ with Zeolite Size at Constant $m_a=0.111\text{kg/s}$ , $T_r=60\text{C}$ , and $N_{RR}=10\text{rpm}$ .....	176
Figure 5.62. Variation of $\varepsilon_{EC}$ with Zeolite Size at Constant $m_a=0.111\text{kg/s}$ ,	

$T_r=60C$ , and $N_{RR}=10rpm$ .....	176
Figure 5.63. Variation of CC with Zeolite Size at Constant $N_{RR}=10rpm$ $N_{DW}=0.1rpm$ and $m_a=0.111kg/s$ .....	177
Figure 5.64. Variation of COP with Zeolite Size at Constant $N_{RR}=10rpm$ $N_{DW}=0.1rpm$ and $m_a=0.111kg/s$ .....	177
Figure 5.65. Variation of CC with Zeolite Size at Constant $N_{RR}=10rpm$ $N_{DW}=0.1rpm$ and $T_r=60C$ .....	178
Figure 5.66. Variation of COP with Zeolite Size at Constant $N_{RR}=10rpm$ $N_{DW}=0.1rpm$ and $T_r=60C$ .....	178
Figure 5.67. Variation of $\Delta w_p$ with Zeolite Size at Constant $N_{RR}=10rpm$ $N_{DW}=0.1rpm$ and $m_a=0.111kg/s$ .....	179
Figure 5.68. Variation of $\Delta w_r$ with Zeolite Size at Constant $N_{RR}=10rpm$ $N_{DW}=0.1rpm$ and $m_a=0.111kg/s$ .....	179
Figure 5.69. Variation of $\Delta w_p$ with Zeolite Size at Constant $N_{RR}=10rpm$ $N_{DW}=0.1rpm$ and $T_r=60C$ .....	180
Figure 5.70. Variation of $\Delta w_r$ with Zeolite Size at Constant $N_{RR}=10rpm$ $N_{DW}=0.1rpm$ and $T_r=60C$ .....	180
Figure 5.71. Variation of $\varepsilon_{RR}$ with Zeolite Size at Constant $N_{RR}=10rpm$ $N_{DW}=0.1rpm$ and $m_a=0.111kg/s$ .....	181
Figure 5.72. Variation of $\varepsilon_{EC}$ with Zeolite Size at Constant $N_{RR}=10rpm$ $N_{DW}=0.1rpm$ and $m_a=0.111kg/s$ .....	181
Figure 5.73. Variation of $\varepsilon_{RR}$ with Zeolite Size at Constant $N_{RR}=10rpm$ $N_{DW}=0.1rpm$ and $T_r=60C$ .....	182
Figure 5.74. Variation of $\varepsilon_{EC}$ with Zeolite Size at Constant $N_{RR}=10rpm$ $N_{DW}=0.1rpm$ and $T_r=60C$ .....	182
Figure 5.75. Effects of Particle Size of Zeolite and Air Flow Rate on Pressure Loss Through DW with $\Delta X_{DW}=10cm$ and Zeolite Size=10 and 20mm.....	183
Figure 5.76. Variation of CC with $\Delta X_{DW}$ at Constant $N_{DW}=0.1rpm$ , $T_r=60C$ and $m_a=0.111kg/s$ .....	187

Figure 5.77. Variation of COP with $\Delta X_{DW}$ at Constant $N_{DW}=0.1$ rpm, $T_r=60$ C and $m_a=0.111$ kg/s.....	187
Figure 5.78. Variation of CC with $\Delta X_{DW}$ at Constant $N_{RR}=10$ rpm, $T_r=60$ C and $m_a=0.111$ kg/s.....	188
Figure 5.79. Variation of COP with $\Delta X_{DW}$ at Constant $N_{RR}=10$ rpm, $T_r=60$ C and $m_a=0.111$ kg/s.....	188
Figure 5.80. Variation of $\Delta w_p$ with $\Delta X_{DW}$ at Constant $N_{DW}=0.1$ rpm, $T_r=60$ C and $m_a=0.111$ kg/s.....	189
Figure 5.81. Variation of $\Delta w_r$ with $\Delta X_{DW}$ at Constant $N_{DW}=0.1$ rpm, $T_r=60$ C and $m_a=0.111$ kg/s.....	189
Figure 5.82. Variation of $\Delta w_p$ with $\Delta X_{DW}$ at Constant $N_{RR}=10$ rpm, $T_r=60$ C and $m_a=0.111$ kg/s.....	190
Figure 5.83. Variation of $\Delta w_r$ with $\Delta X_{DW}$ at Constant $N_{RR}=10$ rpm, $T_r=60$ C and $m_a=0.111$ kg/s.....	190
Figure 5.84. Variation of $\varepsilon_{RR}$ with $\Delta X_{DW}$ at Constant $N_{DW}=0.1$ rpm, $T_r=60$ C and $m_a=0.111$ kg/s.....	191
Figure 5.85. Variation of $\varepsilon_{EC}$ with $\Delta X_{DW}$ at Constant $N_{DW}=0.1$ rpm, $T_r=60$ C and $m_a=0.111$ kg/s.....	191
Figure 5.86. Variation of $\varepsilon_{RR}$ with $\Delta X_{DW}$ at Constant $N_{RR}=10$ rpm, $T_r=60$ C and $m_a=0.111$ kg/s.....	192
Figure 5.87. Variation of $\varepsilon_{EC}$ with $\Delta X_{DW}$ at Constant $N_{RR}=10$ rpm, $T_r=60$ C and $m_a=0.111$ kg/s.....	192
Figure 5.88. Variation of CC with $\Delta X_{DW}$ at Constant $N_{RR}=10$ rpm, $N_{DW}=0.1$ rpm, and $m_a=0.111$ kg/s.....	193
Figure 5.89. Variation of COP with $\Delta X_{DW}$ at Constant $N_{RR}=10$ rpm, $N_{DW}=0.1$ rpm, and $m_a=0.111$ kg/s.....	193
Figure 5.90. Variation of CC with $\Delta X_{DW}$ at Constant $N_{RR}=10$ rpm, $N_{DW}=0.1$ rpm, and $T_r=60$ C .....	194
Figure 5.91. Variation of COP with $\Delta X_{DW}$ at Constant $N_{RR}=10$ rpm, $N_{DW}=0.1$ rpm, and $T_r=60$ C .....	194
Figure 5.92. Variation of $\Delta w_p$ with $\Delta X_{DW}$ at Constant $N_{RR}=10$ rpm, $N_{DW}=0.1$ rpm, and $m_a=0.111$ kg/s.....	195

Figure 5.93. Variation of $\Delta w_r$ with $\Delta X_{DW}$ at Constant $N_{RR}=10\text{rpm}$ , $N_{DW}=0.1\text{rpm}$ , and $m_a=0.111\text{kg/s}$ .....	195
Figure 5.94. Variation of $\Delta w_p$ with $\Delta X_{DW}$ at Constant $N_{RR}=10\text{rpm}$ , $N_{DW}=0.1\text{rpm}$ , and $T_r=60\text{C}$ .....	196
Figure 5.95. Variation of $\Delta w_r$ with $\Delta X_{DW}$ at Constant $N_{RR}=10\text{rpm}$ , $N_{DW}=0.1\text{rpm}$ , and $T_r=60\text{C}$ .....	196
Figure 5.96. Variation of $\varepsilon_{RR}$ with $\Delta X_{DW}$ at Constant $N_{RR}=10\text{rpm}$ , $N_{DW}=0.1\text{rpm}$ , and $m_a=0.111\text{kg/s}$ .....	197
Figure 5.97. Variation of $\varepsilon_{EC}$ with $\Delta X_{DW}$ at Constant $N_{RR}=10\text{rpm}$ , $N_{DW}=0.1\text{rpm}$ , and $m_a=0.111\text{kg/s}$ .....	197
Figure 5.98. Variation of $\varepsilon_{RR}$ with $\Delta X_{DW}$ at Constant $N_{RR}=10\text{rpm}$ , $N_{DW}=0.1\text{rpm}$ , and $T_r=60\text{C}$ .....	198
Figure 5.99. Variation of $\varepsilon_{EC}$ with $\Delta X_{DW}$ at Constant $N_{RR}=10\text{rpm}$ , $N_{DW}=0.1\text{rpm}$ , and $T_r=60\text{C}$ .....	198
Figure 5.100. Effects of $\Delta X_{DW}$ as a function of $m_a$ on $\Delta P$ through DW with $\Delta X_{DW}=10\text{cm}$ and $15\text{cm}$ and $d_z=20\text{mm}$ ,.....	199

## LIST OF SYMBOLS

<u>Symbol</u>	<u>Description</u>
A	: area, ( $m^2$ )
AC	: alternating current
CC	: cooling capacity, ( $kW/kg_{dryair}$ )
COP	: coefficient of performance
$C_z$	: specific heat of Zeolite, ( $kJ/kgK$ )
d	: orifice plate diameter, (mm)
$d_z$	: average zeolite particle size, (mm)
D	: pipe diameter, (mm)
DCS	: desiccant cooling system
DW	: desiccant wheel
EC	: evaporative cooler
f	: function
g	: gravitational constant, ( $m/s^2$ )
h	: enthalpy of moist air, ( $kJ/kg_{dryair}$ )
h'	: head, (m)
ID	: inside diameter, (mm)
k	: thermal conductivity, ( $kJ/Cm$ )
L	: Length, (m)
$m_a$	: mass flow rate of air, ( $kg/s$ )
N	: revolution of the wheel, (rpm)
OCDCS	: open cycle desiccant cooling system
OD	: outside diameter, (mm)
OP	: orifice plate
P	: pressure, (kPa)
p.s.i.	: Paund per inch square
Pr	: Prandtl number
Q	: heat, (kJ)
r	: radius, (mm)
Re	: Reynold number

RH	: relative humidity, (%)
rph	: revolution per hour
rpm	: revolution per minute
RR	: rotary regenerator
RTD	: resistance temperature detector
S.T.P.	: standard temperature pressure
T	: temperature, (C)
U	: velocity of air, (m/s)
w	: humidity ratio of air, ( $\text{kg}_{\text{water vapor}}/\text{kg}_{\text{dry air}}$ )
w'	: uncertainty
X	: thickness of the wheel/matrix, (cm)

### **Greek Letters:**

$\beta'$	: diameter ratio
$\Delta$	: difference
$\beta$	: heat transfer surface area density, ( $\text{m}^2/\text{m}^3$ )
$\varepsilon$	: effectiveness
$\theta$	: manometer inclination angle
$\rho$	: density, ( $\text{kg}/\text{m}^3$ )

### **Subscripts and others:**

a	: air
alc	: alcohol
db	: dry bulb
DW	: desiccant wheel
EC	: evaporative cooler
h	: hydrodynamic
i	: inlet
in	: input



lab	: laboratory
min	: minimum
o	: outlet
OP	: orifices plates
p	: process
r	: regenerator
RR	: rotary regenerator
s	: sensible
t	: thermal
wb	: wet bulb
z	: zeolite
1, 2,.....,9	: state number



## CHAPTER 1

### INTRODUCTION

The decade of the 1990s has brought together a combination of societal concerns which are of particular interest to the refrigeration and air conditioning industries. These concerns range from indoor air quality issues, destruction of the earth's ozone layer, greenhouse warming, increased efficiency standards, and peak electrical energy demands on summer peaking electrical utilities. These issues are now and will continue to have a profound influence on the design of refrigeration equipment used for building space environmental control. The innovative application of desiccant cooling systems offers some attractive advantages among the range of technology options which can address these concerns.

Desiccant Cooling System offers an attractive way of utilizing low-temperature energy (solar, geothermal or waste heat) and reducing the consumption of conventional energy. It also have been proposed as an alternative to conventional vapor compression units.

Desiccant cooling is a potentially environmentally friendly technology which can be used to condition the internal environment of buildings. Unlike a conventional air conditioning system which relies on electrical energy to drive the cooling cycle, desiccant cooling is a heat driven cycle.

Simple evaporative cooling has been used for many years in those parts of the world for which the climate is hot and dry and there is a supply water available. This climate constraint limits the potential markets for

evaporative cooling, excluding many of the world's population areas. The integration of air desiccant with evaporative cooling over the last 50 years has led to the possibility of extending the climate range over which evaporative cooling can be effective. Contemporary desiccant systems treat latent and sensible cooling requirement separately and more efficiently by using equipment specific to that load. Desiccant full air conditioning systems were first developed in the 1950's. There have been many recent developments and desiccant cooling is now acknowledged as available technology for the air conditioning sector and the technology is advancing rapidly.

### **In Favor of Desiccants**

- Avoidance of refrigerant
- Better indoor air quality
- Heat recovery
- Waste heat could be used
- Same capital cost lower running cost
- Lower maintenance cost than chillers
- Longer life
- Less equipment

### **Against Desiccants**

- Concern re-legionnaires' disease
- Could restrict choice of maintenance staff
- Limited cooling capacity
- Current pricing strategy
- Concern about lithium bromide
- Inefficient summer operation
- Concern about good filtration of external air

Advantages of using desiccant cooling systems include the following:  
(1) very small electrical energy is consumed and the source for regenerating thermal energy can be diverse (i.e. solar energy, waste heat, natural gas); (2) a desiccant system is likely to eliminate or reduce the use of ozone depleting

CFCs (depending on whether desiccant cooling is used in conjunction with evaporative coolers or vapor compression systems, respectively); (3) controlling humidity can be achieved better than those cases employing vapor compression systems since sensible and latent cooling occur separately; and (4) improvement in indoor air quality is likely to occur because of the normally high ventilation and fresh air flow rates normally employed. Also desiccant systems have the capability of removing airborne pollutants.

Desiccant cooling is not suitable for small unitary systems, except where heat recovery is already going to be provided and the upgrade cost to a desiccant-coated heat wheel is small. Since the use of heat wheel is not practical when latent cooling loads are low.

Desiccant technologies have numerous current and potential applications. For example:

- Supermarkets use them to reduce frost build up on refrigerated cases and frozen products, extending product shelf life as well as the intervals between expensive, energy consuming defrost cycles.
- Desiccant contribute to a drier, cleaner, more comfortable environment in schools, hospitals, hotels, office buildings and stores of all kinds.

A typical desiccant cooling system consists of a desiccant wheel, a rotary heat exchanger, two evaporative coolers and associated blowers for air movement (Figure 1.1). After the desiccant wheel adsorbs moisture from the process air, this air exits the wheel hot and dry, due to the desiccant's heat of adsorption. For an effective cooling system, all or most of this heat must be rejected. The cooler, dry air leaving the rotary heat exchanger is then passed through an evaporative cooler, which adds moisture to the air, reducing its temperature before it enters the conditioned space. On the regeneration side, air is first reduced in temperature by passing it through an evaporative cooler. This cooled air provides a heat sink for the air-to-air heat exchanger. The hottest air exiting the heat exchanger is used for

regeneration of the desiccant wheel. (The remainder, if any, is normally rejected outside). The regeneration heat source for the desiccant can be the condenser coil of a boiler system, a direct-fired burner or a waste-heat source. The hot air existing the heat source is passed through the regeneration section of the desiccant wheel, and the moisture released by the desiccant is rejected to the flue.

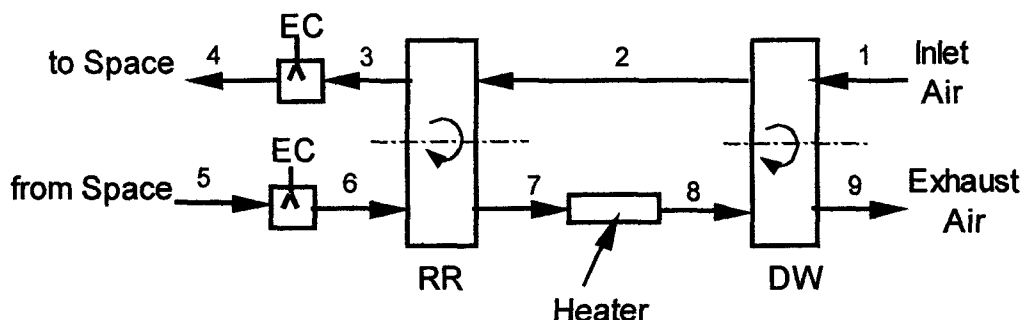


Figure 1.1 Schematic of an open-cycle desiccant cooling system

The performance of a desiccant dehumidifier depends mainly on the type of desiccant material used, the internal geometry of the dehumidifier (i.e., how the desiccant is deployed within the dehumidifier matrix), and the operating parameters. The material type affects size, range of operation (temperature, humidity), efficiency, cost, and service life of a dehumidifier. The desiccant choice also affects the thermal COP and cooling capacity of a system. The geometry of a dehumidifier affects its pressure drop, size, and cost and thus the thermal and electrical COPs and the cost of a cooling system. Control strategies can also affect the overall performance. The optimum combination of desiccants and geometries can provide high efficiency and low cost dehumidifiers for air-conditioning applications.

Desiccants are chemicals with great affinity to moisture. They absorb (or release) moisture because of the difference in vapor pressure between the surface of the desiccant and the surrounding air. Dehumidification said to occur when the vapor pressure of the surface of the desiccant is less than

that of the surrounding air. Dehumidification continues until the desiccant material reaches equilibrium with the surrounding air.

Commercially available desiccants include silica gel, activated alumina, natural and synthetic zeolites, lithium chloride, and synthetic polymers.

Previously there was no cited theoretical and/or experimental study on Desiccant Cooling Systems in Turkey. This study was planned as a first experimental investigation on the system. This study also investigates the applicability of Natural Zeolite (Clinoptilolite type, Biğadiç/Balıkesir) to the Desiccant Cooling Systems for dehumidification of air.

The primary design and construction of a desiccant cooling system was started in 1997. The modifications on designed components, additional component's design, set-up combination, construction of measurement system calibration and operation of the desiccant cooling system were achieved in the time period starting from 2001.

In the second chapter of this thesis, an extensive literature survey on desiccant cooling systems and rotary regenerator and desiccant wheels together with desiccants as dehumidifier medium is presented.

The third chapter is devoted to the design, construction of experimental test set-up and measurements conducted.

In Chapter 4, the method of experiments and calculations performed on the measured data are outlined.

The experiments conducted on the performance of established DCS with defined system parameters are discussed to determine the influence of operating parameters in Chapter 5.

The estimated future studies on DCS in terms of heat and mass transfers are listed in Chapter 6.

The experimental study presented in this thesis was financially supported by the Research Fund of the University of Gaziantep under code MF 97-05.



## CHAPTER 2

### LITERATURE SURVEY

#### 2.1 INTRODUCTION

Developed countries use a significant amount of energy in cooling buildings. In most cases this cooling is done by refrigeration machines using form of high-grade energy (e.g. electricity).

Several studies have investigated alternative methods of providing cooling using lower-grade energy. The system proposed by Dunkle uses a desiccant to reduce the moisture content of air then evaporatively cools it. Systems of this type, which use a desiccant dehumidifier to convert cooling load into sensible load and using evaporative coolers, are known generally as Open-Cycle Desiccant Cooling Systems **Sheridan and Mitchell**, 1985, in [53].

This chapter consists of a summary of the related literature on the manner. The previously conducted theoretical and experimental studies on desiccant cooling systems desiccant wheels as separate components, systems performance, rotary regenerators, performance through heat and mass transfer calculations are analyzed consecutively. The method of presentation is just as following the historical background in time.



## 2. 2 AN OVERALL ANALYSIS ON DESICCANT COOLING SYSTEMS

Desiccant cooling is an environmentally friendly technology which can be used to condition the internal environment of buildings. Unlike conventional air conditioning systems, which rely on electrical energy to drive the cooling cycle, desiccant cooling is a heat driven cycle. Desiccant cooling systems have been used successfully in Northern Europe and a number of studies have demonstrated that solar energy can be used to drive the system in this region. However, to date, desiccant cooling has not been used in Southern Europe. **Mavroudaki, P., Beggs, C. B., Sleight, P. A., and Halliday, S. P.**, in 2002 [1] presented the results of a study, in which a solar desiccant cooling model was used to evaluate the potential for using solar power to drive a single-stage desiccant cooling system in various locations in Southern Europe. The study demonstrated that solar desiccant cooling was feasible provided that the latent heat gains experienced were not excessive. However, if the relative humidities experienced are too high then desiccant cooling becomes impracticable simply because the regeneration temperatures required are excessive.

The desiccant cooling cycle is a novel open heat driven cycle which can be used both to cool and dehumidify air. Being a heat driven cycle, desiccant cooling accords an opportunity to utilize heat which might otherwise be wasted. It can therefore be coupled to solar collectors to produce a cooling system which, in theory, should be environmentally friendly. **Halliday, S. P., Beggs, C. B., and Sleight, P. A.**, in 2002 [2] discussed the feasibility of using solar energy to power the desiccant cooling cycle and also presented a study, in which a solar desiccant cooling model is used to evaluate installations located in the Southeast and East midlands of England, and in the central Scotland. The paper demonstrates that solar powered desiccant cooling is a feasible solution for cooling and heating buildings in the United Kingdom.

HVAC systems with desiccant wheel (DW) are energy efficient, with a low ambient impact, and can be profitable in comparison with the traditional

systems. They also allow a better indoor air quality. In their paper the summer operating costs of both the desiccant and traditional systems were obtained by **Mazzei, P., Minichiello, F., and Palma, D.**, in 2002 [3] using three software codes. Two were based on DOE calculation engine (PowerDOE and DesiCalce), while one (DTPE) was an autonomously developed code, based on a subdivision of the psychrometric chart in zones, each one corresponding to a different air handling. DOE and DTPE took into account the most recent DW performance values. Calculation assumes hourly weather data extracted from the European .le named "Test Reference Year" (TRY) and appropriately processed. With reference to operating costs of the desiccant systems in summer Italian conditions, for a retail store application, interesting savings (up to 35%) were obtained, as well as reduction in thermal cooling power (up to 52%). Starting costs of the desiccant system were generally greater than the ones of the traditional system; considering the present costs of the Italian market, a simple payback of about 5–7 years has obtained. If slightly de-rated DWs were considered, the payback would attain lower values, near to 3–4 years.

A hybrid solar cooling system, which combines the technologies of rotary desiccant dehumidification and solid adsorption refrigeration, has been proposed by **Dai, Y. J., Wang, R. Z., and Xu, Y. X.**, in 2002 [4] for cooling grain. The key components of the system were a rotary desiccant wheel and a solar adsorption collector. The former was used for dehumidification and the later acts as both an adsorption unit and a solar collector. The heating load from sunshine can thus be reduced to a greater extent since the solar adsorption collector was placed on the roof of the grain depot. Compared with the solid adsorption refrigeration system alone, the new hybrid system performs better. Under typical conditions, the coefficient of performance of the system was  $>0.4$  and the outlet temperature was  $<20^{\circ}\text{C}$ . It was believed that the system can be used widely in the regions with abundant solar resources due to such advantages as environmental protection, energy saving and low operation costs. Additionally, some parameters, for example, ambient conditions, the effectiveness of the heat exchanger and evaporative

cooler, mass air-flow rate, etc., which affect system performance, are also analyzed.

In 2001, **Joudi, K. A., and Dhaidan, N. S.**, [7] developed a computer simulation program for evaluating the performance of solar assisted heating and cooling systems for a domestic two story residence located in Baghdad. Simulation of the open cycle solar assisted desiccant cooling system showed that the ambient temperature, regeneration temperature, heat exchanger effectiveness and evaporative cooler effectiveness have major influences on the system performance, whereas the dehumidifier has minor effect.

The use of heat produced by solar thermal collectors was an interesting option for thermal driven air conditioning processes. A thermal driven cooling technique which fits well to non-tracking solar collectors was the desiccant cooling technique. Recently several projects have been carried out which focused on the connection of desiccant cooling systems with solar thermal energy for regeneration of the sorbents. **Henning, H-M., Erpenbeck, T., Hindenburg, C., and Santamaria, I. S.**, in 2001 [8] deal with three main topics: (1) experiences achieved in a realized system which was coupled to a solar collector were discussed, (2) a new concept was presented, in which a solar air collector was integrated into the desiccant cooling cycles as the only heat source and (3) a comparative study was presented which compares system performance for different system configurations and different climatic situations.

In 2000, **Jalalzadeh-Azar, A., A., Steele, G. W., and Hodge, B. K.**, [9] experimentally evaluated and analyzed the performance of a rotary gas-fired desiccant system. The constituents of the study are (1) evaluation of the issues critical to accurate data acquisition and (2) examination of the sensitivities of the system performance parameters to perturbations in a certain design set points.

The experimental system studied in their study was gas-fired, rotary dehumidifier that was commercially available by **Jalalzadeh-Azar, A. A.**, in

2000 [10]. The transient response of the experimental system was observed for two transient scenarios involving brief and prolonged idle modes prior to activating the system. The results for a time-dependent average efficiency were obtained and discussed in evaluating the significance of transient operation. Steady-state performance of the system as a function of inlet humidity ratio and its response to natural gas flow modulation were also discussed.

In 1998, **Vineyard, E. A., Sand, J. S., and Durfee, D. J.**, [11] studied to investigate the impact of varying some of these operating parameters on the performance of a desiccant dehumidification system. They reported their results using more quantitative measures, such as latent capacity and latent coefficient of performance (COP), that better describe the efficiency of the moisture removal process. Two desiccant loadings were tested; one at normal production level and the other with 25% more desiccant applied to the wheel. For both desiccant loadings, it was claimed that the latent capacity and COP increased as desiccant wheel speed increased.

In 2000, **Pons, M., and Kodama, A.**, [12,13] in their consecutive studies paid attention to the thermodynamic analysis. They emphasized the open character of the cycle, and considered especially the consumption of liquid water. Their full second-law analysis showed that there existed an optimal rotation speed which results from a combination between the different entropy productions in the cycle. When the air velocity was increased, together with an accordingly optimized rotational speed, the cooling capacity increased while the COP decreased due to increases in the entropy productions in the dehumidifier and sensible heat exchanger.

Active desiccant systems for ventilating commercial buildings was evaluated by **Harriman, L. G., Czachorski, M., Witte, M. J., and Kosar, D. R.**, in 1999 [14]. Over the last 15 years, active desiccant systems have become a common component of HVAC systems in commercial buildings needing lower-than-usual humidity levels. Ice arenas, supermarkets and refrigerated warehouses all contain refrigeration systems which cool air more

effectively when most of the building's moisture load was removed by an active (heat-reactivated) desiccant system. Cost savings, comfort improvements and "process benefits" of extended-season operation for ice rinks, lower product temperature for supermarkets and improved safety for warehouses were usually enough to make the desiccant component a useful addition to such buildings.

In 1999, **Techajunta, S., Chirarattananon, S. and Exell, R. H. B.**, [15] presented an indoor and analytical study to evaluate the performance of a desiccant cooling system that uses silica gel as desiccant, electric light bulbs to simulate solar radiation, and forced flow of air through an integrated Desiccant Collector. Comparisons between analytical calculations and experimental data indicated good agreement. Meanwhile based on the calculations show that it should be possible to operate this system in tropical humid climates using the regeneration process in the day and the air dehumidification in the night time.

**Belding, W. A., Delmas, M. P., and Holeman, W. D.**, in 1996, [18] studied the loss of a desiccant's equilibrium water adsorption capacity after exposure to thermal cycling as a common method for quantifying desiccant aging. Since isotherm shape and desiccant capacity can be related to overall cooling-system performance, system cooling capacity and coefficient of performance over time can be predicted. Aging curves for a new Type 1M desiccant developed specifically for desiccant cooling applications by LaRoche Industries Inc. were compared to other commonly used desiccants for this purpose.

In 1999, **Davaragere, B. S., Sherif, S. F., and Goswami, D. Y.**, [16, 17] simulated a solid desiccant cooling system with a backup vapor compression system by using TRNSYS and the performance of the system was evaluated in four cities of the USA with different climates. It was seen that the system has higher COP values for the locations with more latent loads. Recommendations to minimize the auxiliary energy costs using

different methods for supplying the thermal energy for desiccant regeneration were also.

**He-Fie Zhang and Jin-Di Yu**, in 1996 [19] developed a mathematical model of a rotary desiccant wheel that was used to calculate the performance of stationary or rotary bed in term of transient or steady state operation. A computer program for this new model has been compiled and some results for computer simulation were compared with experimental data, they were found to be in good agreement.

In 1996, **Jalalzadeh-Azar, A. A., Hodge, B. K., and Steele, W. G.** [20] evaluated the performance of desiccant systems for applications requiring stringent control of humidity under varying load conditions. Feasibility of different alternatives were discussed, and the system performance was examined from both first- and second-law perspectives. The analysis was performed using a program for a commercially available gas-fired desiccant system. The program predicted the properties of supply air once the operating conditions were specified. Use of a single system with a proposed modification vs. dual-unit arrangement is the basis for categorization of the alternatives.

The use of unglazed transpired solar collectors for desiccant regeneration in a solid desiccant cooling cycle was investigated by **Pesaran, A. A. and Wipke, K. B.**, in 1994 [21]. The performance of a desiccant cooling ventilation cycle integrated with either unglazed transpired collectors or conventional glazed flat-plate collectors was studied by using computer models. The thermal coefficient of performance of the cooling system with unglazed collectors was lower than that of the cooling system with glazed collectors because the former system did not use the heat of adsorption released during the dehumidification process. Although the area required for the unglazed collector array was 70% more than that required for the glazed collector array in a 10.56 kW (3 ton) solar cooling system, the cost of the unglazed array was 45% less than the cost of the glazed array.

Dupont, M., et al. in 1994 [22], presented a dynamic study of moist air dehumidification in view of its use in an air conditioning process by evaporative cooling in tropical climates. A special device has been built to study dehumidification of tropical-like inlet air, through a fixed bed of silica gel and activated alumina. The compact desiccant storage was composed of two parallel beds to reduce the pressure drop and the analytical model was used to simulate a complete air conditioning open cycle operating with hot and humid climate.

### 2.3 STUDIES ON DESICCANT WHEELS

Desiccant wheels have two major applications: air dehumidification and enthalpy recovery. Since the operating conditions are different, heat and mass transfer behaviors in the wheels are quite different. The performances of desiccant wheels used in air dehumidification and enthalpy recovery were compared with each other by Zhang, L.Z. and Niu, J.L., in 2002 [5]. To accomplish this task, a two-dimensional, dual-diffusion transient heat and mass transfer model which took into account the heat conduction, the surface and gaseous diffusion in both the axial and the thickness directions has presented. Effects of the rotary speed, the number of transfer units, and the specific area on the performance of the wheel were investigated and compared in the two situations. The cycles that the desiccant and air undergo in the wheel were plotted in psychrometric charts to demonstrate the different heat and moisture transfer mechanisms during the dehumidification and enthalpy recovery processes.

A simplified mathematical model consisting of ordinary differential equations has been proposed and found by Tanthapanichakoon, W., and Prawarnpit, A., in 2002 [6] to accurately predict the dynamic performance of a honeycomb rotary absorption-type dehumidifier in a beverage factory. The model was validated experimentally using the transient measurement data on the air properties at the outlets of both the dehumidification and regeneration sections. Good agreement between the predicted and recorded data at each

Dupont, M., et al. in 1994 [22], presented a dynamic study of moist air dehumidification in view of its use in an air conditioning process by evaporative cooling in tropical climates. A special device has been built to study dehumidification of tropical-like inlet air, through a fixed bed of silica gel and activated alumina. The compact desiccant storage was composed of two parallel beds to reduce the pressure drop and the analytical model was used to simulate a complete air conditioning open cycle operating with hot and humid climate.

### 2.3 STUDIES ON DESICCANT WHEELS

Desiccant wheels have two major applications: air dehumidification and enthalpy recovery. Since the operating conditions are different, heat and mass transfer behaviors in the wheels are quite different. The performances of desiccant wheels used in air dehumidification and enthalpy recovery were compared with each other by Zhang, L.Z. and Niu, J.L., in 2002 [5]. To accomplish this task, a two-dimensional, dual-diffusion transient heat and mass transfer model which took into account the heat conduction, the surface and gaseous diffusion in both the axial and the thickness directions has presented. Effects of the rotary speed, the number of transfer units, and the specific area on the performance of the wheel were investigated and compared in the two situations. The cycles that the desiccant and air undergo in the wheel were plotted in psychrometric charts to demonstrate the different heat and moisture transfer mechanisms during the dehumidification and enthalpy recovery processes.

A simplified mathematical model consisting of ordinary differential equations has been proposed and found by Tanthapanichakoon, W., and Prawarnpit, A., in 2002 [6] to accurately predict the dynamic performance of a honeycomb rotary absorption-type dehumidifier in a beverage factory. The model was validated experimentally using the transient measurement data on the air properties at the outlets of both the dehumidification and regeneration sections. Good agreement between the predicted and recorded data at each



thermal cycling with humid ambient air was 10 percent to 30 percent for all desiccants.

**Collier, R. K., Cohen, B. M., and Slosberg, R. B.,** in 1992 [26] described some of the results of the effect that the properties of various desiccant materials can have on the performance of cooling systems based upon the use of thermally reactivated desiccants. One study was purely analytical in nature and viewed the desiccants as characterized by standard isotherm relationships (e. G., Brunauer). The second study was purely experimental in nature and relied upon sample desiccant cores provided by commercial producers of these materials using silica gel, molecular sieve, lithium chloride, and activated carbon as the desiccants. The results were interesting since behavior that was characterized analytically and led to fairly noteworthy recommendations for preferred desiccant properties for air-conditioning systems supported experimentally in the commercial cores.

**Van den Bulk, E., Mitchell, J. W., and Klein, S. A.,** in 1984 [28, 49] investigated the use of rotary dehumidifiers in open cycle desiccant cooling systems by analyzing the performance of the rotary heat exchanger-rotary dehumidifier subsystem. For a given cooling load, the required regeneration heat supply could be minimized by choosing appropriate values for the regeneration air mass flow rate and the wheel rotation speed. A map was presented showing optimal values for rotational speed and regeneration flow rate as a function of the regeneration air inlet temperature and the process air inlet humidity ratio.

**Matsuki, K., and Saito, Y.,** in 1992 [29] described the recent status of R&D in desiccant cooling in Japan. A number of research projects on desiccant cooling have been carried out since the oil crisis, in many cases financially supported by the government. The desiccants used included LiCl, silica gel, and zeolite, and the desiccant carriers were rotary heat exchangers or beds. In many cases, solar energy was used as the heat source for the regeneration of desiccants. In other cases, the performance of solar desiccant cooling systems has been observed.

thermal cycling with humid ambient air was 10 percent to 30 percent for all desiccants.

**Collier, R. K., Cohen, B. M., and Slosberg, R. B.**, in 1992 [26] described some of the results of the effect that the properties of various desiccant materials can have on the performance of cooling systems based upon the use of thermally reactivated desiccants. One study was purely analytical in nature and viewed the desiccants as characterized by standard isotherm relationships (e. G., Brunauer). The second study was purely experimental in nature and relied upon sample desiccant cores provided by commercial producers of these materials using silica gel, molecular sieve, lithium chloride, and activated carbon as the desiccants. The results were interesting since behavior that was characterized analytically and led to fairly noteworthy recommendations for preferred desiccant properties for air-conditioning systems supported experimentally in the commercial cores.

**Van den Bulk, E., Mitchell, J. W., and Klein, S. A.**, in 1984 [28, 49] investigated the use of rotary dehumidifiers in open cycle desiccant cooling systems by analyzing the performance of the rotary heat exchanger-rotary dehumidifier subsystem. For a given cooling load, the required regeneration heat supply could be minimized by choosing appropriate values for the regeneration air mass flow rate and the wheel rotation speed. A map was presented showing optimal values for rotational speed and regeneration flow rate as a function of the regeneration air inlet temperature and the process air inlet humidity ratio.

**Matsuki, K., and Saito, Y.**, in 1992 [29] described the recent status of R&D in desiccant cooling in Japan. A number of research projects on desiccant cooling have been carried out since the oil crisis, in many cases financially supported by the government. The desiccants used included LiCl, silica gel, and zeolite, and the desiccant carriers were rotary heat exchangers or beds. In many cases, solar energy was used as the heat source for the regeneration of desiccants. In other cases, the performance of solar desiccant cooling systems has been observed.

isotherms, adsorption rate, heat of adsorption, and cyclic aging performance. Properties were measured on individual material components as well as selected component mixtures.

Using computer simulations and recent experimental data on silica gel, the impact of degradation was evaluated by **Pesaran, A. A., and Penney, T. R.**, in 1991 [37]. Hypothetical degradations of desiccants with Type 1 moderate isotherms were also simulated. Depending on degree and type of desiccant degradation, the decrease in thermal COP and cooling capacity of the system was 10% to 35%. The 35% loss in system performance occurs when desiccant degradation was considered as the worst case. The simulations showed that the COP and, to a lesser degree, the cooling capacity of these degraded systems could be improved by increasing the rotational speed of the dehumidifier. However there is no information on the influence of rotational speed of the dehumidifier.

## **2.4 ANALYSIS ON PERFORMANCE OF DESICCANT COOLING SYSTEMS**

The performance of a gas-fired cooling system operating in the recirculation mode was optimized by modeling, using different desiccant materials. Design and operating parameters were investigated by **Worek, W. M., Zheng, W., Belding, W. A., Novasel, D., and Holeman, W. D.**, in 1991 [38] included the fraction of the wheel that was heated in regeneration, termed the “staged regeneration fraction,” the regeneration temperature, the sorption time (inversely proportional to wheel rpm), and desiccant moisture uptake. Performance results documented included the optimum system coefficient of performance (COP) and cooling capacity along with operating conditions, staged regeneration fraction, and sorption time corresponding to the optimum. The performance of the system operating in the recirculation mode was also compared to the performance of an optimally designed system operating in the ventilation mode.

a cooled-bed cooling system, operating in the recirculation mode, at variable indoor and outdoor conditions. The effect of regeneration temperature on the performance of the cooled-bed system was also documented.

**Parsons, B. K., Pesaran, A. A., Bharathan, D., and Shelpuk, B.**, in 1989 [42] examined the merits of coupling a desiccant dehumidification subsystem to a gas-engine-driven vapor compression air conditioner. System used a rotary, silica gel, parallel-plate dehumidifier. Dehumidifier data and analysis were based on recent tests. The dehumidification subsystem processed the fresh air portion and handled the latent portion of the load.

**Kang, T. S., and Maclaine-cross, I. L.**, in 1989 [43] suggested that solid desiccants in open cooling cycles used low temperature heat efficiently making them be attractive for solar air conditioning. Advanced cycles using nearly reversible evaporative coolers have previously been proposed and shown to have high ideal performance. Their parametric study indicated that, with real components comparable to those used in studies of classical cycles, these open cycles can give more than twice the thermal coefficient of performance of a ventilation cycle.

The performance of an open-cycle, adiabatic, solid, desiccant cooling system operating in the ventilation mode was modeled numerically by **Charoensupaya, D., and Worek, W. M.**, in 1988 [46]. The effects of nondimensional dehumidifier channel length, desiccant mass fraction and desiccant isotherm shape were investigated. The results yielded conditions for which the system had an optimum thermal coefficient of performance (COP).

**Löf, G. O. G., Cler, G., and Brisbane, T.**, in 1988 [47] investigated the performance of a solar desiccant cooling system. The cooling unit was operated in the ventilation mode, fresh air being dried in a rotating desiccant matrix, and cooled by heat exchange and evaporative cooling. Return air was used as a cooling medium in a rotating heat exchange matrix, heated by solar energy in a heat exchange coil, and discarded through the rotating

desiccant bed. The solar-driven system provided over 90 percent of the seasonal cooling requirements in an experimental, residence type building at average COP levels of 1.0 and solar collection efficiencies of 50 percent when supplied with solar heated water at temperature of 50 to 65C.

In another experimental investigation a solar assisted open adsorption cooling system has been designed and tested by **Joudi, K. A., and Madhi, S. M**, in 1987 [48] under the local weather conditions of Basrah, Iraq. Data were obtained from June to September, inclusive, 1984. Test were carried out hourly with a direct supply of hot air from a corrugated absorber solar air heater for regeneration. Also, tests were conducted at a constant regeneration temperature of 70C using auxiliary heat. Adsorption was carried out by a rotary disk of silica gel. Three mass flow rates of process air were employed without recirculation. The performance of the solar air heater was obtained for both seasons, and the instantaneous efficiency was evaluated experimentally and analytically with results compared. Daily and seasonal coefficient of performance were obtained for the cooling system for the mass flow rates employed. A maximum seasonal average value of 2.8 was obtained for a mass flow rate of 0.075 kg/s. The system performance improved with higher regeneration temperature, higher process air mass flow rate and dry weather. It was possible to generate a cool supply of air at satisfactory conditions using solar energy only for all clear days under the local weather conditions.

**Calton, D. S.**, in 1985 [50] presented the field analysis of a desiccant-assisted HVAC system. It was shown that reduced circulated air flow rates of 0.5cfm/ft<sup>2</sup> of sales area were possible without compromise to uniform sales area temperatures. An air-distribution strategy of supplying two-thirds of the air to the front of the store and returning air under the refrigerated fixtures was employed. Reduced air flow rates have not shown any ill effect on odor control either. Reducing store relative humidity to 40% has shown a reduction in both refrigerated fixture load and frost formation on fixture coils and products. The total package system used heat reclaim from the refrigerating condensing units for winter heating of the store. The desiccant-regeneration

air was preheated by reclaiming a portion of the heat rejection from air-conditioning condensing units.

**Manley, D. L., Bowlen, K. L., and Cohen, B. M.,** in 1985 [51] presented that the using of gas-fired desiccant dehumidification for supermarket air conditioning afforded many benefits. Since supermarkets have a disproportionately high latent-to-sensible load ratio. Air conditioners must overcool the air to achieve adequate dehumidification and then reheat the air to control dry-bulb temperature. This results in inefficient operation. Depressed humidity levels, which are easily achieved only by desiccant systems, provide additional savings by reducing the latent load on refrigerated cases. A computer model was formulated to allow the extension of field test results to many climates, system types, store types, and shopping patterns. Results indicate a favorable scenario in climates of moderate and high humidity, with utility rate structures that favor the switch from electricity to gas. The trend toward energy-efficient architecture and increased food-refrigeration capacity, both of which increase latent-to-sensible load ratio, and electrical rate penalties for peak power demand suggest that the concept will be even more cost-effective in the future. As a result, an integrated system, which incorporates the most desired features and the best balance of desiccant-based and vapor-compression cooling, should be under development.

**Burns, P. R., Mitchell, J. W., and Beckman, W. A.,** in 1985 [52] studied the performance of three possible hybrid system configurations in supermarket applications and compared their performance with the traditional vapor compression system. Results presented suggest a total air-conditioning savings of 60% with hybrid systems for the design condition considered.

**Sheridan, J. C., and Mitchell, J. W.,** in 1985 [53] considered a cycle which combined indirect evaporative cooling with a dehumidifier for covering latent loads and vapor compression refrigeration unit for covering sensible load. The cycle has been studied for two climate types and two different

loads representative of those likely to be met in commercial buildings, with the use of a solar energy system regenerating the desiccant dehumidifier.

**Epstein, M., Glormes, M., Davidson, K., and Kosar, D.,** in 1985 [55] studied a simple algebraic model of wave motion arising in the adiabatic fixed-desiccant bed dehumidification of an air stream for the prediction of the performance potential of a desiccant air conditioning system. The model was used to explain the increase in cooling system performance that has been realized through the use of mixed inert-desiccant material adsorption beds. The response of cooling system performance to changes in external process conditions was examined and conclusions were drawn relative to optimization of system characteristics.

A generic model of a cooled dehumidifier suitable for use in estimating the seasonal performance of cooled desiccant dehumidifier air-conditioning systems was developed by **Schultz, K. J., Mitchell, J. W., and Beckman, W. A.,** in 1982 [56]. A system configuration appropriate for using a cooled dehumidifier was presented. Estimates of the seasonal performance of the cooled system were presented in comparison with adiabatic dehumidifier system performance. Both gas-fired and solar-assisted operations were considered. It was found that the cooled system could be competitive with the adiabatic ventilation system, particularly in solar-assisted applications if a high level cooled dehumidifier could be developed.

A feasibility study of open cycle air conditioning systems that use solid desiccants and solar energy had been performed by **Nelson, J. S., Bekman, W. A., Mitchell, J. W., and Close, D. J.,** in 1978 [57]. Two configurations evaluated were the ventilation mode, in which ambient air was continually introduced into the room, and the recirculation mode, in which room air is recirculated. Seasonal simulations for Miami, Florida, indicated that the auxiliary energy requirement for the ventilation mode was about half that for the recirculation mode. The seasonal COP for the system using solar energy as the auxiliary was approximately 0.75. A conventional flat plate solar

energy system of moderate size could provide a large fraction of the energy required to meet the sensible and latent loads of a typical house.

## 2.5 STUDIES ON ROTARY REGENERATORS

An effective prediction was proposed by **Kodama, A., Hirayama, T., Goto, M., Hirose, T., and Critoph, R. E.**, in 2001 [100] to estimate the optimal rotational speed and performance of a rotary adsorber, in which simultaneous enthalpy and humidity changes were dealt with separately by visualizing changes of state of product or exhaust air on psychrometric chart. Assuming that the adsorbent rotor is completely regenerated to equilibrium with the regeneration air during the corresponding period, the optimal rotational speed corresponds to the region of the short time adsorption in which penetration theory holds and enthalpy change between both streams through the adsorbent rotor follows the behavior of a rotary sensible heat exchanger at lower revolution rates. The change of the product/exhaust air condition with increasing rotational speed is presented as a set of simple equations. Also, by considering the relative humidity of product air and that of regeneration air to be almost the same at a sufficiently high flow rates of regeneration air, an optimal rotational speed and the product air condition are easily found by simple calculation. In comparison with experiments, the proposed method gives a rotational speed near the "optimum" and the humidity and temperature of the product air are predicted almost exactly.

Waves analysis using psychrometric chart, a method aiming to evaluate the rotary desiccant dehumidification, was presented by **Dai, Y. J., Wang, R. Z., and Zhang, H. F.**, in 2001 [101]. The continuity and energy conservation equations for the transient coupled heat and mass transfer were established and solved using a finite differential model. The locus of points of outlet air states along the rotational direction was plotted as two wave fronts and one breakthrough point for both dehumidification and regeneration processes. Thermal wave, concentration wave, and middle zone point were explained in terms of the different characteristics of their own. The rules to



improve the performance of dehumidification according to the wave shape were proposed and some important parameters, such as heat capacity, adsorption heat, rotational speed, regeneration temperature, thickness of the desiccant matrix and the desiccant isotherm shape, are discussed in detail using psychrometric chart. It was demonstrated that the chart method has feasible and rapid in evaluating the performance of the rotary dehumidifier.

Desiccant air conditioning system that incorporate rotary heat and mass exchangers are getting a closer look in view of the pressure on the industry to decrease the use of chlorofluorocarbons and for fuel economies. Heat and mass exchangers that utilize LiCl, silica gel and other desiccants have been considered by **Neti, S., and Wolfe, E. I.**, in 2000 [102] as possibilities. The performance features of the silica gel rotary mass exchanger wheel, which is the primary component in a desiccant system, has been measured. The process air flow velocities and temperatures ranged from 0.5 to 2.5m/s, and 20 to 30C with 30 to 100% relative humidities. Similar velocity and relative humidity conditions were used for regeneration air. The desiccant data were compared to two different theories from the literature; the method of characteristics and a numerical approach. The method of characteristics appears to be good for only a small range of conditions, generally for low values of specific capacities. The numerical approach appears to predict the trends well, through sometimes with large errors.

Controlling the performance of HVAC systems and air-to-air energy exchangers, to prevent overheating and overhumidifying of the supply air during part-load operating conditions was discussed by **Simonson., C. J., Shang, W., and Besant, R. W.**, in 2000 [59] Equations were developed to facilitate the calculation of the optimal energy exchanger performance and the optimal recirculation air flow rate during part-load operating conditions. If these optimal values were applied, it was possible to save energy and improve indoor air quantity simultaneously. Numerical and experimental investigations can be applied to investigate the potential of using wheel speed control the energy and moisture transfer rates. A numerical model is necessary to predict the part-load performance because the performance is

affected by the operating conditions. The effectiveness decreases as the wheel speed decreases for some of the operating conditions, while the effectiveness increases as the wheel speed decreases for some other operating conditions.

**Simonson., C. J., Shang, W., and Besant, R. W.,** in 2000 [60] investigated the potential of bypassing some of the supply air flow around energy wheels to control their performance. The required bypass flow depends on the building design conditions, the fraction of the recirculated air, the energy wheel effectiveness , and the outdoor conditions. Numerical and experimental results were presented that demonstrate the performance of the energy wheels during bypass control or unbalanced supply and exhaust flow rates. To make bypass control easier to implement into energy simulation programs and building control systems, effectiveness correlations were presented that allow the designer to calculate the sensible, latent, and total effectiveness of energy wheels without detailed simulations. These correlations for effectiveness during unbalanced supply and exhaust mass flow rates were in agreement with simulation data within  $\pm 3\%$ .

**Shah, R.K. and Skiepko, T.,** 1999 [61] proposed a comprehensive modeling for leakages and thermal performance of rotary regenerators. They represented a substantial refinement over that available in the literature. Two separate models are proposed for the energy transfer in the regenerator. The first refers to the heat transfer and pressure drop process. The second, based on a gas flow network, represents modeling of leakage distribution within the regenerator. The solution of both models has obtained iteratively with proper input data and yielded the thermal/flow design parameters of a rotary regenerator. These models use experimental correlations describing the Nusselt number, friction factor and seal discharge coefficients. A design procedure was outlined for the rating problem and details were referenced. Keeping the pressure leakage factor constant, the rating problem has been solved for different distributions of leakages through radial, peripheral and axial seals. The results clearly demonstrated that a significant reduction

could occur in the thermal energy transfer to the cold fluid even with reasonably small (5% or so) individual leakages.

A numerical model for coupled heat and moisture transfer in rotary energy exchanger was developed by **Simonson, C. J., and Besant, R. W.**, in 1997 [103,104]. The numerical model was one dimensional , transient and was formulated using the finite volume method with an implicit time discretization. The model was developed from the physical principles with a limited number of simplifying assumptions. This enables the study of several assumptions and their effect on the predicted performance of regenerative energy exchangers. Results from the numerical model for coupled heat and mass transfer in rotary energy exchangers were compared with experimental data. The agreement between the measured and simulated effectiveness (sensible, latent, and total energy) was close and within the experimental uncertainty. In addition, the effects of certain assumptions were investigated for sensitivity on the predicted performance of regenerative energy exchangers.

The design-point dehumidification performance (i. E., at ARI conditions) of a rotary dehumidifier wheel depends on its rotational speed, the sorption properties of desiccant, the heat and mass transfer characteristics of the matrix, and the size of the dehumidifier. However, the real operating conditions of a rotary dehumidifier can vary significantly from the design point, given the large variations in operating conditions (i.e., the outdoor, indoor, and regeneration temperature, and humidities) for various locations during different times of the year. **Zheng, W., Worek, W. M., and Novasel, D.**, in 1995 [105] investigated the variability of the dehumidification performance of a rotary dehumidifier and its dependence on operating conditions. Also, the effect of the operating conditions on the optimum rotational speed of a rotary dehumidifier, where the performance of a rotary dehumidifier was optimized, was described.

A generalized representation of desiccant isotherms was developed by **Jekel, T. B., Mitchell, J. W., and Klein, S. A.**, in 1993 [116] for microporous

adsorbents, a class of desiccant materials that have pore diameters of less than about 20 Å. The adsorption potential theory developed by Dubinin and Polanyi for microporous adsorbents was used to describe the isotherms. The adsorption potential was defined as the change in Gibb's free energy of adsorption of an ideal gas, and using the Clausius-Claypeyron equation was shown to be equal to the difference between the heat of adsorption and heat of vaporization at the same temperature. A single-sited Dubinin isotherm form, which was the simplest form, was used to describe the different isotherm shapes. The advantage of this formulation is that for many desiccants the only temperature dependence through the adsorption potential. The adsorption potential theory is applicable for a variety of adsorbents, including silica gel, zeolites, and molecular sieves.

The equilibrium performance of desiccant materials can also be evaluated using the method of characteristics and shock wave theory for the processing and regenerating periods, respectively. The performance of a simple desiccant cooling cycle is evaluated at the design point to illustrate the desirable desiccant properties. The desiccant dehumidifier outlet is assumed to be at the intersection point, thus illustrating the maximum attainable performance.

To prevent the carry-over of contaminated air to the fresh air in rotary heat regenerators, a small part of the incoming fresh air is used to purge the heat transfer matrix during its transfer from the hot to the cold zone. This purging causes a loss in the effectiveness of heat transfer in the regenerator. A simple numerical scheme employing heat transfer theory for elemental heat exchangers has been developed by **Worsøe-Schmidt, P.**, in 1991, [66]. This scheme was obtained by dividing the gas stream and the 'stream' of matrix material into a number of flow channels, and the effect of fresh air purging has been calculated over a wide range of parameters. The results were presented numerically, graphically, and in the form of approximate algebraic expressions.

A hybrid numerical method, combining finite differences with respect to space and a Laplace transform with respect to time, was proposed by **Kawasaki, K., Matsuhisa, T., Sakai, I., and Hijikata, K.**, in 1991 [67] to determine the heat transfer in a rotary heat exchanger used as a rotating ceramic regenerator for automotive gas turbine. The temperature distributions of the core and of the working fluids were solved for given boundary and initial conditions of a rotary regenerators using this method. An advantage of the present method is that it can be applied when the core and the working fluids have dissimilar temperature distributions. The temperature change in the ceramic honeycomb core was determined from start up to periodic steady state operation. The heat exchanger effectiveness was obtained for an extruded ceramic core used in automotive gas turbine applications.

Experimental design data ( $St$  vs  $Re$ ,  $Nu$  vs  $x^*$ , and  $f$  vs  $Re$ ) were presented by **Sunden, B., and Karlsson, I.**, in 1991 [63] for four trapezoidal ducts with corrugated walls and one with smooth (noncorrugated) walls with constant wall temperature boundary conditions. The trapezoidal channel has top and bottom walls corrugated in the flow direction, while the two side walls are smooth. A smooth (noncorrugated) channel was used as a reference. For rotary regenerators used in a air conditioning systems, such trapezoidal channels with all four walls smooth are common. The corrugated walls then yield heat transfer enhancement. A test rig has been built, and measurements have been taken for one smooth and four corrugated channels using a steady-state oil-to-air heat transfer. The corrugated height and wave length of the top and bottom walls were varied. The investigation covered a Reynolds number range of  $500 < Re < 5000$ . The corrugated channel with the largest corrugation height and smallest wavelength provides the best enhancement of the heat transfer (about 100%), but the pressure drop penalty was very large (about 270% increase). Flow area goodness factor and volume goodness factor comparisons of the heat transfer surfaces were made for the assessment of investigated channels.

The behavior of the air-water vapor-desiccant system is of central interest for modeling rotary heat and mass exchangers in desiccant cooling systems. Lithium chloride is commonly used as desiccant in commercial systems, primarily because of the low humidities it supports. **Rau, J. J., Klein, S. A., and Mitchell, J. W.**, in 1991 [118] provided a relationships to describe the sorption equilibria of the air-water vapor-LiCl system. Rotary heat and mass exchangers were described by two conservation laws and two transfer equations. A system of two coupled non linear hyperbolic partial differential equations and two ordinary differential equations were formed. Since isotherm and isopiestic of LiCl exhibit discontinuities, conventional numerical methods that solve this system could not be used. A modified method based on the finite difference model by Maclaine-cross (A theory of combined heat and mass transfer in regenerators, Ph. D. Thesis, Monash University (1979)) was presented. This method predicted the outlet conditions of the air streams and determines temperature and moisture content profiles of the matrix.

British Gas and Munters Ltd., Huntingdon have recently completed a joint development of gas fired desiccant wheel dehumidifier. Desiccant wheel technology has been available for over 40years but the high cost of electrical power has been barrier in their competition with electric refrigeration units. The gas-fired desiccant wheel has, however, more than halved running costs. This article introduces the concept of desiccant technology and describes how the gas-fired system was developed can be found in the study of **Pearson, J., and Thompson, K.**, in 1991, [107].

A computer program for prediction of mass and heat transfer in a rotary-type dehumidifier was developed by **Borde, I., Korin, E., and Eliasy, R.**, in 1991 [117]. The theoretical model considered the mass transfer resistance to be accounted by surface and Knudsen diffusion effects. The theoretical model was used to investigate the influence of the adsorption properties on the drying process. A comparison between adiabatic and isothermal breakthrough curves for silica gel and zeolite 5A showed that considerable improvement in the efficiency of the air drying process could be

obtained by heat removal from the silica gel bed compared with insignificance of this effect in the case of zeolite 5A. The theoretical model was also applied to investigate the drying performance of various compositions of a combined bed composed of silica gel in the front part and zeolite 5A in the back part. The results demonstrated that a significant improvement in dehumidifier performance could be obtained by arranging a suitable proportion of silica gel to zeolite 5A in the combined bed in comparison with a bed containing only silica gel. However, the optimal composition of the combined bed has to be considered in the light of the fact that of zeolite has been regenerated at 130-150C compared with 70-90C for silica gel.

Rotary regenerator exit gas temperature responses to step changes in mass flow rates were presented by Romie, F., E., in 1990 [68]. When the step changes is the same for both gases the responses are shown to have a decaying oscillation to the final values of the exit gas temperatures. The source of oscillations is explained. The responses are found by dividing the regenerator into pie-shaped segments and approximating the area-mean gas temperature leaving a segment as the temperature of the gas leaving a small regenerator located on the central radius of the segment.

A hybrid heat wheel has been developed by Chakravarty, M., and Kayal, T., in 1990 [69] by combining the design and incorporating the advantages of a metallic and ceramic heat wheel. The final heat wheel has loose ceramic packings inside a metallic basket rotating around a vertical axis. It has been operated with maximum stream flow rates up to 350nm<sup>3</sup>/hr and hot gas inlet temperatures up to 860C. It may not be suitable for attachment to a coal-fired furnace because of possible clogging of packing voids by non-combustible coal ash.

The kinetics of sorption in most commercial adsorbents (e.g. charcoals or zeolites) results from the interaction of several distinct steps of mass transfer. In order to understand and analyze the compound kinetics it is expedient to design experiments so that the rate of individual steps can be

observed by **Riekert, L.**, in 1989 [145] independently. Otherwise, the rate of diffusion in micropores or in cavities of zeolite crystals is likely to be obscured by resistance to mass transfer in intercrystalline voids of the sample or in the macropores of a pellet. Temperature excursion in the solid sorbent owing to exothermicity of sorption can be controlled through direct contact of the solid sorbent with a heat sink of sufficient capacity.

A heuristic “pseudo-steady-state” model of the heat and mass transfer occurring in desiccant dehumidifiers, embodied in the program DESSIM, has been proposed by **Schultz, K. J., and Mitchell, J. W.**, in 1989 [108] as a conceptually and numerically simple analysis tool (**Barlow, 1982**). A comparison is made with a finite difference solution to determine the accuracy and limitations of the pseudo-steady-state model. The comparison indicates that the pseudo-steady-state model can produce accurate results of dehumidifier performance relative to the finite difference solution when used carefully, although at greater computational expense. Substitution of the finite difference solution into the overall DESSIM program results in a potentially accurate and useful analysis tool.

The transient heat transfer in a rotating counter flow regenerator was analyzed by **Huettner, W., and Niggemann, M.**, in 1989 [71], analytically and numerically with the assumption of constant mass flows on both sides of the regenerators. Moreover, first results for the case of temperature-dependent mass flows were presented.

Exit gas temperature responses of the counter flow rotary regenerator were found for a unit step increase of the inlet temperature of either gas. An analytical solution applicable during the first part of the transient shows that the responses could not be smooth. The overall responses is found by **Romie, F. E.**, in 1988 [77] by dividing the regenerator disk into pie-shaped segments and approximating the area mean gas temperature leaving a segment as the temperature of the gas leaving a small regenerator located at the center of the segment. The method is shown to give good accuracy and is in agreement with predictions of the analytic solution.



**Van den Bulck, E., Klein, S. A., and Mitchell, J. W.**, in 1988 [109] presented a second law analysis of solid desiccant rotary dehumidifiers. The equations for entropy generation for adiabatic flow of humid air over a solid desiccant were developed. The generation of entropy during operation of a rotary dehumidifier with infinite transfer coefficients was investigated and the various sources of irreversibility were identified and quantified. As they pass through the dehumidifier, both the process and regeneration air streams acquire non-uniform outlet states, and mixing both of these air streams to deliver homogeneous outlet streams was irreversible. Transfer of mass and energy between the regeneration air stream and the desiccant matrix occurs across finite differences in vapor pressure and temperature and these transfer processes generate entropy. The second law efficiency of the dehumidifier was given as a function of operating conditions and the effect of finite transfer coefficients for an actual dehumidifier was discussed. It was shown that operating the rotary dehumidifier at conditions that minimize regeneration energy also yielded a local maximum for the second law efficiency.

**Atthey, D. R.**, in 1988 [75] described an approximate thermal analysis of a regenerative heat exchanger. The approximation used relies on the fact that the dimensionless parameters, known as the reduced periods, are not too large, a condition which is made more precise, and which is true for all power station air heaters. There is no upper limit on the reduced lengths with which the method can cope. The method gives time averaged fluid outlet temperatures which are equivalent to those deduced from an analysis of an equivalent recuperator by Hausen. The results are compared with a finite difference solutions of the regenerator problem for sets of plan data. The ability of method to cope with long regenerators was also demonstrated, and the results were compared with Hausen's solution and with other standard results of the literature.

**Skiepko, T.**, in 1988 [71] considered two models describing transport phenomena in rotary heat exchangers as: either disregarding or the other

including heat conduction in the matrix. Both models were described by the system of energy conservation equations which is solved by analytical methods. On the basis of these solutions the effect of the matrix longitudinal heat conduction on the temperature fields of gases and matrix was studied.

Rotary regenerators, also referred to as periodic flow or storage type heat exchangers were used in gas-to-gas heat transfer applications, and mainly in waste heat recovery applications. The basic thermal design theory was first summarized by **Shah, R. K.**, in 1988 [76] for the regenerator including the effect of rotation, longitudinal and transverse conduction, pressure leakage and carry over. Then detailed step-by-step solution procedures were outlined for rating (performance) and sizing (design) of a counter flow rotary regenerator with a specific example.

The operation of the symmetric counter flow regenerative heat exchanger was described by **Romie, F. E.**, in 1987 [79] for conditions under which the thermal capacitance of the contained fluid could not be set equal to zero. The solution of the system equations is found by use of the Laplace transform method. The thermal effectiveness was presented for a range of parameters believed to cover most applications of the symmetric regenerator.

Diffusion mechanisms of moisture within silica gel particles were investigated by **Pesaran, A. A., and Mills, A.**, in 1987 [110]. It is found that for microporous silica gel surface diffusion was the mechanism of moisture transport, while for macroporous silica gel both Knudsen and surface diffusions were important. A model was proposed for simultaneous heat and mass transfer in a thin packed bed of desiccant particles, which account for diffusion of moisture into the particles by both Knudsen and surface diffusions. Using finite difference methods to solve the resulting partial differential equations, predictions were made for the response of thin beds of silica gel particles to a step change in air inlet conditions, and compared to a pseudo-gas-side controlled model commonly used for the design of desiccant dehumidifiers for solar desiccant cooling applications.

Experiments have been performed by **Pesaran, A. A., and Mills, A.**, in 1987 [111] to obtain the transient response of a thin adiabatic packed bed of silica gel after a step change in inlet air conditions. Comparisons were made with predictions using a solid-side resistance model and a pseudo-gas-side controlled model and better agreement obtained with the former model. An apparent dynamic hysteresis for adsorption/desorption with microporous silica gel was clearly in evidence, which could be due to a solid-side effective diffusion coefficient which decreased with increasing moisture content, or to a lesser extent to a hysteresis in the adsorption isotherm itself.

The Galerkin method was applied by **Baclic, B. S.**, in 1985 [81] to solve the symmetric and balanced counter flow thermal regenerator problem. In this approach, the integral equation, expressing the reversal condition in periodic equilibrium of regenerator matrix, is transformed into a set of algebraic equations for the determination of the expansion coefficients associated with the representation of the matrix temperature distribution at the start of cold period in a power series in the space variable. The method was easy and straightforward to apply and leads to the explicit analytical expressions for expansion coefficients. As explicit analytical formula for regenerator effectiveness is derived and the corresponding numerical values were computed. An excellent agreement is found between the present results and those reported in the literature by different numerical methods. The convergence towards the exact results by carrying out the computations to higher order terms, as well as the extension of this method to the more general counter flow regenerator problem was discussed.

A theory was presented by **Van den Bulck, E., Mitchell, J. W., and Klein, S. A.**, in 1985 [120] for modeling rotary heat and mass exchangers with infinite transfer coefficients. The continuity and energy conservation equations for one-dimensional transient flow were established and analyzed. Solutions to the equations were obtained by method of characteristics and the shock wave method. Both methods provided a set of analytical equations that allow performance prediction of the heat and mass exchanger with infinite transfer coefficients for any inlet and operating conditions. A

regenerator-operating chart was introduced to show the fundamental modes of operating for rotary heat and mass exchanger.

## **2.6 STUDIES REGARDING THE PERFORMANCE OF DESICCANT COOLING SYSTEMS IN TERMS OF HEAT AND MASS TRANSFER**

Heat recovery from exhaust air in air conditioning systems using rotary regenerators is common in the United State of America and Canada and it is shown that installations in Australia are well justified economically.

**Van den Bulck, E., Mitchell, J. W., and Klein, S. A.**, in 1985 [121] presented correlations for the effectiveness of rotary dehumidifiers with finite transfer coefficients. A finite-difference model for performance prediction of rotary dehumidifiers with finite transfer coefficients was used in combination with the ideal dehumidifier model to establish effectiveness correlations. Correlations for the humidity and enthalpy effectiveness for silica gel regenerators were given as functions of the dehumidifier number of transfer units (NTU). An Effectiveness-NTU model, incorporating the corrections for the effectiveness an ideal dehumidifier performance, allowed rapid calculation of the dehumidifier performance. The corrections were valid for a wide range of operating conditions and account for the effect of unbalanced flow and high Lewis numbers.

Coupled heat and mass transfer between fluid streams by a regenerator with a sorbent matrix was predicted by **Banks, P. J.**, in 1985 [122, 123] by the superposition of two independent regenerators, in each of which transfer was driven by a combined potential, analogous to temperature in a similar regenerator for energy recovery or dehumidification with convective transfer controlling is considered. The combined potentials and associated specific capacities are examined, and the nature of the analogy explored, in view of the dependence of matrix sorption properties on state. Approximate nonlinear expressions for the combined potentials, applicable to air-conditioning regenerators, were derived and utilized.

The performance of a counterflow, rotary heat exchanger operating with either transient or nonuniform inlet temperatures was investigated by **Brandemuehl, M. J., and Banks, P. J.**, in 1984 [84]. The effect of transient inlet temperatures was analyzed in terms of the response of the outlet fluid temperatures to a step change in temperature of one of the inlet fluid streams. The effect of temperature nonuniformities was analyzed in terms of the change in steady-state effectiveness due to circumferential temperature distribution in one of the inlet fluid streams. A finite difference model of the governing differential equations, using finite transfer coefficient, was employed to obtain a detailed numerical analysis of heat exchanger performance. Results for the complete range of matrix to fluid capacity rate ratio were presented for a balanced and symmetric regenerator. An experimental analysis has also been conducted using a counterflow, parallel passage, rotary heat exchanger made from polyester film.

The exit fluid temperature responses were presented by **Romie, F. E.**, in 1984 [83] for a unit step increase in the entrance temperature of either of the fluids of a counterflow heat exchanger. The exit temperature response histories were functions of four parameters, three of which were commonly used to define the steady-state temperature distributions in the exchanger. The responses were found using a finite difference method and were represented by empirical equations for a range of the four parameters believed appropriate for many technical applications.

The average process stream outlet humidity ratio of an adiabatic counterflow dehumidifier can be lowered if a portion of the process outlet stream is purged from the bulk flow. The purged stream can be recirculated and introduced at the inlet of regenerating period. The performance of such a purged counterflow dehumidifier was studied by **Jurinak, J. J., and Mitchell, J. W.**, in 1984 [113]. Two purged geometries that result in a spatially nonuniform inlet condition in the regenerating period were considered. The effect of the recirculated purge on the process stream outlet states of high performance silica gel dehumidifiers with low and high thermal capacitance matrices operated at nearly optimal rotational speeds was evaluated.

A finite difference model of counterflow rotary dehumidifier was used studied by **Jurinak, J. J., and Mitchell, J. W.**, in 1984 [114] to determine the effect of six matrix properties of dehumidifier performance. The matrix properties considered were the sorption isotherm shape, the maximum sorbent water content, the heat of sorption, the matrix thermal capacitance, matrix moisture diffusivity, and sorption isotherm hysteresis. The results of the finite difference calculations have shown that the shape of the isotherm had a greater effect on dehumidification than the maximum water content. The analysis has indicated that commercially available solid desiccants could result in nearly optimal dehumidifier performance.

**Romie, F. E.**, in 1983 [84] indicated that the transient mixed mean temperatures of the two gases leaving a crossflow heat exchanger were found for a unit step increase in the entrance temperature of either gas. The temperature responses were given in graphical form for the range of parameters:  $Ntu$  from 1 to 8, capacity rate ratio from 0.6 to 1.67, and conductance ratio from 0.5 to 2.0. The solutions were found by using the Laplace transform method by applying to single-pass crossflow exchangers with neither gas mixed.

A mathematical model to predict the thermal performance of regenerators with steam addition into the combustion air has been presented by **Chawla, O. P., and Khandwala, A. L.**, in 1981 [87]. The governing performance equations have been solved by Alternating Direction Approximation Method. On account of 15% steam addition to combustion air, overall heat transfer coefficient during cooling period was doubled, with an increase by 15% during the heating period. The savings in fuel costs have been calculated by considering the depreciation, maintenance and operating costs of a waste heat boiler. It has been predicted that the steam injection was more beneficial for long and low capacity regenerators. The net optimum savings in fuel costs range between 1.3 and 4.2 million rupees annually for the various cases worked out.

A mathematical model of condensation, evaporation and heat transfer in a regenerator having a non sorbing matrix was derived by **van Leersum, J., G., and Ambrose, C. W.**, in 1981 [124]. Good agreement between heat and moisture effectivities was predicted by a simulation of the model, in comparison to the corresponding results from an independently derived equilibrium model for a particular case.

Increased energy costs have brought about increased concern by building owners as well as governments about the operating costs and energy budgets for buildings and power plants. This growing energy conservation consciousness has brought a considerable interest in reclaiming waste heat from residential, commercial, industrial, and institutional ventilation systems. Based on the considerations, the design and the performance of a small rotary heat exchanger for residential houses was tested by **Younis, M., and Shauky, M.**, in 1981 [86]. Laboratory results reveal a high sensible heat recovery maximum effectiveness of 85% with acceptable levels of pressure drop and cross leakage. Cost saving analysis indicates annual energy savings up to 15%, with ever larger savings in the size of the heating and cooling equipment up to 42%. As expected greatest savings could occur when large amounts of outside air are required for ventilation.

The regenerator alternately stores and supplies heat to two gases which enter at different but constant temperatures and flow counter-currently and sequentially through the same flow passages for periods  $t_a$  and  $t_b$ . The periodic steady-state temperatures of the two gases and the regenerator solid are found as functions of time and position. The analysis is based on the use of polynomials of the positions coordinate to represent the matrix temperature distributions at the beginning of each flow periods. The subsequent gas and matrix temperatures were expressed in terms of functions by **Romie, F. E.**, in 1979 [91] by use of a computer. The initial, time average, final temperatures of the gas leaving the regenerator were tabulated. Results for a single regenerators were applied to the rotating regenerator and to switched regenerators.

Simultaneous heat and mass transfer in periodic-flow heat and mass exchangers, or regenerators, with hygroscopic matrix materials has been analyzed by **Holmberg, R. B.**, in 1979 [125]. The coupled heat and mass transfer equations were derived for boundary-layer controlled heat and mass transfer and included longitudinal heat conduction in the matrix. A numerical method of finite difference type was applied to the steady-state performance. Results for a water vapor-air mixture have shown the influence of matrix heat and moisture capacities on the temperature and humidity efficiencies. Distributions of air temperature, air humidity, matrix temperature and adsorbent moisture content were calculated in drying as well as in recovery operations.

Heat and mass transfer in rotary heat exchangers with nonhygroscopic rotor materials have been investigated by **Holmberg, R. B.**, in 1977 [126]. A numerical method of the finite-difference type was applied to the steady-state performance under conditions of finite rotational speed and finite longitudinal heat conduction. Temperature and absolute humidity distribution were calculated for a set of rotary heat exchanger parameters typical in air conditioning. Temperature and humidity efficiencies were evaluated for different inlet air conditions.

The heat transfer, mass transfer and pressure drop characteristics of rotary regenerative sensible heat exchangers or regenerators were also discussed by **Dunkle, R. V., Maclaine-Cross, I. L., and Grad, B. E., and Aust, I. E.**, in 1970 [95]. The literature on the theory of heat exchange by regenerators performance were expressed in terms of the important design variables to simplify the comparison of alternative designs. Effectivity charts were presented for balanced and unbalanced flow. The advantages of the parallel plate regenerator developed by the authors were discussed and a simple design procedure was given.



## 2.7 CONCLUSION

An extensive literature survey on desiccant cooling systems was outlined in this chapter. There exists numerous studies both theoretical and experimental on the overall performance of desiccant systems and on the separate components of the system. Since design, construction and test of open cycle desiccant cooling system is the primary goal of this study available literature is referred paying attention to what is known in terms of theory of desiccant cooling systems and what was done up to date.

In this chapter it is also aimed to provide a complete reference list to consult for whom attending to study on the manner, somehow as a starting point.



## **CHAPTER 3**

### **EXPERIMENTAL SET-UP AND MEASUREMENTS**

#### **3.1 INTRODUCTION**

In this chapter, design, construction and calibration of the experimental test set-up and measurement principles of the collaborated devices are presented.

The chapter consists of the presentation of the set-up as a whole, description of its major components and the measurement methods. The calculations performed on the measured data and methods of experimental study are presented in the succeeding chapter.

#### **3.2 DESIGN AND CONSTRUCTION OF THE EXPERIMENTAL SET-UP**

In this study, an open cycle desiccant cooling system (OCDACS) operating on the ventilation mode test set-up was designed and constructed. The experimental test set-up was consisted of the following basic parts as shown in Figure 3.1.

1. Inlet fan
2. Outlet fan
3. Rotary regenerator
4. Desiccant wheel
5. Pipe system

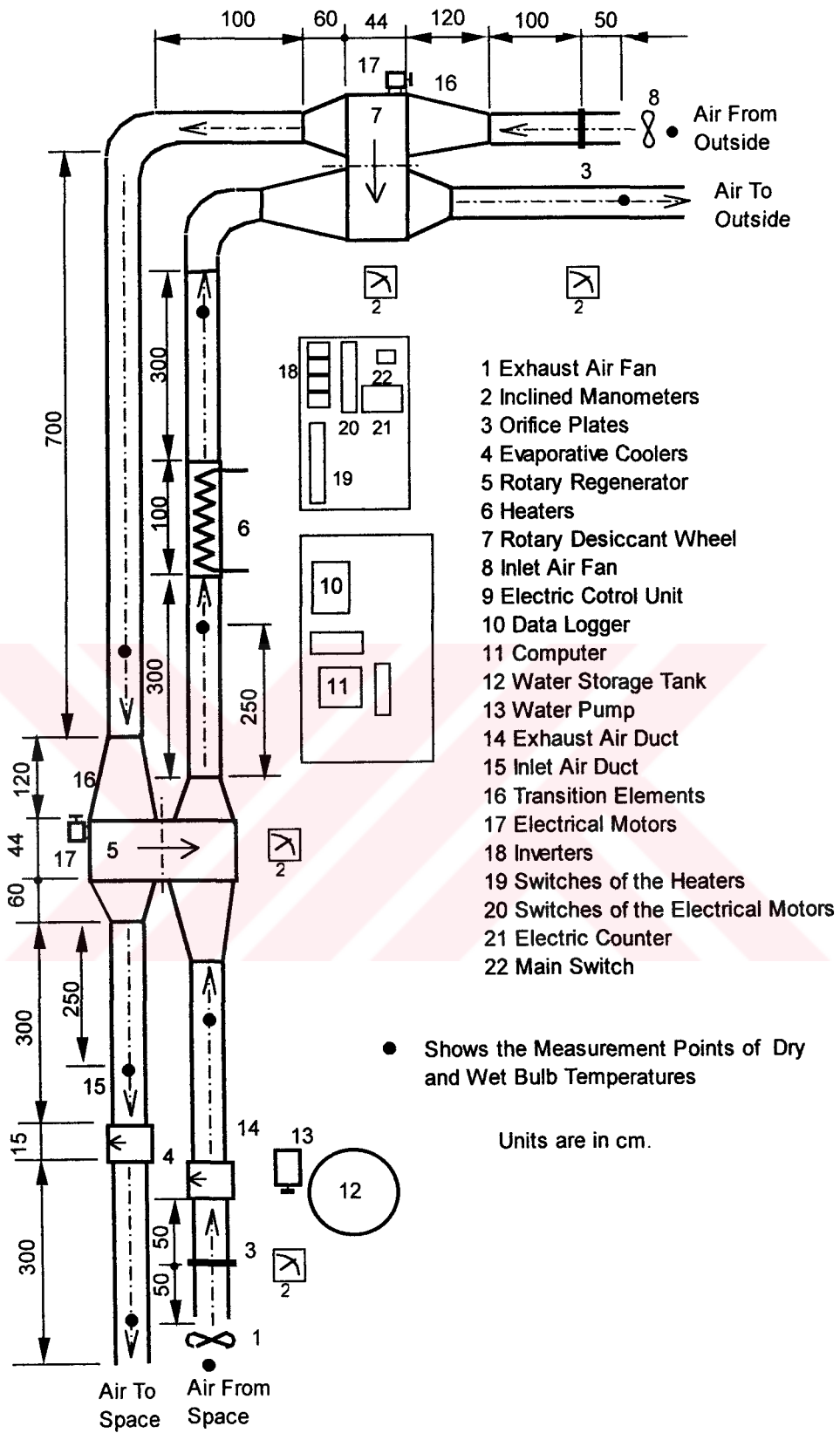


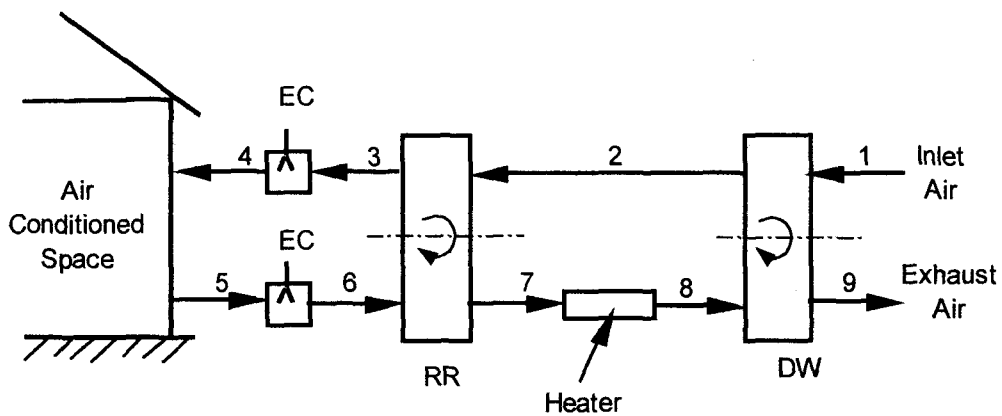
Figure 3.1 A Schematic Layout of the Experimental Test Set-Up

6. Desiccant wheel
7. Pipe system
8. Transition parts
9. Evaporative coolers
10. Heaters
11. Measurement Devices

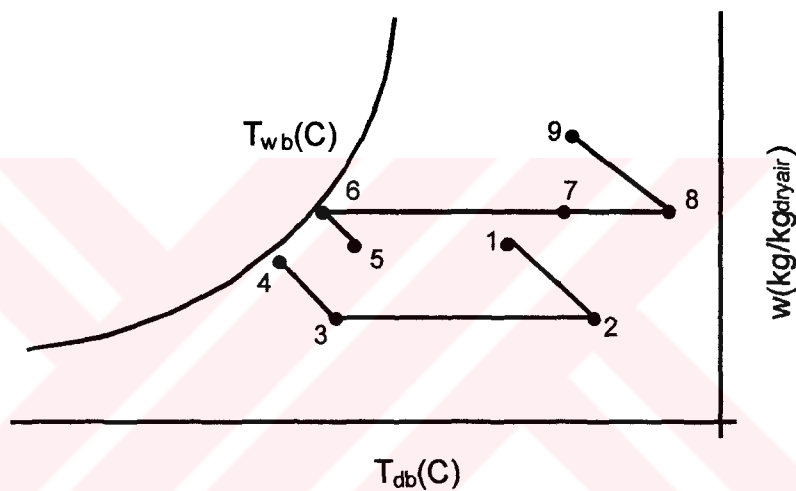
In desiccant air conditioning systems, air is dried by passing it over the desiccant and heat of sorption is removed by sensible cooling. The air is further cooled by adiabatic humidification and is directed into the residence as cool dry air. The component configurations and psychrometric processes of the ventilation cycle are illustrated in Figure 3.2.

Parameters influencing system performance are regeneration air inlet temperature, wheel revolution speed, desiccant mass, and the ratio of regeneration air to process air mass flow rates. An optimal choice of these parameters will reduce the regeneration heat required for a given load. Minimizing both air stream mass flow rates may also reduce the electrical fan power.

OCDACS utilizes a desiccant to remove moisture from air. Dry air is cooled in evaporative coolers (EC) and rotary regenerators are used to meet both sensible and latent air conditioning loads. Solar, waste, or other energy sources are used to regenerate the desiccant. The emphasis in this study is on systems using solid desiccants. Design point calculations were made to establish optimum air flow rates and wheel thicknesses. In the ventilation mode, ambient air is dried and heated by the dehumidifier, regeneratively cooled by exhaust air, evaporatively cooled, and introduced into the house. The process can be controlled so that the temperature and humidity of the supply air are lower than that in the house, and this allows the sensible and latent loads to be met. The exhaust air is first evaporatively cooled to provide a low temperature sink for the heat transfer from the supply air in the regenerator. The air is then heated by an energy supply which could be either a conventional fuel, a source, e.t.c. Passage of the heated air through



(a)



(b)

Figure 3.2 a) A Schematic of Ventilation Mode of Open-Cycle DCS  
 b) Psychrometric Diagram of Ventilation Mode

the dehumidifier regenerates the desiccant and cools the air. The psychrometric diagram Figure 3.2.b shows the states of the air for typical operating conditions. Ambient conditions change over the course of the day, with resulting changes in the sensible and latent loads as can be seen in the psychrometric diagram.

Improving Marketability:

To make desiccant systems more marketable, to;

- Develop advanced desiccant materials, components, and systems with lower costs and improve performance,
- Develop a uniform method for testing desiccant materials and dehumidifier, adsorption sections and whole systems in the laboratory,
- Demonstrate desiccant systems in real-world environments,
- Develop performance benchmarks to establish consumer confidence in manufacturer claims,
- Develop markets for desiccant systems that will improve indoor air quality and reduce environmental pollution.

### 3.2.1 DESICCANT WHEEL

The performance of desiccant dehumidifier depends mainly on the desiccant materials used, the internal geometry of the dehumidifier (i.e., how the desiccant is developed within the dehumidifier matrix), and the operating parameters.

The material type affects size, range of operation (temperature, humidity), efficiency, cost, and, service life of a dehumidifier. The desiccant choice also affects the thermal COP and cooling capacity of the system. The geometry of a dehumidifier affects its pressure drop, size, and cost, and, thus, the thermal and electrical COPs and cost of a cooling system. Control strategies can also affect the overall performance. The optimal combination of desiccants and geometries can provide high-efficiency and low cost dehumidifiers for air-conditioning applications, as was stated by **Belding et al.**, in 1996 [18] in the following list:

Desiccant wheels used for cooling applications are designed with channels which provide laminar flow, maintaining the heat and mass transfer area as high as possible with a minimum pressure drop. Process and regeneration sections of the wheel are sealed to minimize cross-leakage. To

achieve a small wheel size and optimum wheel efficiency, the following characteristics are desirable in the wheel:

1. High surface area to volume ratio for fast heat and mass transfer,
2. High-temperature regeneration to minimize the size of the regeneration section,
3. Desiccant having a Type 1M isotherm shape to enhance the containment of moisture wavefronts on adsorption and the temperature wavefront on regeneration,
4. High desiccant/substrate loading ratio,
5. Desiccant having a low heat of adsorption or a high percentage of its capacity within a low temperature range,
6. Desiccant able to withstand direct-fired regeneration to eliminate losses in efficiency from a boiler,
7. Desiccant properties which are stable over the projected life.

A desiccant is a substance that can absorb and release water vapor from air and can be either solid or liquid. Solid desiccant such as; silica gel and molecular sieves are the desiccants presently under investigation for DCS. Effect of the six matrix properties on the steady-state performance of a DW considered are the sorption isotherm shape, the maximum sorbent water content, heat of sorption, the matrix thermal capacity, maximum moisture diffusivity, and sorption isotherm hysteresis.

Adsorption is the condensation of vapor on a surface at a pressure below the normal pressure of the vapor.

Some of the variables that influence the results of a dynamic dehumidification operation are listed by ASHRAE (Equipment Handbook, 1975) as follows:

- A. Variables concerning the desiccant bed:
  1. Type of desiccant,
  2. Dry weight of desiccant,

3. Particle size,
4. Bulk density,
5. Shape of bed,
6. Area of bed normal to gas flow,
7. Depth of bed,
8. Packing of the desiccant in the bed,
9. Pressure drop through bed.

**B. Variables concerning the gas to be dried:**

1. Flow rate,
2. Temperature,
3. Moisture content,
4. Pressure,
5. Contact time between gas and sorbent; a function of inlet face velocity and bed depth.

**C. Variables concerning reactivation:**

1. Reactivation temperature,
2. Rate and magnitude of heat supply,
3. Heat storage capacity of the bed,
4. Temperature gradient of the bed,
5. Amount of insulation,
6. Gas flow rate.

**D. Miscellaneous:**

1. Cycle time or rotational speed of rotary equipment,
2. Leakage from the apparatus.

For commercially dehumidifying systems and equipment, a sorbent should have the following characteristics, [ASHRAE Handbook of Fundamental]:

1. Suitable vapor pressure characteristics including high adsorptive or absorptive capacity.



2. Stability, should not break down structurally or chemically in range and type of use and resist contamination from impurities.
3. Should be noncorrosive, odorless, nontoxic and nonflammable.
4. Capable of regeneration or reactivation with methods and temperatures generally available.
5. Should be readily available at moderate cost.

In this study, a desiccant wheel, DW using zeolite was designed and constructed. Zeolites including crystalline zeolites, also called molecular sieves, are aluminosilicate minerals and occur naturally. Many types of synthetic zeolites have been developed for special applications. For example, molecular sieves, using types 4A, 5A, 10A, and 13X which have been developed by the Linde Co., U.S.A. These substances have cavity volumes in the range of 0.05 to 0.30cm<sup>3</sup>/gr. However, they may be heated to about 500C without damages occurring to their adsorption and regeneration properties. Type 4A (also termed as NaA by other manufacturers), is used for drying and separation of hydrocarbon mixtures. For example, type 5A (or CaA) is used to separate paraffines and some cyclic hydrocarbons, and type 10X (or CaX) and 13X (or NaX) adsorb quite a wide range of adsorbates because of their larger diameter of inlet necks of their pores as was said by **Srivastava**, in 1998 [186]. Heat of adsorption of natural zeolite have lower values than synthetic zeolites.

Zeolites are micro-porous crystalline alumina silicates, having internal voids consist of channels or cavities; various silicates having internal voids consist of channels or cavities; various considerable vapors and gases (water, ammonia, carbon dioxide, methanol) are strongly adsorbed on the large internal surface area (~1000m<sup>2</sup>/gr) of them, and they have special affinity for water. There exist more than 150 types synthetic and 34 types of natural zeolites.

### 3.2.1.1 Design-Construction and Modification of DW

In designed DW of present study, as a solid desiccant Clinoptilolite type Zeolite of Balıkesir was used by Ülkü, in 1986 [151]. The major properties are given as density,  $\rho_z=1450\text{kg/m}^3$ , thermal conductivity,  $k=0.60\text{W/(mC)}$ , and specific heat,  $C_z=1.1\text{ kJ/kgK}$ .

For the construction of DW as shown in Figure 3.3 in the form of parallel-plate rotary dehumidifier, raw zeolite as shown in Figure 3.4 was cracked. These cracked zeolites were sieved with different sieve meshes such as 1, 2, 3, 4, 6, 10, and 15mm sizes. Due to irregular shape, sieved zeolite has a size 6mm also includes different sizes that is greater than 4mm and less than 6mm.

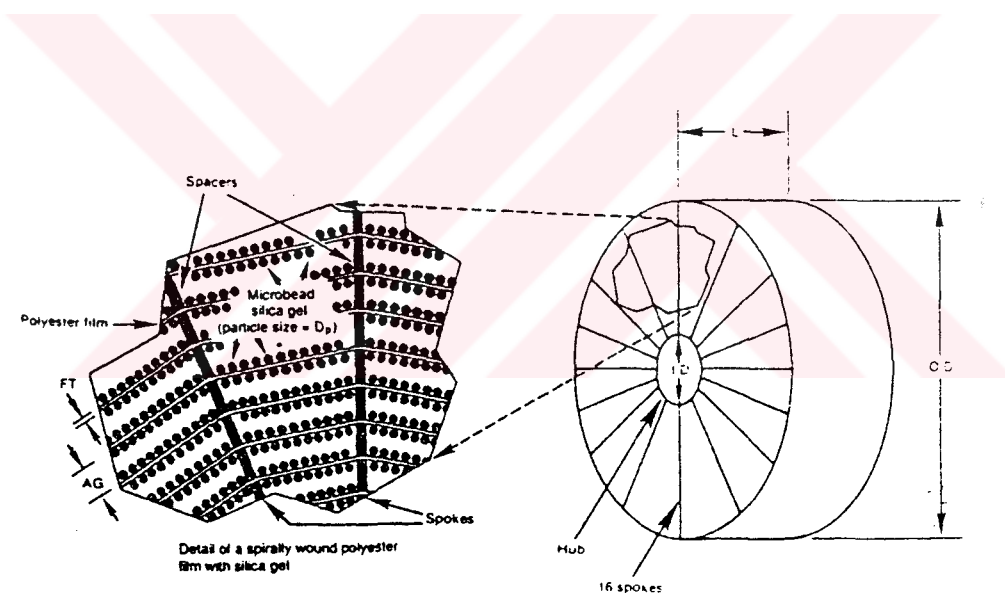


Figure 3.3 Schematic of a parallel-plate rotary dehumidifier [37]

First design construction for DW was tried similar to the arrangement as shown in Figure 3.3. Zeolite was attached to a base material like leather with the use of different glues. However, this form of desiccant bed failed in the construction of DW. Because zeolite is a natural material and its smooth adhesion was not possible (Figure 3.5.a). Zeolite particles were sewed in the form of consecutive packets along cloth. This cloth material was rounded in

DW (Figure 3.5.b). But this arrangement of DW resulted in failure in the DCS operation due to high temperature and mixing of process and regeneration air flow streams. The construction trials finally reached to the last improved DW shape as shown in Figure 3.5.d. As can be seen in Figure 3.5.d instead of using glued or cloth filled zeolite; zeolite were filled in the new designed housing of DW. Both surface of the housing were closed with 1mm thickness and 4mm diameter drilled iron plate. Circumference was closed with flat plate that has six caps for filling zeolite freely in the housing.

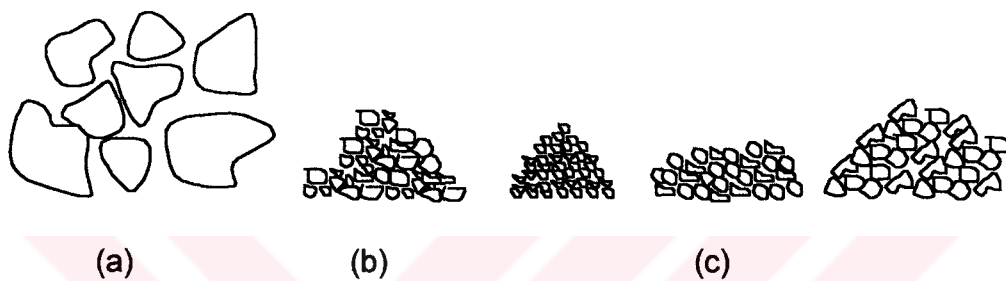


Figure 3.4 Preparation of the zeolite as desiccant

a) Raw Zeolite, b) Cracked Zeolite, c) Sieved Zeolite

The original design and construction of DW was modified according to the tests conducted for the operation of DCS. With the first design; the failure in the system operation was due to air-transfer between process and regeneration lines. The shape of desiccant bed was in the form of 4 sections in the original construction. However the desiccant bed was modified in the form of 12 equally shaped sections along the circumference as can be seen in Figure 3.5.d. The dimensions of DW were 110mm and 550mm inside and outside diameter respectively, with a thickness of (two zones such as; 100mm plus 150mm) 250mm. The designed and constructed DW was 100mm plus 150mm) 250mm. The designed and constructed DW was mounted in a housing made of iron profiles and sheets. The frame was constructed by using 0.8mm sheet iron separated into twelve sections of 30° each along the circumference. Therefore in the final construction of DW shape of the bed was 30° triangular sections with 250mm thickness in the

form of freely packed zeolites. A corrosion resistant 0.5mm aluminum sheet was used along the circumference to have a complete sealing. The rotor and air ducts connections were well fitted by means of rubber gaskets used. The detailed pictorial drawings of DW can be found in Figure 3.5.d.

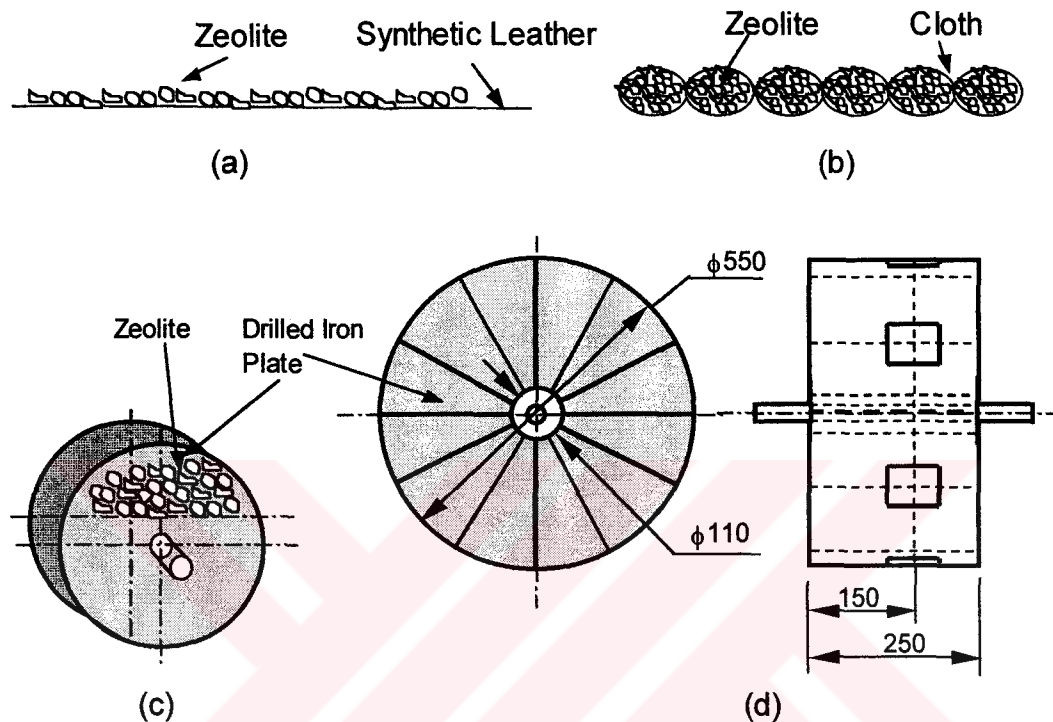


Figure 3.5 Development and modified of DW matrix material arrangement tried

- a) Zeolite glued to synthetic leather
- b) Zeolite filled to cloth sachet
- c) Metal housing has a four zone
- d) Metal housing with twelve zone and two thickness

### 3.2.2 ROTARY REGENERATOR

Rotary regenerator (RR) is the main part of the DCS. RR is used for transferring heat from exhaust air to fresh air, and visa-versa. RR's are highly compact heat transfer devices. The ratio of the heat transfer surface area to the total volume of the heat exchanger is defined as "heat transfer surface area density,  $\beta$ ". If  $\beta$  is greater than  $700\text{m}^2/\text{m}^3$  then that exchanger is called

“compact heat exchanger.” A disk type RR simply consist of the disk which contains undulated sheets with many small channels between them. These channels are called “matrix” and constitute heat transfer surface and flow passages. The rotor in which the matrix is packed is placed in a duct. The inlet and exit to the matrix is so arranged that hot and cold fluids flow parallel to the axis of rotation of the rotor and due to many parallel channels in the matrix fluid streams do not mix with each other and certain number of channels are exposed to the hot stream while the remaining channels are exposed to the cold stream. As the disk is slowly rotated the channels of the matrix is exposed to hot and cold gases alternately.

### **3.2.2.1 Design-Construction and Modification of RR**

In this study, likewise the design of DW; due to the need in DCS operation the original design and construction of RR was modified.

The RR was constructed of a light honeycomb structure made of copper foil sheets with a center hole to accommodate the rotating shaft. The rotor was mounted in a reinforced iron frame divided into two sections to accommodate the supply and exhaust ducts and was allowed to rotate via two bearings. The duct sectors of the wheel were well sealed by a rubber. The wheel was driven by a 0.25 kW gear motor via a belt arrangement. The rotor speed was variable in the range of 1-40 rpm by a speed control unit. The rotor was 500mm in diameter, with a 250mm max. length.

In general as a matrix material corrosion-resistant high thermal conductivity sheet are used. The thickness of the sheet should be as thin as possible for better heat transfer characteristics.

In this study, matrix material of the RR was Cu plate were whose thickness was 0.075mm with a special shape as shown in Figure 3.6. In the first construction of RR, Cu matrix materials were simply rounded around the shaft with dimensions of 48 and 560mm in the inner and outer diameters

respectively as can be seen in Figure 3.7.a. However due to the observed failure in DCS operation a modification was made with the arrangement of the Cu plates as shown in Figure 3.7.b. In both arrangements compactness of the matrix material which is defined as the heat transfer area to the volume of matrix  $\beta$  is approximately  $3600 \text{ m}^2/\text{m}^3$ . The housing and sealing RR was similar to that of DW discussed in the previous part.

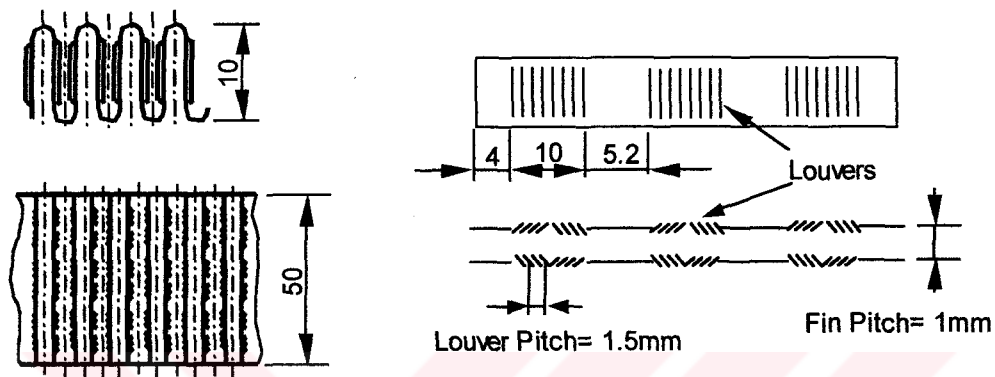


Figure 3.6 Special shape Cu plate RR matrix material

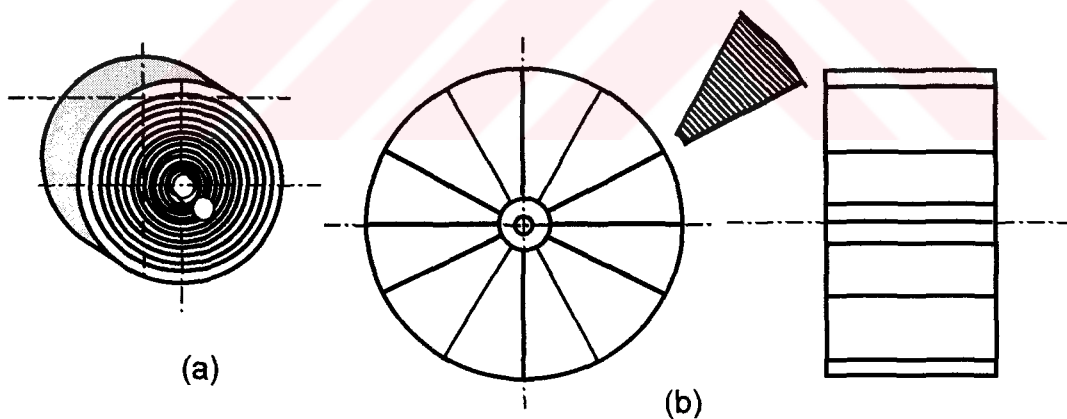


Figure 3.7 a) RR Cu matrix rounded on the shaft  
b) Modified RR matrix material housing

As a result of the tests in the operation of DCS; the RR circumference was divided into 12 sectors to avoid the mixing problem. The dimensions of the wheel are 110mm and 550mm inside, and outside diameters,

respectively. Axial divisions of the RR were 10 to 25cm with 5cm thickness. The original and modified RR are shown in Figure 3.7 respectively.

Furthermore the frames of the RR and DW were made of iron profiles and sheets. Connections were made by bolts, screw, and welding, that caused the RR and DW assembly and disassembly of the set-up quite practical. The frames of the housings were designed and constructed for balanced flow, the details of housings are given in Figure 3.8.

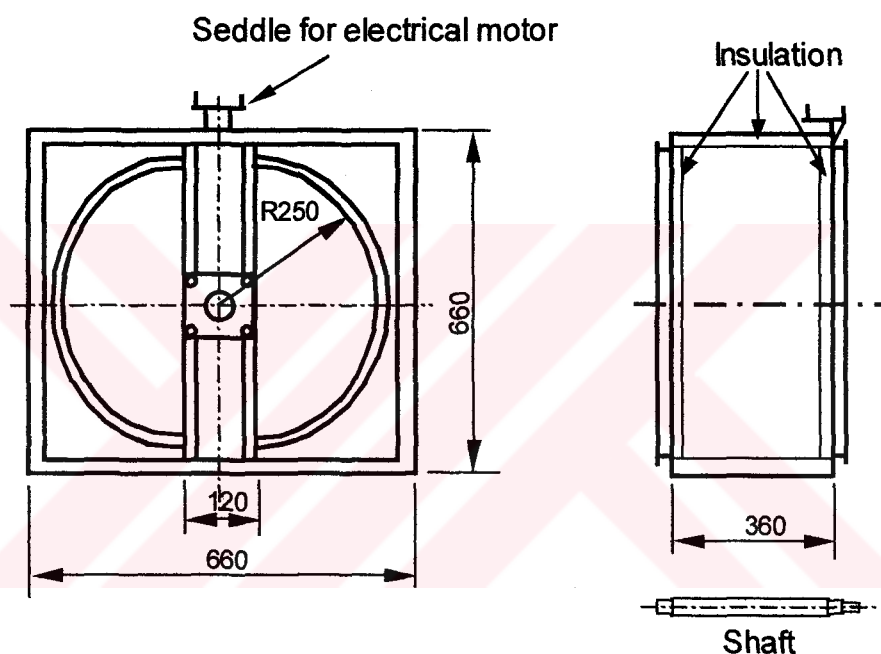


Figure 3.8 Balanced flow housing for RR and DW

### 3.2.3 EVAPORATIVE COOLERS

The primary component of a desiccant cooling system is the dehumidifier, but without evaporative cooler the system cannot be operated. The evaporative cooler acts as a cooler on the one hand to remove heat from the cooling water by evaporative cooling, whereas, on the other hand it is used to cool the air preliminarily with assistance of a heat exchanger.

Two EC's were used in this study. One was in collaboration with DW while the other one was used for transfer of sensible heat of water from exhaust air to fresh air through RR.

The designed evaporative coolers are shown in Figure 3.9. The primary parts of the EC are frame, sprayer, and filling material used for increasing contact area of water droplets and air stream. Secondary parts of the EC's are water storage tank, pump hose, valves, and fittings.

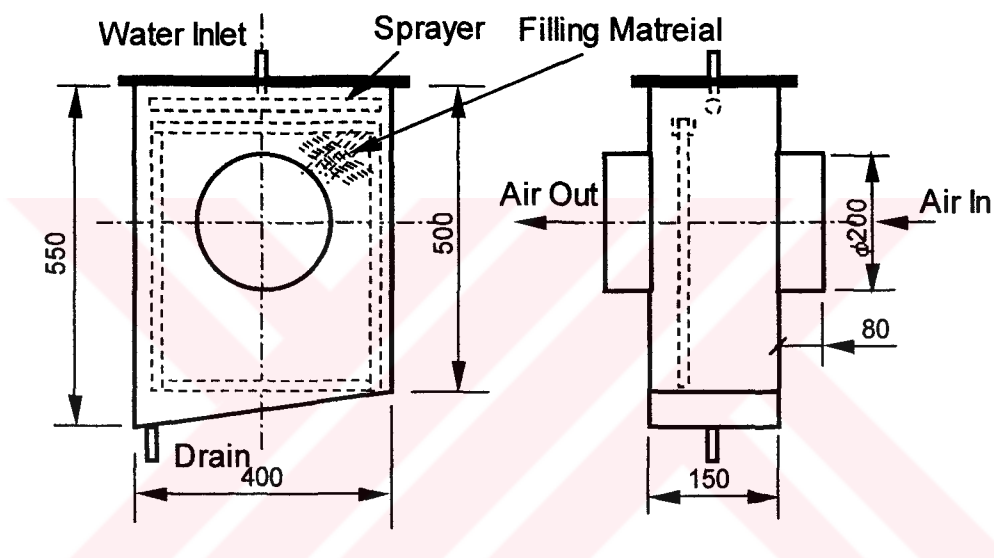


Figure 3.9 Evaporative Cooler and Filling Material

### 3.2.4 PIPE-LINE

A PVC tube of inner diameter  $D=200\text{mm}$  was used in the pipe system. The 200cm of the pipe downstream of the fan/wheel is called the entrance part, providing sufficient length to have a fully developed turbulent flow of exhaust/inlet air as 250cm. The test section along which the dry and wet bulb temperatures are taken has a length of 250cm from the inlet of any pipe, due to the analysis on hydrodynamic and thermal entry lengths. In laminar flow  $L_h$ ,  $L_t$  are given approximately as



$$L_{h,laminar} \approx 0.05ReD$$

$$L_{t,laminar} \approx 0.05RePrD$$

In turbulent flow, the hydrodynamic and thermal entry lengths are known to be independent of Re or Pr and are generally taken to be

$$L_{h,turbulent} \approx L_{t,turbulent} \approx 10D \quad \text{Çengel, in 1998 [159]}$$

### 3.2.5 PIPE-LINE TRANSITION ELEMENTS

There are two types of connection parts; one of them was for inlet of air to the RR and DW, the other was for the exit of air from the RR and DW. They were designed and produced with a galvanized steel plates with a thickness 0.5mm. Experiments show that, in straight-sided diffusers whose divergence exceeds the limiting angle, separation of the flow always occurs near the inlet. This is due to the pressure gradient along the diffuser. The best results were given by the form of diffuser, starting with a gentle curve and terminating in a straight-sided cone whose total angle should not exceed 35-40° Ower and Pankhurst, in 1966 [161].

In this study, two diffuser shape transition elements were designed and constructed. One of their sides was circular and 200mm in diameter, and other side was a semi-circle and 500mm in diameter. Divergence and convergence angles were taken as 23° and 40°, respectively as shown in Figure 3.10. The location of pressure tappings on transition elements can also be seen in Figure 3.10.

### 3.2.6 HEATERS

The regeneration compartment contained eight electrical heaters, each with 2.0kW of heating capacity. The construction of electrical heaters in

the form of compartments is shown in Figure 3.11. Each one of them has an electrical switch and one of them also has a variac to control the heat input to the regeneration air.

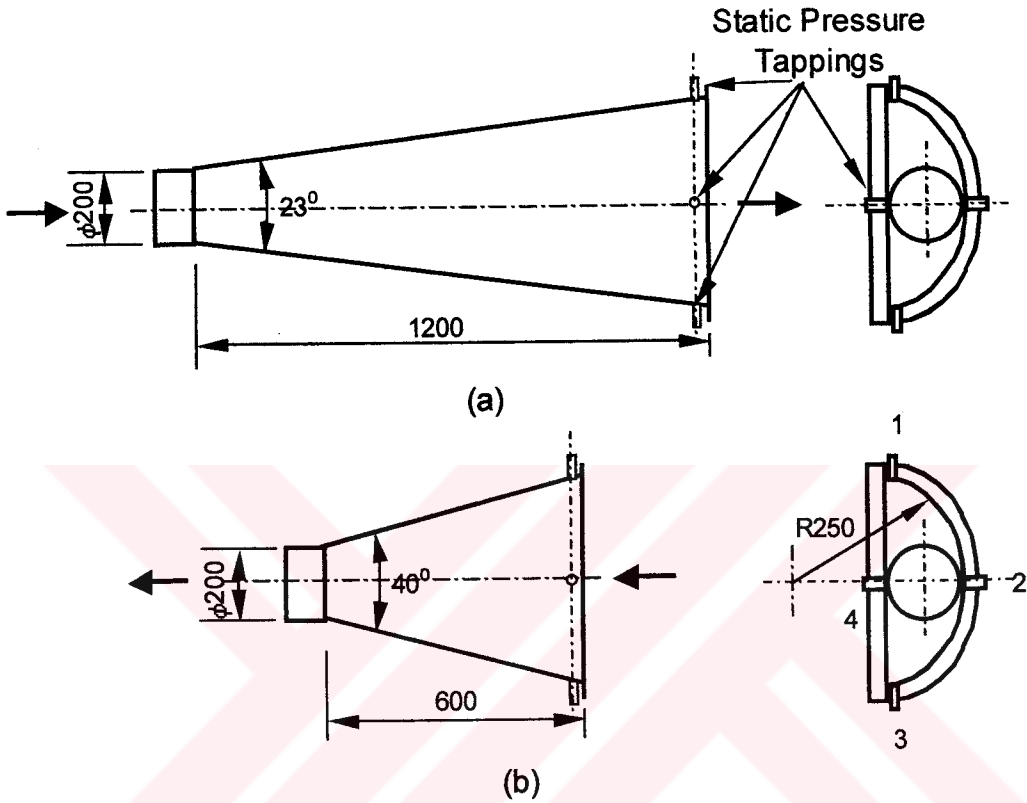


Figure 3.10 Pipe-Line Transition Elements a) For Inlet, b) For Outlet

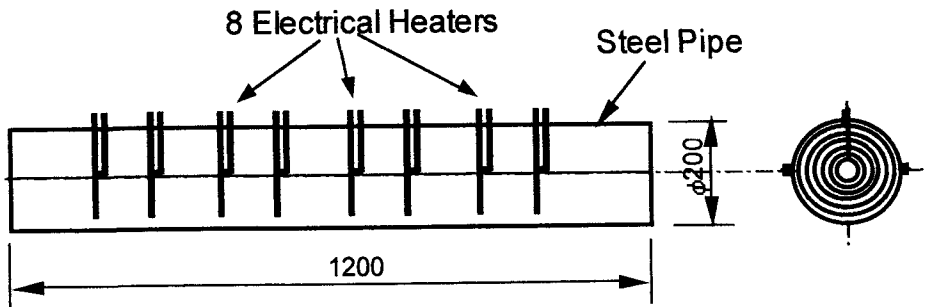


Figure 3.11 Electrical Heaters

### 3.2.7 CENTRIFUGAL FAN

Two centrifugal fans were used in the set-up. One for the process air and other for the regeneration air flows.

A horizontal shaft centrifugal fan is capable of delivering  $0.5\text{m}^3/\text{s}$  of air under a head of 150mmWC when running at 1380 rpm, was used in the set-up. It had an impeller 360mm outer and 140mm inner diameters respectively, having 12 backward curved blades. The fan was driven by 1.1 kW, 1380 rpm AC electric motor. Driving motor of the fan was controlled by an AC motor speed controller unit which controls the rotational speed of the motor by changing the frequency of the input voltage. The technical specifications of the drive unit of the fan consisted of a motor and a speed control unit are given in Appendix 1. The rotational speed of the motor could be changed safely from 0 to 1410 rpm via the motor speed control unit. Thus the air flow rate through the pipe could be controlled.

### 3.2.8 DRIVING COMPONENTS OF RR AND DW

In this system, RR and DW were rotated by an AC motor and gear box. The combination of the casing and the gear boxes was done by means of a belt and two pulleys. The process and regeneration airs were blown through the ducts and the components by fans which were driven by AC motors. Each one of these four AC motors was coupled with an AC motor speed controlled unit which controlled the rotational speed of the motor by changing the frequency of the input voltage. The technical specifications of the drive units of the RR and DW consisted of a motor and a speed control unit are given in Appendix 2 and Appendix 3.

### **3.2.9 SPEED CONTROL UNITS**

The MicroMaster and MidiMaster are a range of inverters with a voltage DC-link circuit for variable speed AC drives. Various models are available, ranging from the compact 250 W MicroMaster up to the 37 kW MidiMaster.

Both types of inverter are microprocessor-controlled. A special pulse-width modulation method with selectable pulse frequency permits extremely quiet motor operation. Complete inverter and motor protection is provided by various protective functions.

### **3.2.10 TEST SET-UP INSULATION MATERIALS**

For avoiding the heat transfer from surrounding to the air stream or visa versa pipes, transition parts and frame of the RR and DW were well insulated. Pipes and transition parts were insulated with a 6cm glass wool and covered with a cloth. The frames were insulated from inside with a suitable thickness 2, 3, and 4cm foam board.

## **3.3 MEASUREMENT METHODS AND UTILIZED DEVICES**

### **3.3.1 Temperature Measurement**

Dry and wet bulb temperatures  $T_{db}$  and  $T_{wb}$  of the air streams at 9 points shown in Figure 3.2 in the pipe line were measured by T-type thermocouples connected to the Hilton Data Logger.

Temperature measurement and control were the main part of the experiments. The easy way of the temperature measurement for PC application using DATA logging system and thermocouple in the form of temperature probes were employed.

### 3.3.1.1 Thermocouple Configuration

Thermocouples are pairs of wires, of dissimilar metals, connected to both ends. When two junctions are subjected to different temperatures, and electrical potential is set up between them, or if they carry a current from an external source, the two junctions will assume different temperatures. When one of the junctions is maintained at a fixed temperature, say that of melting ice the other junction may be used as thermometer, and the voltage curve is higher reliable and reproducible.

Any convenient size of wire may be used for thermocouples, but a good electrical contact at the junctions and good insulation of the rest of the wire are important. Insulations may be enamel, plastic, silk, or cotton for low temperatures and asbestos, glass, porcelain, or other refractory materials for high temperatures.

The temperature of the “hot junction” can be determined only by reference to cold junction of known temperature. A vacuum bottle filled with cracked ice and water is a good junction container, provided that there is enough ice. For noncopper couples, two cold junctions will be necessary if copper lead wires are desired. Although the ice point is the most common reference temperature, any constant temperature can be used, and for high temperature work the cold junctions are sometimes buried underground, deep enough so that the seasonal temperature change is negligible.

Another reference junction scheme uses an external source of controlled voltage instead of thermocouple sources. Mercury batteries or rectified alternating current is used with a bridge circuit and balanced so as to produce a voltage equivalent to that representing ice immersion of the original cold junction. Cold junction compensators may also be built into the indicating or recording instruments themselves. A technique is to provide software compensation in the data acquisition system. In this technique the temperature of the measurement junction(s) is (are) measured with a RTD or thermistor and compensation provided with a build in microprocessor. Direct

digital readout of temperature is then provided. With appropriate switching one use the same junction(s) for several types of thermocouples. Such compensation assumes a polynomial relation, and if the thermocouple wire and/or junctions do not conform to the NBS standard, then an error in measurement will result. To alleviate this difficulty, the wires and junctions may be calibrated against known standard and known temperature.

### **3.3.1.2 Dry Bulb Temperature Probe**

Dry bulb temperature measurement was done by a probe which was designed and constructed as shown in Figure 3.12. Probe material was a copper tube and a T type (Cu-Constantan) thermocouple was selected. It consisted of three parts; thermocouple, sensing part, and support. Glue and plastic tube were used as insulator and connector for these two parts. Hot junction thermocouple was soldered to the Cu tube probe. The probe dimensions were 3.2mm inside diameter, 4.6mm outside diameter, and 25mm length.

For calibration of the probe; dry-bulb temperature of the air stream was measured with a calibrated mercury thermometer and a digital thermometer. These measured values were compared with the value measured by the Hilton Data Logger. All of these three results were approximately same.

### **3.3.1.3 Wet Bulb Temperature Probe**

The probe designed for dry bulb temperature measurement was used for wet bulb temperature determination. However, the probe was covered with a 40mm cotton sleeving. Other end of the cotton sleeving was submerged into water to get wetness. For a thermocouple unit with wick feed a length of wick 0.5 to 1cm long, below the thermocouple junction, must be

exposed to the air flow to minimize errors due to heat conduction from the water reservoir and also to ensure the feeding of water to the sleeve at about wet bulb temperature Hickman, in 1970 [160]. Two small water containers which were connected by a Cu pipe that had 2.2mm outside and 1.1mm inside diameters with each others. Inside container was used for wetting the cotton sleeving, outside was used for adding make-up water. Detailed configurations was shown in Figure 3.12.

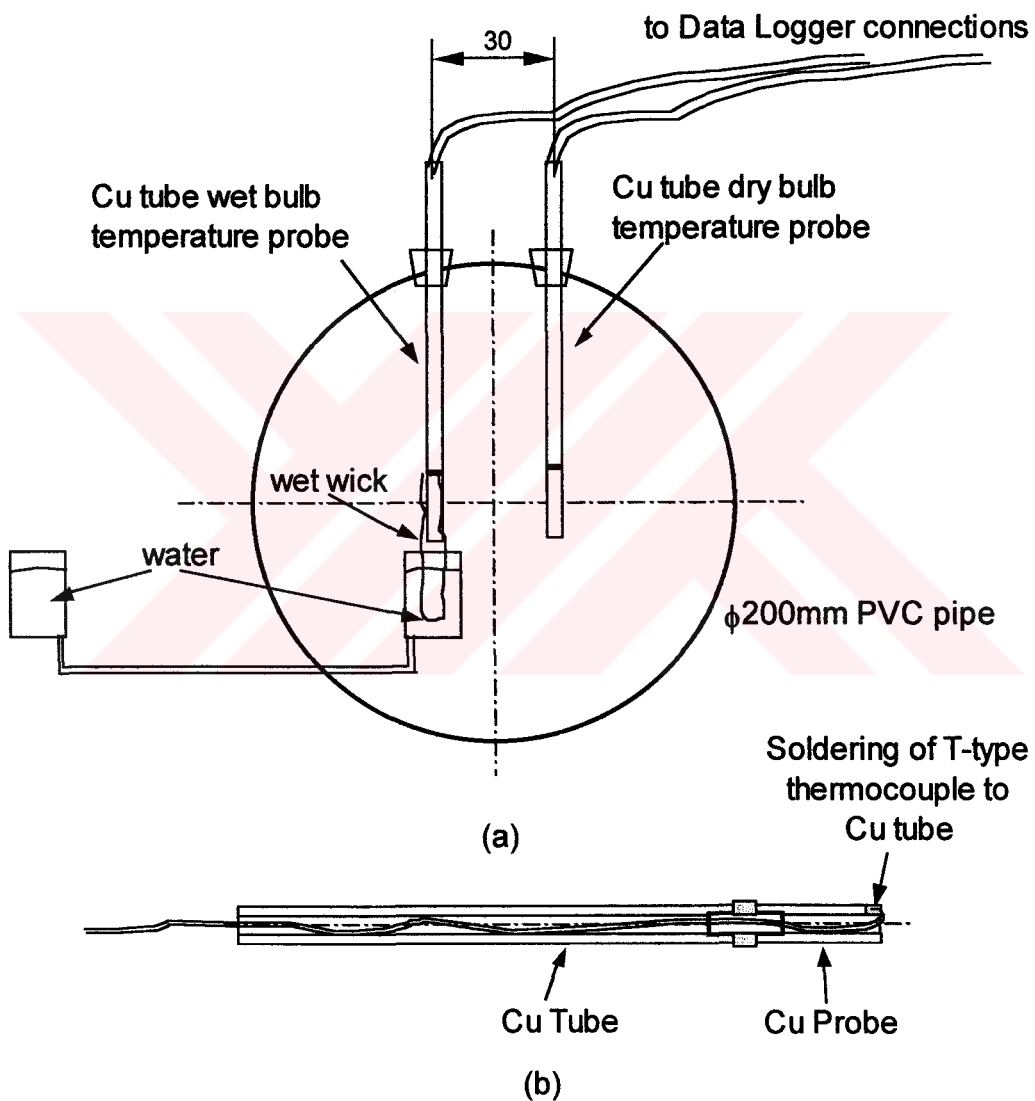


Figure 3.12 a) Location of dry and wet bulb temperature probes in the pipe  
b) Detail of the temperature probe

For calibration of the wet-bulb temperature probe; in the first trial; again a calibrated mercury thermometer and a digital thermometer were used. But, in this calibration bulb of the thermometer and junction of thermocouple of digital thermometer were covered with wet wicks. It showed that there was a big difference especially between wet-bulb temperature measured with mercury or digital thermometer and wet-bulb temperature measured by the Data Logger. Reason for this difference was due to high temperature and pressure inside the duct when the set-up started to run. So that, distance between bulb and water level could not stay constant such as 0.5-1.0cm as mentioned above. Also, wet bulb was effected with conduction of Cu tube due to high temperature.

In the second calibration trial; configuration was used according to ASHRAE standards on temperature measurement [177]. However, result of this wet-bulb temperature measurement was not good due to the high temperatures in most of the states in DCS operation.

Therefore, the solder was broken for the wet-bulb temperature probe. Cu tube was used only as a support for wet-bulb temperature measuring thermocouple. Junction of the thermocouple was freely covered with wick and submerged into the water. Pressure effect was also eliminated with the use of a multiplication coefficient for calibration of wet-bulb temperature probe readings to obtain accurate  $T_{wb}$  values.

For calibration of the probe; wet-bulb temperature of the air stream was measured with a calibrated mercury thermometer and a digital thermometer. These measured values were compared with the value measured by the Hilton Data Logger. All of these three results were approximately same with a maximum error of 11%.



### 3.3.2 Flow Rate Measurement

Process and regeneration air flow rates were measured by orifice plates. Inclined manometers were employed for the required pressure drop measurements.

#### 3.3.2.1 Orifice Plate; Design, Construction and Calibration

An orifice plate as shown in Figure 3.13 was designed, manufactured and calibrated.

The orifice plate, OP was selected for measuring the air flow rate. The pressure drop of the OP was minimized by choosing a large diameter ratio,  $\beta' = 0.7$ . Brass sheets having a thickness of 1mm was used as orifice plates. This thickness let to use square-edged orifice plate. The diameter of OP was 140mm for the pipe inside diameter 200mm. Brass orifice plate was fastened between two flanges with two rubber gaskets which had a thickness of 3mm. For inlet and exit pressure locations 1D and 1/2D were used for the pressure connections.

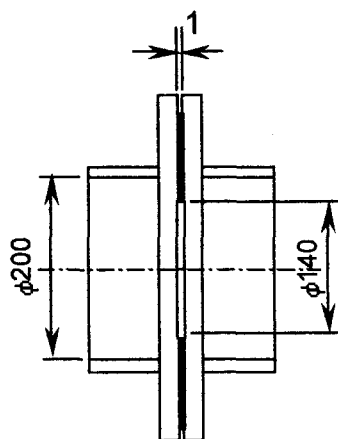


Figure 3.13 Orifice plate

For calibration of the orifice plate a calibration set-up was designed, constructed and the tests were done. The set-up is shown in Figure 3.14.a. It consists of a fan, OP, pitot tube, pitot tube traverse mechanism, U-tube, and inclined manometer. For driving mechanism an AC motor coupled with fan and for obtaining different flow rate an AC motor speed controller were used.

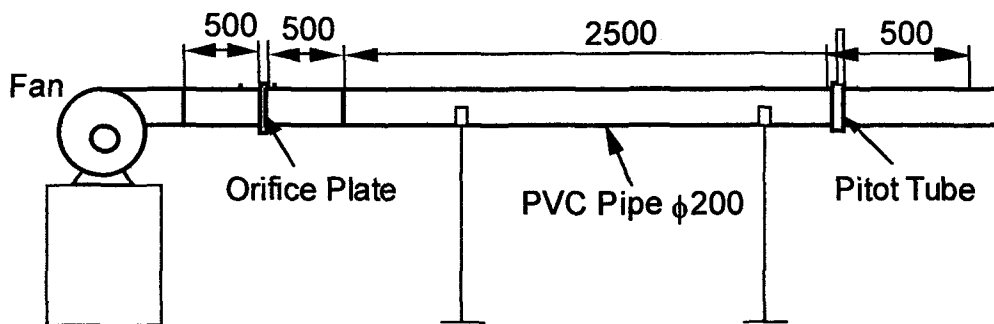


Figure 3.14 a) Set-up for calibration of the orifice plate

Tests were done for the frequency from 15 to 50Hz with an interval 5Hz to get different flow rates. When set-up run at a certain frequency, pressure drop at the OP was measured from U-tube manometer, and pressure drop at the pitot tube station was traversed and measured from radius,  $r=0$  to 100mm.

The details of flow velocity and flow direction measurement by using pressure probes have been described by Ower and Punkhurst, in 1966 [161]. An L shaped copper pitot tube of 2.2mm OD and 1.1mm ID located at 300cm upstream of the OP with a wall static pressure tapping were used to measure the mean velocity at the section. The pitot tube traversed across the pipe cross-section with an accuracy of  $\pm 0.025$ mm by means of a traverse mechanism to find the position of the pitot tube at which the mean velocity was measured. Since the average velocity is measured approximately at the same distance from the pipe wall for fully developed turbulent flows.

From the following derivation of the equations for  $U_{\text{mean}}$  was calculated for pitot tube;

$$\Delta P = \rho_{alc} g h' \sin \theta \quad (3.1)$$

where  $\theta$  is the inclination angle of the manometer

$$P = \frac{1}{2} \rho_{air} U_1^2 \quad (3.2)$$

$$\frac{1}{2} \rho_{air} U_1^2 = \rho_{alc} g h' \sin \theta \quad (3.3)$$

$$U_1 = \sqrt{\frac{\rho_{alc} g h' \sin \theta}{\frac{\rho_{air}}{2}}} \quad (3.4)$$

$$U_{mean} = \frac{1}{r} \sum_{r=0}^{r=r1} U_1 \quad (3.5)$$

For the same frequency pressure drop at the OP is converted to velocity.

Bernoulli equation is written for OP,

$$P_1 + \rho \frac{U_1^2}{2} = P_2 + \rho \frac{U_2^2}{2} \quad (3.6)$$

$$P_2 - P_1 = \frac{\rho}{2} (U_2^2 - U_1^2) \quad (3.7)$$

Continuity equation for OP,

$$Q = U_1 A_1 = U_2 A_2 \quad (3.8)$$

$$U_2 = \frac{U_1 A_1}{A_2} \quad (3.9)$$

$$\Delta P = \frac{\rho}{2} U_1^2 \left( \frac{A_1^2}{A_2^2} - 1 \right) \quad (3.10)$$

$$\Delta P = \rho_{alc} g h'_{alc} \quad (3.11)$$

$$U_1 = \sqrt{\frac{\rho_{alc} g h'_{alc}}{\frac{\rho_{air}}{2} \left( \frac{D^4}{d^4} - 1 \right)}} \quad (3.12)$$

$$U_{mean} = C_{OP} U_1 \quad (3.13)$$

By considering the ratio of  $U_{mean}$  and  $U_1$  a calibration coefficient for the OP was defined:

$$C_{OP} = U_{mean} / U_1 \quad (3.14)$$

$C_{OP}$  is the calibration coefficient for the designed, constructed, and used OP in the set-up. The average value of  $C_{OP}$  was found to be 0.568 for the covered Re (Figure 3.14.b).

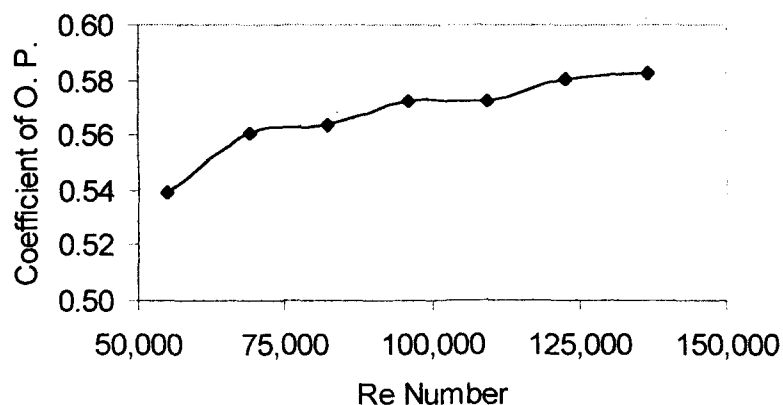


Figure 3.14 b) Calibration curve of the orifice plate

### 3.3.3 Pressure Drop Measurements

Pressure drops were measured between inlet and exit of RR and DW as seen in Figure 3.15.a. Pipes were connected with transition parts to the faces of RR and DW at their semi-circular ends. Pressure measured at 4 points at the inlet and exit of the wheels and their average were measured by an inclined alcohol manometer which were connected to static pressure taps located in the duct walls. Semi-circular side of the transition parts have straight face, circular face, and two narrow section as shown in Figure 3.10 and wheel rotates. As a result, average pressures should be measured by a specially designed and constructed parts as shown in Figure 3.15.b. It takes the average pressure from 4 points. Difference of the average pressure between inlet and exit of the wheel gives the pressure drop of the RR and DW.

The average pressure drops through the RR and DW were measured with inclined alcohol manometers (Figure 3.15.c).

### 3.3.4 Manometers

An inclined micro-manometer, the manometer fluid being alcohol, was used in collaboration with the pitot tube and orifice plate. The pressure measurement sensitivity was such that the pressures as low as 0.35 Pa could be measured.

The atmospheric pressure and the ambient temperature were measured during each experiment; because all experimental data was taken under varying atmospheric conditions. In order to avoid the effect of ambient temperature and atmospheric pressure changes on the manometer readings; all readings; were converted to the ones at standard temperature and pressure, STP. condition. Appendix 4 was used to correct the manometer readings to STP. condition.

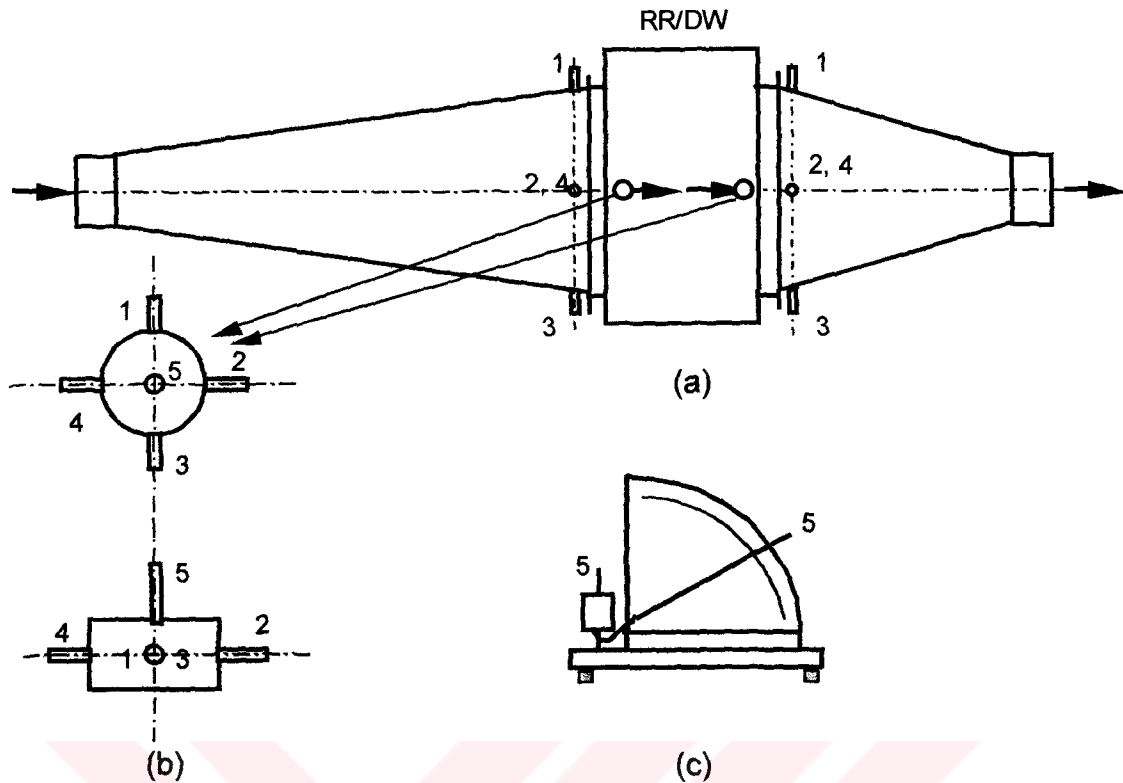


Figure 3.15 a) Pressure drop measurement

b) 4 point average pressure measuring device

c) Inclined manometer

### 3.3.5 Hilton Data Logger

The Hilton Data Logger is a microprocessor controlled computer interface that may be simply configured as a combined data logger and controller (Appendix 5). The unit is designed to be operated on a computer serial link responding to simple (ASCII) alphanumeric commands and returning numeric data.

Up to 7 interfaces may be operated on single RS232 serial link with each being identified by its own ident number.

The Hilton Computer Interface is a multi-channel analogue and digital unit with both input and output capability. Commands and data are

transferred via a 5 wire RS232 serial link using ASCII character strings sent and received by a controlling computer.

The controlling computer may be an IBM or IBM compatible running either the Hilton data logging software or any other software package designed to use the following command formats.

As the interface has its own on board computer or microprocessor and independent memory, it is possible to set up the system to return data from most standard transducers in the form required by the user or the user's software.

For example, if a particular pressure transducer has a range of 0-300 p.s.i., then data may be returned in either p.s.i. or any other set of units, such as Pascals, inches water gauge and so on.

Once all of the required channels have been set up to return data in the required format than the whole system configuration may be stored on computer disc. For use in different situations on different sets of transducers a library of these disc configurations may be built up by the user and loaded into the interface as required.

Up to 15 thermocouple inputs may be addressed and these connect to terminals labeled D1+D1-D2+D2-etc. Either type T or type K thermocouples may be used but not a mixture of both unless external cold junction compensation is used with additional software.

On High Gain the maximum readable input voltage corresponds to approximately 500C. On low Gain the corresponding maximum is approximately 1300C.

An isolated thermocouple is, for example measuring the temperature of a plastic coated surfaces or one that is fully isolated from ground. In this

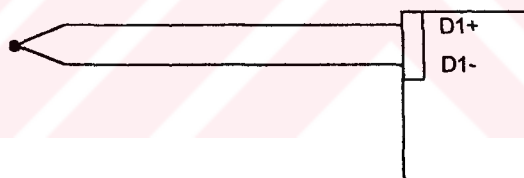
case switch associated with the thermocouple channel inside the case is pushed down.

In the case of a thermocouple connected, for example, to copper pipe work that is at some points connected to an earth that can be traced back to the interface, then the tip is effectively grounded. In this case the associated switch is pulled up.

For enhanced stability it is preferable to connect isolated thermocouples to channels 1-8.

Corresponding grounded thermocouples are best connected to channels 9-15.

However, in either case this is essential as all channels will give acceptable readings for normal purpose.

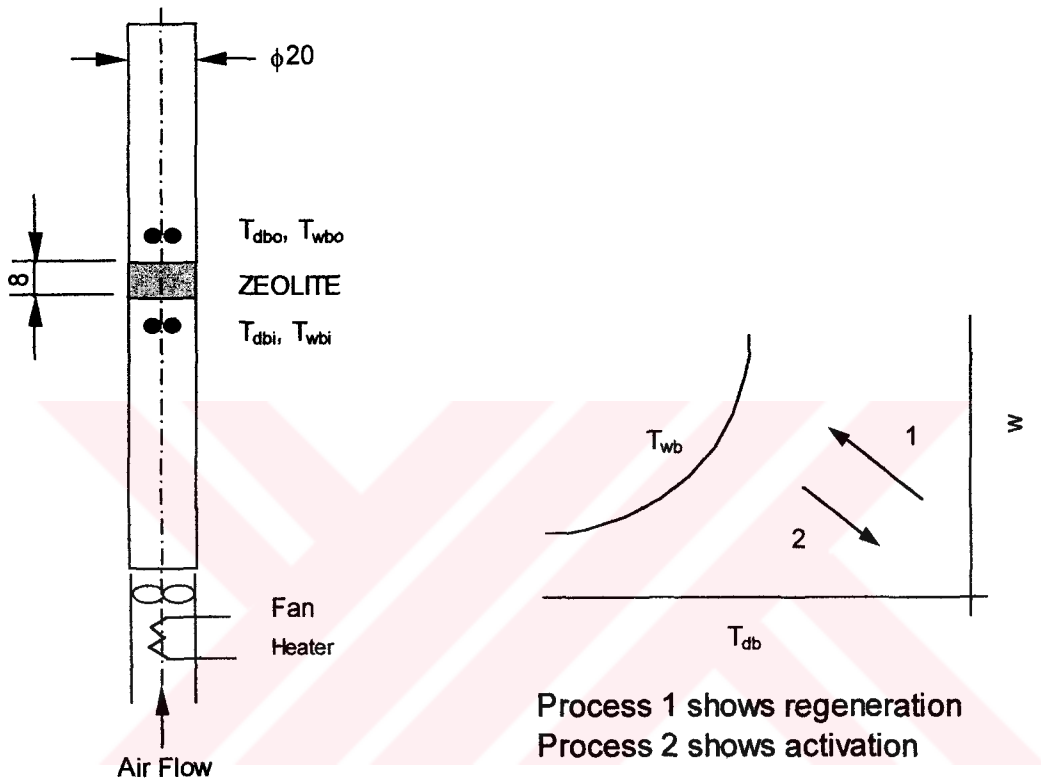


The Hilton Data Logger used in the study has its own cold junction compensator. An execute program called as TALK.EXE allows single channels to be accessed and updated rapidly, useful when testing the response of a new sensor. Talk is also used to calibrate the cold junction compensator which effect 15 temperature channels equally.

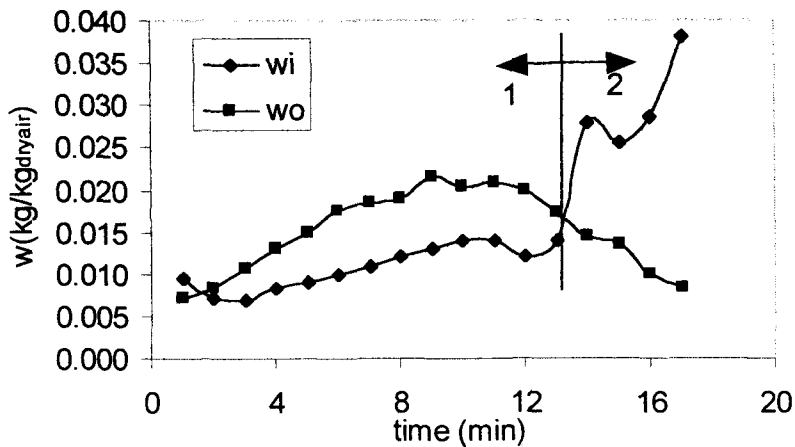


### 3.4 TEST OF ZEOLITE AS A DESICCANT

Two tests were made on zeolite to determine its basic characteristic in the cooling operation, in other words to determine its suitability as a desiccant.



a) Zeolite test set-up      b) Psychrometric representation of the processes



c) First Test Result on Zeolite  
(Variation of zeolite moisture content with/without heat wrt. time)

Figure 3.16

The first test was done for humidification and dehumidification of air by the Zeolite. For this test a small set-up was constructed with an electrical heater, an axial fan, 200mm diameter two pipes, and 80mm thick and 200mm diameter Zeolite section. The set-up was shown in Figure 3.16.a.

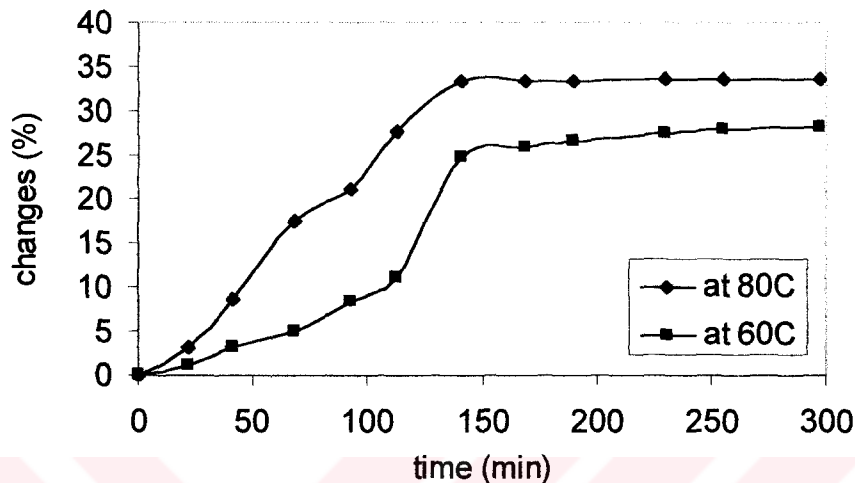


Figure 3.17 Second Test Result on Zeolite  
(Changes of "Zeolite Weight Loss" with time)

In the second test to define the moisture capacity and adsorption-desorption of the Zeolite approximately, 1500gr Zeolite was waited in water for 24 hours. Before, start to dry into a fixed temperature furnace, it was weighted. After start to dry, it was weighted for a time interval of 20 minutes. Drying was continued until when its mass was not changed with heating. Decrease in the mass shows the moisture content of the Zeolite. Test was repeated for 60C and 80C. The results are shown in Figures 3.16 and 3.17.

It is seen that selection of Zeolite is appropriate for the purpose in designed DCS. The selection of Zeolite as a desiccant for DCS was supported by graph in Figure 3.18. Because, adsorption capacity of the silica gel and natural zeolite are same at 20% relative humidity that is approximately equal to relative humidity of Gaziantep summer design condition as  $T_{db}=39C$  and  $T_{wb}=23C$ . For high relative humidity, mass of desiccant should be increased.

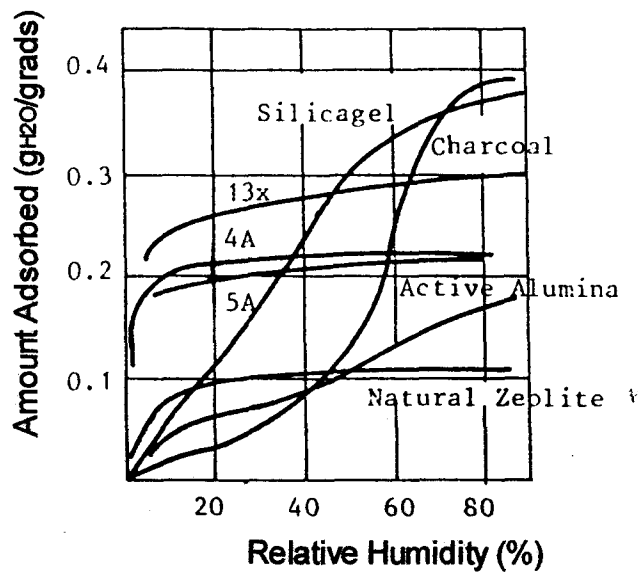


Figure 3.18 Adsorption isotherms for Adsorbent-water pairs[147]

### 3.5 CONCLUSION

In the operation of DCS moisture from process ambient air was removed by zeolite bed contained in the rotating DW. The perforated disk rotated horizontally between two chambers, one for adsorption and the other for desorption. Dehumidified ambient air was then sensibly cooled by a water cooled RR, made of Cu-plate matrix. The process air was finally evaporatively cooled through a wet pad 150mm thick and delivered to the conditioned space. The system contains two fans; one for the process air and the other for the regeneration air.

Exhaust air was blown through the EC, RR, auxiliary heater by the centrifugal fan and then drawn through the regeneration chamber of the DW, finally discharged to the atmosphere. The regeneration compartment contained an electrical heaters for auxiliary heating to the desired regeneration temperature. One of the heater output controlled by a switch, and variac, others with only switch.

Temperature at 9 different points of the system were (Figure 3.2) determined by Copper-Constantan thermocouples and Hilton Data Logger. Process and regeneration air flow rates were varied and controlled. The pressure drops through RR and DW were also measured.



## CHAPTER 4

### EXPERIMENTAL STUDY AND EVALUATION OF DATA

#### 4.1 INTRODUCTION

In the designed and constructed set-up, the influence of several system and operating parameters such as thickness of RR and DW, compactness of RR matrix material, size of zeolite, internal geometry of DW, sector angle of DW, DW rotational speed  $N_{DW}$ , RR rotational speed  $N_{RR}$ , regeneration temperature  $T_r$ , air flow rate  $m_a$ , can be controlled to determine the performance of DCS. Performance of DCS can be evaluated in terms of moisture removal capacity  $\Delta w$ , cooling capacity, CC, and coefficient of performance, COP of the DCS considered. There are in fact so many design parameters that influence the operation of a DCS that is difficult to quantify their impact and the interactions on system performance.

The purpose of this study is to investigate the impact of varying some of these operating parameters on the performance of DCS. The results will be used to improve the understanding of the operation of DCS and optimize the performance by changing certain operating and system parameters or improving the system components. In this chapter the experimental procedure and the calculations on the measured parameters are discussed.

## 4.2 EXPERIMENTAL PROCEDURE

### 4.2.1 Setting of Air Flow Rates in Process and Regeneration Lines

The following procedure was followed for setting the air flow rates:

First of all, the ambient pressure was measured by means of a mercury barometer, and ambient temperature was measured with an alcohol thermometer. This was necessary for recording the coefficient,  $c$ , for alcohol. Because, alcohol was used in the manometers to measure pressures. From the correction chart in Appendix 4, the  $c$  value is found corresponding to the measured ambient pressure and temperature. The alcohol height is reduced to STP conditions from the ratio;

$$h'_{alc} / (h'_{alc})_{STP} = c, \quad (4.1)$$

$$(h'_{alc})_{STP} = h'_{alc} / c \quad (4.2)$$

The alcohol height in the inclined manometer leg for a specific flow velocity was determined as follows:

As the blower unit is running at an unknown velocity, the alcohol level in the manometer had shows a value, but this is random. The required height is found with respect to the required velocity. The value read on the manometer-leg corresponds to the difference of total pressure and static pressure. Because, the pressure sensed by the pitot tube is sum of the static and dynamic pressure of the flow and this total pressure is applied on the reservoir of the manometer. The static pressure from the wall static pressure tapping is applied to the leg of the manometer. That is, the pressure from the pitot tube increasing the alcohol height while that from the tapping decreases the alcohol height in the manometer-leg. Thus, the resulting height of the alcohol is the difference between the total and static pressure. In other words, this height represents the dynamic pressure of the flow. So,

$$P_{\text{Total}} - P_{\text{Static}} = P_{\text{Dynamic}} \quad (4.3)$$

$$\Delta P = P_{\text{Dynamic}} \quad (4.4)$$

The dynamic pressure is also expressed by the relation;

$$P_{\text{Dynamic}} = \rho_a U^2 / 2 \quad (4.5)$$

Where, density of air,  $\rho_a$  is in  $\text{kg/m}^3$ , flow velocity  $U$  in  $\text{m/s}$  and pressure,  $P$  is in Pascal.

The difference between total and static pressure,  $\Delta P$  in the manometer-leg in terms of alcohol height,  $h'_{\text{alc}}$  is given by:

$$\Delta P = \rho_{\text{alc}} g h'_{\text{alc}} \quad (4.6)$$

Where,  $\rho_{\text{alc}}$  is the density of alcohol in  $\text{kg/m}^3$ . Taking into consideration manometer's inclination angle,  $\alpha$  and  $h'_{\text{alc}}$  from the Equation 4.4, following equation is obtained:

$$\Delta P = \rho_{\text{alc}} g (h'_{\text{alc}} / c) \sin \alpha \quad (4.7)$$

Substituting Equation 4.6 and 4.7 into Equation 4.5, following relation was obtained:

$$\rho_{\text{alc}} g (h'_{\text{alc}} / c) \sin \alpha = (\rho_a U^2 / 2) \quad (4.8)$$

It is seen that  $h'_{\text{alc}}$  can be evaluated from Equation 4.8, since all the parameters in this equations are known. Therefore, the required velocity together with the other parameters are inserted into Equation 4.8 and  $h'_{\text{alc}}$  can be calculated. Thus, the frequency of the blower's motor is regulated with

the speed control units (it is increased or decreased) until calculated alcohol height from Equation 4.8 is achieved.

#### 4.2.2 STEPS IN EXPERIMENT

During the experiments, before the measurements were taken certain steps were passed. Process and regeneration air fans were turned on. The electrical heaters were adjusted to the planned power. To give the right rotational speed of the RR and DW driven by electrical motors coupled with pulley and the belt system was adjusted by speed control unit. At an adjusted frequency the rotational speed of the RR and DW was measured by a digital tachometer. The temperature measuring system Hilton Data Logger was prepared. Pump of the EC was turned on. Make up water reservoir for the  $T_{wb}$  measurement was completed and checked for certain time intervals. The entire system was allowed to run around half an hour before the measurements were taken to provide steady-state operation of the DCS. The measurements were taken in 5 minutes intervals in an operation time of 15 minutes. The data corresponding to the steady state case were selected and used; as can be seen with sample output given in (Appendix 6). Once it was observed that the system was running under steady state measurements were taken.

##### **Detailed Description of the Steps:**

A) Before starting the experiment;

1. Define  $c$  from correction chart in Appendix 4 by reading  $T_{lab}$  and  $P_{lab}$  and multiply  $m_a$  by  $c$ . Find  $h_{alc}$  for the Orifice Plate.
2. Adjust  $m_a$  by changing frequency of fan's electrical motor with changing head of OP inclined manometer for both process and regeneration air mass flow rates equally.
3. Open the computer and the Data Logger



4. Give heat input by starting switch of electrical heaters and adjust variac to reach a suitable  $T_r$  that was temperature of experiment done.

After half an hour, set-up reached the steady-state condition for defined  $T_r$ , and  $m_a$ .

B) Then;

1. Set-up runs 15 minutes for each  $N_{RR}$  of four  $N_{RR}$ , at each  $N_{DW}$  of four  $N_{DW}$ .
2. When four values of  $N_{RR}$  were completed,  $N_{DW}$  was changed to the other value, and repeated step 1.
3. After tests were completed, for four different values of  $N_{RR}$  at each different values of four  $N_{DW}$ ,  $m_a$  changed to new value by changing the frequency.  $Q_{in}$  also was adjusted to heat the new  $m_a$ , to a temperature that is  $T_r$ . Repeat step 1 and 2.
4. For one of the four different  $T_r$ , steps from 1-3 were repeated.

The following data were taken for each case:

1. Temperature and pressure of the air inside measured with barometer.
2. Dry and wet bulb temperatures ( $T_{db}$  and  $T_{wb}$ ) of the outdoors (ambient) and indoors (laboratory) measured with a whirling hygrometer in two hours intervals.
3. At measurement points (7) on the set-up dry and wet bulb temperatures ( $T_{db}$  and  $T_{wb}$ ). (Three data sets were saved during 15 minutes at each 5 minutes, by the computer coupled with the Data Logger.)
4. Pressure loss  $\Delta P$  at the RR and DW.

### 4.3 EVALUATION OF MEASUREMENTS

$T_{db}$  and  $T_{wb}$  measurements at 7 stations were used to determine the corresponding moisture  $w$  and enthalpy  $h$  in reference to psychrometric chart given in Appendix 7. Referring to the related literature following parameters were calculated (Figure 4.1).

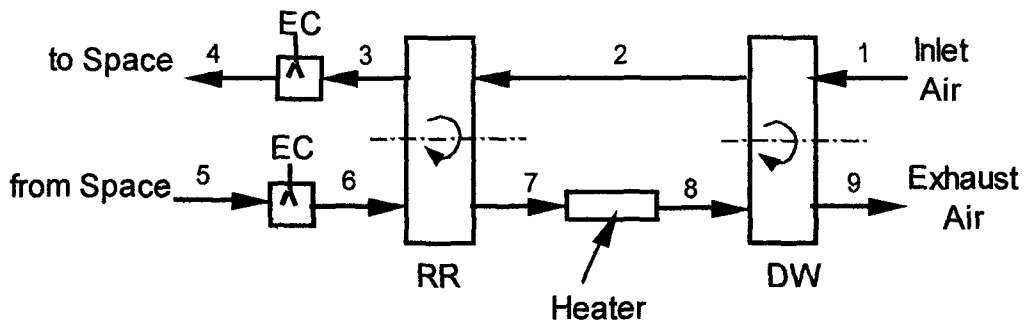


Figure 4.1 Schematic of the Open-Cycle DCS Tested

Moisture removal capacity which is an operating parameter for (DW) i.e. DCS

For the process side of DW;

$$\Delta w_p = w_1 - w_2 \quad (4.9)$$

For the regeneration side of DW;

$$\Delta w_r = w_8 - w_9 \quad (4.10)$$

Due to the nature of the experimental set-up heat transfer occurring in the system were analyzed in terms of sensible cooling capacity,  $CC_s$  and sensible coefficient of performance  $COP_s$ .

The sensible cooling capacity of the system is;

$$CC_s = m_{air}(h_5 - h_{4'}) \quad (4.11)$$

where  $h_{4'}$  is the enthalpy of point 4' which shows sensible cooling effect of the point 4 on psychrometric chart (Figure 4.2).

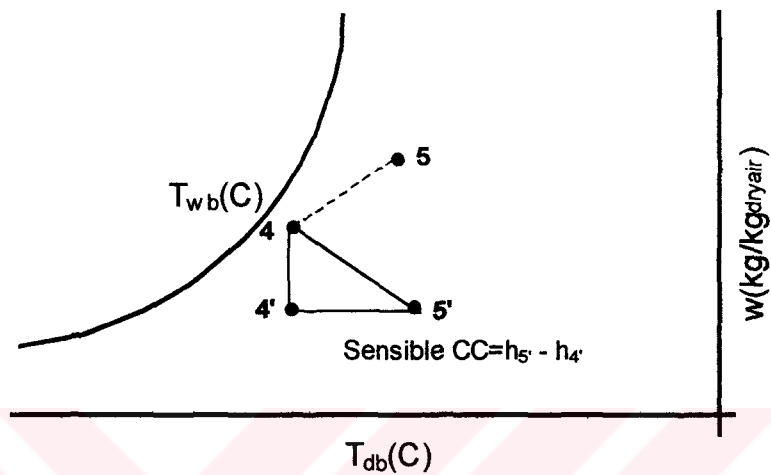


Figure 4.2 Sensible cooling capacity analysis of DCS

The heat input to the system for regeneration is;

$$Q_{in} = m_{air}(h_8 - h_7) \quad (4.12)$$

In ventilation mode;

$$(m_{air,R} \equiv m_{air,p} \equiv m_{air}) \quad (4.13)$$

So that the  $COP_s$  is;

$$COP_s = \frac{h_5 - h_{4'}}{h_8 - h_7} \quad (4.14)$$

Furthermore, in terms of effectiveness  $\epsilon$ ;

The effectiveness of the evaporative cooling process generally known as;

$$\varepsilon_{EC} = \frac{T_{cool} - T_{in}}{T_{wb} - T_{in}} \quad (4.15)$$

For the operation of the system designed (Figure 4.1);  $\varepsilon_{EC}$  is defined as;

$$\varepsilon_{EC} = \frac{T_{4db} - T_{3db}}{T_{3wb} - T_{3db}} \quad (4.16)$$

The effectiveness of RR,  $\varepsilon_{RR}$  generally known as:

$$\varepsilon_{RR} = \frac{C_h(T_{hi} - T_{ho})}{C_{min}(T_{hi} - T_{ci})} \quad (4.17)$$

where  $C = c_p m$ , and  $C_{min} = (C_h, C_c)$ ,  
but with  $C_h$  is equal to  $C_{min}$   $\varepsilon_{RR}$  is;

$$\varepsilon_{RR} = \frac{T_{hi} - T_{ho}}{T_{hi} - T_{ci}} \quad (4.18)$$

For the operation of system designed (Figure 4.1)  $\varepsilon_{RR}$  is defined as:

$$\varepsilon_{RR} = \frac{T_2 - T_3}{T_2 - T_6} = \frac{T_7 - T_6}{T_2 - T_6} \quad (4.19)$$

### Uncertainty Analysis of The Study

Any experimental result will involve some level of uncertainty that may originate from cause such as the lack of accuracy in measurement equipment, random variation in the measurands, and approximations in data

reduction relations. All these individual uncertainties eventually translate into uncertainty in the final results. Uncertainty analysis is performed during the design stage of an experiment to assist in the selection of measurement technique and devices. It is also performed after the data taking has been completed to demonstrate the validity of the results. Uncertainty analysis is also a useful tool for identification of corrective actions while validating and performing experiments.

The experimental data will provide industry and end users with independent performance evaluation and help researchers assess the energy savings potential of the technology. Accurate determination of humidity ratio is critical to this work and an understanding of the capabilities of the available instrumentation is central to its proper application. Historically, heating, ventilation and air conditioning (HVAC) test labs have measured wet-bulb, dry-bulb and pressure to use in evaluating humidity.

In most experiments it is possible for the experimenter to estimate the uncertainty,  $w'_x$ , of each of the measurands,  $x$ . These uncertainty estimates should include lack of precision in the experiments (precision error) and estimated maximum fixed error (bias error).

In the general case, consider the result,  $R$ , to be a function of  $n$  measured variables  $x_1, x_2, \dots, x_n$  as

$$R=f(x_1, x_2, \dots, x_n)$$

The uncertainty is given by

$$w'_R = \left[ \sum_{i=1}^n \left( w_{xi} \frac{\partial R}{\partial x_i} \right)^2 \right]^{1/2}$$

In this study the exact theoretical expressions for the CC, COP of the DCS and  $\Delta w, \varepsilon$ 's for RR and EC as a function of the operating parameters

are not known. Therefore based on the experiments following functional relationships can be proposed.

$$CC=f(m_a, T_r, N_{RR}, N_{DW})$$

$$COP=f(m_a, T_r, N_{RR}, N_{DW})$$

$$\Delta W =f(m_a, T_r, N_{RR}, N_{DW})$$

$$\varepsilon =f(m_a, T_r, N_{RR}, N_{DW})$$

However a theoretical study for the similarity analysis (Bunkinham's theorem) of these functional relationships was not carried out. Therefore, uncertainty effects of each components should be considered separately, as orifice plate, OP, Cu-constantan,  $T_{wb}$ , measurement technique, pressure, P, electrical power (for regeneration), Q, data logger, measurement of rotational speeds, N, speed control units and reading error of psychrometric chart on the performance of DCS can be mentioned. The measured dry-bulb and wet-bulb temperature values were under the effect of all other parameters.

Uncertainty of orifice plate, (or in  $m_a$ )

$$m_a = AU = AC \sqrt{\frac{\rho_a g h'_{alc}}{2 \left( \frac{D^4}{d^4} - 1 \right)}}$$

$C=0.568 \pm 0.0217$ , calibration coefficient for the OP,

$A=0.0314m^2 \pm 0.0004mm^2$ , flow area,

$d=0.14m \pm 0.02mm$ , OP diameter,

$D=0.2m \pm 0.02mm$ , pipe diameter,

$h'=10mm \pm 0.0000435mm$ , head of alcohol

Uncertainty of Cu-constantan for all db, and wb temperature measurements,

$$T=100C \pm 0.5C$$

Uncertainty of  $T_{wb}$  measurement is a function of correction factor of the  $T_{wb}$  measurement devices, its maximum value is 0.11.

Uncertainty of pressure measurement,

$$\Delta P=350Pa \pm 0.35Pa$$

Uncertainty of the Data Logger,

$$T=100C \pm 0.1C$$

Uncertainty of rotational speeds of RR and DW,

$$N=40rpm \pm 0.0005rpm \text{ (from used contact type digital tachometer catalogue)}$$

Uncertainty of speed control units;

It is clearly seen in its catalogue, they have not output error. They adjust the output frequency of the current with 0.0% error.

Uncertainty of reading of psychrometric chart. It can be divided in to two errors in moisture capacity, and in enthalpy readings.

$$w=0.01kg/kg_{dryair} \pm 0.118kg/kg_{dryair}$$

$$h=120kJ/kg_{dryair} \pm 0.0193kJ/kg_{dryair}$$

It can be clearly seen in the above uncertainty analysis CC, COP,  $\Delta w$ , and  $\epsilon$ 's of the system are affected with all of the above uncertainties coming from measurements and calculations.

#### 4.4 CONCLUSION

In this study, selected operating parameters which affect the CC and COP of the DCS were 3 constant 4 variable parameters are given in Table 4.1. The variables in the covered test cases are given in Table 4.2. The first tests were done with the certain system parameters such as compactness, thickness of the RR and the DW and zeolite size staying constant ( $\Delta X_{RR}$ ,  $\Delta X_{DW}$  and size of zeolite). Variable parameters were rotational speed of the RR and the DW, flow rate of air (process and regeneration air flow rate were taken to be same), and the regeneration temperature  $T_r$ . The performance of these test cases are given in Chapter 5.

Table 4.1 System Description

DCS:		
	Operation Mode	: Open-Cycle (ventilation)
DW:		
	Desiccant Type	: Solid Desiccant
	Matrix Material	: Natural Zeolite (Clinoptilolite)
	Matrix Density	: 800kg/m <sup>3</sup>
	Mass of Desiccant	: 19kg
	Total Frontal Area	: 0.068m <sup>2</sup> for process
		: 0.068m <sup>2</sup> for regeneration
	Matrix Dept.	: 0.1m
	Adsorption/Regeneration	: Balanced flow and balanced area
	Heat of Sorption	: 2.700kJ/kg <sub>H<sub>2</sub>O</sub>
	Dehumidifier Operation Mode	: Adiabatic
RR:		
	Matrix Materail	: Louvered Copper Sheet
	Fin Thickness	: 0.07mm
	Density of Matrix Material	: 878kg/m <sup>3</sup>
	Mass of Matrix Material	: 25kg



Table 4.2 Operating Parameters of the DCS

$\Delta X_{RR}(\text{cm})$	$d_z(\text{mm})$	$\Delta X_{DW}(\text{cm})$	$T_r(^{\circ}\text{C})$	$m(\text{kg/s})$	$N_{DW}(\text{rpm})$	$N_{RR}(\text{rpm})$
10*	6	10*	60	0.056	0.1	5
15	10*	15**	70	0.083	0.2	10
20	20**	25	80	0.111	0.3	15
			90	0.139	0.4	20

\* shows tested sizes

Table 4.3 Ranges of the variables in the conducted experimental study

$\Delta X_{RR}(\text{cm})$	$d_z(\text{mm})$	$\Delta X_{DW}(\text{cm})$	$T_r(^{\circ}\text{C})$	$m(\text{kg/s})$	$N_{DW}(\text{rpm})$	$N_{RR}(\text{rpm})$
10	10	10	60	0.056	0.1	5, 10, 15, 20
10	10	10	60	0.056	0.2	5, 10, 15, 20
10	10	10	60	0.056	0.3	5, 10, 15, 20
10	10	10	60	0.056	0.4	5, 10, 15, 20
10	10	10	60	0.084	0.1	5, 10, 15, 20
10	10	10	60	0.084	0.2	5, 10, 15, 20
10	10	10	60	0.084	0.3	5, 10, 15, 20
10	10	10	60	0.084	0.4	5, 10, 15, 20
10	10	10	60	0.111	0.1	5, 10, 15, 20
10	10	10	60	0.111	0.2	5, 10, 15, 20
10	10	10	60	0.111	0.3	5, 10, 15, 20
10	10	10	60	0.111	0.4	5, 10, 15, 20
10	10	10	60	0.139	0.1	5, 10, 15, 20
10	10	10	60	0.139	0.2	5, 10, 15, 20
10	10	10	60	0.139	0.3	5, 10, 15, 20
10	10	10	60	0.139	0.4	5, 10, 15, 20
10	10	10	70	0.056	0.1	5, 10, 15, 20
10	10	10	70	0.056	0.2	5, 10, 15, 20
10	10	10	70	0.056	0.3	5, 10, 15, 20
10	10	10	70	0.056	0.4	5, 10, 15, 20
10	10	10	70	0.084	0.1	5, 10, 15, 20
10	10	10	70	0.084	0.2	5, 10, 15, 20
10	10	10	70	0.084	0.3	5, 10, 15, 20
10	10	10	70	0.084	0.4	5, 10, 15, 20
10	10	10	70	0.111	0.1	5, 10, 15, 20
10	10	10	70	0.111	0.2	5, 10, 15, 20
10	10	10	70	0.111	0.3	5, 10, 15, 20
10	10	10	70	0.111	0.4	5, 10, 15, 20
10	10	10	70	0.139	0.1	5, 10, 15, 20
10	10	10	70	0.139	0.2	5, 10, 15, 20
10	10	10	70	0.139	0.3	5, 10, 15, 20
10	10	10	70	0.139	0.4	5, 10, 15, 20

Table 4.3 Ranges of the variables in the conducted experimental study (contd.)

$\Delta X_{RR}(\text{cm})$	$d_z(\text{mm})$	$\Delta X_{DW}(\text{cm})$	$T_r(^{\circ}\text{C})$	$m(\text{kg/s})$	$N_{DW}(\text{rph})$	$N_{RR}(\text{rpm})$
10	10	10	80	0.056	0.1	5, 10, 15, 20
10	10	10	80	0.056	0.2	5, 10, 15, 20
10	10	10	80	0.056	0.3	5, 10, 15, 20
10	10	10	80	0.056	0.4	5, 10, 15, 20
10	10	10	80	0.084	0.1	5, 10, 15, 20
10	10	10	80	0.084	0.2	5, 10, 15, 20
10	10	10	80	0.084	0.3	5, 10, 15, 20
10	10	10	80	0.084	0.4	5, 10, 15, 20
10	10	10	80	0.111	0.1	5, 10, 15, 20
10	10	10	80	0.111	0.2	5, 10, 15, 20
10	10	10	80	0.111	0.3	5, 10, 15, 20
10	10	10	80	0.111	0.4	5, 10, 15, 20
10	10	10	80	0.139	0.1	5, 10, 15, 20
10	10	10	80	0.139	0.2	5, 10, 15, 20
10	10	10	80	0.139	0.3	5, 10, 15, 20
10	10	10	80	0.139	0.4	5, 10, 15, 20
10	10	10	90	0.056	0.1	5, 10, 15, 20
10	10	10	90	0.056	0.2	5, 10, 15, 20
10	10	10	90	0.056	0.3	5, 10, 15, 20
10	10	10	90	0.056	0.4	5, 10, 15, 20
10	10	10	90	0.084	0.1	5, 10, 15, 20
10	10	10	90	0.084	0.2	5, 10, 15, 20
10	10	10	90	0.084	0.3	5, 10, 15, 20
10	10	10	90	0.084	0.4	5, 10, 15, 20
10	10	10	90	0.111	0.1	5, 10, 15, 20
10	10	10	90	0.111	0.2	5, 10, 15, 20
10	10	10	90	0.111	0.3	5, 10, 15, 20
10	10	10	90	0.111	0.4	5, 10, 15, 20
10	10	10	90	0.139	0.1	5, 10, 15, 20
10	10	10	90	0.139	0.2	5, 10, 15, 20
10	10	10	90	0.139	0.3	5, 10, 15, 20
10	10	10	90	0.139	0.4	5, 10, 15, 20

In the second part of the study one different zeolite size and one different desiccant wheel thickness were tested 20mm and 15cm respectively to determine their effects on the performance of the DCS.

For testing the  $d_z$  and  $\Delta X_{DW}$ , instead of covering all of the operating parameters, experiments were done for the selected constant design and

operating parameters. That means one of the four operating parameters was changed in the previously selected range, remaining three of them stays constant as shown in Table 4.4. The detailed variation of the operating parameters are given in Tables 4.5, and 4.6.

Table 4.4 Ranges of the variables in the conducted experimental study for testing  $\Delta X_{DW}$  and  $d_z$

$\Delta X_{RR}(\text{cm})$	$d_z(\text{mm})$	$\Delta X_{DW}(\text{cm})$	$T_r(^{\circ}\text{C})$	$m(\text{kg/s})$	$N_{DW}(\text{rpm})$	$N_{RR}(\text{rpm})$
10	20	10	60*	0.056	0.1*	5*
		15	70	0.083	0.2	10
			80	0.111*	0.3	15
			90	0.139	0.4	20

\* shows the constant operating parameters

Table 4.5 Ranges of the variables in the conducted experimental study for testing  $\Delta X_{DW}=10\text{cm}$  and  $d_z=20\text{mm}$

$\Delta X_{RR}(\text{cm})$	$d_z(\text{mm})$	$\Delta X_{DW}(\text{cm})$	$T_r(^{\circ}\text{C})$	$m(\text{kg/s})$	$N_{DW}(\text{rpm})$	$N_{RR}(\text{rpm})$
10	20	10	60	0.111	0.1	5
			70			
			80			
			90			
10	20	10	60	0.056	0.1	5
				0.083		
				0.111*		
				0.139		
10	20	10	60	0.111*	0.1	5
					0.2	
					0.3	
					0.4	
10	20	10	60	0.111*	0.1	5
						10
						15
						20

Table 4.6 Ranges of the variables in the conducted experimental study for testing  $\Delta X_{DW}=15\text{cm}$  and  $d_z=20\text{mm}$

$\Delta X_{RR}(\text{cm})$	$d_z(\text{mm})$	$\Delta X_{DW}(\text{cm})$	$T_r(^{\circ}\text{C})$	$m(\text{kg/s})$	$N_{DW}(\text{rpm})$	$N_{RR}(\text{rpm})$
10	20	15	60	0.111	0.1	5
			70			
			80			
			90			
10	20	15	60	0.056	0.1	5
				0.083		
				0.111*		
				0.139		
10	20	15	60	0.111*	0.1	5
					0.2	
					0.3	
					0.4	
10	20	15	60	0.111*	0.1	5
						10
						15
						20

For comparison of the results of these two different  $d_z$  and  $\Delta X_{DW}$ , with the previous, data which were obtained under the same operating conditions were selected.

The experimental study was composed of three sets of test cases. One of them composed of 256 tests with  $\Delta X_{DW}=10\text{cm}$ ,  $d_z=10\text{mm}$  to investigate the effects of operating parameters in the selected ranges on the performance of the DCS. Second one was composed of 16 tests with  $\Delta X_{DW}=10\text{cm}$ ,  $d_z=20\text{mm}$  to investigate the effects of particle size of zeolite,  $d_z$ , and third one was also composed of 16 tests with  $\Delta X_{DW}=15\text{cm}$ ,  $d_z=20\text{mm}$  to investigate the effects of DW thickness,  $\Delta X_{DW}$ , on the performance of the DCS with the selected constant operating parameters.

## CHAPTER 5

### PERFORMANCE OF DCS IN TERMS OF OPERATING PARAMETERS FOR SELECTED SYSTEM CONSTRAINTS

#### 5.1 INTRODUCTION

An experimental study was conducted in the DCS with the system constraints: thickness of RR;  $\Delta X_{RR}=10\text{cm}$ , thickness of DW;  $\Delta X_{DW}=10\text{cm}$  and  $15\text{cm}$  with the particle size of zeolite,  $d_z$ ;  $10\text{mm}$  and  $20\text{mm}$  on average, with a variety of operating parameters.

In this chapter; evaluated data were expressed in terms of graphs related to the processes occurring in the system operation. Psychrometric charts were drawn and the parameters  $CC_s$ ,  $COP_s$ ,  $\Delta W_p$ ,  $\Delta W_r$ ,  $\epsilon_{EC}$  and  $\epsilon_{RR}$  defined in the previous chapter were given as their dependence with particularly  $N_{RR}$ , and  $N_{DW}$  at different mass flow rates  $m_a$ , and regeneration temperatures  $T_r$ . The covered range of the operating parameters aimed to minimized the energy input of the DCS.

First of all, experimental and predicted processes of DCS are represented based on selected sample test cases in terms of psychrometric charts. Effects of  $N_{RR}$ ,  $N_{DW}$ ,  $T_r$ , and  $m_a$  on  $CC_s$ ,  $COP_s$ ,  $\Delta W_p$ ,  $\Delta W_r$ ,  $\epsilon_{EC}$  and  $\epsilon_{RR}$  for all of the experiments conducted are analyzed later.

## 5.2 ANALYSIS OF THE DCS-OPERATION THROUGH PSYCHROMETRIC CHARTS

Predicted (i.e. theoretical) behavior of DCS is illustrated in Figure 5.1. As shown in Figure 5.3.a-h based on experimental study conducted some selected sample processes were drawn on psychrometric charts. Test results indicated a deviation from the predicted processes-regeneration lines in psychrometric chart.

The reasons for this deviation are suggested to be as follows;

1. Approximately 10% of process and regeneration air flow streams were mixed through the sealing influenced by pressure differences in DW and RR. This phenomena was checked by running one of the air flow fans.
2. For different air flow rates, pressure effects are different on the wet-bulb temperature measurements. It was previously mentioned that due to these pressure effects there were differences between the actual and measured  $T_{wb}$ . However, multiplication factors were used for correction of wet bulb temperatures. But due to the need of this correction in  $T_{wb}$  the realized psychrometric chart representation have shown a deviation from the predicted/theoretical one.
3. One of the most important point for the test set-up is the absence of air-conditioned space that coupled with the set-up satisfying the state 4 to 5 . Therefore instead of state 4 state 4' was resulted.
4. As shown in psychrometric representation of DCS processes, from state 2 to state 3 moisture removal capacity of process air increases due to (the condensation/evaporation of moisture in

regeneration air at state 6) mass transfer from regeneration air to process air at RR for especially the case with  $T_r > 60\text{C}$ .

5. Reason for the deviation between predicted and obtained behavior of process from state 7 to 8 is due to the condensation of moisture of regeneration air. The condensation occurs due to high pressure and low wall temperature of long pipe lines between 7-8 states.

As can be seen from the behavior of process-regeneration lines in psychrometric charts;  $T_r$  seems to be dominant parameter effecting the operation in comparison to  $N_{RR}$ ,  $N_{DW}$ ,  $m_a$ . However the realization of the process-regeneration lines seems to be under the interactive influence of  $N_{RR}$ ,  $N_{DW}$ ,  $m_a$ . The matching of the process line in Figure 5.3.a, and b to the theoretical one imply the significance of the parameters  $T_r=60\text{C}$ ,  $N_{RR}=10\text{rpm}$ ,  $N_{DW}=0.2\text{rpm}$ ,  $m_a=0.056\text{kg/s}$  and  $T_r=60\text{C}$ ,  $N_{RR}=5\text{rpm}$ ,  $N_{DW}=0.1\text{rpm}$ ,  $m_a=0.083\text{kg/s}$ .

The matching of the regeneration line in Figure 5.3.c, and d approaches to the theoretical ones with the parameters  $T_r=70\text{C}$ ,  $N_{RR}=15\text{rpm}$ ,  $N_{DW}=0.1\text{rpm}$ ,  $m_a=0.111\text{kg/s}$  and  $T_r=70\text{C}$ ,  $N_{RR}=10\text{rpm}$ ,  $N_{DW}=0.1\text{rpm}$ ,  $m_a=0.139\text{kg/s}$ .

In predicted the theoretical operation of DCS process and regeneration lines exhibit parallel behavior (Figure 5.1). However in the experimental study there existed discrepancies from the theoretical operation. The dependency of the system operation on operating parameters is clearly observed. (Figures 5.3.a through 5.3.h) The system operation seems to be continuous since the matching of process and regeneration lines in a complete cycles, particularly for the cases given in Figure 5.3.c, d, f, g, and h. The slope of the separate parts in both process and regeneration lines seem to be under the severe influence of  $T_r$ ; as  $T_r$  increases slopes have shown increases. However there seems to discuss on this deduction more in later times to result in exactly.

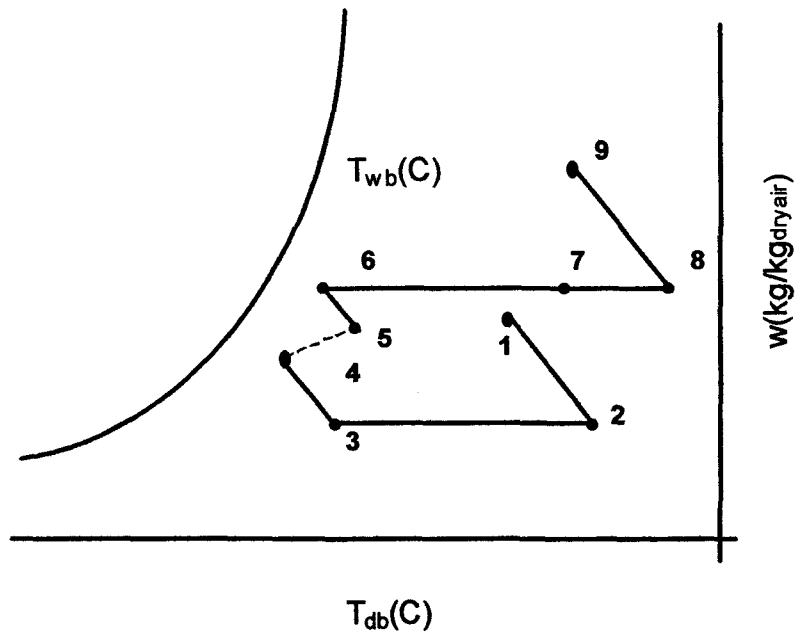


Figure 5.1 Predicted Psychrometric representation of DCS processes

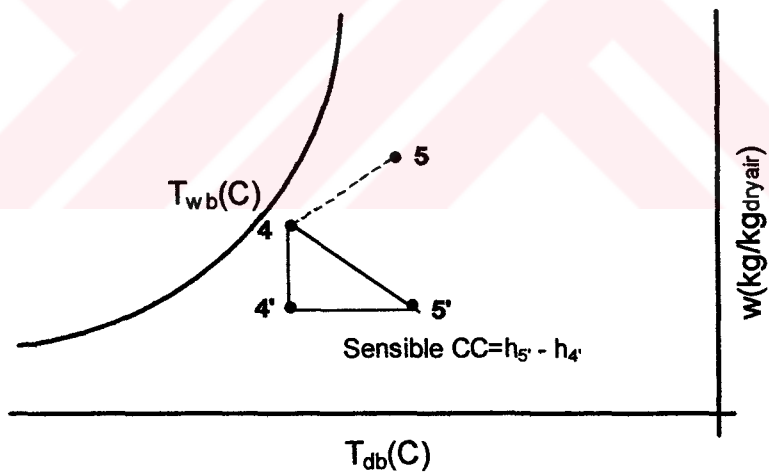
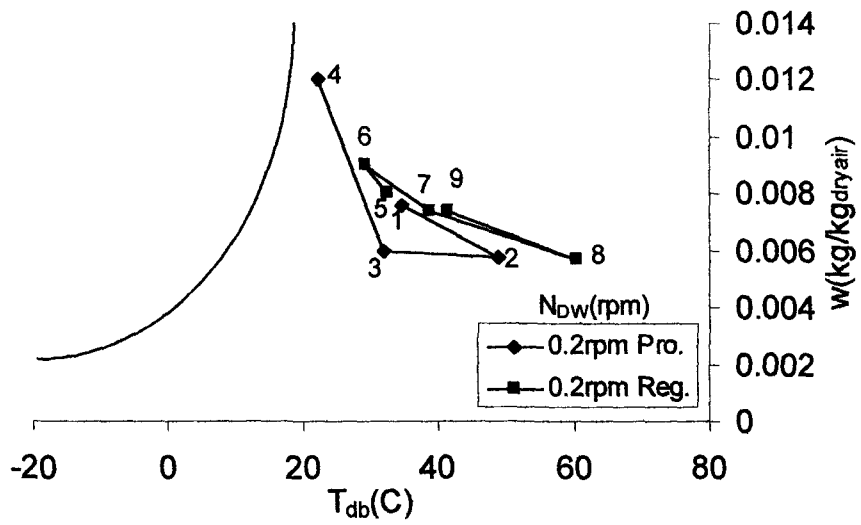
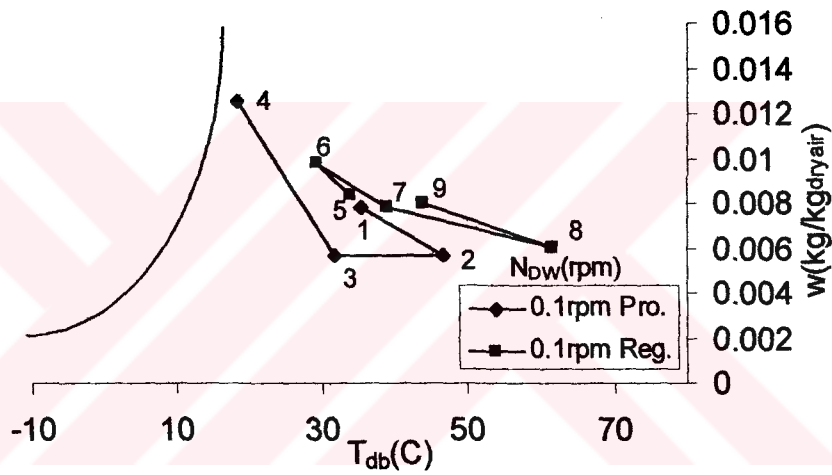


Figure 5.2 Sensible cooling capacity analysis of DCS

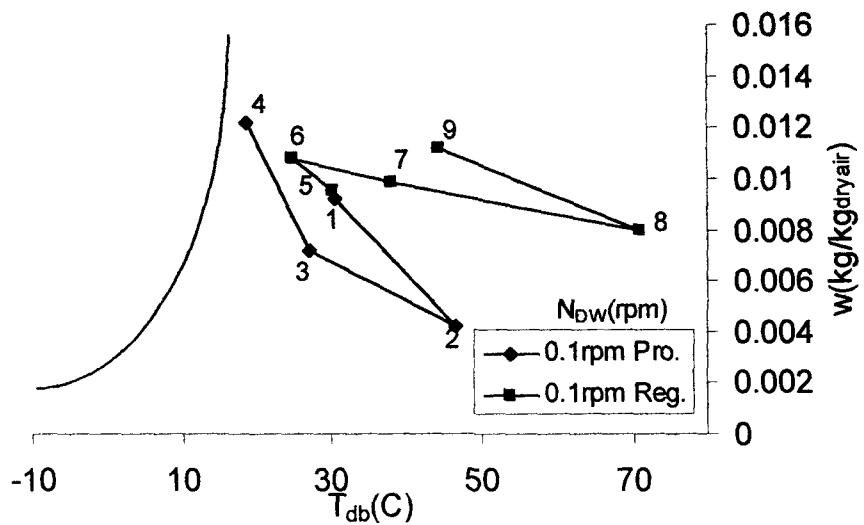




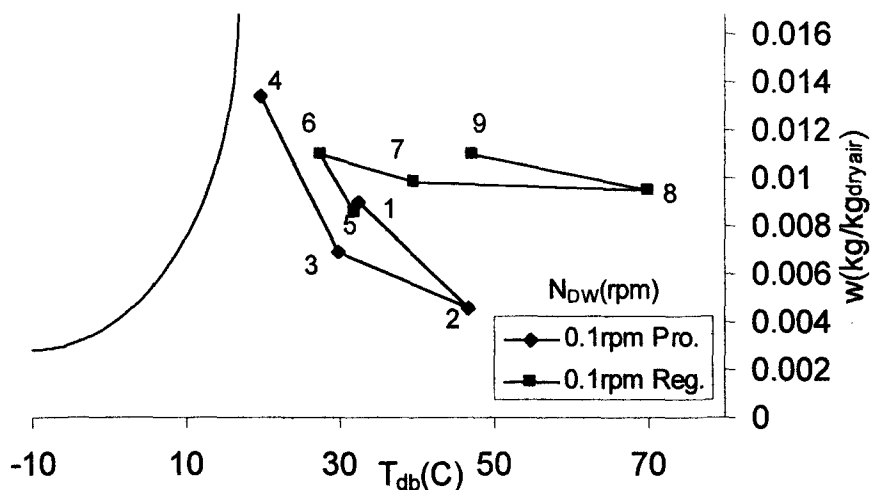
(a)  $m_a=0.056$ kg/sec,  $T_r=60$ C and  $N_{RR}=10$ rpm



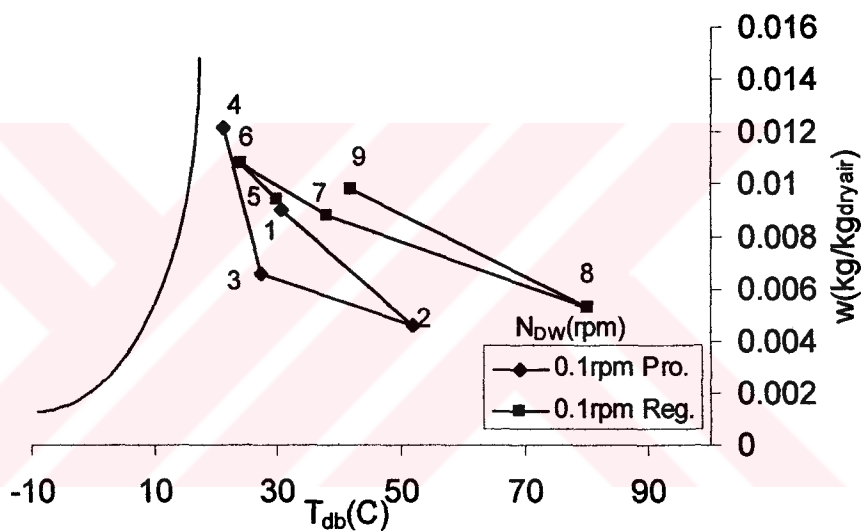
(b)  $m_a=0.083$ kg/s,  $T_r=60$ C and  $N_{RR}=5$ rpm



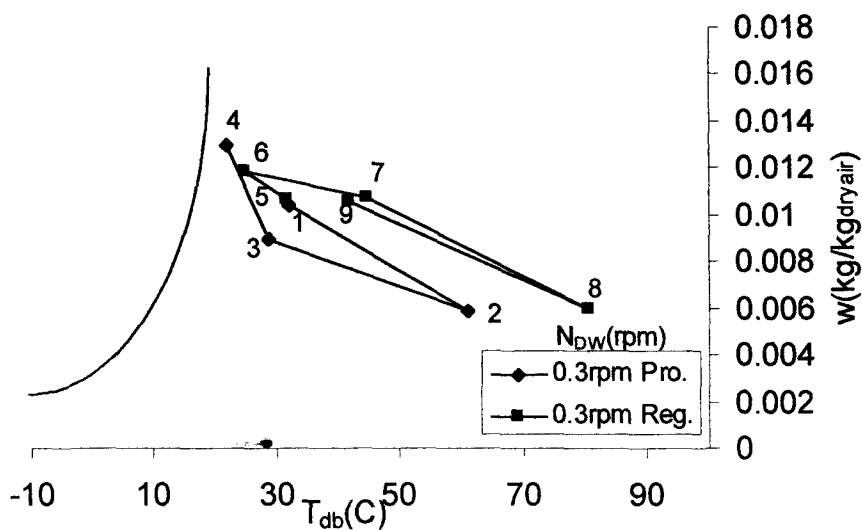
(c)  $m_a=0.111$ kg/s,  $T_r=70$ C and  $N_{RR}=15$ rpm



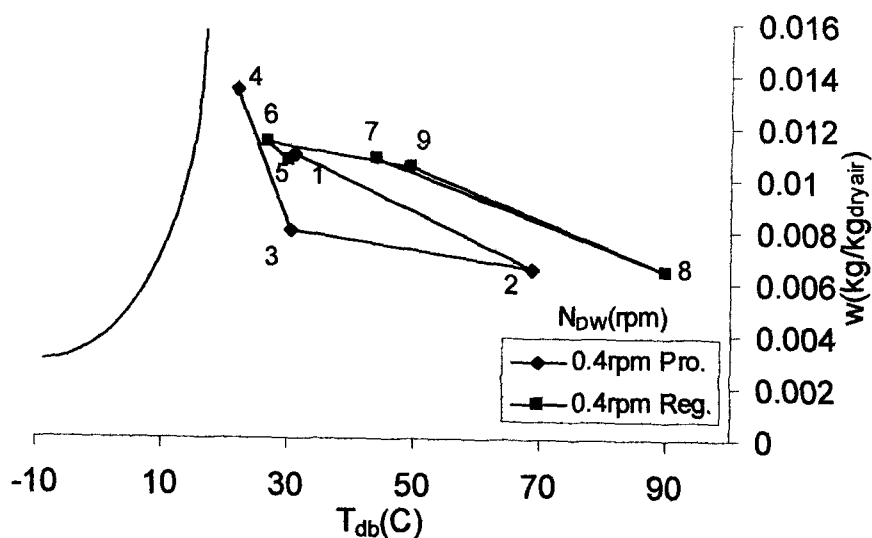
(d)  $m_a=0.139\text{kg/s}$ ,  $T_r=70\text{C}$  and  $N_{RR}=10\text{rpm}$



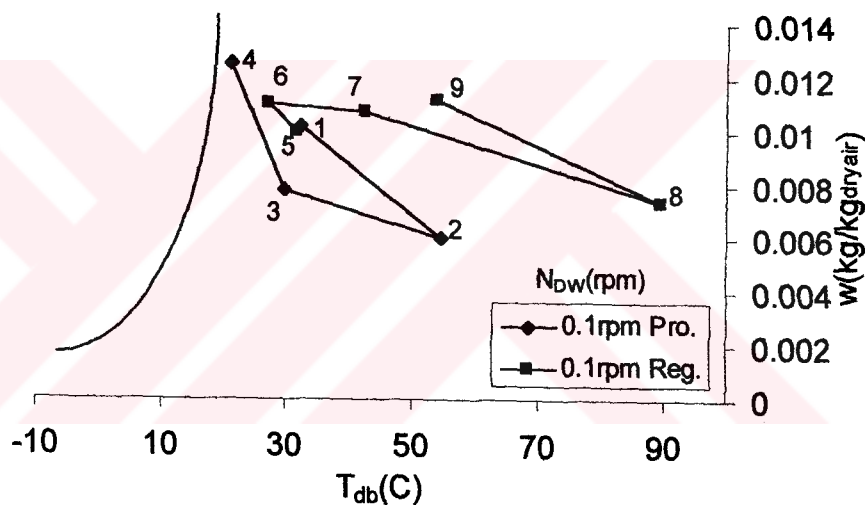
(e)  $m_a=0.056\text{kg/s}$ ,  $T_r=80\text{C}$  and  $N_{RR}=5\text{rpm}$



(f)  $m_a=0.083\text{kg/s}$ ,  $T_r=80\text{C}$  and  $N_{RR}=10\text{rpm}$



(g)  $m_a=0.111\text{kg/s}$ ,  $T_r=90\text{C}$  and  $N_{RR}=5\text{rpm}$



(h)  $m_a=0.139\text{kg/s}$ ,  $T_r=90\text{C}$  and  $N_{RR}=5\text{rpm}$

Figure 5.3 Psychrometric Representation of the Same Sample Test Result of DCS

### 5.3. EFFECTS OF $N_{RR}$ AND $N_{DW}$

The rotational speed of the dehumidifier affects the outlet air temperature and humidity from the dehumidifier and therefore affects the performance of the cooling system. The DW is rotated at a speed where the desiccant will be near total saturation at a point just before it rotates out of

the process air stream into the regeneration stream. Similarly, regeneration temperature,  $T_r$  should be designed so that dried desiccant rotated out of the regeneration air path and into the process path right at the point where the last few molecules of absorbed water are removed from the desiccant loaded on the wheel. Wheel speeds that are too high do not utilize all of the active desiccant process-side water removal or allow for total desiccant regeneration, which results in lower capacity and thermal cycling with sub optimal moisture removal connected to the low efficiency. Desiccant wheel speeds are too slow allow saturated desiccant to remain in the process air stream too long and excess heating of already activated desiccant, which also translates into capacity and efficiency losses. To determine effects of  $N_{RR}$  and  $N_{DW}$  the parameters  $CC_s$  and  $COP_s$  are selected in the analysis.

### 5.3.1 Effects of $N_{RR}$ and $N_{DW}$ on CC and COP

Variation of sensible CC with  $N_{RR}$  are given for different  $N_{DW}$  in Figures 5.4-19. As it can be seen from Figures 5.4-7,  $T_r=60C$  is the common parameter while  $m_a$  is varied as 0.056kg/s, 0.083kg/s, 0.111kg/s, and 0.139kg/s. The variation of CC with  $N_{RR}$  for different mass flow rates seems to be different in terms of  $N_{DW}$ . From these figures, effect of  $N_{RR}$  on variation of CC is negligible but effect of  $N_{DW}$  on CC is clearly seen to be dominant.

Variation of CC with  $N_{RR}$  the selection of  $T_r$  by itself is not enough to determine the functional relationship. It seems that the selected parameters  $N_{DW}$ ,  $m_a$ , is important. This states that all of the covered parameters influence the relationship (CC vs  $N_{RR}$ ) in a complicated manner which can not be estimated in a simple way. As it can be seen in Figures 5.12.a –19.a, CC decreases when the  $N_{DW}$  increases at  $T_r=80C$  and  $90C$ .

Some close inspection to the Figures 5.4.a through 5.19.a in terms of CC variation with  $N_{RR}$  following conclusions can be derived.

1. For  $T_r=60C$ ,  $m_a=0.056kg/s$  CC variation with  $N_{RR}$  is directly under the influence of  $N_{DW}$ . (Figure 5.4.a). At  $N_{DW}=0.4rpm$  and  $0.3rpm$  CC stays constant independent of  $N_{RR}$  with a value of  $14kW/kg_{dryair}$ . This means that it is not important to have a change in RR speed for this case. The variation of CC with  $N_{RR}$  seems to be similar for  $N_{DW}=0.2rpm$  and  $N_{DW}=0.1rpm$ .
2. For  $T_r=60C$   $m_a=0.083kg/s$  (Figure 5.5.a) CC variation with  $N_{RR}$  seems to be independent of  $N_{DW}$  with negligible data scattering taking in a range of  $16kW/kg_{dryair}$ ,  $13kW/kg_{dryair}$ . CC variation as a function of  $N_{RR}$  with different  $N_{DW}$  are seen to be close to each other with a value near to  $1kW/kg_{dryair}$  which means that  $N_{DW}$  is not seriously affecting the relationship between CC and  $N_{RR}$ .
3. However at  $T_r=60C$   $m_a=0.111kg/s$  CC variation with  $N_{RR}$  seems (Figure 5.6.a) to be influenced by  $N_{DW}$ . For  $N_{DW}=0.1rpm$  and  $0.2rpm$  CC values almost irrespective of  $N_{RR}$  stay in the order of  $10kW/kg_{dryair}$ . For  $N_{DW}=0.3rpm$  and  $0.4rpm$  CC value almost in the order of  $14kW/kg_{dryair}$  is observed. This means that for this case magnitude of  $N_{DW}$  becomes important on the cooling capacity of the system. At  $m_a=0.139kg/s$ ,  $N_{DW}=0.1rpm$  and  $0.2rpm$ , CC values are higher than CC values for  $N_{DW}=0.3rpm$  and  $0.4rpm$ . As can be seen in Figure 5.4.a, 5.5.a, 5.6.a and 5.7 the highest CC is obtained as  $16kW/kg_{dryair}$  at  $N_{DW}=0.1rpm$ ,  $m_a=0.083kg/s$  or  $0.139kg/s$  and  $T_r=60C$
4. As can be seen from Figures 5.8.a, 5.9.a, 5.10.a, 5.11.a for  $T_r=70C$  with varying  $m_a$  values the functional relationship of CC with  $N_{RR}$  seem to be influenced severely with the variations in  $N_{DW}$ . It is difficult to estimate the reasons of these behavior. Similar observations are made for  $T_r=80C$  (Figures 5.12.a through 5.14.a). The magnitude of CC does not increase with  $T_r$ . CC stays constant at  $8kW/kg_{dryair}$  for  $T_r>70C$  as it can be seen from Figures 5.4.a through 5.19.a.

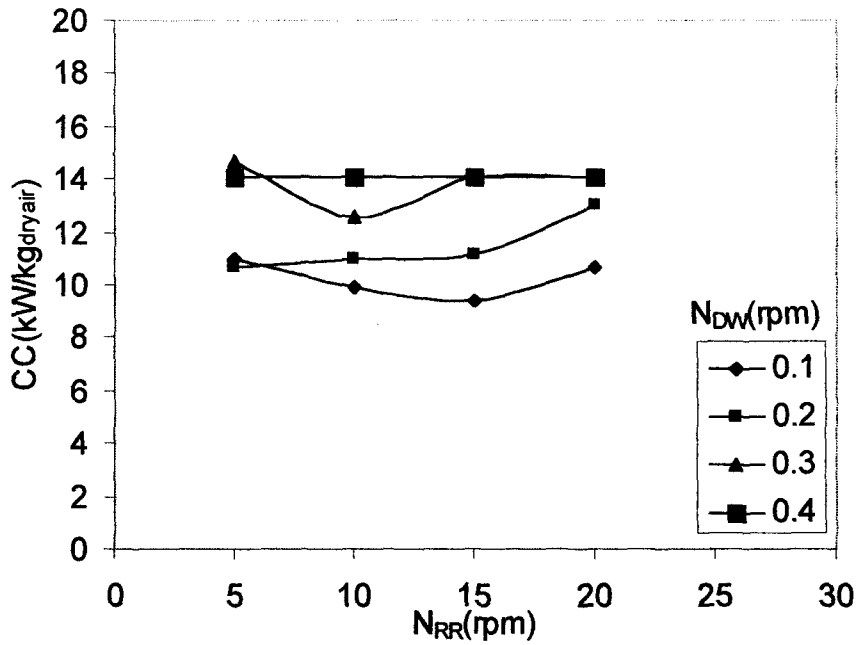
5. As can be seen from Figures 5.16.a through 5.19.a at  $T_r=90\text{C}$  the behavior of CC with  $N_{RR}$  under the influence of  $m_a$  and  $N_{DW}$  shows a considerable change. Since for  $m_a=0.056\text{kg/s}$  (Figure 5.16.a) at  $N_{DW}=0.1\text{rpm}$  CC stays constant almost with a value of  $8\text{kW/kg}_{\text{dryair}}$  while at  $N_{DW}=0.2\text{rpm}$  and  $0.3\text{rpm}$  it decreases with increase in  $N_{RR}$  from  $8\text{kW/kg}_{\text{dryair}}$  to  $7\text{kW/kg}_{\text{dryair}}$ . Meanwhile at  $N_{DW}=0.4\text{rpm}$  CC stays almost constant at  $7\text{kW/kg}_{\text{dryair}}$ . While with increase in  $m_a$  (Figure 5.17.a, 5.18.a, 5.19.a) CC at  $N_{DW}=0.1\text{rpm}$  and  $N_{DW}=0.2\text{rpm}$  stays constant at  $11\text{kW/kg}_{\text{dryair}}$ . At  $N_{DW}=0.3\text{rpm}$  and  $0.4\text{rpm}$  CC stays constant at  $8\text{kW/kg}_{\text{dryair}}$  irrespective of  $N_{RR}$ . Therefore it can be said that  $N_{RR}$  is not a dominant parameter in comparison to  $N_{DW}$ , on the cooling capacity of the DCS operation under the considered case of high  $T_r=90\text{C}$ .
6. The obtained highest magnitude of  $\text{CC}=16\text{kW/kg}_{\text{dryair}}$  is also the highest for the selected  $T_r$  range. It seems that the most effective operating parameters influencing CC in the selected ranges of  $N_{RR}$ ,  $N_{DW}$ ,  $m_a$ , and  $T_r$  are  $m_a$  and  $N_{DW}$  due to mass transfer in DW.

COP variation with  $N_{RR}$  for different  $N_{DW}$  are given also in Figure 5.4-19 in the same manner as CC. Variation of COP with  $N_{RR}$  seems to be independent of  $N_{DW}$ ; as can be seen from COP values remaining in the ranges of 0.7-1 for  $m_a=0.139\text{kg/s}$  and  $T_r=60\text{C}$  from Figure 5.7.b, 0.3-0.45 for  $m_a=0.111\text{kg/s}$ , and  $T_r=70\text{C}$  from Figure 5.10.b, 0.25-0.4 for  $m_a=0.139\text{kg/s}$ ,  $T_r=70\text{C}$  from Figure 5.11.b, and 0.2-0.35, for  $m_a=0.139\text{kg/s}$ ,  $T_r=90\text{C}$  from Figure 5.19.b. For another condition, COP varies randomly with  $N_{RR}$  and  $N_{DW}$ . But it can be said that the highest COP is reached at low  $N_{RR}$  and  $T_r=60\text{C}$ . However as  $T_r$  increases COP decreases, commonly.

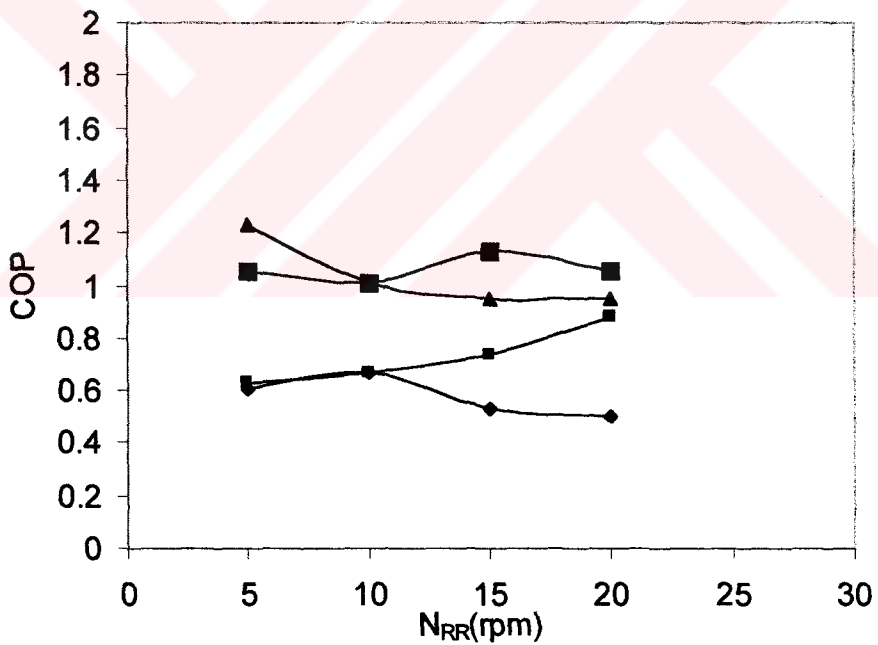
Some close inspection to the Figures 5.4.b through 5.19.b COP variation with  $N_{RR}$  following conclusions can be derived.

1. As can be seen from Figures 5.4.b COP variation with  $N_{RR}$  is seriously influenced by  $N_{DW}$  at  $T_r=60C$ , and  $m_a=0.056kg/s$ . Increase in  $N_{DW}$  is somehow resulted in increase in COP. (i.e. at  $N_{DW}=0.2rpm$  COP increases from 0.6 to 0.9 with  $N_{RR}$  increase however at  $N_{DW}=0.4rpm$  COP varies between 1 and 1.1 with  $N_{RR}$  increases.) The highest magnitude of COP is obtained as 1.3 at  $m_a=0.083kg/s$ ,  $T_r=60C$ ,  $N_{RR}=20rpm$  and  $N_{DW}=0.4rpm$  as shown in Figure 5.5.b.
2. COP variation with  $N_{RR}$  is also influenced by  $m_a$ . Since increases in  $m_a$  to 0.083kg/s at the same  $T_r=60C$  (Figure 5.5.b) causes irregular variation of COP with  $N_{RR}$  in the band of 0.9-1.3 which is irrespective of  $N_{DW}$ . However as can be seen from Figure 5.6.b at  $T_r=60C$ ,  $m_a=0.111kg/s$  for the variation of COP with  $N_{RR}$ ,  $N_{DW}$  becomes effective. While further increase in  $m_a$  at the same  $T_r=60C$  (Figure 5.7.b) COP variation with  $N_{RR}$  under the effect of  $N_{DW}$  takes the magnitudes between 0.7-0.9 in the covered range of  $N_{RR}$ .
3. Increase in  $T_r$  to 70C, 80C resulted in similar behavior of COP with  $N_{RR}$  (Figure 5.8.b through Figure 5.15.b) with lower magnitudes of COP.
4. At the higher magnitude of  $T_r=90C$  (Figure 5.16.b through Figure 5.19.b) COP variation with  $N_{RR}$  is seriously influenced by the magnitudes of  $m_a$  and  $N_{DW}$ .
5. COP variation with  $N_{RR}$  as a function of  $N_{DW}$  is with considerable amounts only for the cases in which as can be seen from Figure 5.4.b. On the other hand the relationship between COP and  $N_{RR}$  is almost independent of  $N_{DW}$  for most of the cases.

Finally it can be said that for COP behavior of DCS operation both  $N_{DW}$  and  $N_{RR}$  are serious factors besides  $m_a$  and  $T_r$ .



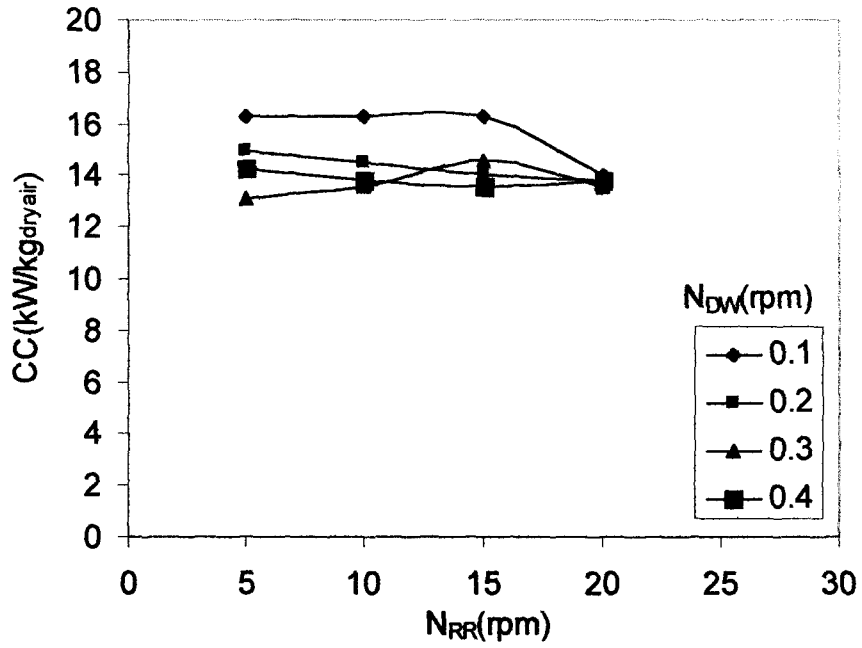
(a)



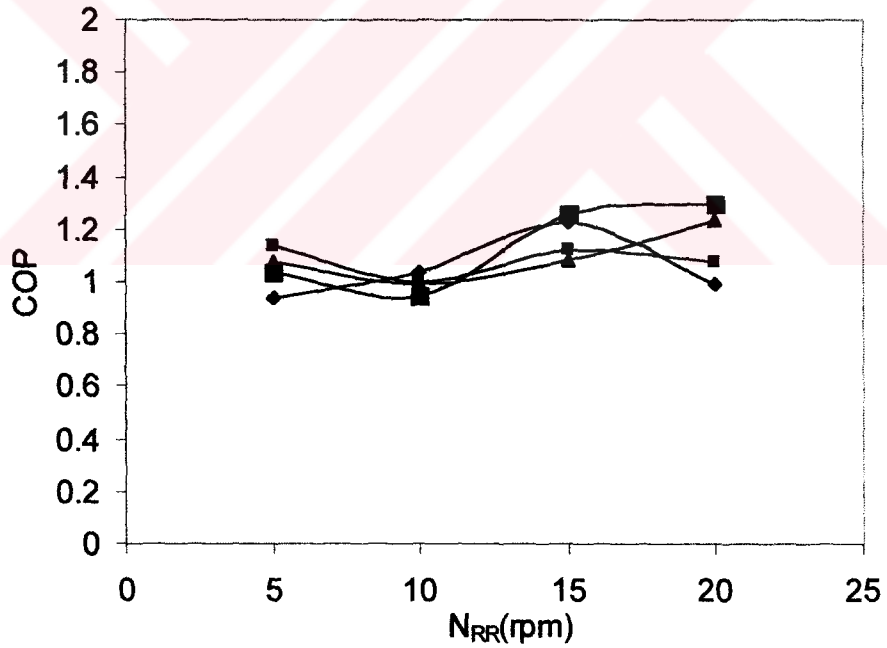
(b)

Figure 5.4 a) Variation of Sensible Cooling Capacity of DCS with  $N_{RR}$  and  $N_{DW}$  for  $m_a=0.056\text{kg/s}$  and  $T_r=60\text{C}$   
 b) Variation of Sensible COP of DCS with  $N_{RR}$  and  $N_{DW}$  for  $m_a=0.056\text{kg/s}$  and  $T_r=60\text{C}$



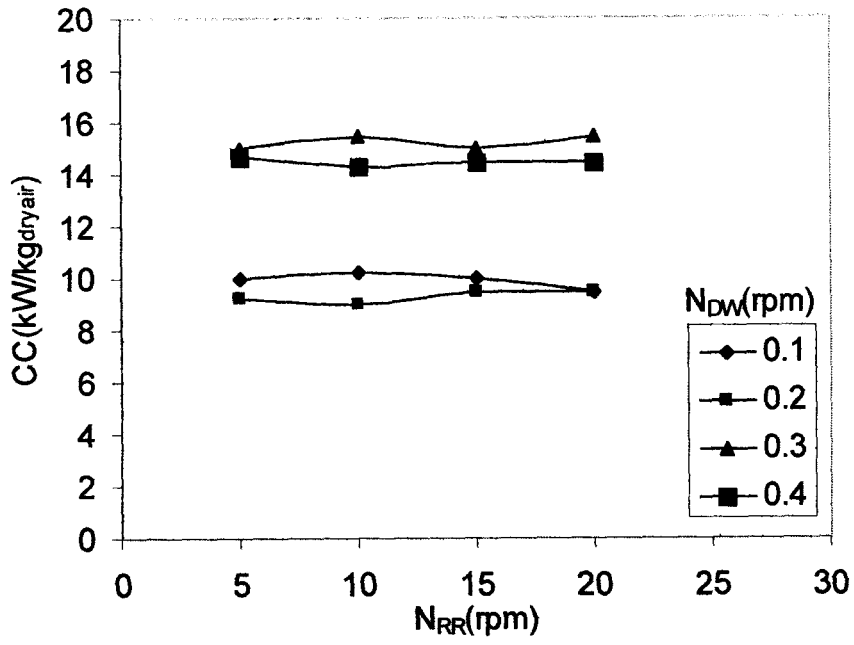


(a)

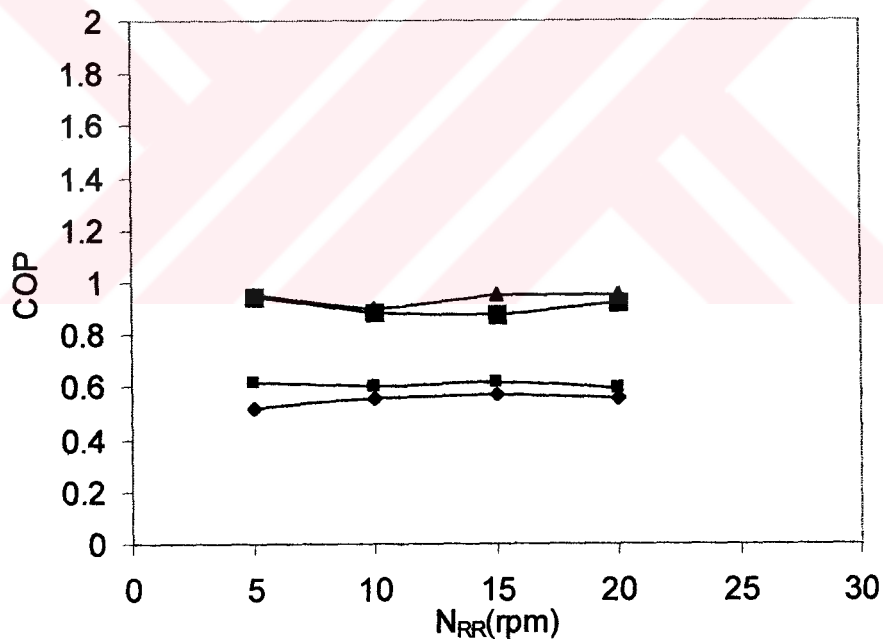


(b)

Figure 5.5 a) Variation of Sensible Cooling Capacity of DCS with  $N_{RR}$  and  $N_{DW}$  for  $m_a=0.083\text{kg/s}$  and  $T_r=60\text{C}$   
 b) Variation of Sensible COP of DCS with  $N_{RR}$  and  $N_{DW}$  for  $m_a=0.083\text{kg/s}$  and  $T_r=60\text{C}$

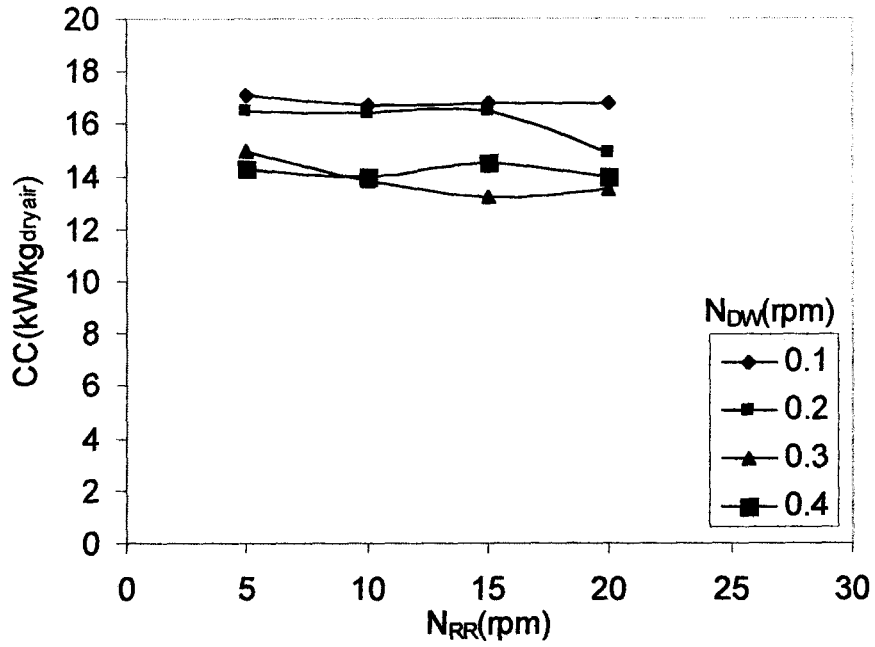


(a)

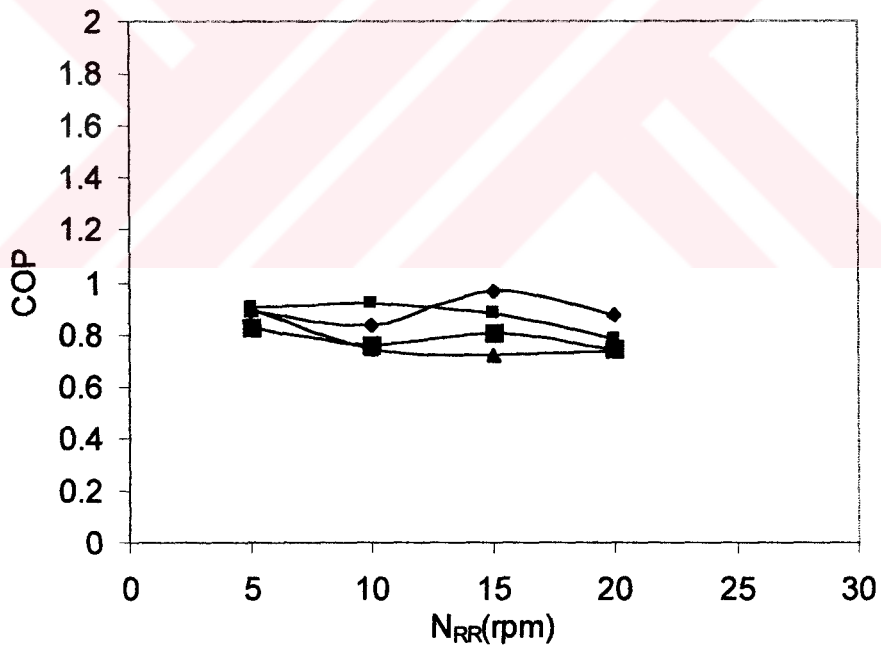


(b)

Figure 5.6 a) Variation of Sensible Cooling Capacity of DCS with  $N_{RR}$  and  $N_{DW}$  for  $m_a=0.111\text{kg/s}$  and  $T_r=60\text{C}$   
 b) Variation of Sensible COP of DCS with  $N_{RR}$  and  $N_{DW}$  for  $m_a=0.111\text{kg/s}$  and  $T_r=60\text{C}$



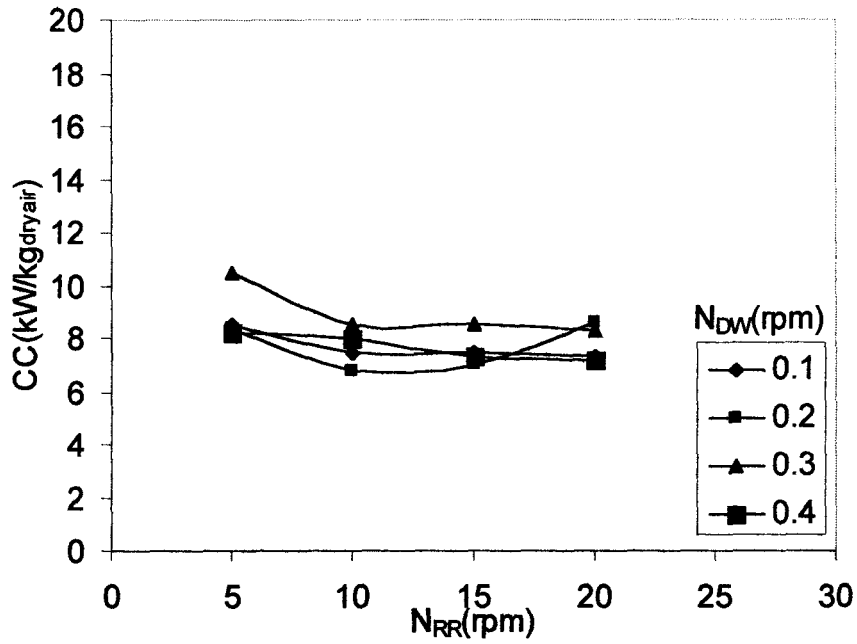
(a)



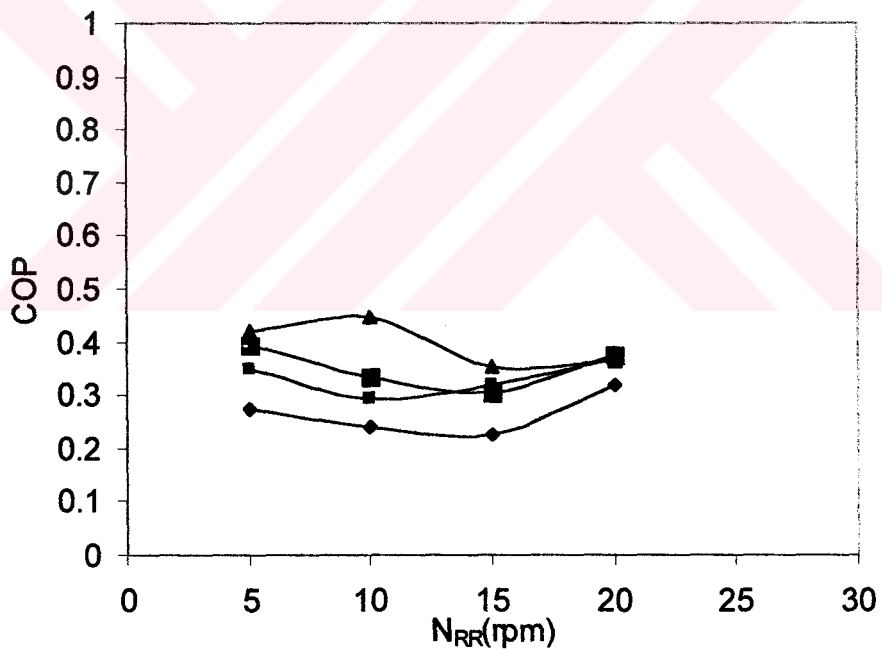
(b)

Figure 5.7 a) Variation of Sensible Cooling Capacity of DCS with  $N_{RR}$  and  $N_{DW}$  for  $m_a=0.139\text{kg/s}$  and  $T_r=60\text{C}$

b) Variation of Sensible COP of DCS with  $N_{RR}$  and  $N_{DW}$  for  $m_a=0.139\text{kg/s}$  and  $T_r=60\text{C}$

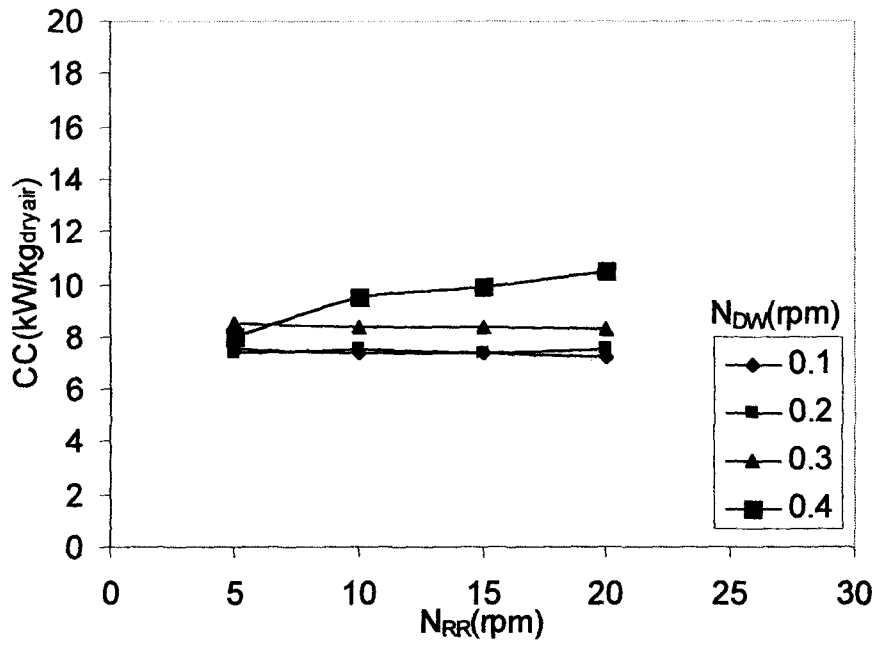


(a)

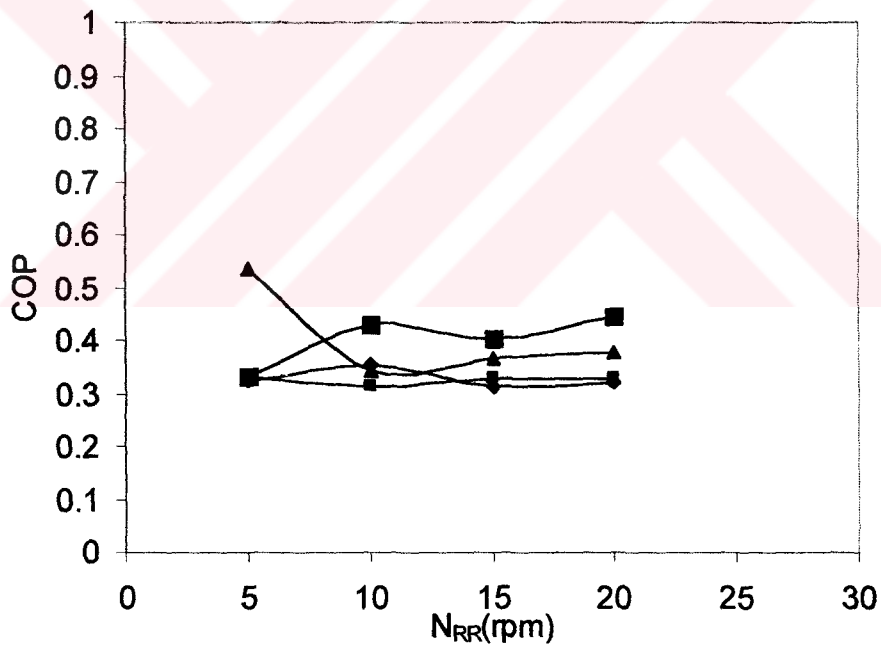


(b)

Figure 5.8 a) Variation of Sensible Cooling Capacity of DCS with  $N_{RR}$  and  $N_{DW}$  for  $m_a=0.056\text{kg/s}$  and  $T_r=70\text{C}$   
 b) Variation of Sensible COP of DCS with  $N_{RR}$  and  $N_{DW}$  for  $m_a=0.056\text{kg/s}$  and  $T_r=70\text{C}$



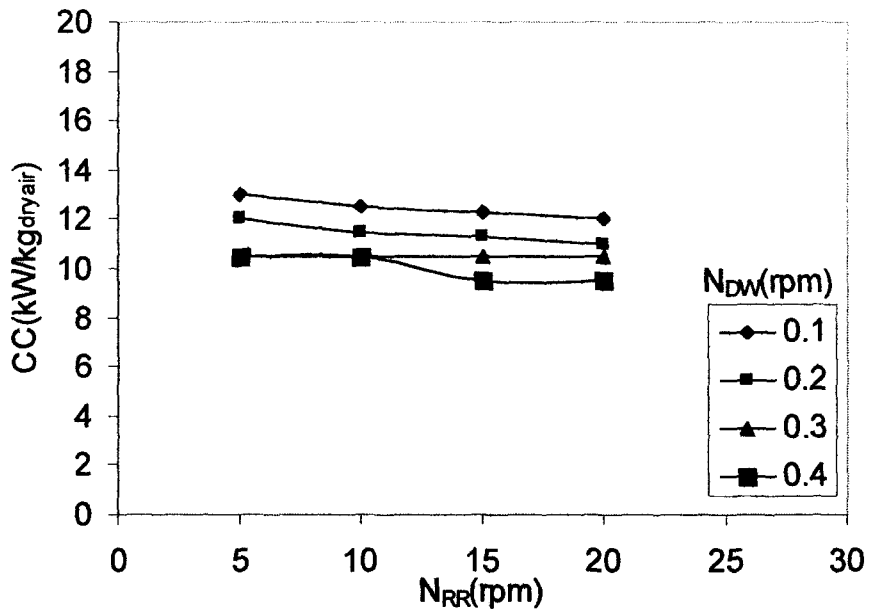
(a)



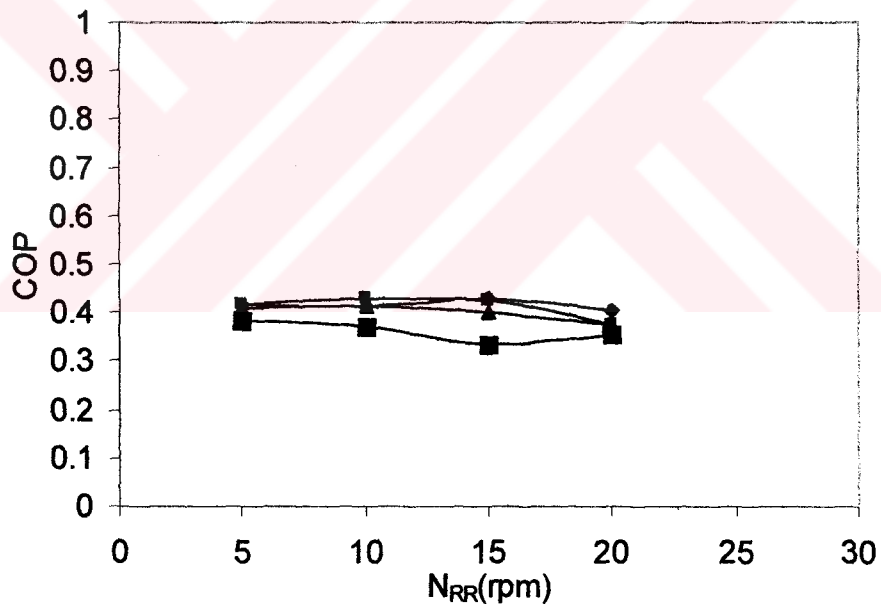
(b)

Figure 5.9 a) Variation of Sensible Cooling Capacity of DCS with  $N_{RR}$  and  $N_{DW}$  for  $m_a = 0.083 \text{ kg/s}$  and  $T_r = 70^\circ\text{C}$

b) Variation of Sensible COP of DCS with  $N_{RR}$  and  $N_{DW}$  for  $m_a = 0.083 \text{ kg/s}$  and  $T_r = 70^\circ\text{C}$



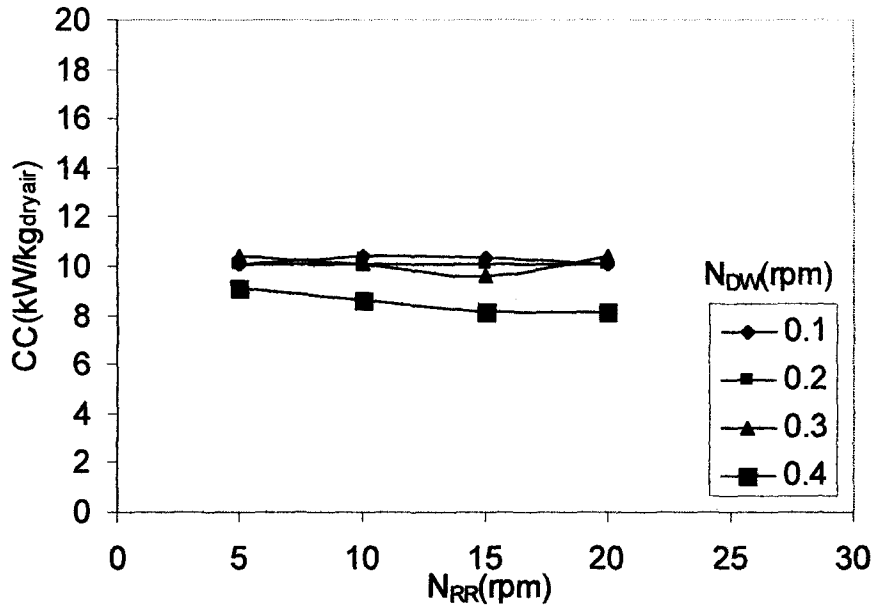
(a)



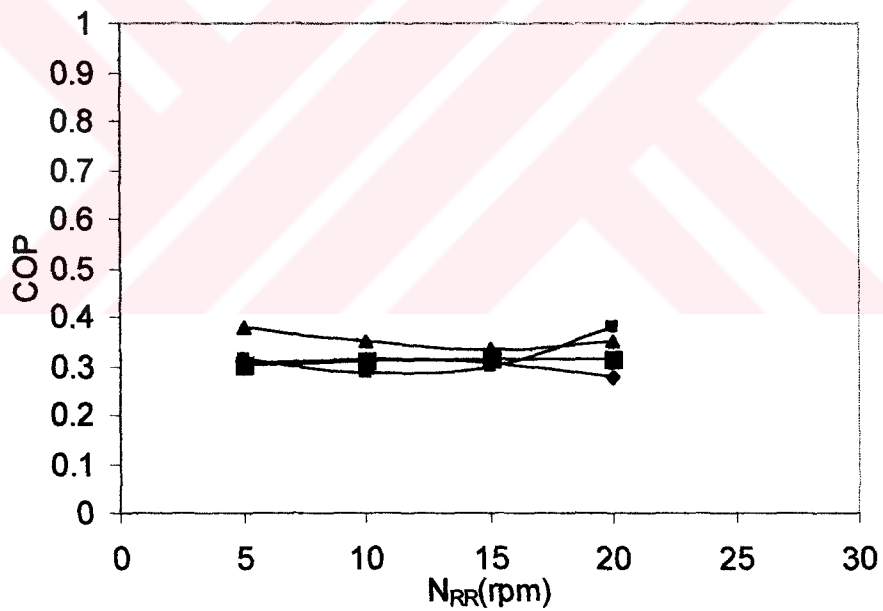
(b)

Figure 5.10 a) Variation of Sensible Cooling Capacity of DCS with  $N_{RR}$  and  $N_{DW}$  for  $m_a=0.111\text{kg/s}$  and  $T_r=70\text{C}$

b) Variation of Sensible COP of DCS with  $N_{RR}$  and  $N_{DW}$  for  $m_a=0.111\text{kg/s}$  and  $T_r=70\text{C}$

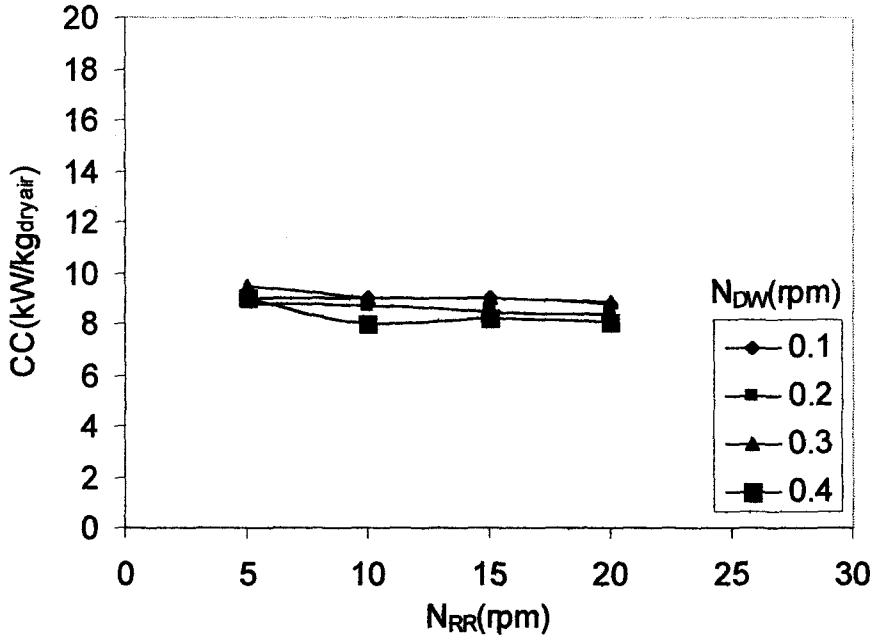


(a)

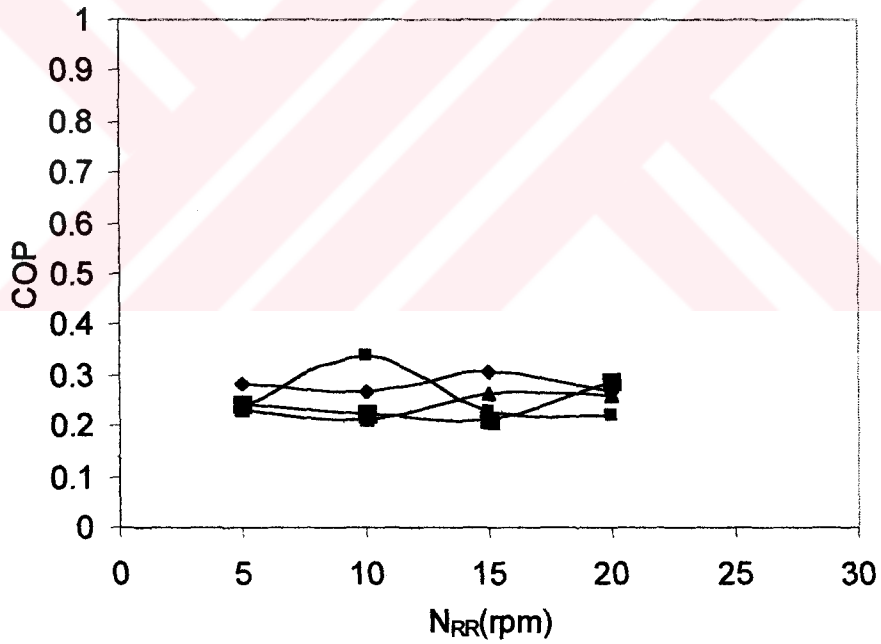


(b)

Figure 5.11 a) Variation of Sensible Cooling Capacity of DCS with  $N_{RR}$  and  $N_{DW}$  for  $m_a=0.139\text{kg/s}$  and  $T_r=70\text{C}$   
 b) Variation of Sensible COP of DCS with  $N_{RR}$  and  $N_{DW}$  for  $m_a=0.139\text{kg/s}$  and  $T_r=70\text{C}$



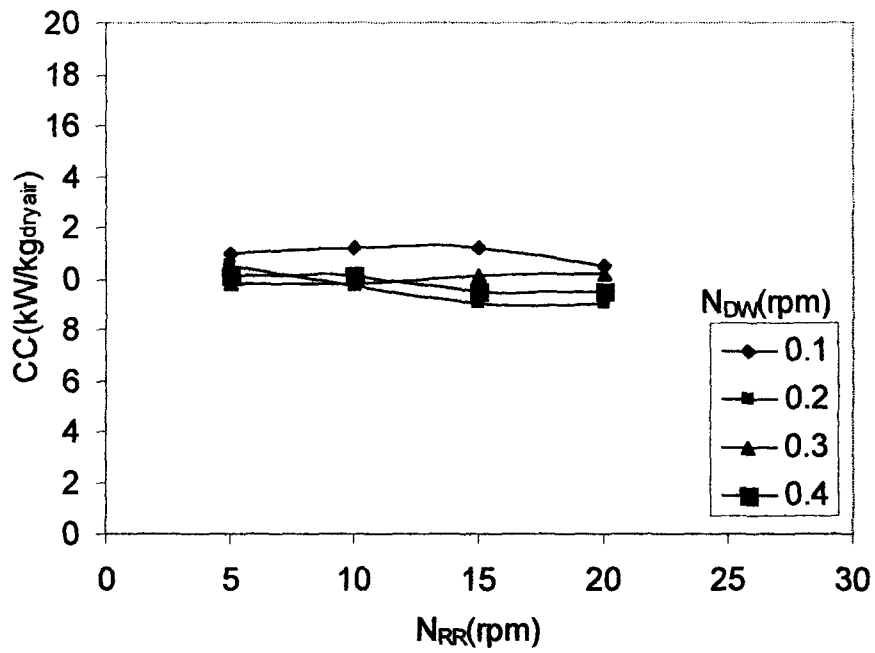
(a)



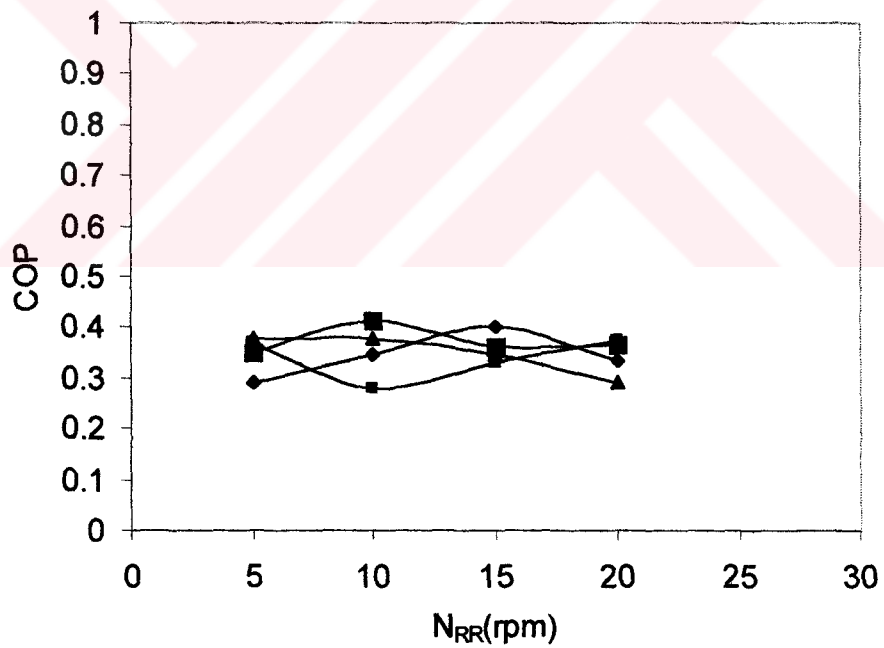
(b)

Figure 5.12 a) Variation of Sensible Cooling Capacity of DCS with N<sub>RR</sub> and N<sub>DW</sub> for m<sub>a</sub>=0.056kg/s and T<sub>r</sub>=80C  
 b) Variation of Sensible COP of DCS with N<sub>RR</sub> and N<sub>DW</sub> for m<sub>a</sub>=0.056kg/sec and T<sub>r</sub>=80C



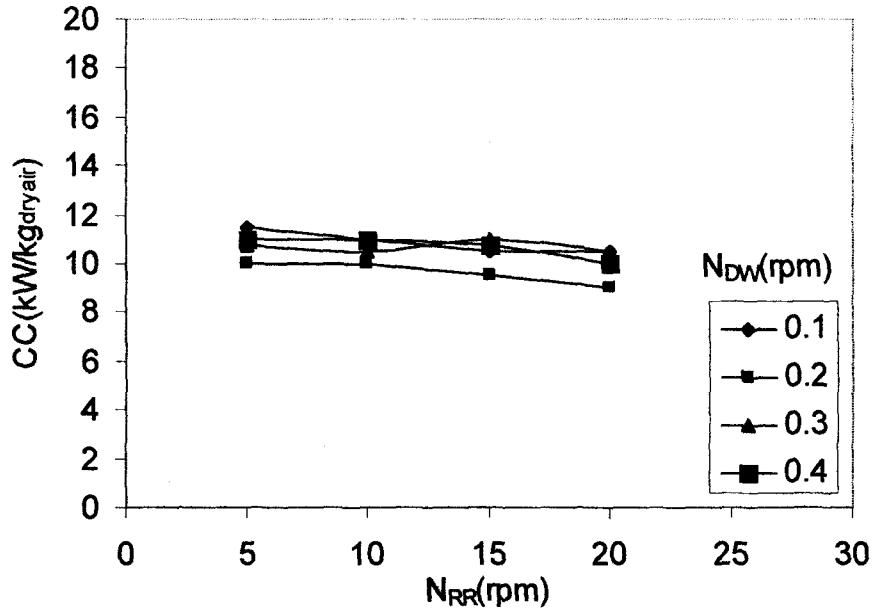


(a)

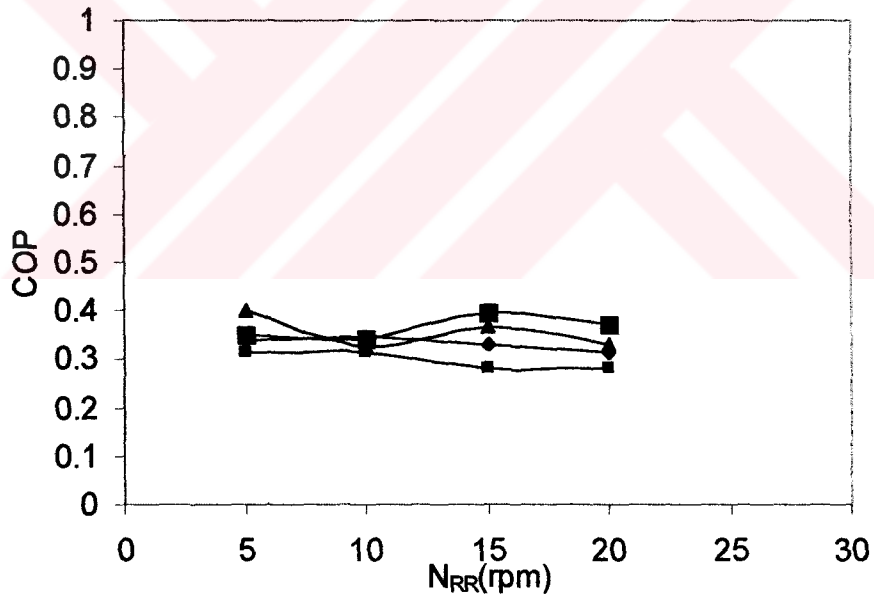


(b)

Figure 5.13 a) Variation of Sensible Cooling Capacity of DCS with  $N_{RR}$  and  $N_{DW}$  for  $m_a=0.111\text{kg/s}$  and  $T_r=80\text{C}$   
 b) Variation of Sensible COP of DCS with  $N_{RR}$  and  $N_{DW}$  for  $m_a=0.111\text{kg/s}$  and  $T_r=80\text{C}$

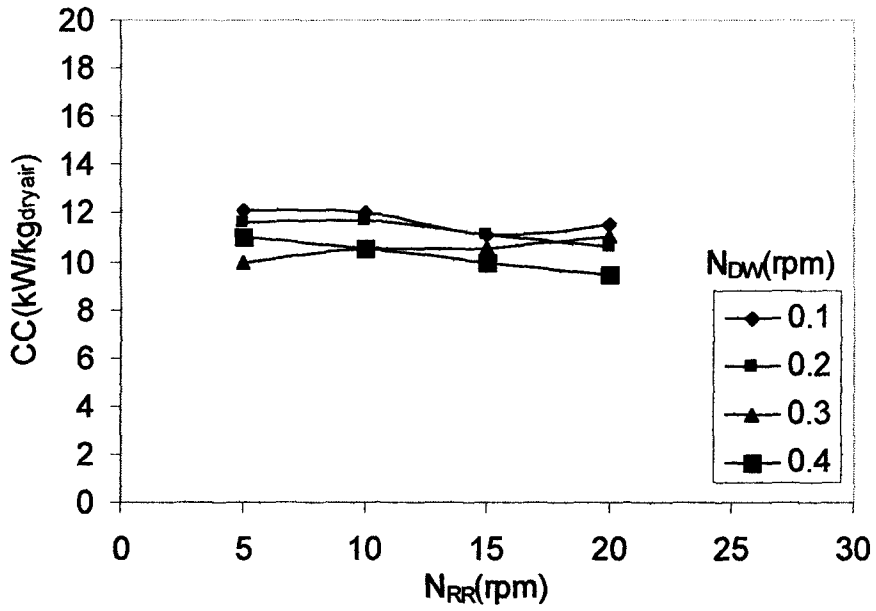


(a)

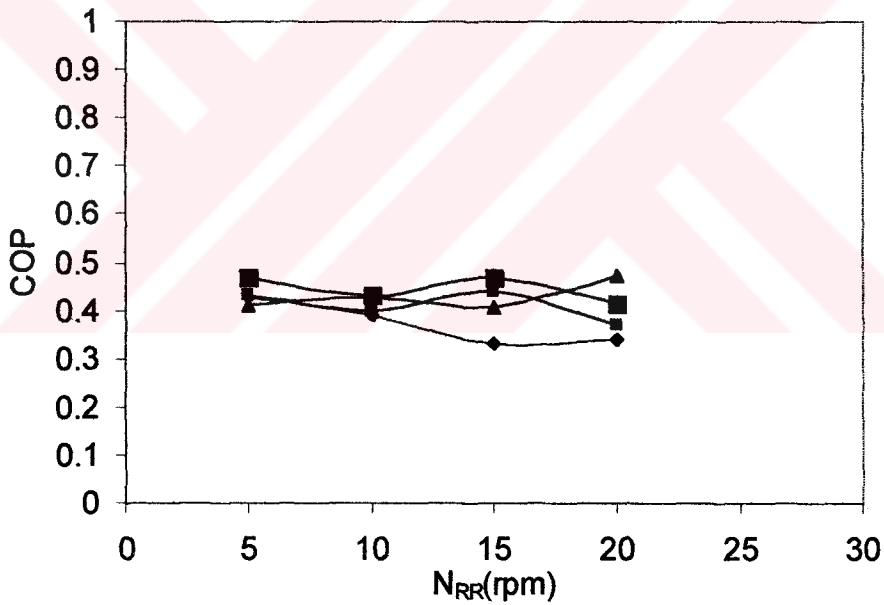


(b)

Figure 5.14 a) Variation of Sensible Cooling Capacity of DCS with  $N_{RR}$  and  $N_{DW}$  for  $m_a=0.111\text{kg/s}$  and  $T_r=80\text{C}$   
 b) Variation of Sensible COP of DCS with  $N_{RR}$  and  $N_{DW}$  for  $m_a=0.111\text{kg/s}$  and  $T_r=80\text{C}$

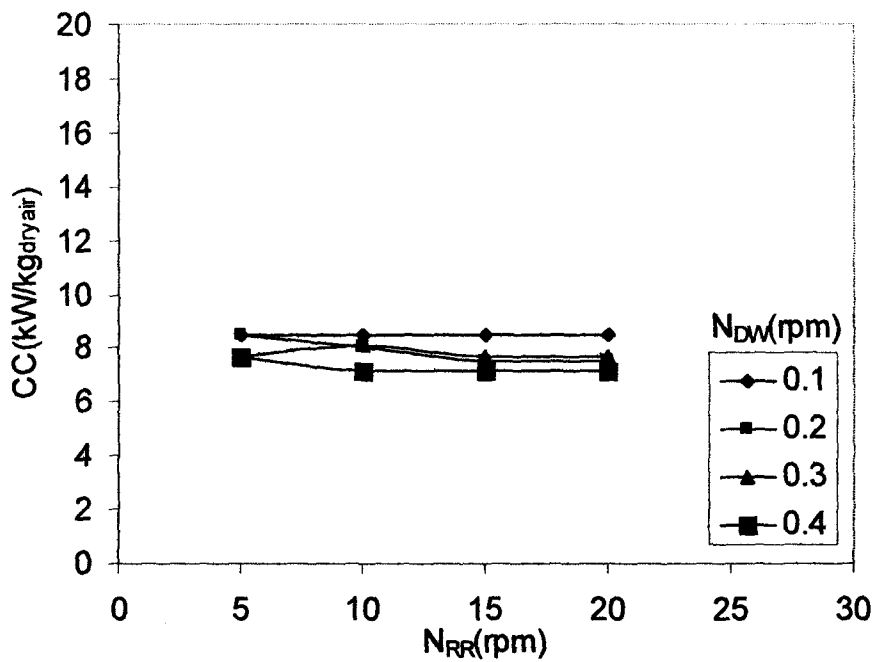


(a)

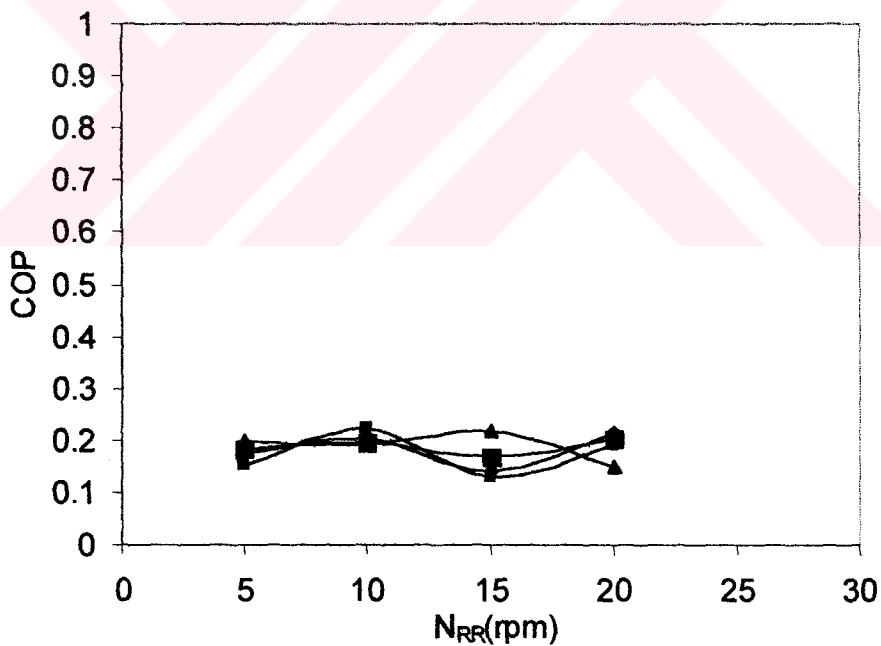


(b)

Figure 5.15 a) Variation of Sensible Cooling Capacity of DCS with  $N_{RR}$  and  $N_{DW}$  for  $m_a=0.139\text{kg/s}$  and  $T_r=80\text{C}$   
 b) Variation of Sensible COP of DCS with  $N_{RR}$  and  $N_{DW}$  for  $m_a=0.056\text{kg/sec}$  and  $T_r=80\text{C}$

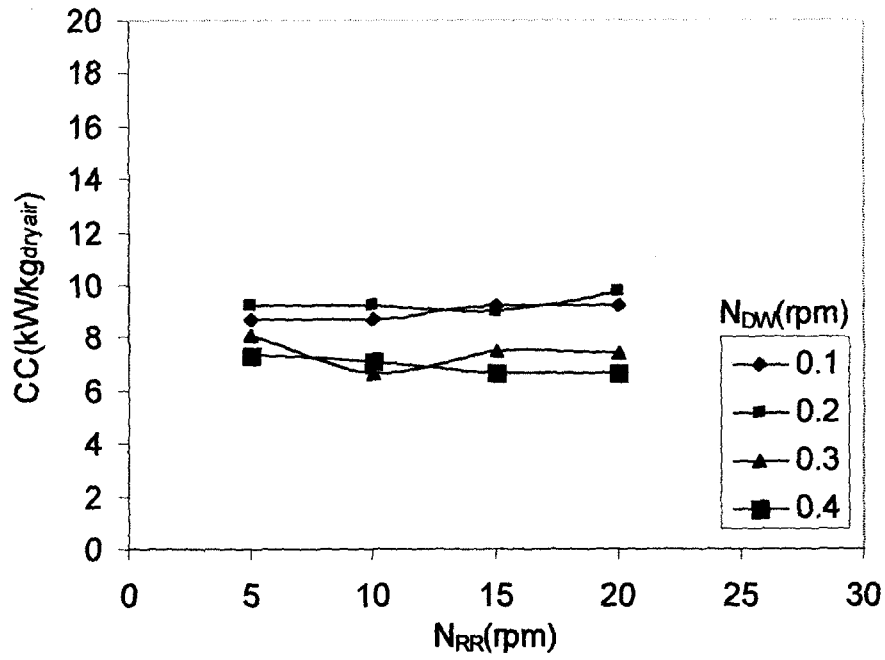


(a)

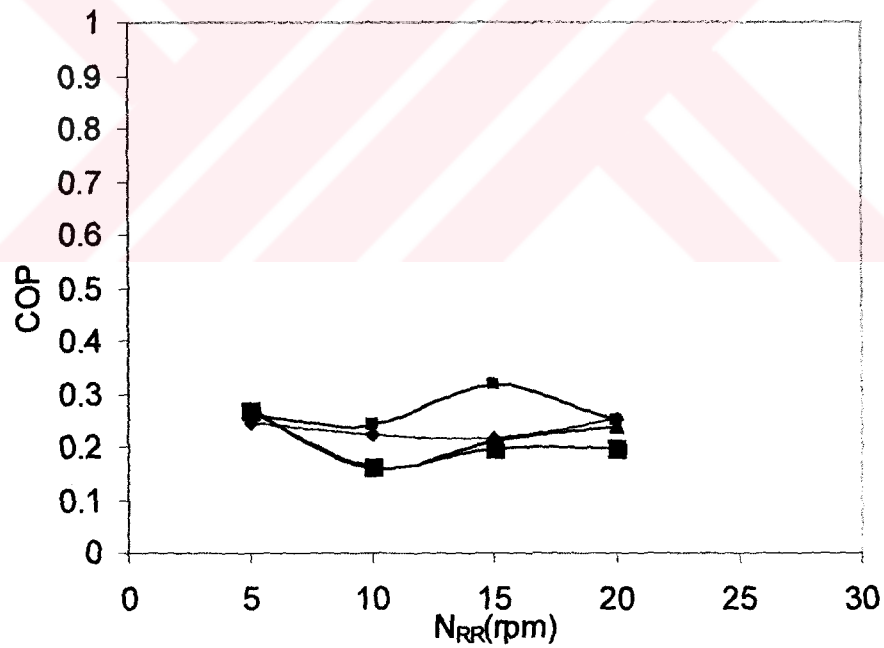


(b)

Figure 5.16 a) Variation of Sensible Cooling Capacity of DCS with  $N_{RR}$  and  $N_{DW}$  for  $m_a = 0.056 \text{ kg/s}$  and  $T_r = 90^\circ\text{C}$   
 b) Variation of Sensible COP of DCS with  $N_{RR}$  and  $N_{DW}$  for  $m_a = 0.056 \text{ kg/s}$  and  $T_r = 90^\circ\text{C}$

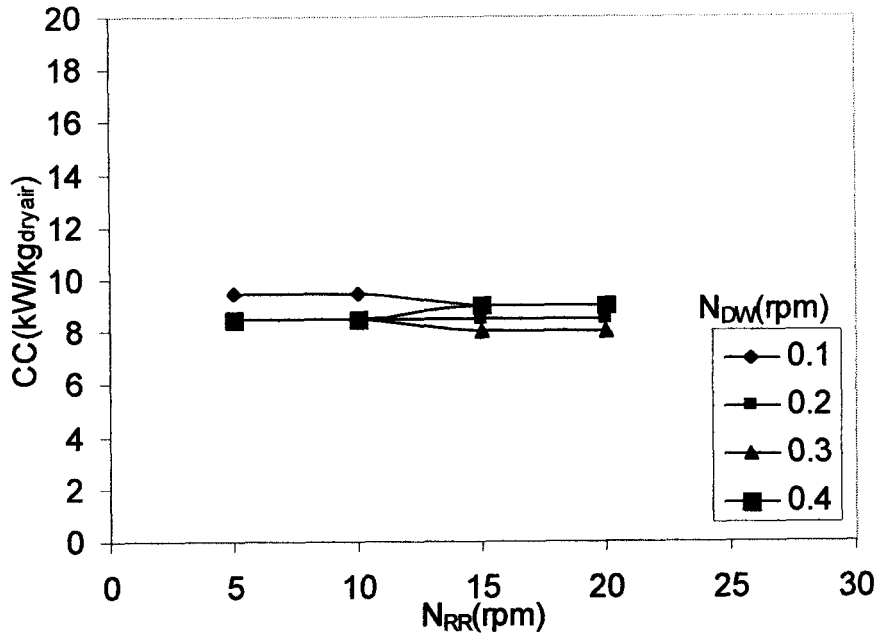


(a)

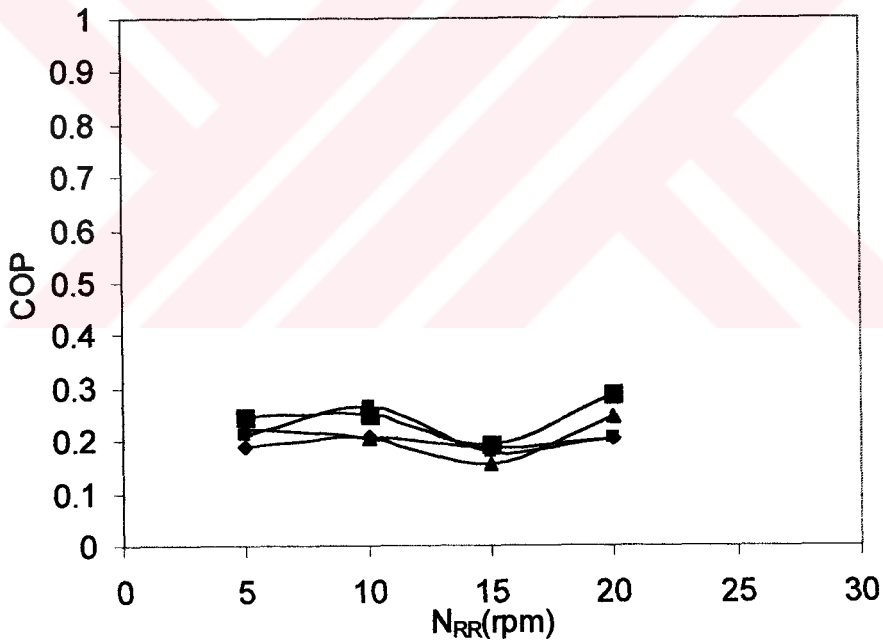


(b)

Figure 5.17 a) Variation of Sensible Cooling Capacity of DCS with  $N_{RR}$  and  $N_{DW}$  for  $m_a=0.083\text{kg/s}$  and  $T_r=90\text{C}$   
 b) Variation of Sensible COP of DCS with  $N_{RR}$  and  $N_{DW}$  for  $m_a=0.083\text{kg/s}$  and  $T_r=90\text{C}$

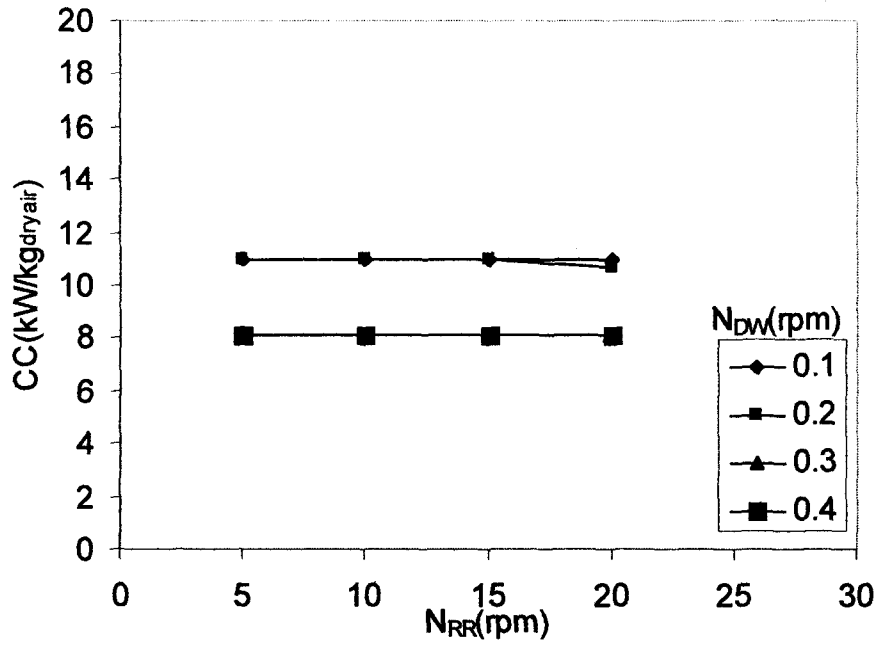


(a)

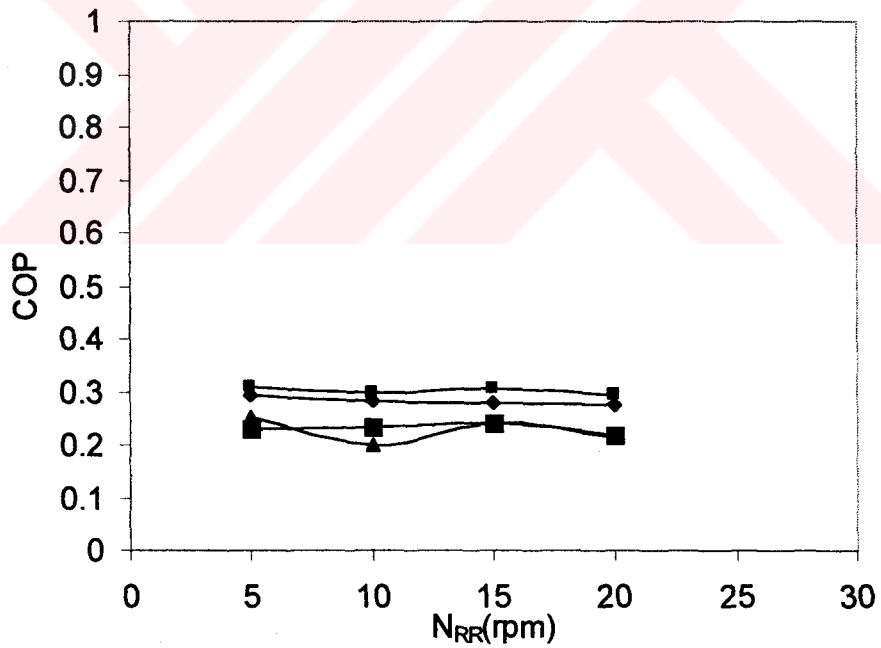


(b)

Figure 5.18 a) Variation of Sensible Cooling Capacity of DCS with  $N_{RR}$  and  $N_{DW}$  for  $m_a=0.111\text{kg/s}$  and  $T_r=90\text{C}$   
 b) Variation of Sensible COP of DCS with  $N_{RR}$  and  $N_{DW}$  for  $m_a=0.111\text{kg/s}$  and  $T_r=90\text{C}$



(a)



(b)

Figure 5.19 a) Variation of Sensible Cooling Capacity of DCS with  $N_{RR}$  and  $N_{DW}$  for  $m_a=0.139\text{kg/s}$  and  $T_r=90\text{C}$   
 b) Variation of Sensible COP of DCS with  $N_{RR}$  and  $N_{DW}$  for  $m_a=0.139\text{kg/s}$  and  $T_r=90\text{C}$

### 5.3.2 Effects of $N_{RR}$ and $N_{DW}$ on $\Delta w_p$ and $\Delta w_r$

In order to determine DCS operation in terms of occurred mass transfers variation of  $\Delta w$  in process/regeneration lines with  $N_{RR}$ ,  $N_{DW}$ ,  $m_a$ ,  $T_r$  were considered.

In reference to Figures 5.20.a, b to 5.34.a, b the functional relationship between  $\Delta w_p$  vs  $N_{RR}$  and  $\Delta w_r$  vs  $N_{RR}$  are given as influenced by the main variables of the study;  $N_{DW}$ ,  $T_r$ ,  $m_a$ . As an overall suggestion from the analysis of these figures.

1. All of the considered parameters are effective on mass transfer. It is difficult to estimate the dominant influence of a single parameter.
2. Instead more than one parameter as a group seem to be governing the mass transfer.
3. The relative order of magnitudes of  $N_{RR}$ , and  $N_{DW}$  seem to be seriously important.
4. The mass adsorption in process side seems to be greater than the mass desorption in regeneration side.
5. The amounts of  $m_a$  seems to be of secondary importance.
6. As can be seen in Figure 5.20.a, b, and Figure 5.24.a, b  $N_{DW} \geq 0.2 \text{rpm}$ ,  $N_{RR}$  in the interval  $T_r = 60-70^\circ\text{C}$   $\Delta w_p$  taking (-) values in process side meaning reverse moisture transfer occurs in DW i.e. moisture desorption. However for  $T_r > 70^\circ\text{C}$  this reverse mass transfer is not observed in process line which means the importance and influence of  $T_r$ . The similar idea in regeneration line is seen Figure 5.23.b, Figures 5.26.b-30.b, and Figures 5.32.b-



34.b in some sample cases. However it seems that it is difficult to have critical values for governing parameters due to the close dependence of them.

7. As it can be seen that; high mass transfer rates as adsorption in process line and desorption in regeneration lines occur at low  $N_{DW}$  which is still a function of  $N_{RR}$ .

$\Delta w_p$  increases when  $N_{DW}$  decreases under the influence of  $N_{RR}$  as it can be seen in Figures 5.20-5.35.

As shown in Figures 5.20.a, and 5.25.a, in adsorption side of DW, instead of adsorption, desorption occurs at  $m_a=0.056\text{kg/s}$ ,  $T_r=60\text{C}$  for  $N_{DW}>0.2\text{rpm}$  and  $N_{DW}>5\text{rpm}$ . Similar phenomena occurs for the condition  $N_{RR}=10\text{rpm}$ ,  $N_{DW}=0.2\text{rpm}$ ,  $m_a=0.056\text{kg/s}$ , and  $T_r=70\text{C}$ .  $\Delta w_p$  should be equal to  $\Delta w_r$ . For the condition the highest COP  $\Delta w_p \cong \Delta w_r$ . Adsorption or desorption in process and regeneration side of DW show that moisture adsorbed or desorbed by the zeolite is under its capacity.

In regeneration side instead of desorption, adsorption occurs at  $m_a=0.139\text{kg/s}$ ,  $T_r=60\text{C}$ ,  $N_{DW}=0.4\text{rpm}$  and  $5<N_{RR}<20$  as shown in Figure 5.23.b. Same phenomena occurs in Figures 5.26.b, 5.27.b, 5.28.b, 5.29.b, 5.32.b, 5.33.b, and 5.34.b.

For the covered test cases the condition of  $\Delta w_p \cong \Delta w_r$  were obtained at the particular selection of operating parameters as can be seen:

in Figure 5.20, at  $N_{RR}=15\text{rpm}$ ,  $N_{DW}=0.2\text{rpm}$ ,  $m_a=0.056\text{kg/s}$ , and  $T_r=60\text{C}$

in Figure 5.21, at  $N_{RR}=5\text{rpm}$ ,  $N_{DW}=0.1\text{rpm}$ ,  $m_a=0.083\text{kg/s}$  and  $T_r=60\text{C}$ ,

in Figure 5.24, at  $N_{RR}=15\text{rpm}$ ,  $N_{DW}=0.1\text{rpm}$ ,  $m_a=0.056\text{kg/s}$  and  $T_r=70\text{C}$ ,

in Figure 5.24, at  $N_{RR}=20\text{rpm}$ ,  $N_{DW}=0.1\text{rpm}$ ,  $m_a=0.056\text{kg/s}$  and  $T_r=70\text{C}$ ,

in Figure 5.25, at  $N_{RR}=10\text{rpm}$ ,  $N_{DW}=0.4\text{rpm}$ ,  $m_a=0.083\text{kg/s}$  and  $T_r=70\text{C}$ ,

in Figure 5.28, at  $N_{RR}=5\text{rpm}$ ,  $N_{DW}=0.1\text{rpm}$ ,  $m_a=0.056\text{kg/s}$  and  $T_r=80\text{C}$ ,

in Figure 5.33, at  $N_{RR}=5\text{rpm}$ ,  $N_{DW}=0.2\text{rpm}$ ,  $m_a=0.083\text{kg/s}$  and  $T_r=90\text{C}$ , and

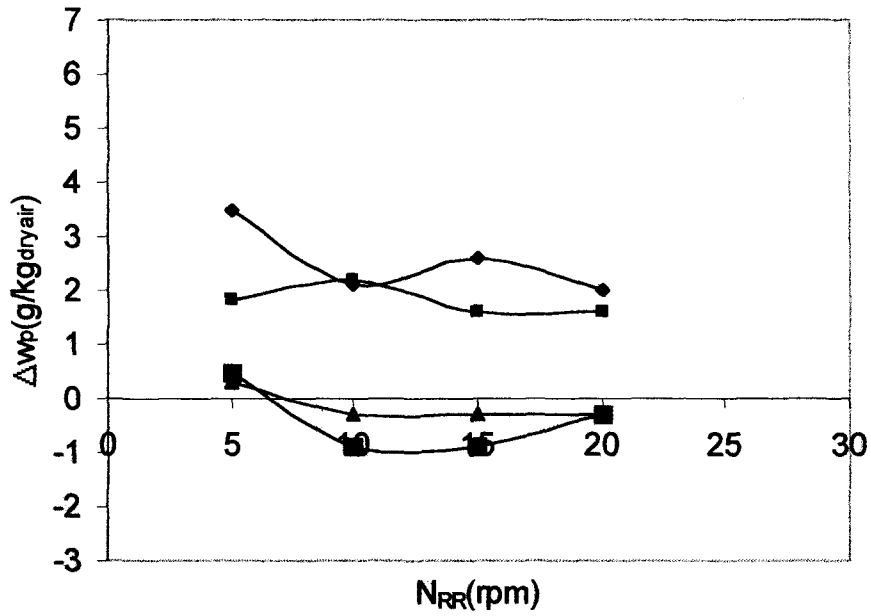
in Figure 5.35. at  $N_{RR}=5\text{rpm}$ ,  $N_{DW}=0.1\text{rpm}$ ,  $m_a=0.139\text{kg/s}$  and  $T_r=90\text{C}$ .

For all other test cases in the constructed test system  $\Delta w_p \neq \Delta w_r$  was obtained. In order to achieve  $\Delta w_p \cong \Delta w_r$  DW should be operated in unbalanced flow mode. It can be concluded from Figures 5.20-5.35 that  $\Delta w$  decreases with increasing  $N_{DW}$  in process and regeneration side of DW.

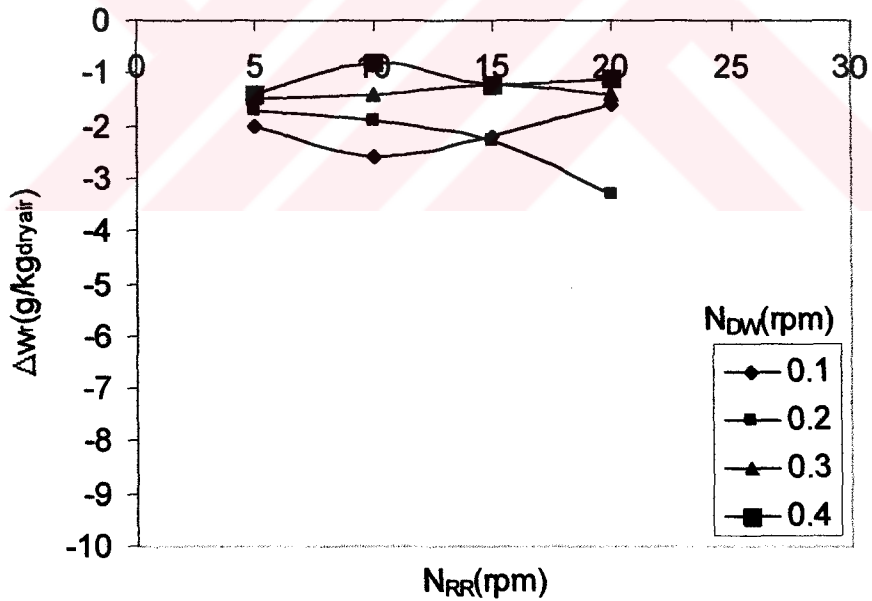
Furthermore following points can also be derived by close inspection of the related figures:

As can be seen from Figure 5.21.a, b, Figure 5.22.a, b, and Figure 5.24.a, b as the sample ones moisture removal capacity of DW in process and regeneration lines is severely influenced by  $N_{RR}$  and  $N_{DW}$ . This means that rotational speeds of both RR and DW are very important for the case of mass transfers. The magnitudes of moisture removal are also affected by  $m_a$  and  $T_r$  as logically expected. However the physics of mass transfer is so complicated that it seems to be impossible to evaluate the relative order of importance of the parameters  $m_a$  and  $T_r$  as well as  $N_{RR}$  and  $N_{DW}$ .

It is also difficult to determine the similarities in process and regeneration lines since the behavior of the curves plotted in a and b parts of figures is not the same or at least similar all the time.



(a)



(b)

Figure 5.20 Variation of moisture removal capacity of DW as a function of  $N_{RR}$  and  $N_{DW}$  at  $m_a=0.056\text{kg/s}$ , and  $T_r=60\text{C}$   
 a) For process side, b) For regeneration side

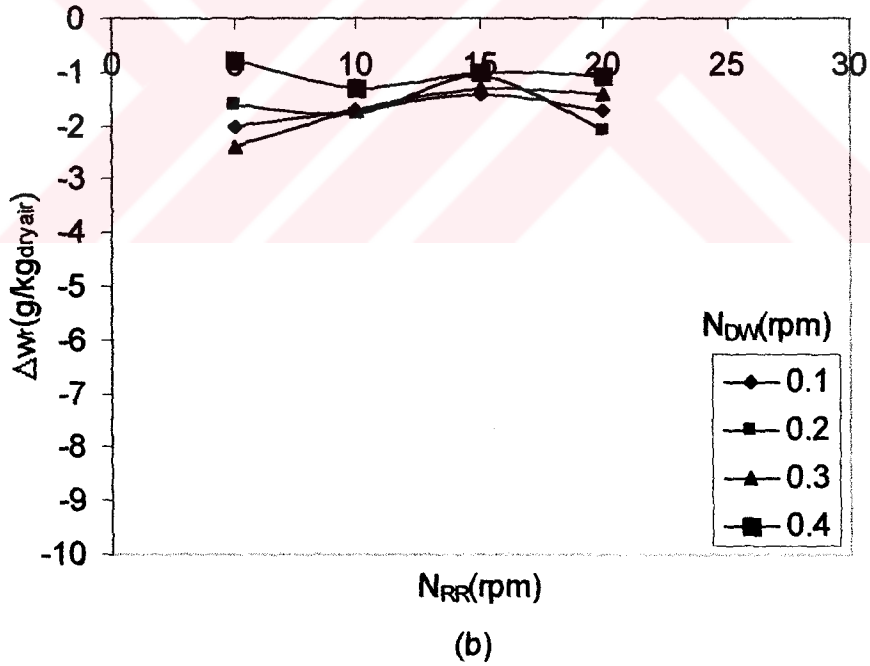
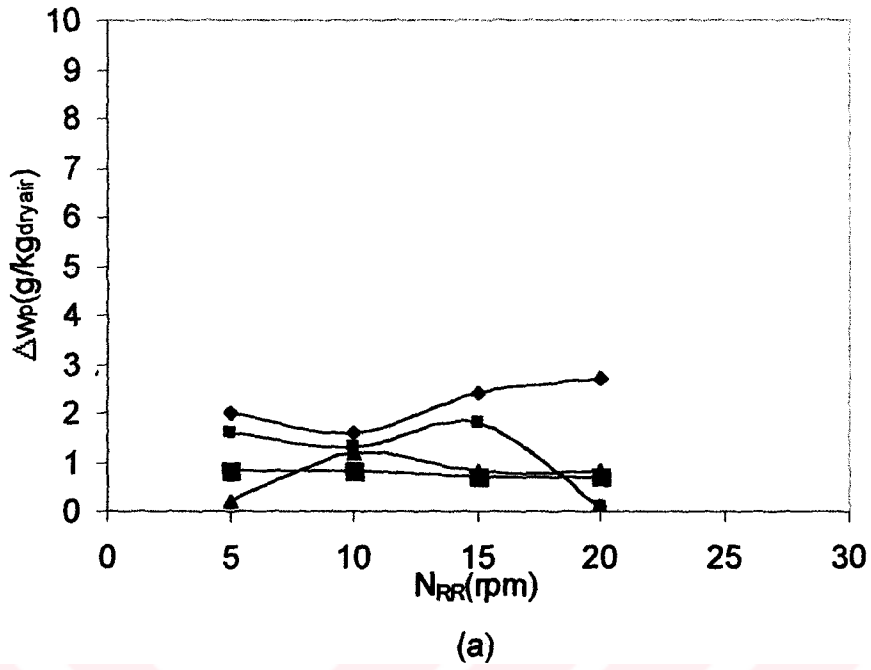


Figure 5.21 Variation of moisture removal capacity of DW as a function of  $N_{RR}$  and  $N_{DW}$  at  $m_a=0.083\text{kg/s}$ , and  $T_r=60\text{C}$   
 a) For process side, b) For regeneration side

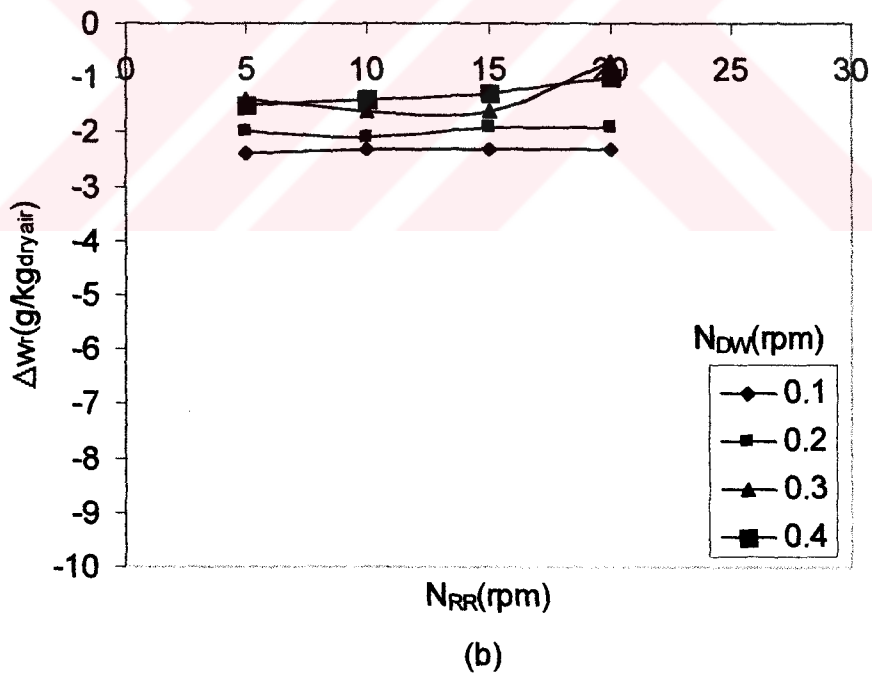
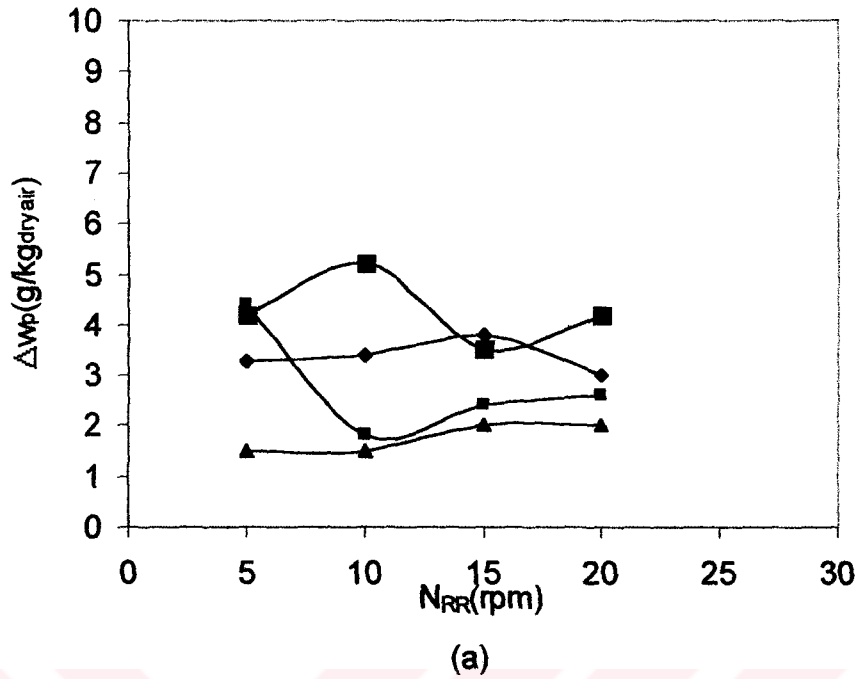
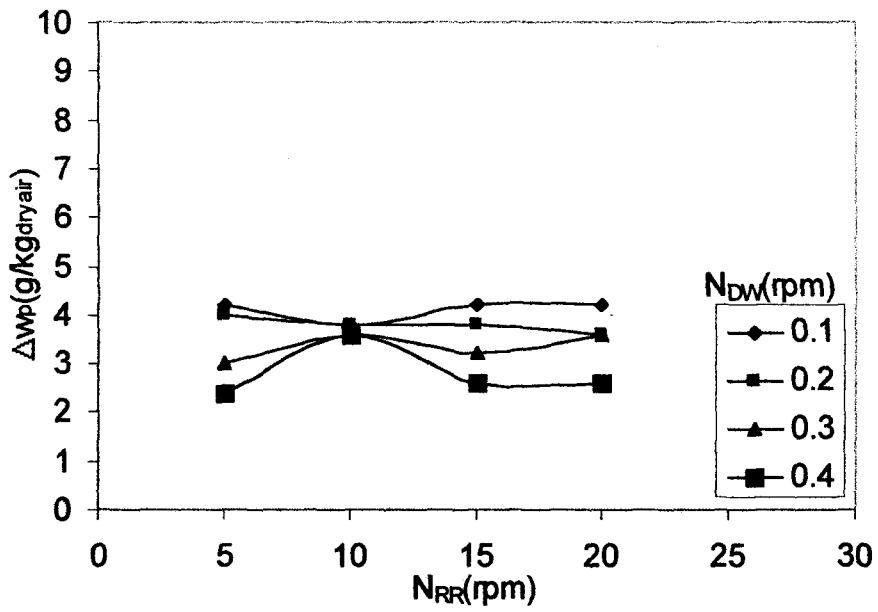
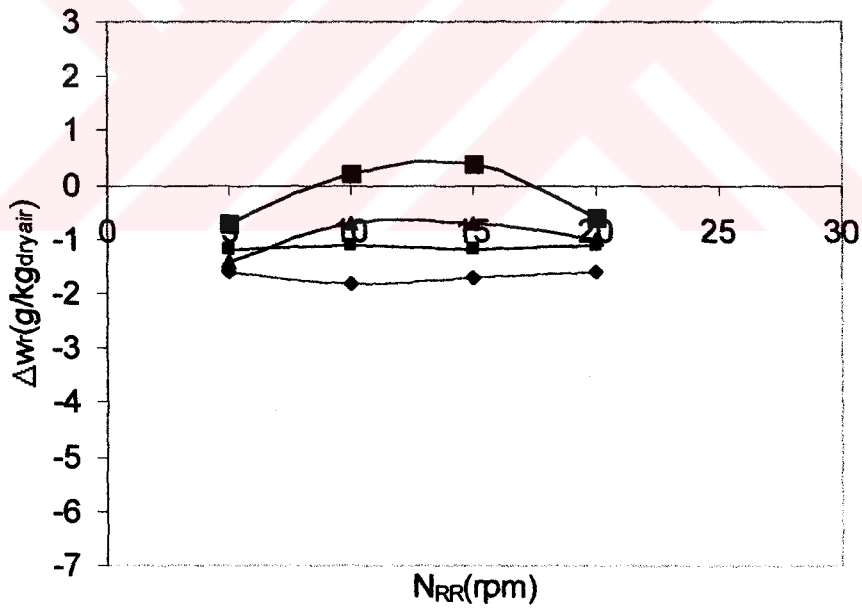


Figure 5.22 Variation of moisture removal capacity of DW as a function of  $N_{RR}$  and  $N_{DW}$  at  $m_a=0.111\text{kg/s}$ , and  $T_r=60\text{C}$   
 a) For process side, b) For regeneration side

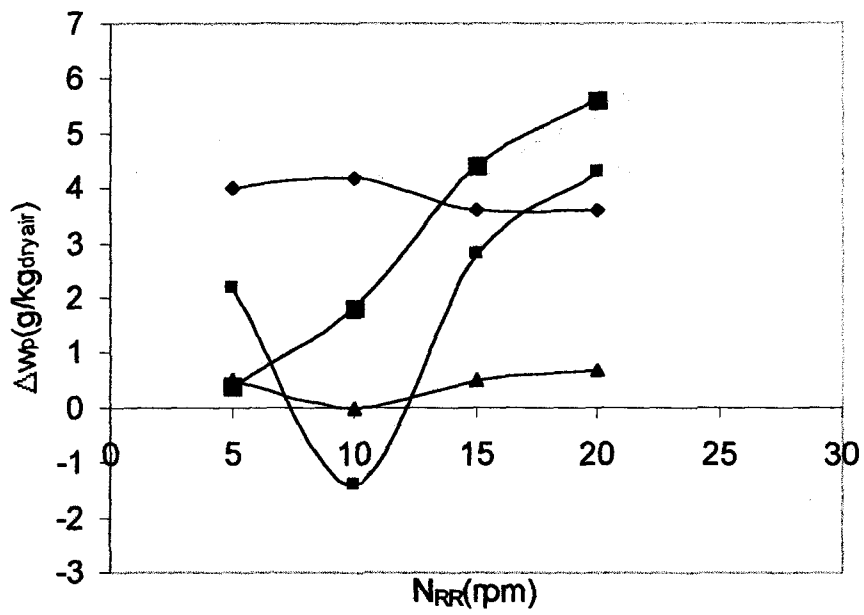


(a)

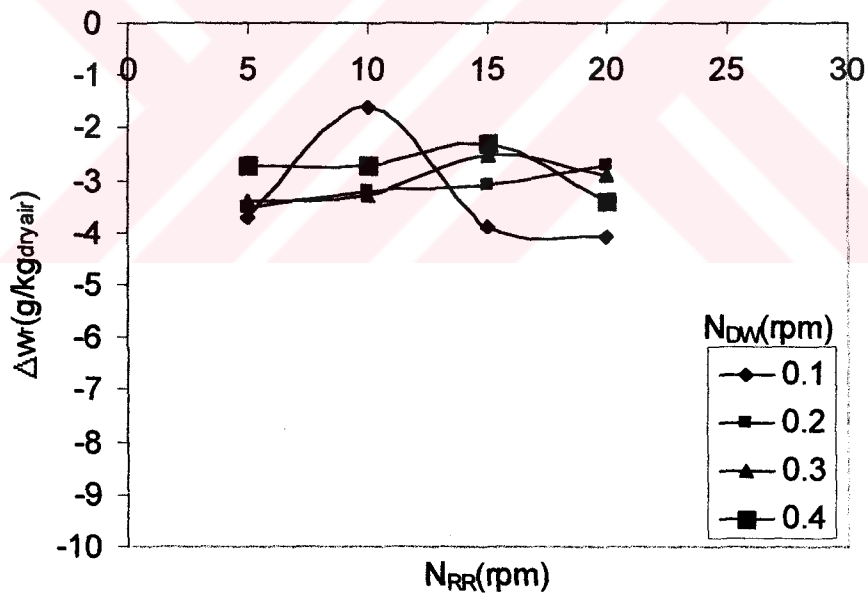


(b)

Figure 5.23 Variation of moisture removal capacity of DW as a function of  $N_{RR}$  and  $N_{DW}$  at  $m_a = 0.139 \text{ kg/s}$ , and  $T_r = 60^\circ\text{C}$   
 a) For process side, b) For regeneration side

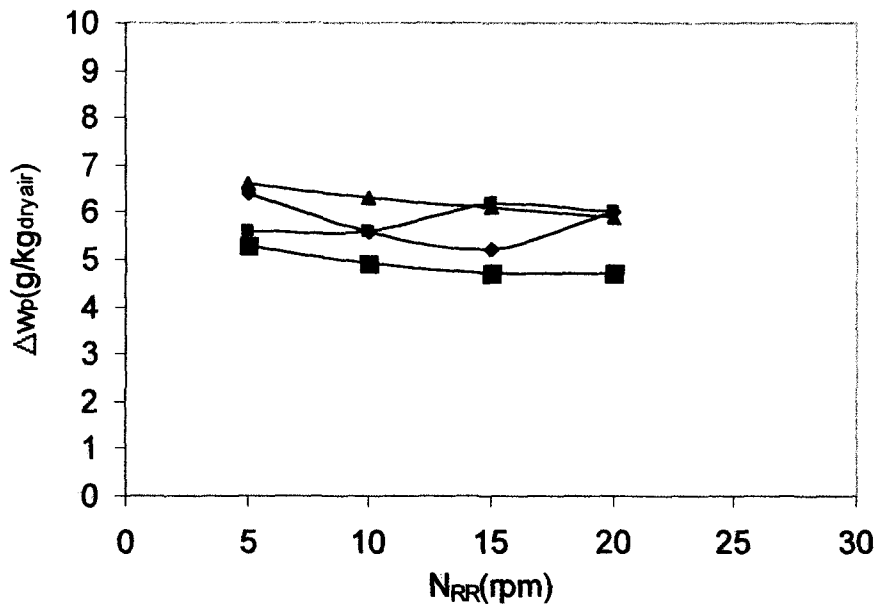


(a)

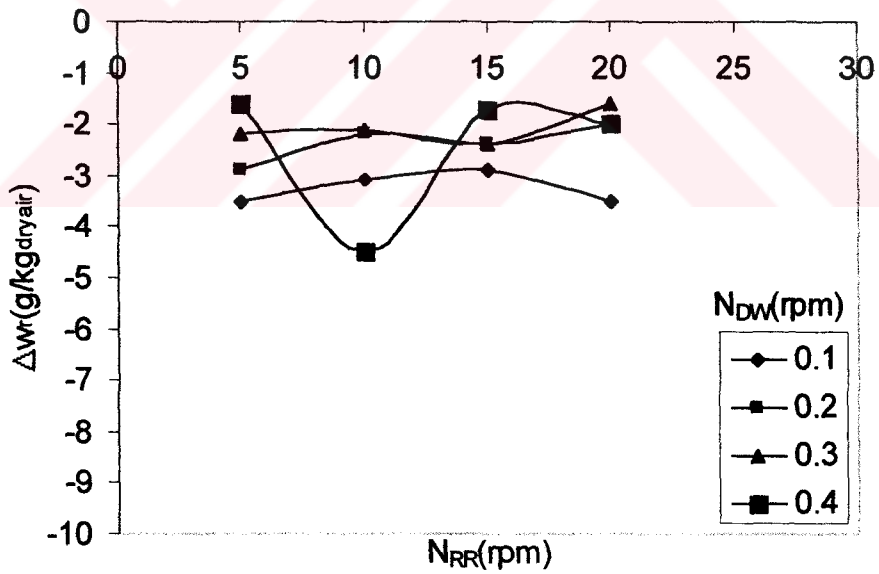


(b)

Figure 5.24 Variation of moisture removal capacity of DW as a function of  $N_{RR}$  and  $N_{DW}$  at  $m_a=0.056\text{kg/s}$ , and  $T_r=70\text{C}$   
 a) For process side, b) For regeneration side



(a)



(b)

Figure 5.25 Variation of moisture removal capacity of DW as a function of  $N_{RR}$  and  $N_{DW}$  at  $m_a=0.083\text{kg/s}$ , and  $T_r=70\text{C}$   
 a) For process side, b) For regeneration side



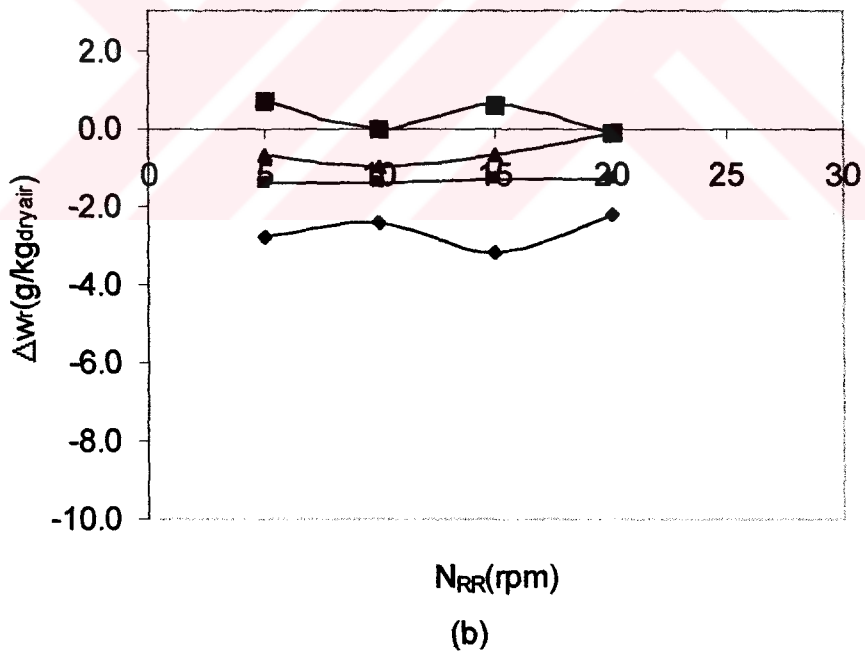
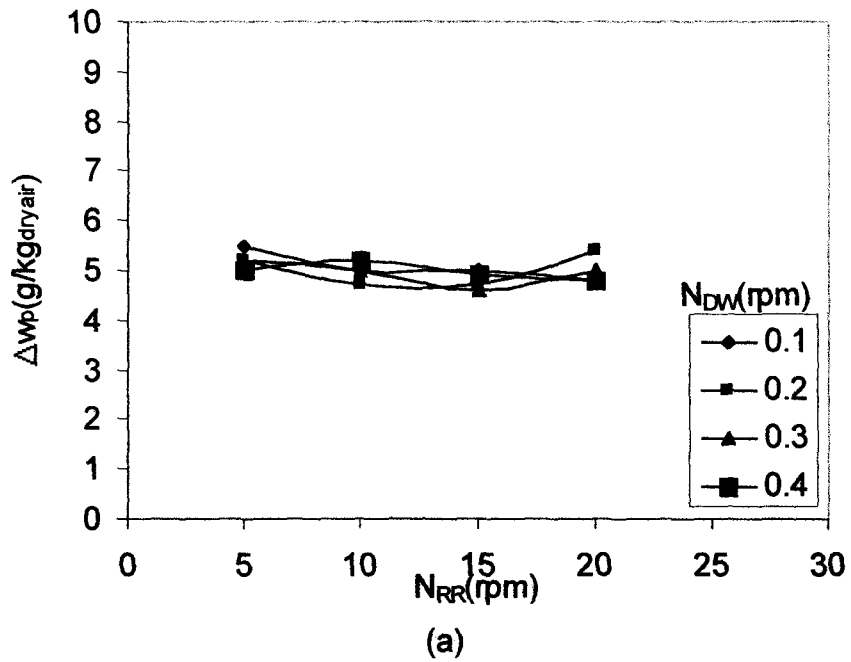
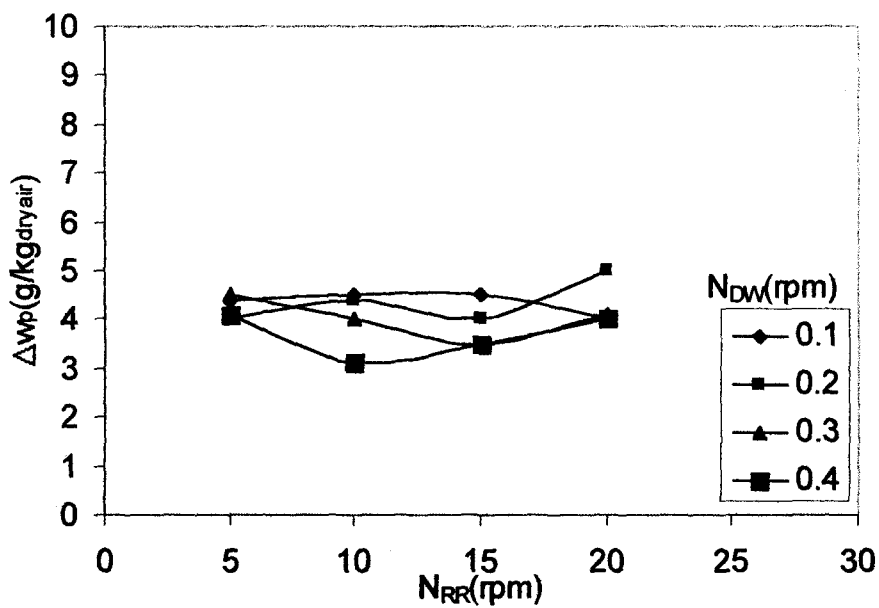
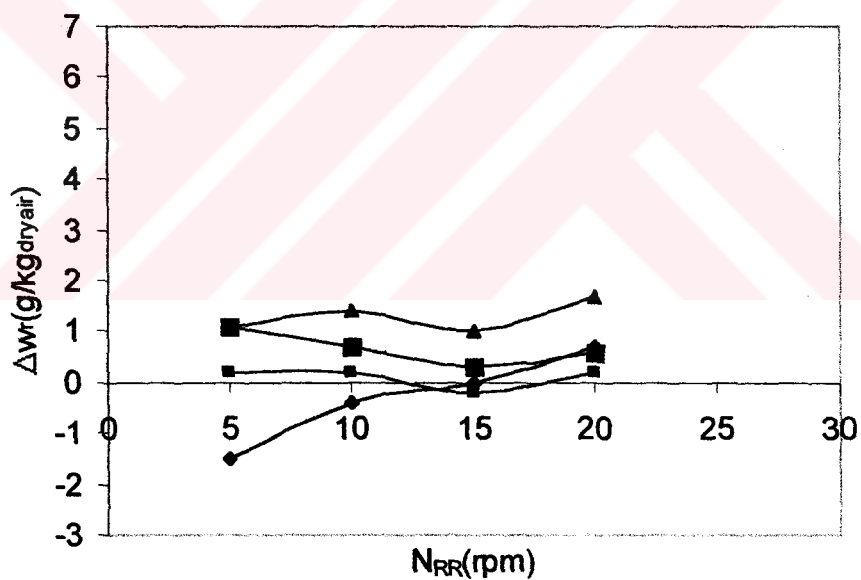


Figure 5.26 Variation of moisture removal capacity of DW as a function of  $N_{RR}$  and  $N_{DW}$  at  $m_a=0.111\text{kg/s}$ , and  $T_r=70\text{C}$   
 a) For process side, b) For regeneration side

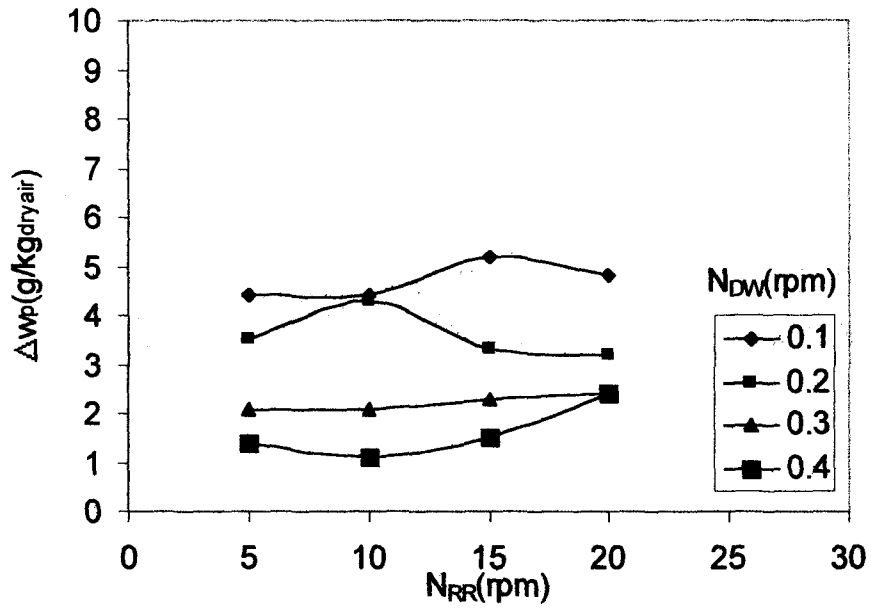


(a)

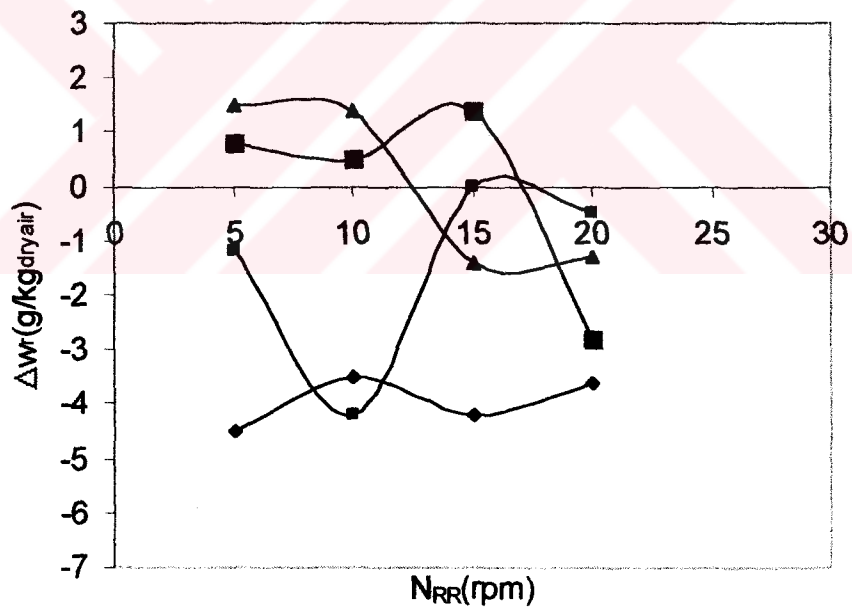


(b)

Figure 5.27 Variation of moisture removal capacity of DW as a function of  $N_{RR}$  and  $N_{DW}$  at  $m_a=0.139\text{kg/s}$ , and  $T_r=70\text{C}$   
 a) For process side, b) For regeneration side



(a)



(b)

Figure 5.28 Variation of moisture removal capacity of DW as a function of  $N_{RR}$  and  $N_{DW}$  at  $m_a=0.056\text{kg/s}$ , and  $T_r=80\text{C}$   
 a) For process side, b) For regeneration side

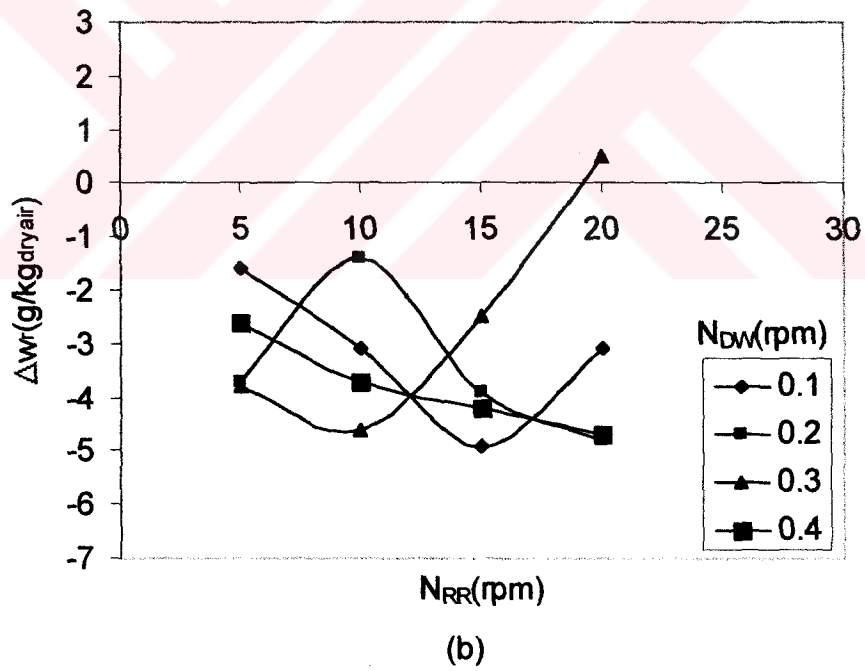
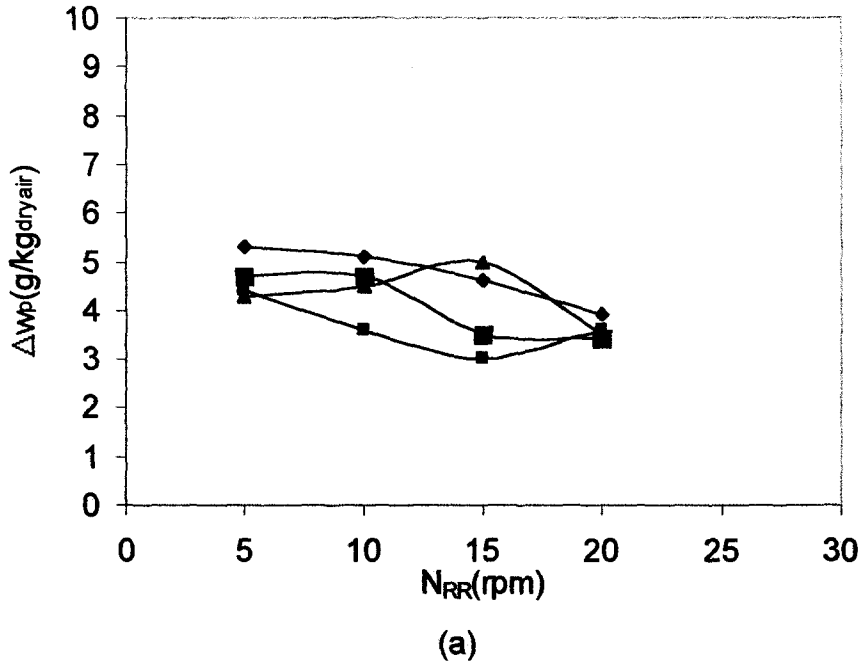
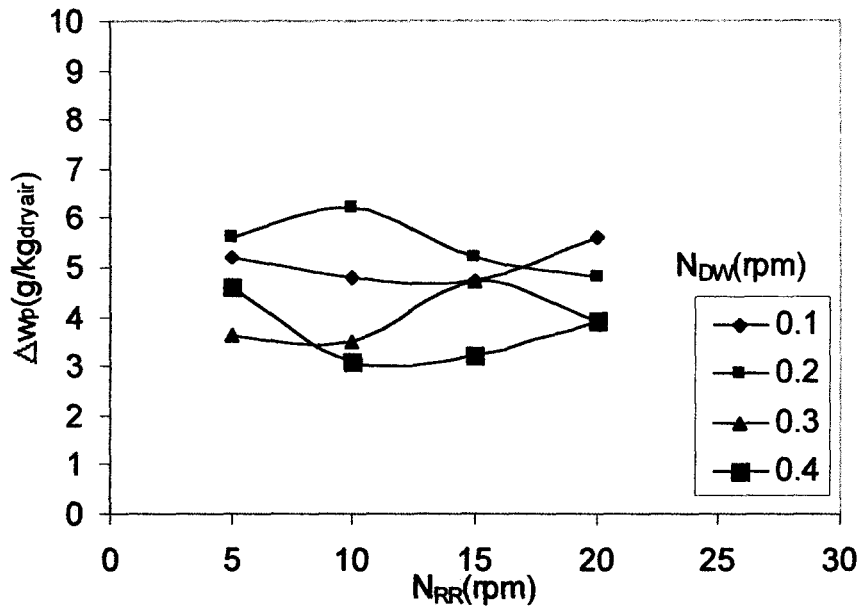
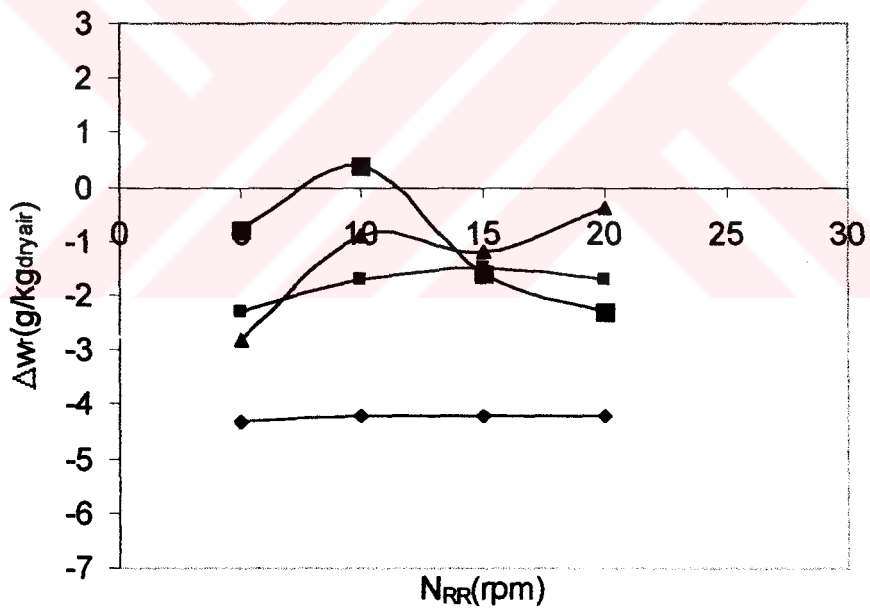


Figure 5.29 Variation of moisture removal capacity of DW as a function of  $N_{RR}$  and  $N_{DW}$  at  $m_a=0.083\text{kg/s}$ , and  $T_r=80\text{C}$   
 a) For process side, b) For regeneration side

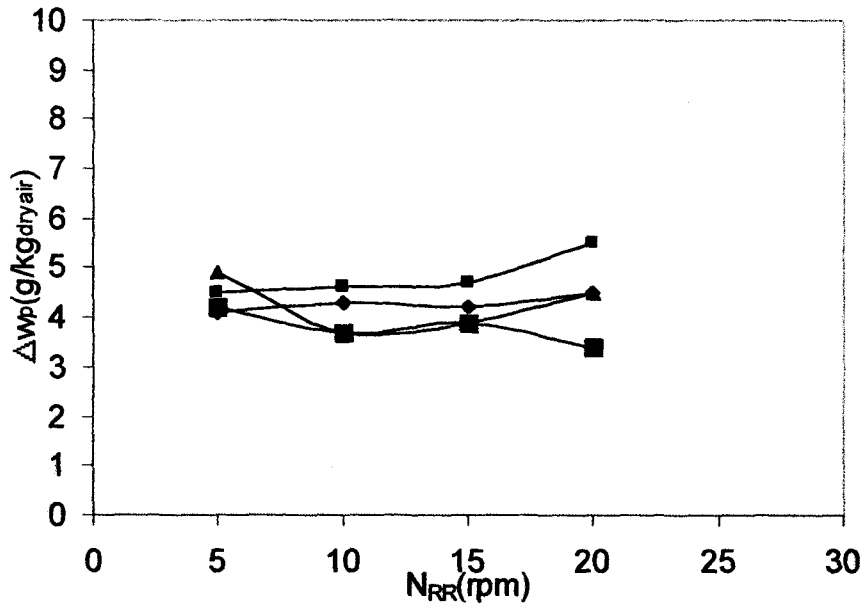


(a)

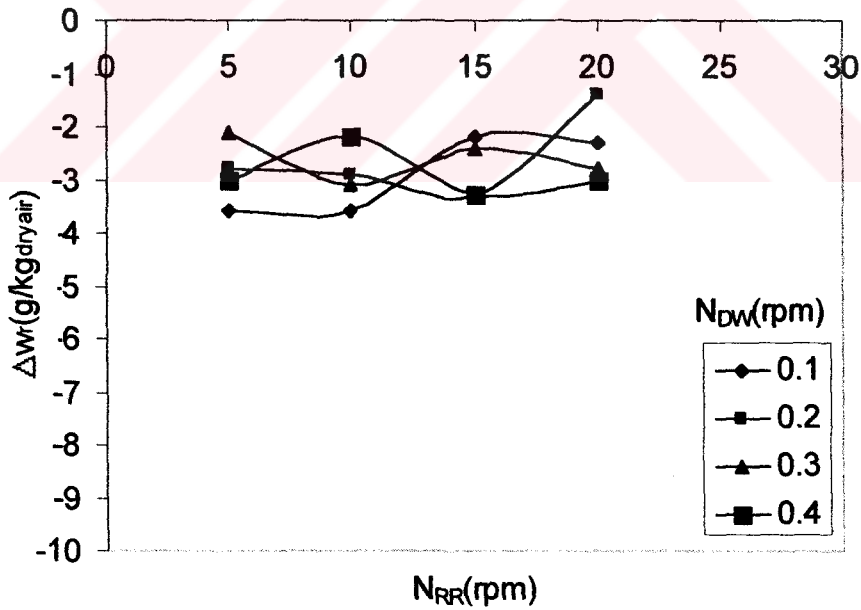


(b)

Figure 5.30 Variation of moisture removal capacity of DW as a function of  $N_{RR}$  and  $N_{DW}$  at  $m_a=0.111\text{kg/s}$ , and  $T_r=80\text{C}$   
 a) For process side, b) For regeneration side

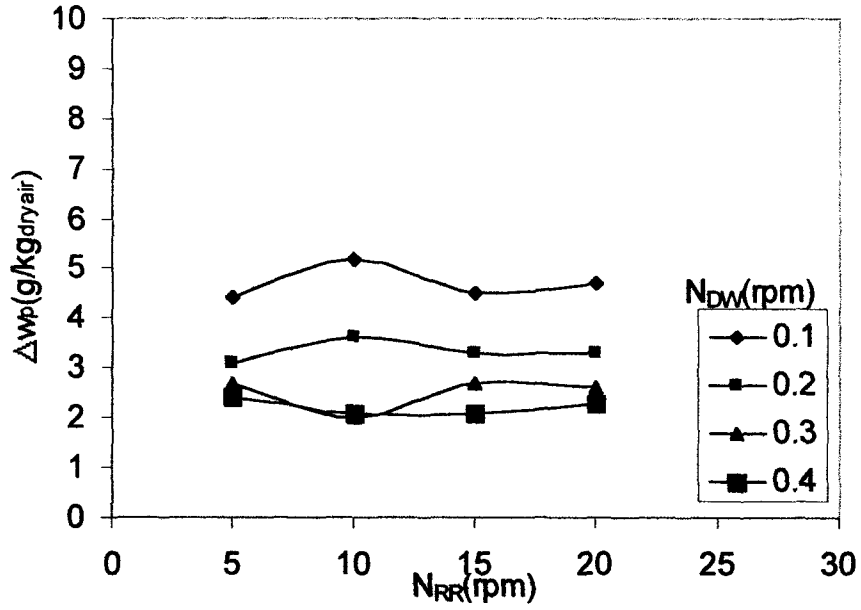


(a)

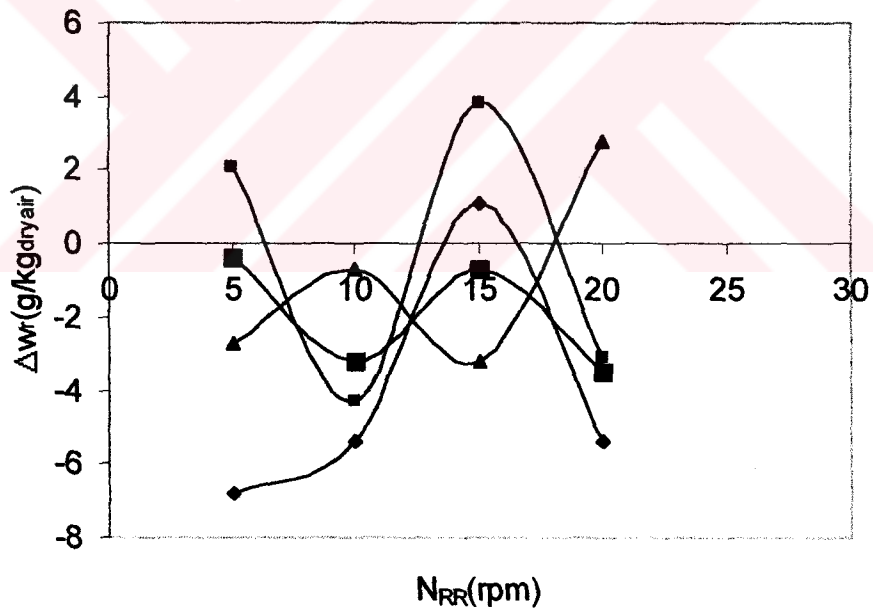


(b)

Figure 5.31 Variation of moisture removal capacity of DW as a function of  $N_{RR}$  and  $N_{DW}$  at  $m_a=0.139\text{kg/s}$ , and  $T_r=80\text{C}$   
 a) For process side, b) For regeneration side

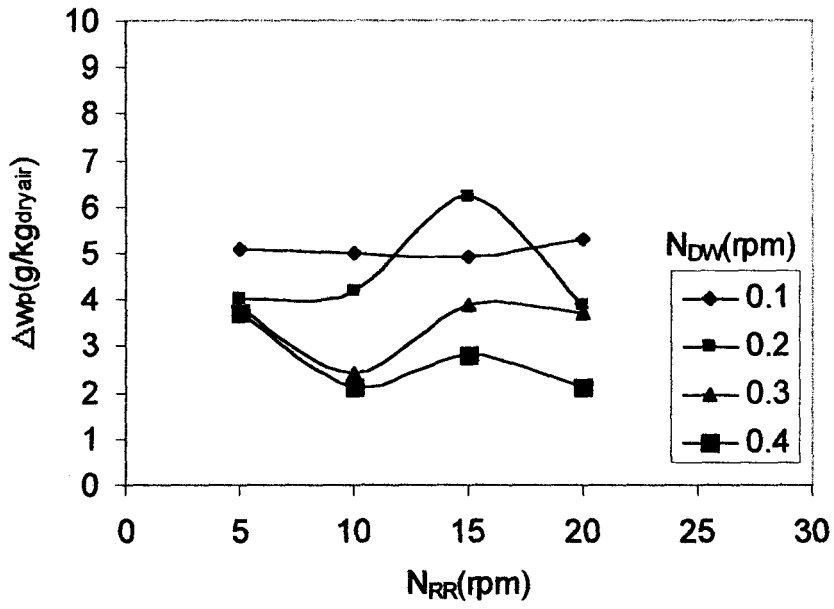


(a)

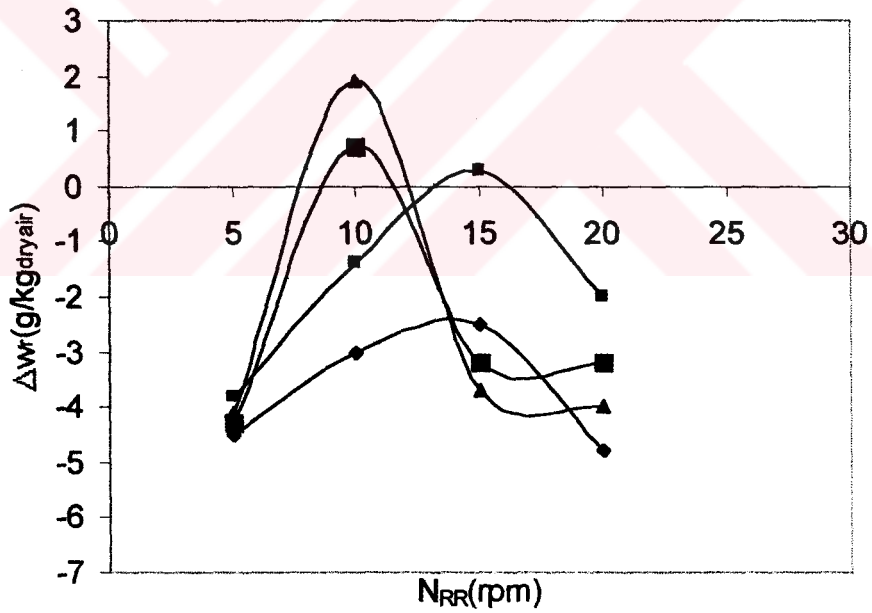


(b)

Figure 5.32 Variation of moisture removal capacity of DW as a function of  $N_{RR}$  and  $N_{DW}$  at  $m_a=0.056\text{kg/s}$ , and  $T_r=90\text{C}$   
 a) For process side, b) For regeneration side



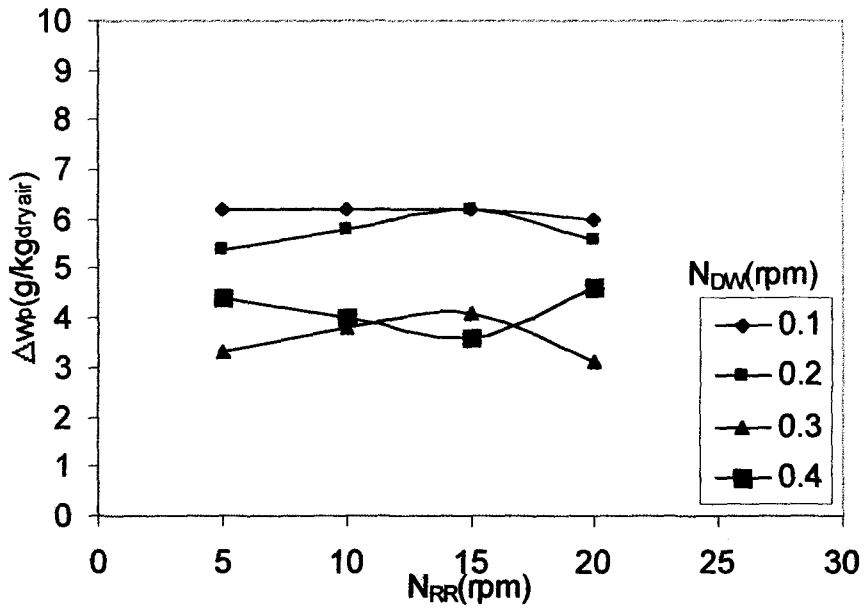
(a)



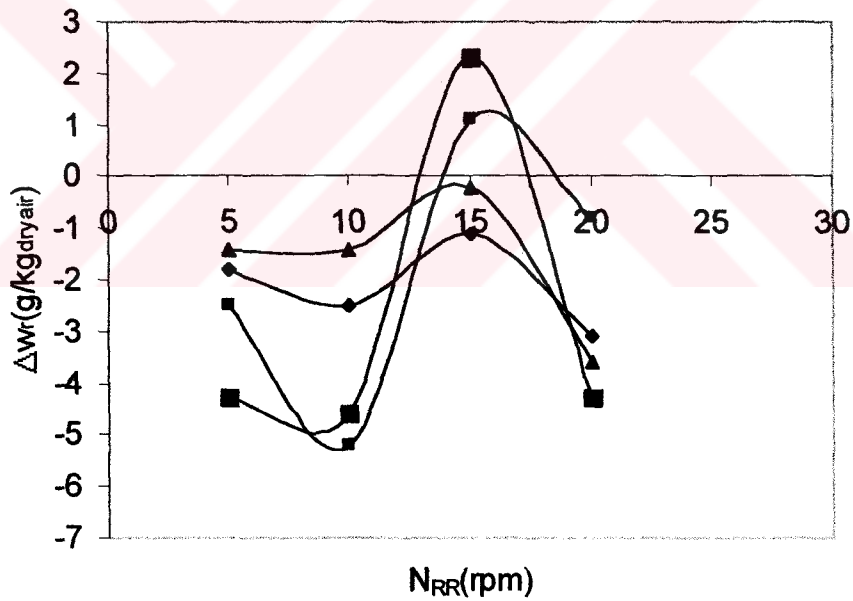
(b)

Figure 5.33 Variation of moisture removal capacity of DW as a function of  $N_{RR}$  and  $N_{DW}$  at  $m_a=0.083\text{kg/s}$ , and  $T_r=90\text{C}$   
 a) For process side, b) For regeneration side



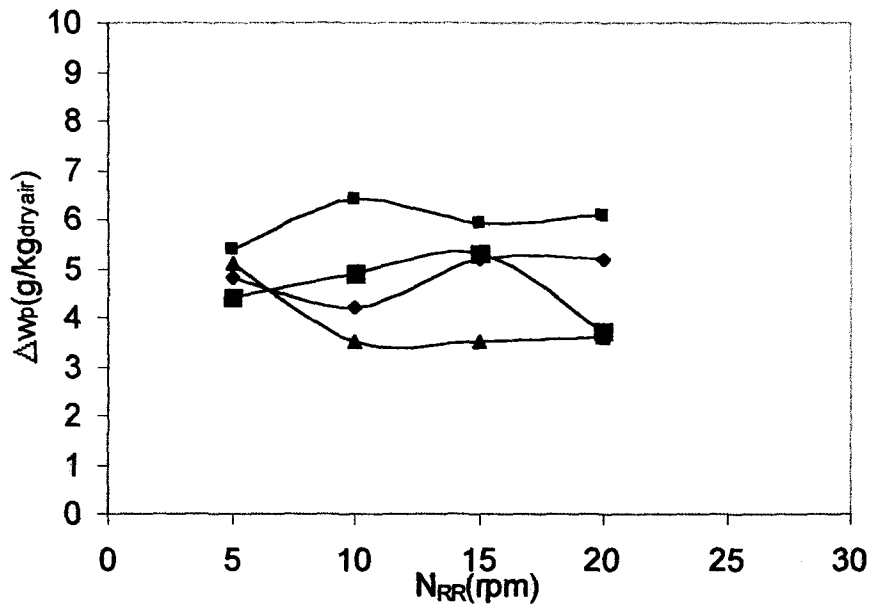


(a)

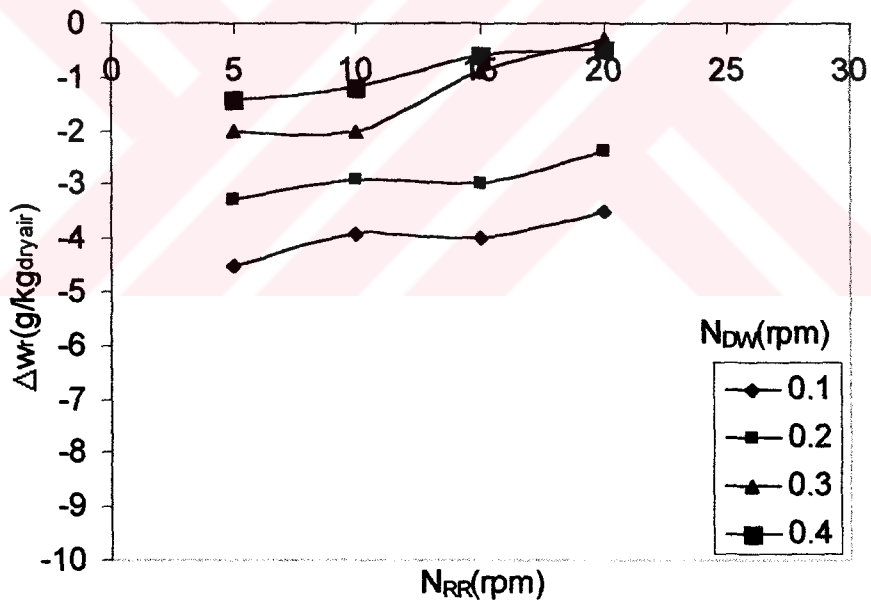


(b)

Figure 5.34 Variation of moisture removal capacity of DW as a function of  $N_{RR}$  and  $N_{DW}$  at  $m_a=0.111\text{kg/s}$ , and  $T_r=90\text{C}$   
 a) For process side, b) For regeneration side



(a)



(b)

Figure 5.35 Variation of moisture removal capacity of DW as a function of  $N_{RR}$  and  $N_{DW}$  at  $m_a=0.139\text{kg/s}$ , and  $T_r=90\text{C}$   
 a) For process side, b) For regeneration side

### 5.3.3 Effects of $N_{RR}$ and $N_{DW}$ on $\varepsilon_{RR}$ and $\varepsilon_{EC}$

Two  $\varepsilon$  factors one defined for RR and the other for EC are given as a function of  $N_{RR}$  for different  $N_{DW}$  with  $T_r$ ,  $m_a$  variables covered as can be seen in Figures 5.36-43

As it can be seen in Figures 5.36-39,  $\varepsilon_{RR}$  are close to each other for different  $N_{DW}$  after  $N_{RR}=20\text{rpm}$ , with negligible deviations. Effectiveness of RR is high at  $m_a=0.056\text{kg/s}$ , and  $N_{DW}=0.1\text{rpm}$  for all  $T_r$ . But for high mass flow rates of air, when  $N_{DW}$  increases  $\varepsilon_{RR}$  increases as a function of  $N_{RR}$ .

Figures 5.40-43 indicate that; effectiveness of RR does not rapidly changed with the  $N_{RR}$  and  $N_{DW}$  except Figure 5.40.a, b, and Figure 5.41.a.

As shown in Figures 5.36-43 magnitudes of  $\varepsilon_{EC}$  seem to be between at 0.6-0.7 almost independent of magnitude of  $N_{DW}$  for the case  $T_r=80$  and  $90\text{C}$  at different  $m_a$ . On the other hand for  $\varepsilon_{EC}$  and  $T_r=70\text{C}$   $N_{RR}$  seem to be influenced by both  $N_{DW}$  and  $m_a$  (Figure 5.40.a-d and Figure 5.41.a-d)

$\varepsilon_{RR}$  vs  $N_{RR}$  is seriously influenced by  $N_{DW}$ ,  $m_a$ ,  $T_r$ . It is difficult to estimate which one is the dominant parameter.

In reference to the some of the selected figures in the given series following conclusions can be given for the behavior of  $\varepsilon_{RR}$  and  $\varepsilon_{EC}$  with  $N_{RR}$  under the influence of  $N_{DW}$ ,  $m_a$  and  $T_r$ .

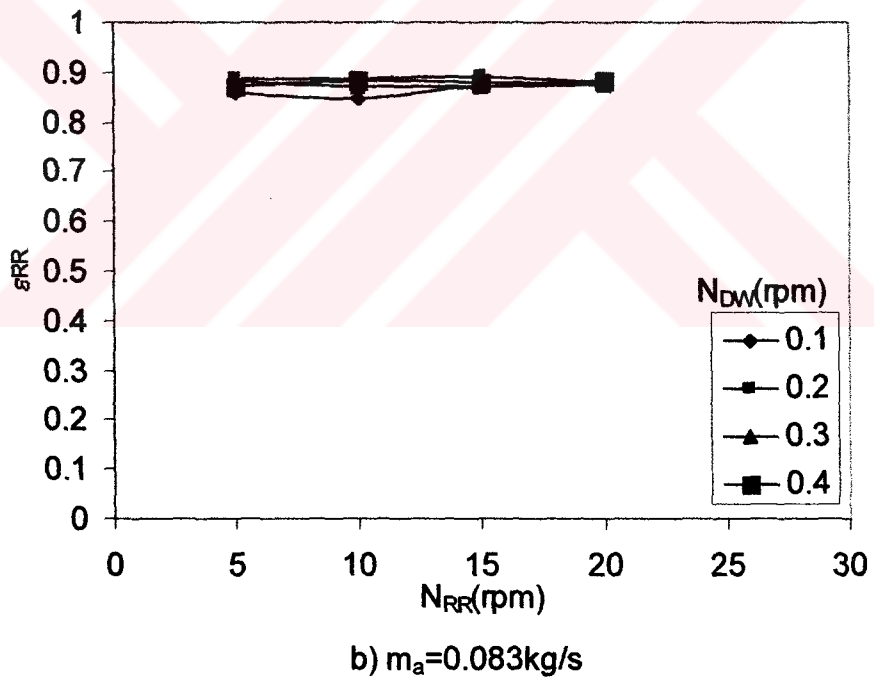
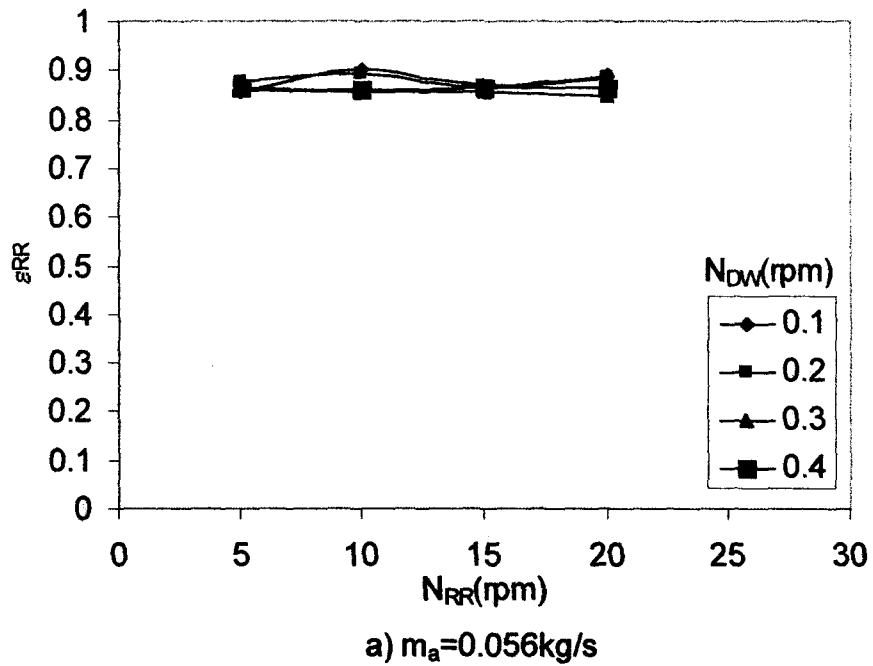
1. At  $T_r=60\text{C}$  and  $T_r=70\text{C}$   $\varepsilon_{RR}$  dependence on  $N_{RR}$  is such that variations in  $N_{DW}$  and  $m_a$  is resulted in severe functional changes (Figures 5.36, and 5.38). The similar observation is seen for the variation of  $\varepsilon_{EC}$  with  $N_{RR}$  (Figures 5.37, and 5.39).
2. With an increase in  $T_r=80\text{C}$ ,  $T_r=90\text{C}$  the behavior of  $\varepsilon_{RR}$  with  $N_{RR}$  and  $\varepsilon_{EC}$  with  $N_{RR}$  become different (Figures 5.40, 5.41, 5.42, and

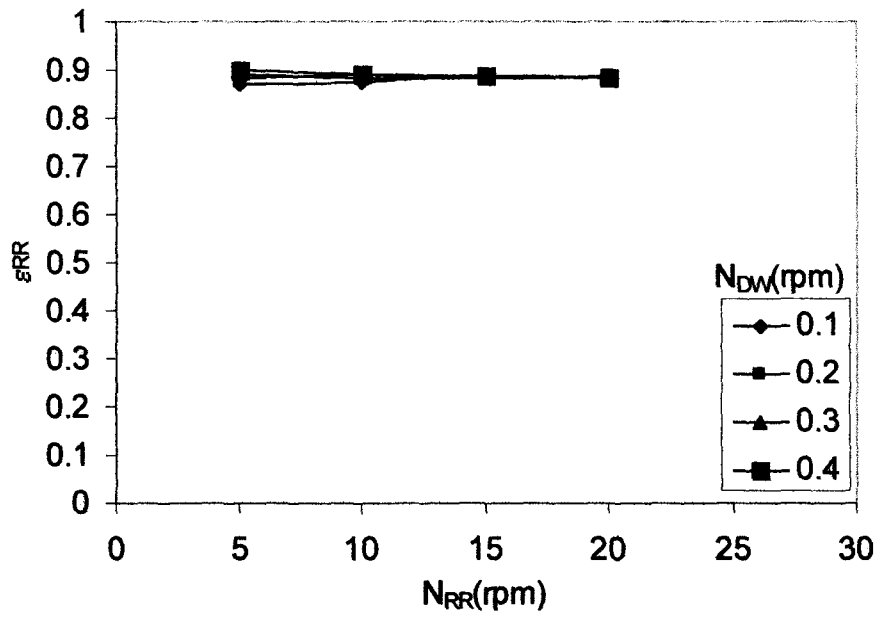
5.43). Since  $m_a$  seems to lose its importance as is seen from Figure 5.43 for the operation of evaporative cooler, with the loss of importance in the magnitude of  $N_{DW}$  (Figure 5.43.b-d). Therefore it can be said that  $\epsilon_{EC}$  as an overall estimation is not seriously influenced by  $m_a$ ,  $N_{DW}$  at high  $T_r > 80C$ . However it is difficult to suggest similar behavior for  $\epsilon_{RR}$ .

As it can be seen in Figures 5.36, 5.38, 5.40, and 5.42, the effectiveness of RR is not seriously influenced by the operating parameters such as  $N_{RR}$ ,  $N_{DW}$ ,  $m_a$ , and  $T_r$ .  $\epsilon_{RR}$  is approximately 0.9 (90%) for the selected ranges of the operating parameters with small deviations.

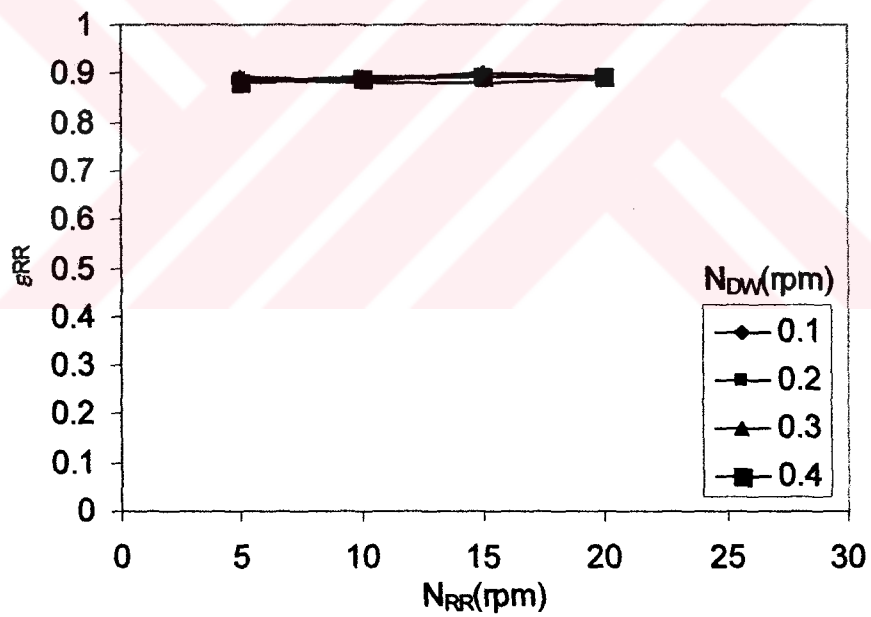
Meanwhile  $\epsilon_{EC}$  is under the influence of all operating parameters as it can be seen in Figures 5.37, 5.39, 5.41, and 5.43. It is clearly seen in the figures  $\epsilon_{EC}$  decreases with increasing  $T_r$ .

Effects of  $N_{RR}$  and  $N_{DW}$  on  $\epsilon_{EC}$  is seen in Figure 5.37 at  $T_r = 60C$ . Influences of  $N_{RR}$  and  $N_{DW}$  decreases for  $T_r > 70C$ . The magnitude of  $\epsilon_{EC}$  are close to each other for all  $N_{RR}$ ,  $N_{DW}$ , and  $m_a$  at  $T_r > 70C$ .  $\epsilon_{EC}$  also approach to each other for  $N_{RR} = 20\text{rpm}$  and  $T_r = 60C$ .



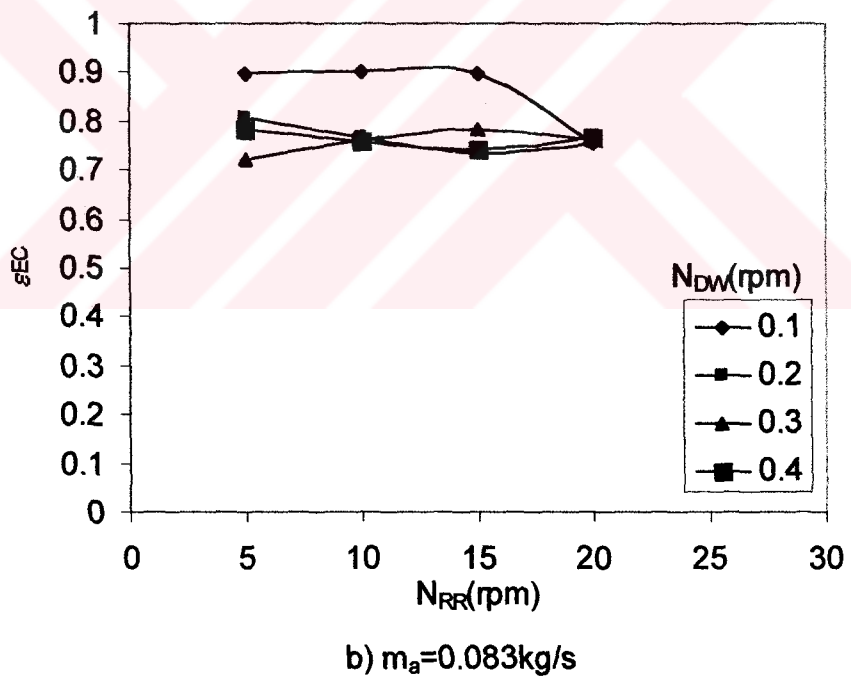
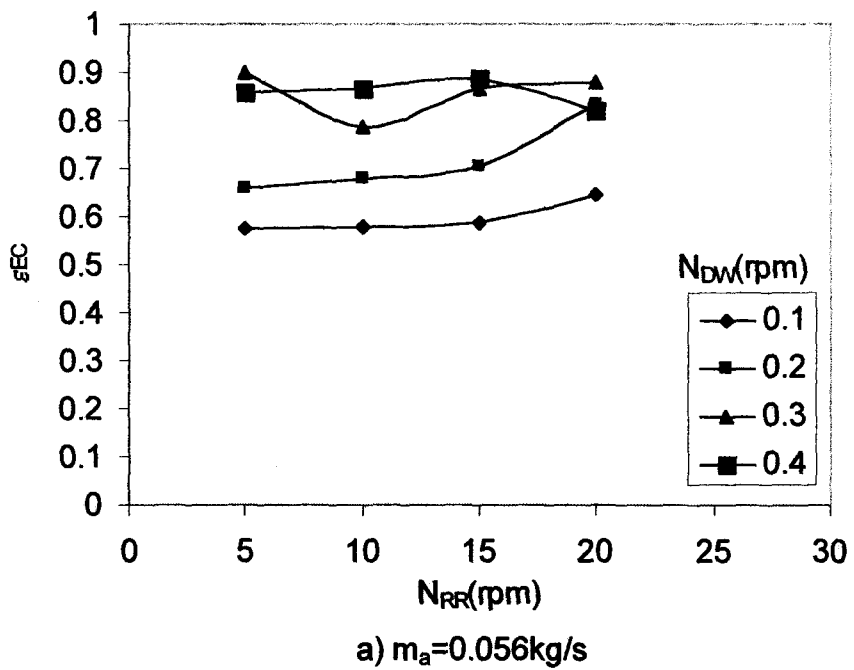


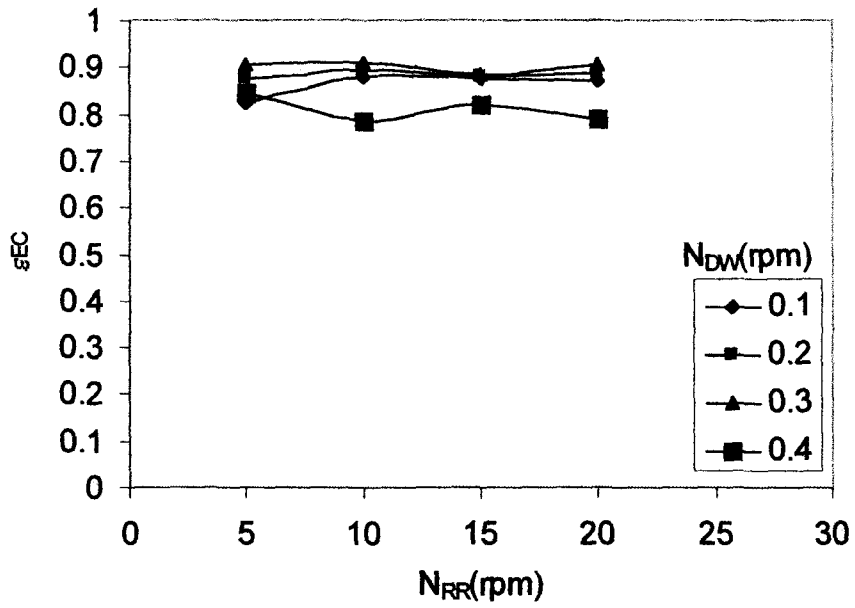
c)  $m_a = 0.111 \text{ kg/s}$



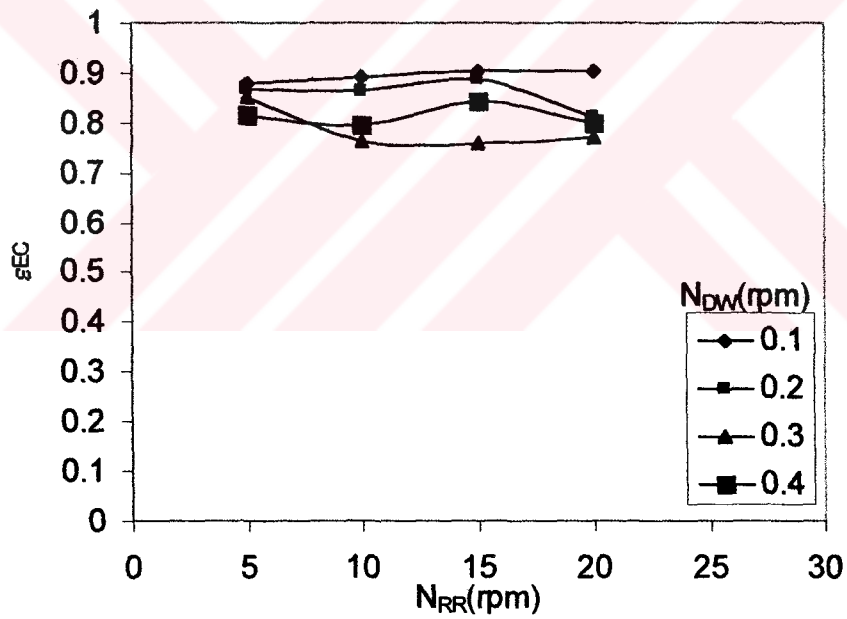
d)  $m_a = 0.139 \text{ kg/s}$

Figure 5.36 Effectiveness of RR as a function of  $N_{RR}$  and  $N_{DW}$  for  $T_r = 60^\circ\text{C}$





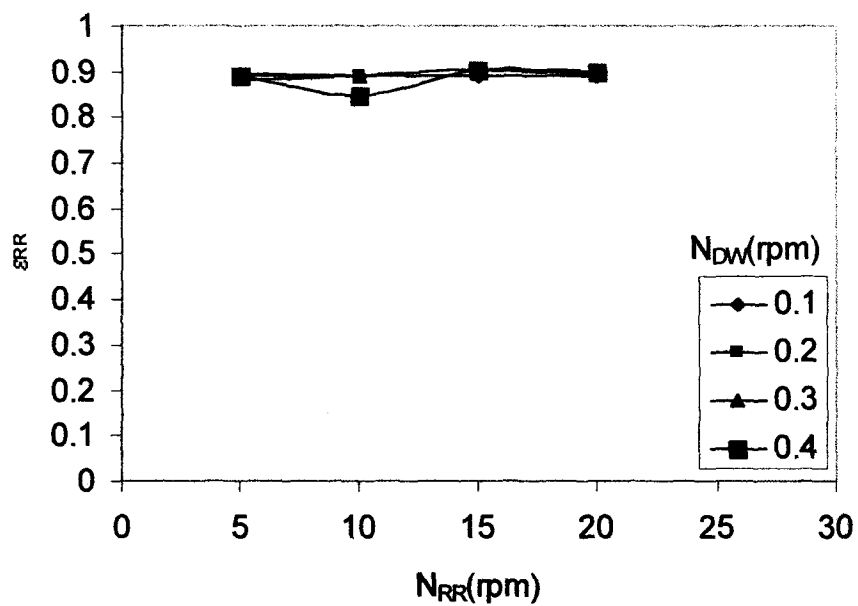
c)  $m_a = 0.111 \text{ kg/s}$



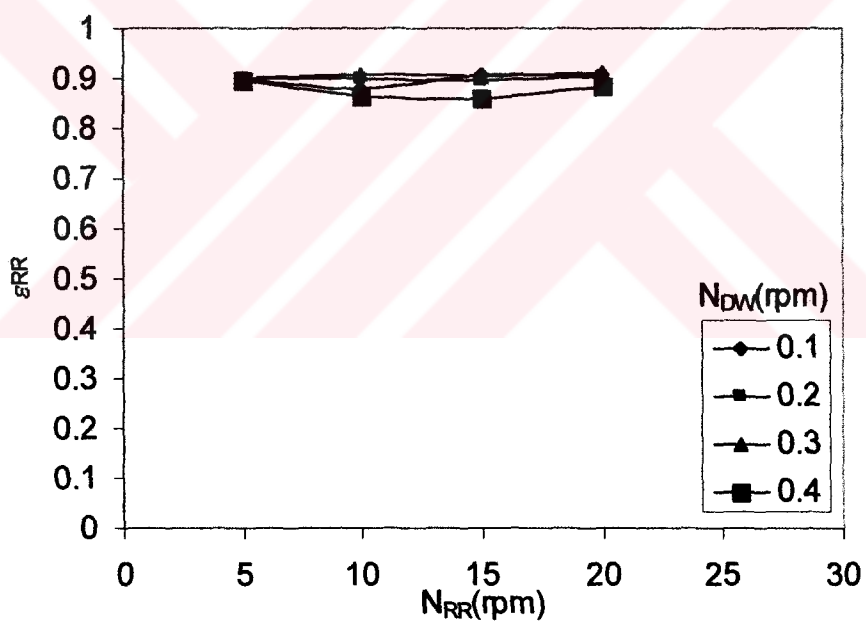
d)  $m_a = 0.139 \text{ kg/s}$

Figure 5.37 Effectiveness of EC as a function of  $N_{RR}$  and  $N_{DW}$  for  $T_r = 60\text{C}$

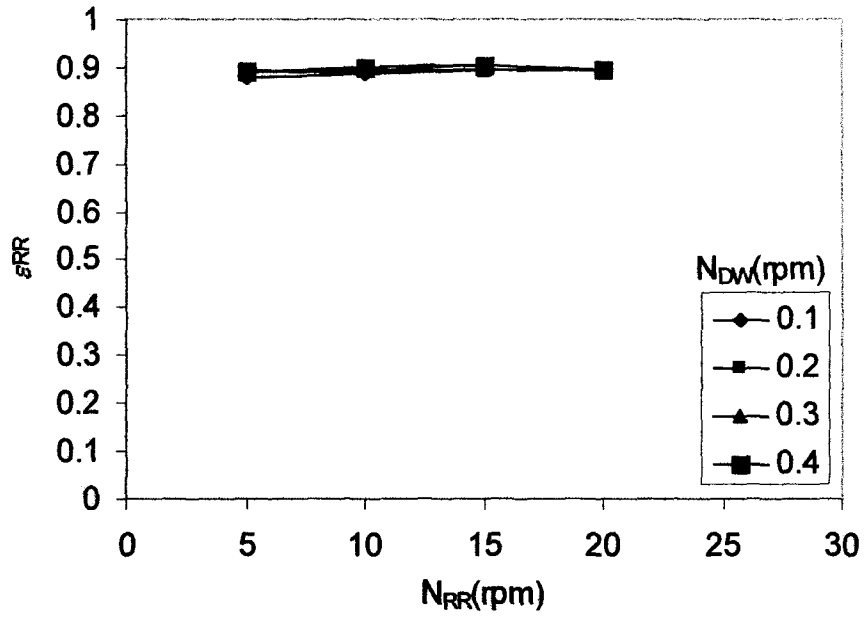




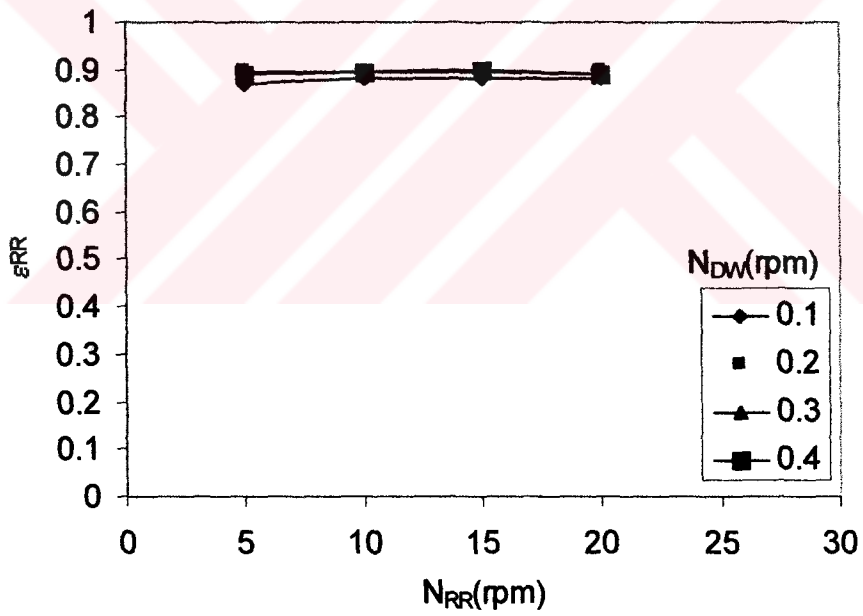
a)  $m_a = 0.056 \text{ kg/s}$



b)  $m_a = 0.083 \text{ kg/s}$

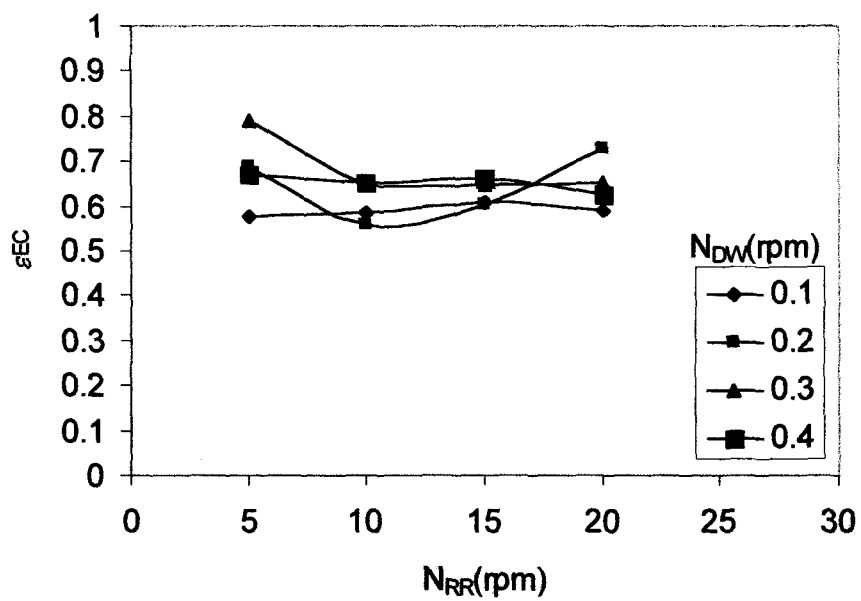
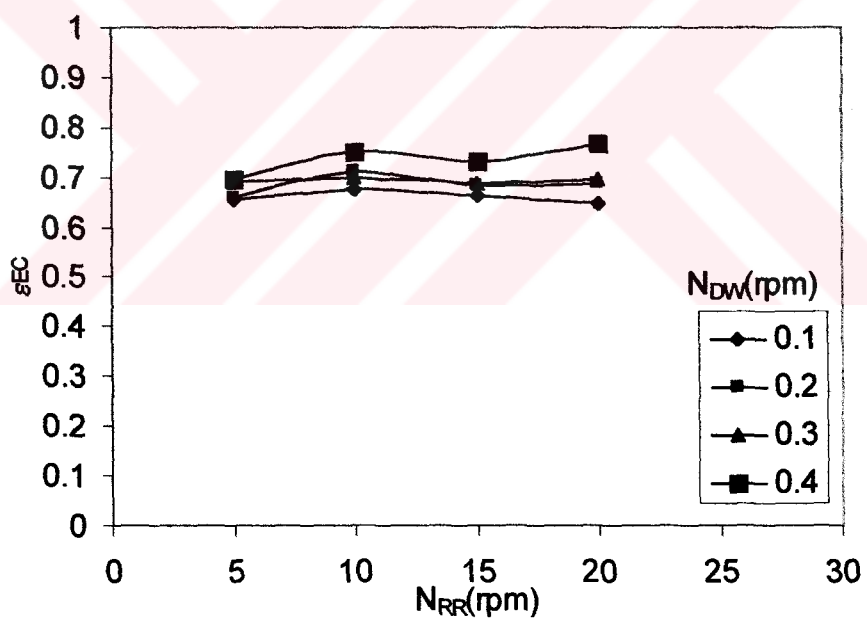


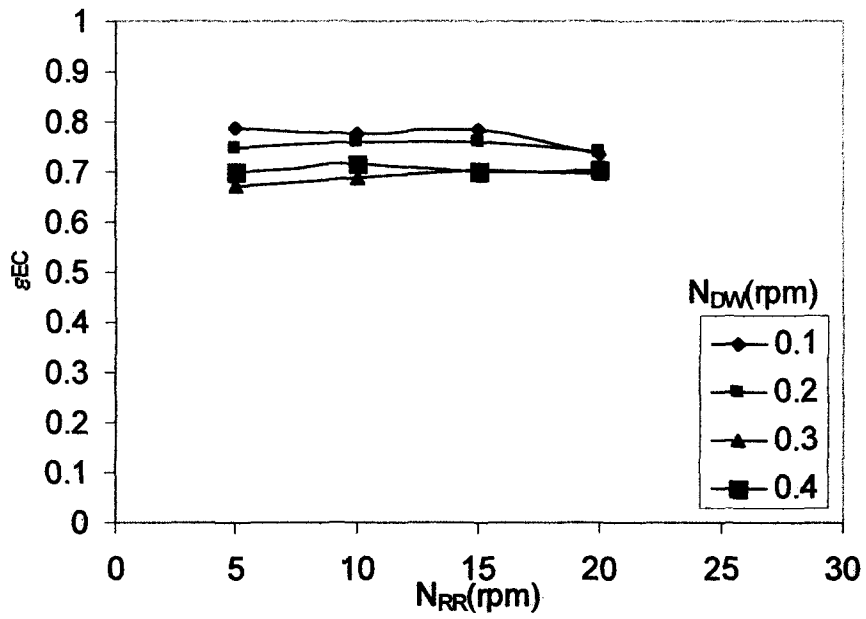
c)  $m_a = 0.111 \text{ kg/s}$



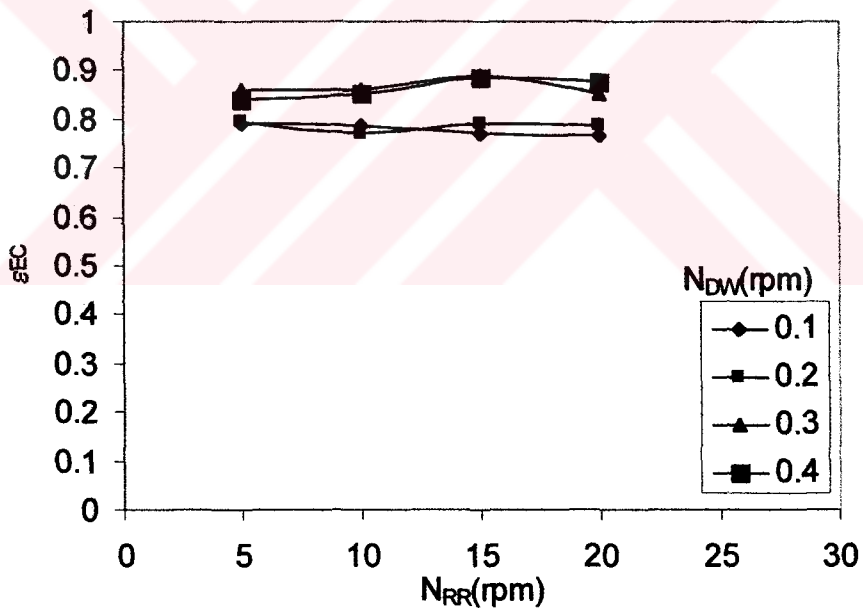
d)  $m_a = 0.139 \text{ kg/s}$

Figure 5.38 Effectiveness of RR as a function of  $N_{RR}$  and  $N_{DW}$  for  $T_r = 70\text{C}$

a)  $m_a = 0.056 \text{ kg/s}$ b)  $m_a = 0.083 \text{ kg/s}$

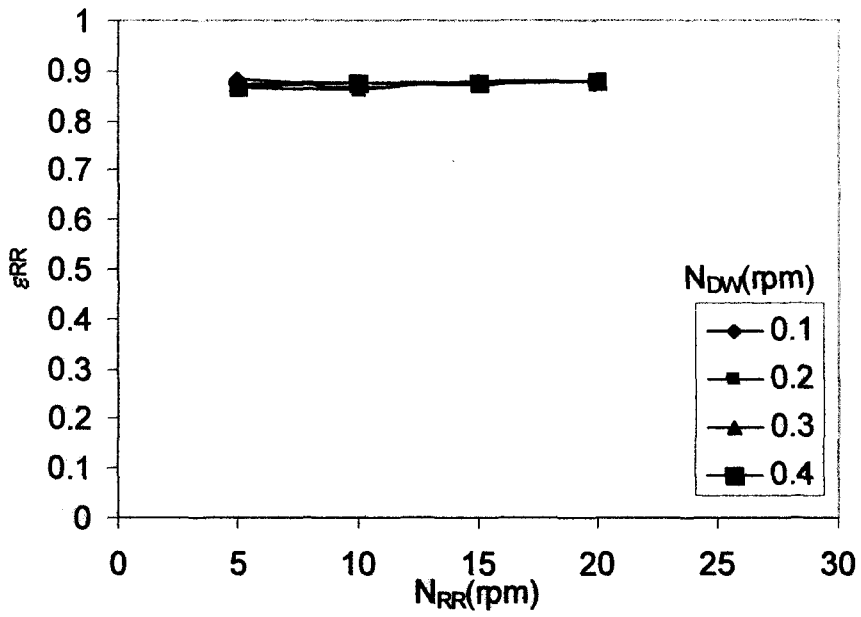
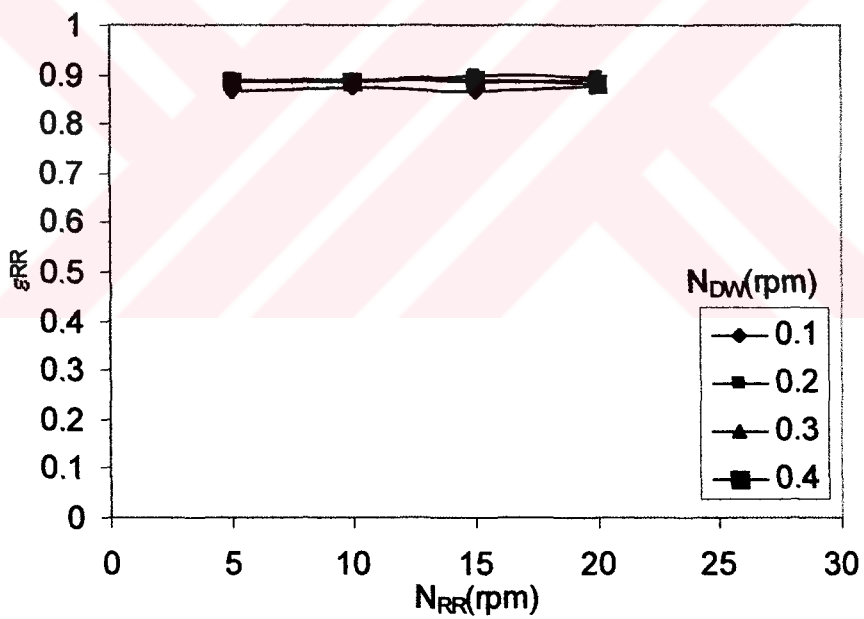


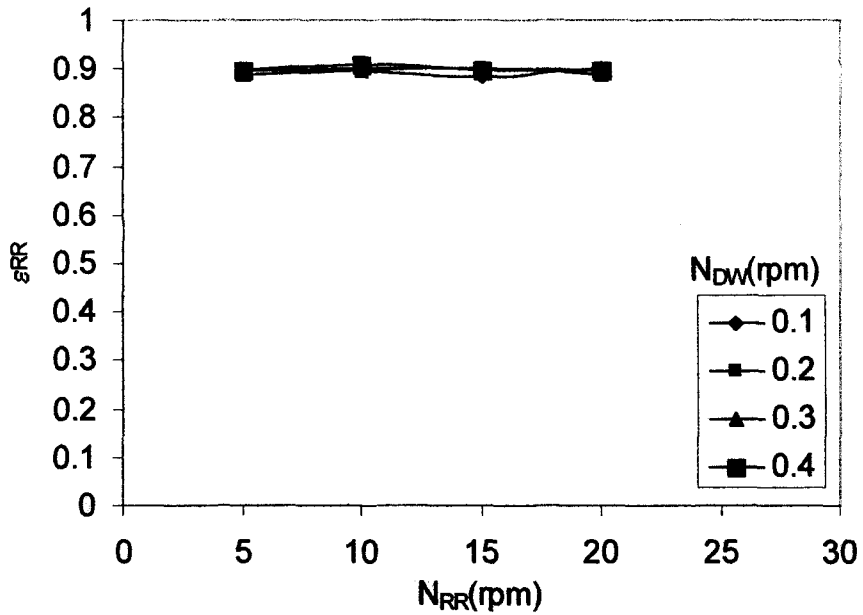
c)  $m_a = 0.111 \text{ kg/s}$



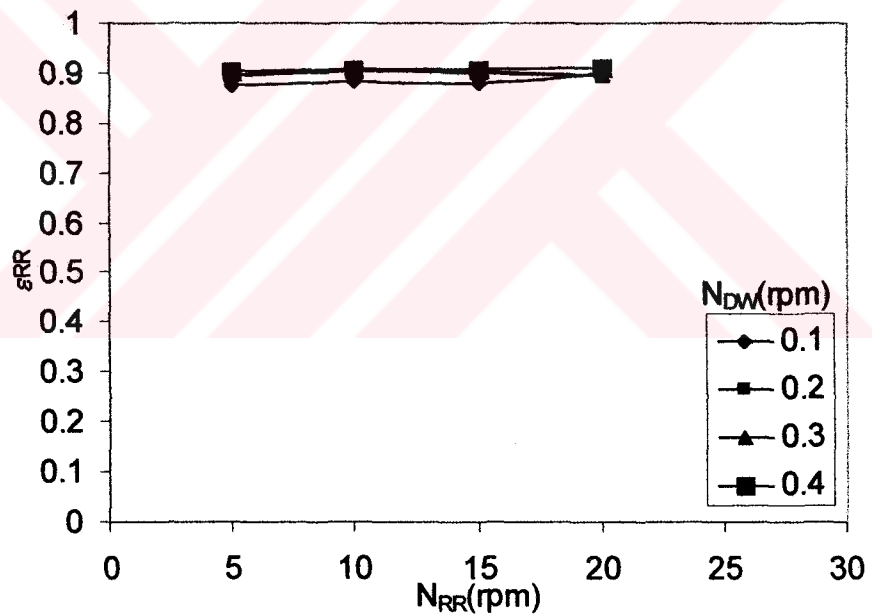
d)  $m_a = 0.139 \text{ kg/s}$

Figure 5.39 Effectiveness of EC as a function of  $N_{RR}$  and  $N_{DW}$  for  $T_r = 70^\circ\text{C}$

a)  $m_a=0.056\text{kg/s}$ b)  $m_a=0.083\text{kg/s}$

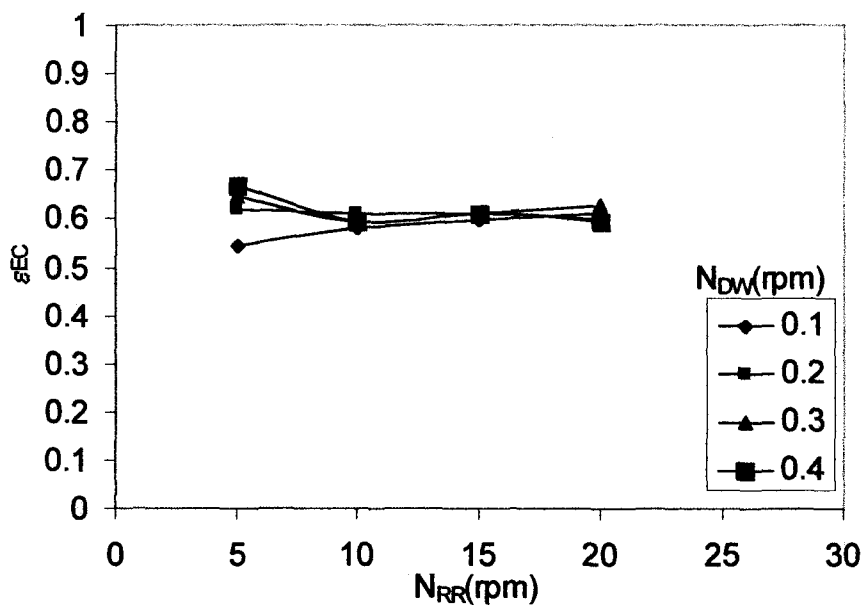
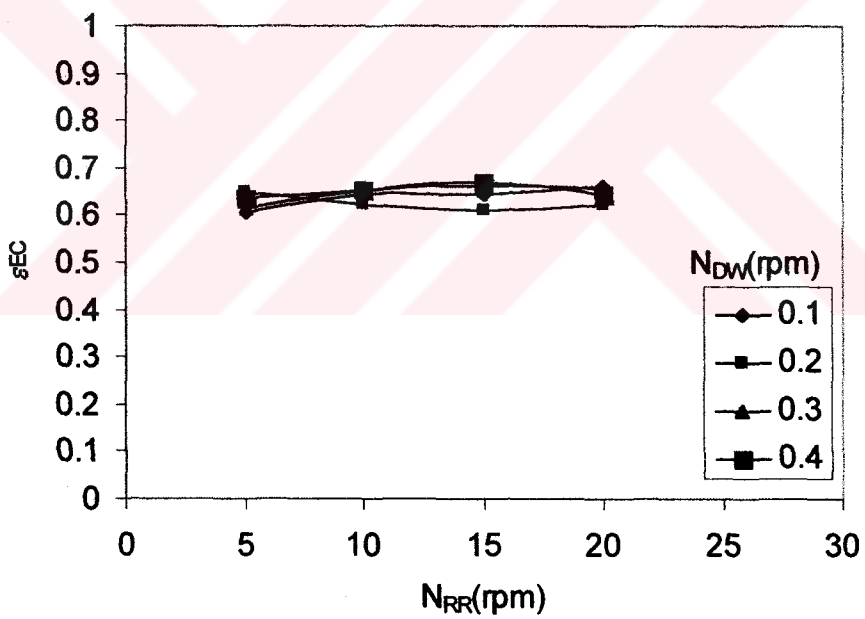


c)  $m_a = 0.111$  kg/s



d)  $m_a = 0.139$  kg/s

Figure 5.40 Effectiveness of RR as a function of  $N_{RR}$  and  $N_{DW}$  for  $T_r = 80$  C

a)  $m_a=0.056\text{kg/s}$ b)  $m_a=0.083\text{kg/s}$

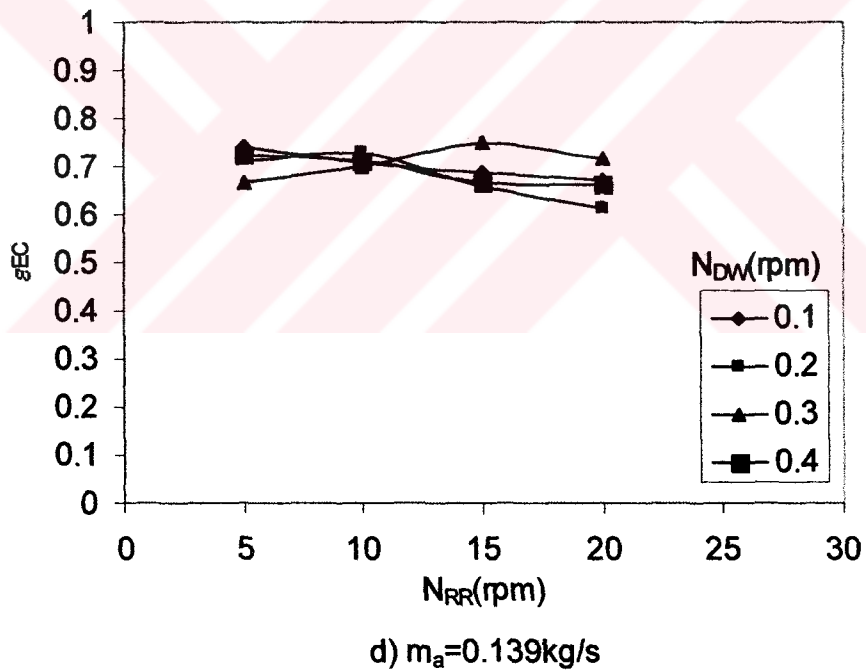
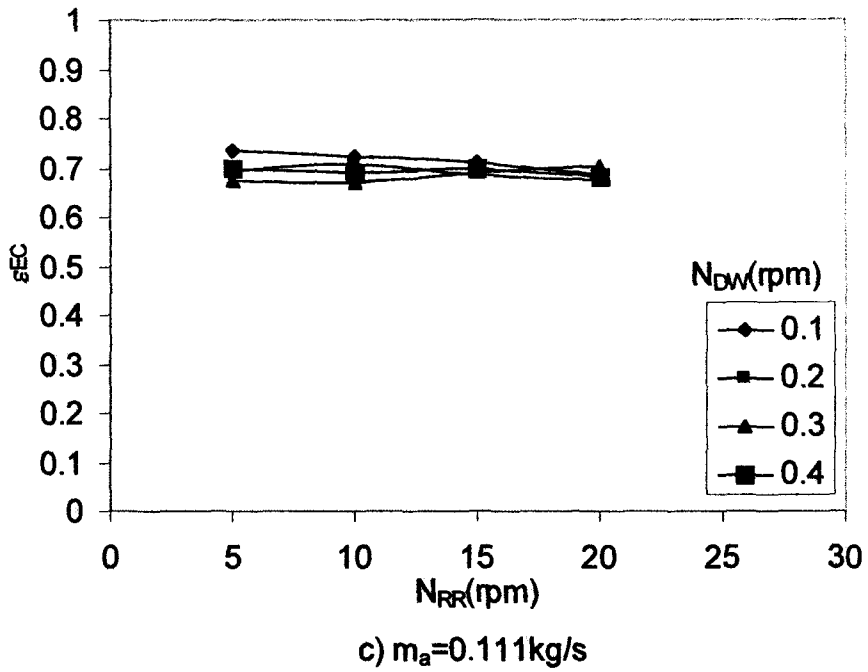
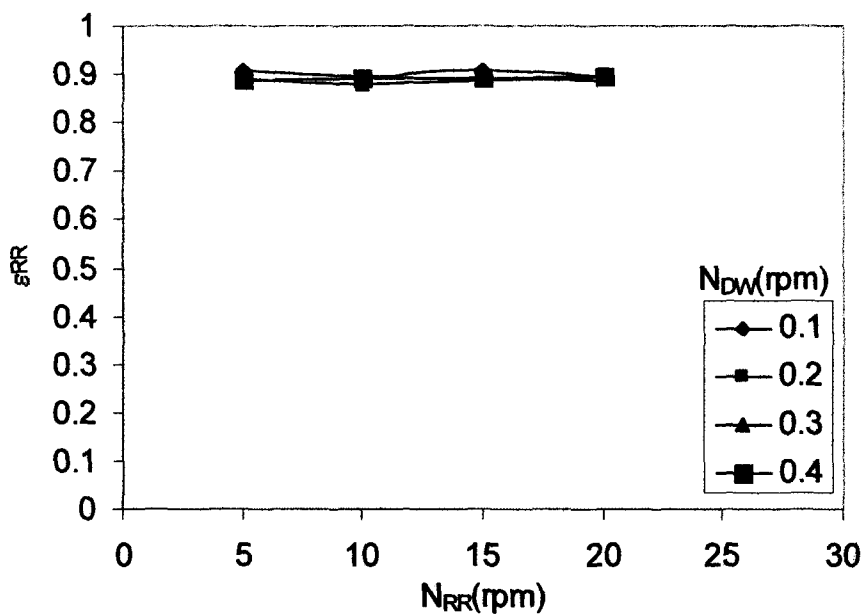
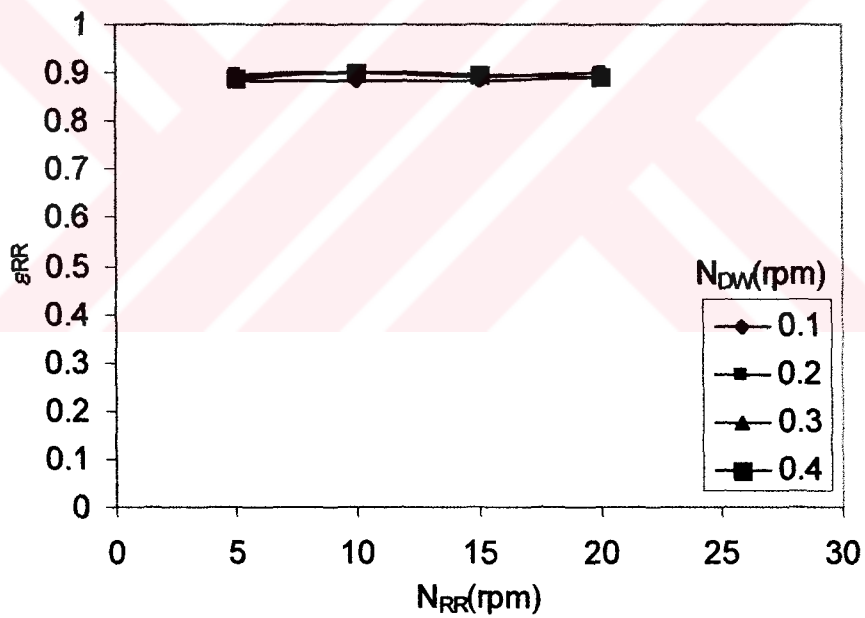
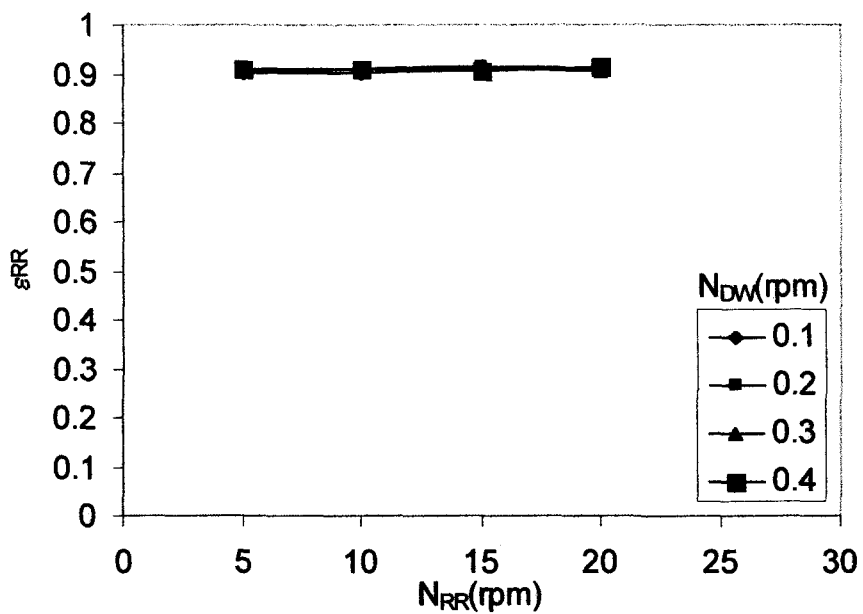


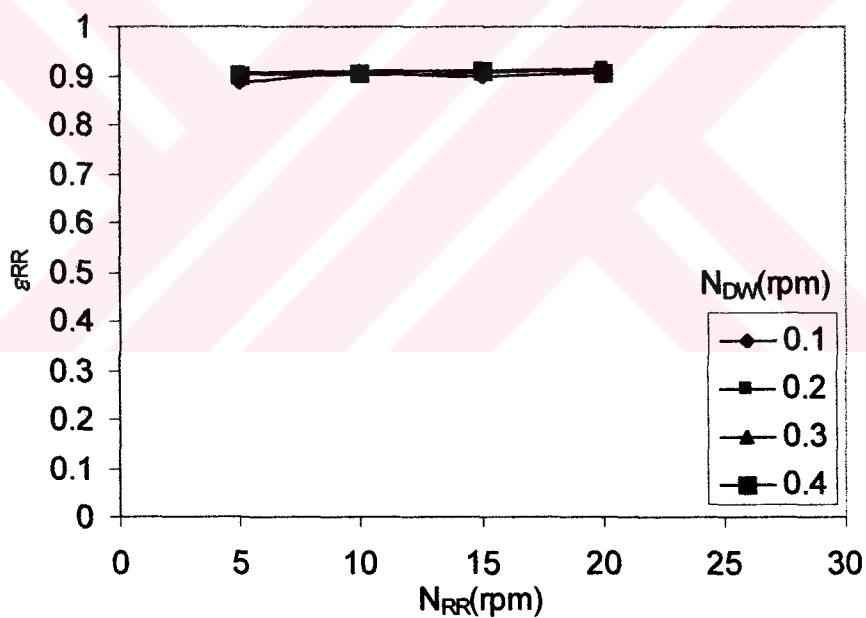
Figure 5.41 Effectiveness of EC as a function of  $N_{RR}$  and  $N_{DW}$  for  $T_r = 80^\circ\text{C}$



a)  $m_a = 0.056 \text{ kg/s}$ b)  $m_a = 0.083 \text{ kg/s}$

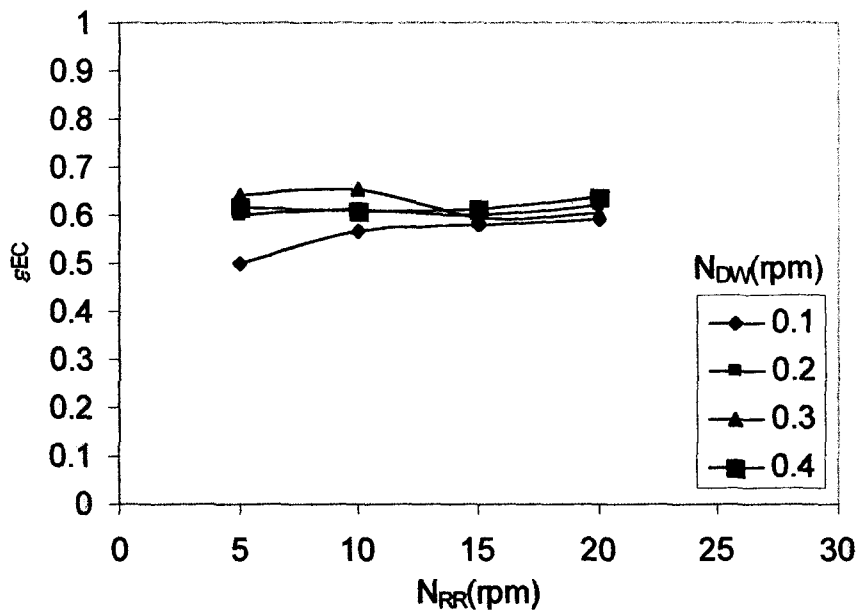
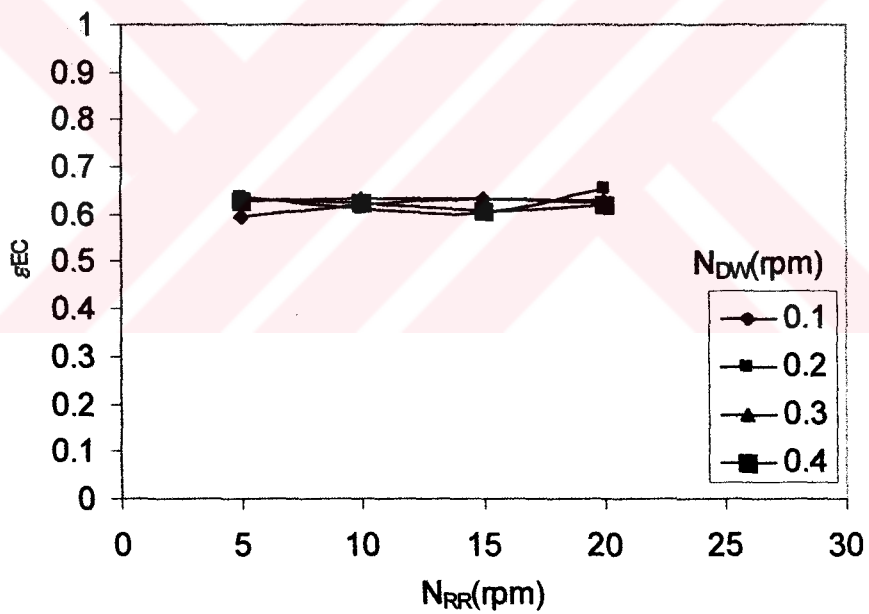


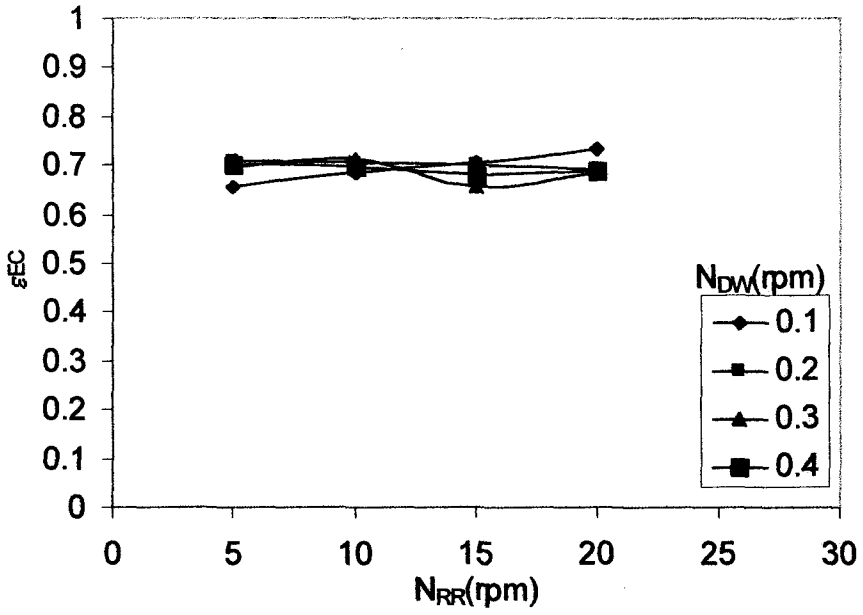
c)  $m_a = 0.111 \text{ kg/s}$



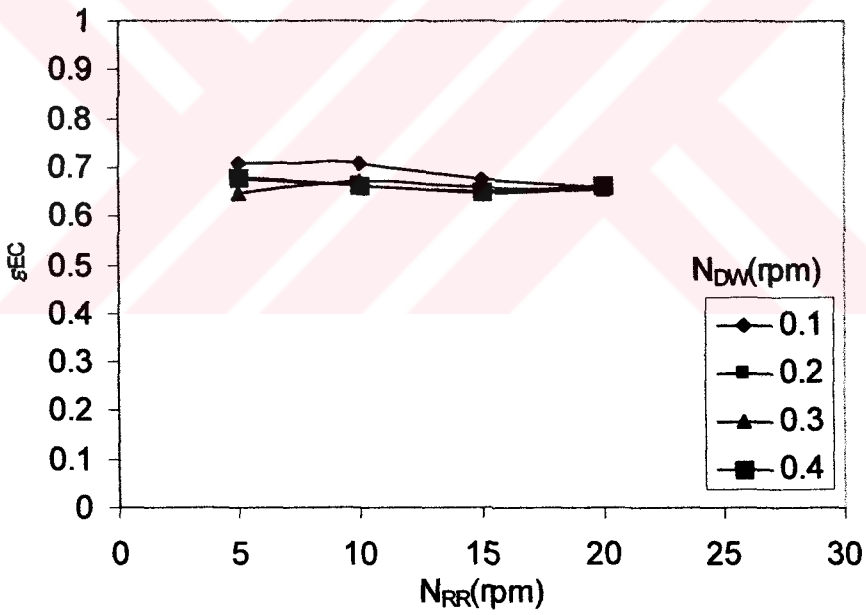
d)  $m_a = 0.139 \text{ kg/s}$

Figure 5.42 Effectiveness of RR as a function of  $N_{RR}$  and  $N_{DW}$  for  $T_r = 90^\circ\text{C}$

a)  $m_a = 0.056 \text{ kg/s}$ b)  $m_a = 0.083 \text{ kg/s}$



c)  $m_a = 0.111 \text{ kg/s}$



d)  $m_a = 0.139 \text{ kg/s}$

Figure 5.43 Effectiveness of EC as a function of  $N_{RR}$  and  $N_{DW}$  for  $T_r = 90^\circ\text{C}$

#### 5.4 ANALYSIS OF THE PRESSURE LOSSES THROUGH RR AND DW

Figure 5.44 shows the pressure losses through the designed and constructed RR and DW. As it can be seen in the figures pressure loss through the DW is greater than pressure loss through the RR at a certain  $m_a$ . Pressure loss of DW increases rapidly with respect to RR pressure loss as a function of air mass flow rate,  $m_a$ .

If the pressure loss of DW considered with geometry of DW, it shows that effect of  $\phi 4.5\text{mm}$  drilled (with central distances 7mm) iron sheet is large. Because, the ratio of empty area to the frontal area is approximately 0.667.

The geometry of RR and DW affects their pressure drop, size and cost and thus thermal COP of a cooling system.

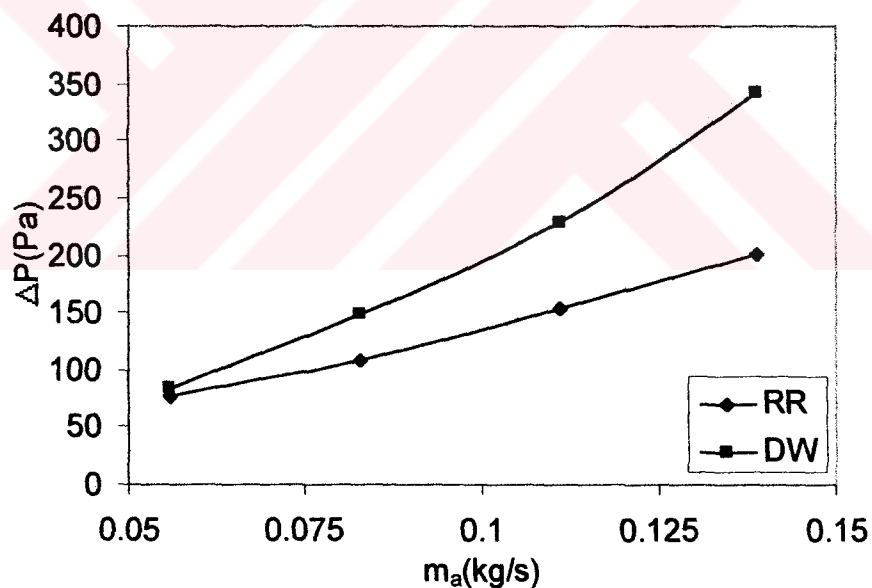


Figure 5.44 Effect of air flow rate on pressure loss through RR and DW with  $\Delta X_{RR}=10\text{cm}$ ,  $\Delta X_{DW}=10\text{cm}$  and  $d_z=10\text{mm}$

## 5.5 CORRELATION TRIALS ON DOMINANT HEAT AND MASS TRANSFER PARAMETER

For the correlation trials cross plots of CC, COP,  $\Delta W_p$ ,  $\Delta W_r$ ,  $\varepsilon_{RR}$  and  $\varepsilon_{EC}$  were plotted as a function of  $T_r$  and  $m_a$  for selected  $N_{RR}=5\text{rpm}$ , and  $N_{DW}=0.1\text{rpm}$ . The selection of these speeds is based on the analysis in the proceeding parts. Since the system performance seems to be the best for lower rotational speeds of DW and RR.

The variations of COP with  $T_r$  for different  $m_a$  are shown in Figure 5.45.a and with  $m_a$  for different  $T_r$  are shown in Figure 5.45.b respectively. Several conclusions may be drawn from Figure 5.45.a and Figure 5.46.a as; high values of CC and COP may be obtained at low  $T_r$ . However, the capacity of the system is low even though energy is used effectively. At  $T_r > 60\text{C}$ , CC and COP decreases significantly. A high regeneration temperature  $T_r$ , produces a very low humidity in the process line after DW but the resulting wet bulb temperature after RR is not correspondingly reduced. As a result only a slightly greater load is met with the greatly increased supply energy not by increasing  $T_r$ .

When the water vapor component of the air-vapor mixture is adsorbed by the desiccant material, the heat evolved in the sorption process causes the temperature of the bed to rise. Thus in the desiccant dehumidification of air-water vapor mixtures, the heat and mass transfers are combined processes. Figure 5.47.a shows the moisture reduction in process line as a function of  $T_r$  for different  $m_a$  and as a function of  $m_a$  for different  $T_r$  is given in Figure 5.47.b. As it can be seen moisture reduction in process line increases with  $T_r$  and  $m_a$ . Figure 5.48.a and b show the moisture reduction in regeneration line with  $T_r$  and  $m_a$  for different  $m_a$  and  $T_r$  respectively. In regeneration line same trend can be seen but high moisture reduction can be reached at  $m_a=0.056\text{kg/s}$  and  $T_r=90\text{C}$ .

Design and control of DW should consider that there is a difference in the time required to complete the drying and the regeneration process. Equal times for drying and regeneration may be sub-optimal conditions.

As can be seen from Figure 5.49.a, and b the variation of  $\varepsilon_{RR}$  with  $T_r$  is influenced by the magnitude of  $m_a$  however there seems to be no direct relationship with  $m_a$  (i.e. increase in  $m_a$  is not reflected in a linear change in  $\varepsilon_{RR}$  versus  $T_r$ ). Furthermore in terms of  $T_r$  dependence the nature of low regeneration temperatures can be observed as reflections in  $\varepsilon_{RR}$ . (i.e. at  $T_r=60C$   $\varepsilon_{RR}$  increases with  $m_a$ , at  $T_r=70C$ ,  $\varepsilon_{RR}$  decreases with  $m_a$ , while at  $T_r=80C$  and  $T_r=90C$ ,  $\varepsilon_{RR}$  shows a periodic decrease-increase with  $m_a$ ).

Finally for  $\varepsilon_{EC}$  variation with  $T_r$  and  $m_a$  as can be seen from Figure 5.50.a, and b the existence of sound and regular relationships are apparent. (i.e. as  $m_a$  increases magnitudes of  $\varepsilon_{EC}$  increases with similar behavior curves of  $\varepsilon_{EC}$  versus  $T_r$ , and as a function of  $T_r$ , increase in  $T_r$  resulted in decrease in magnitudes of  $\varepsilon_{EC}$  with similar behavior curves of  $\varepsilon_{EC}$  versus  $m_a$ ).

Besides this overall analysis some of the details to be referred are outlined here:

For the selected  $N_{RR}=5rpm$  and  $N_{DW}=0.1rpm$  test cases;

1. It can be seen from Figure 5.45 CC is under the influence of  $m_a$  and  $T_r$ . From this figure it can be said that CC decreases when  $T_r$  increases (with negligible deviation). As shown in Figure 5.45.b CC is obtained as  $16kW/kg_{dryair}$  at  $m_a=0.083kg/s$  and  $m_a=0.139kg/s$  for  $T_r=60C$ . But, CC magnitude increases with  $m_a$  for different  $T_r$ .
2. As it can be seen in Figure 5.46.a and b COP is in similar behavior as CC. The significance of high  $T_r$  is apparent since at  $T_r=90C$  COP values corresponding to different  $m_a$  coincide at an approximate value of  $COP=0.25$ .

3. The situation of  $\Delta w_p \cong \Delta w_r$  is seen in separate cases.  $\Delta w_p$  and  $\Delta w_r$  are under the effect of  $m_a$  and  $T_r$  as seen in Figures 5.47, and 5.48.  $\Delta w_p$  increases with increasing  $T_r$  and  $m_a$  with a small trend. At  $T_r=60C$  and  $m_a=0.083kg/s$ ,  $\Delta w_p$  is minimum, at  $T_r=70C$  and  $m_a=0.083kg/s$   $\Delta w_p$  is maximum.  $\Delta w_p$  also close to each other for  $m_a \geq 0.139kg/s$  and  $T_r \geq 90C$  with small deviations. In regeneration side of DW, behavior of  $\Delta w_r$  is not in similar behavior of  $\Delta w_p$ . It is not possible to say anything for  $\Delta w_r$  behavior, however it is rapidly changed with  $m_a$  and  $T_r$ .
4.  $\varepsilon_{RR}$  is not effected by  $m_a$  and  $T_r$  as shown in Figure 5.49.a, and b. But  $\varepsilon_{EC}$  decreases when  $T_r$  increases and  $\varepsilon_{EC}$  increases with increasing  $m_a$ .



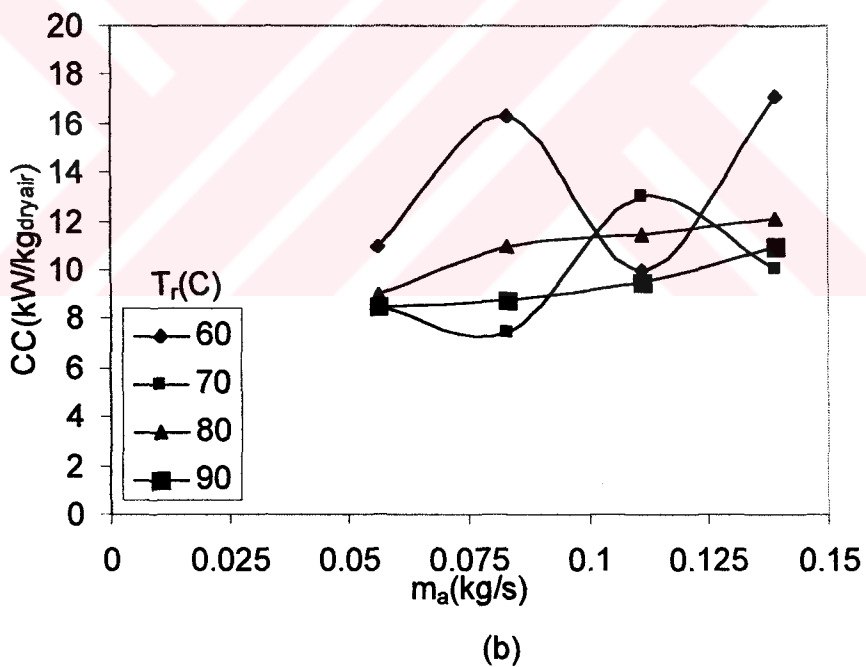
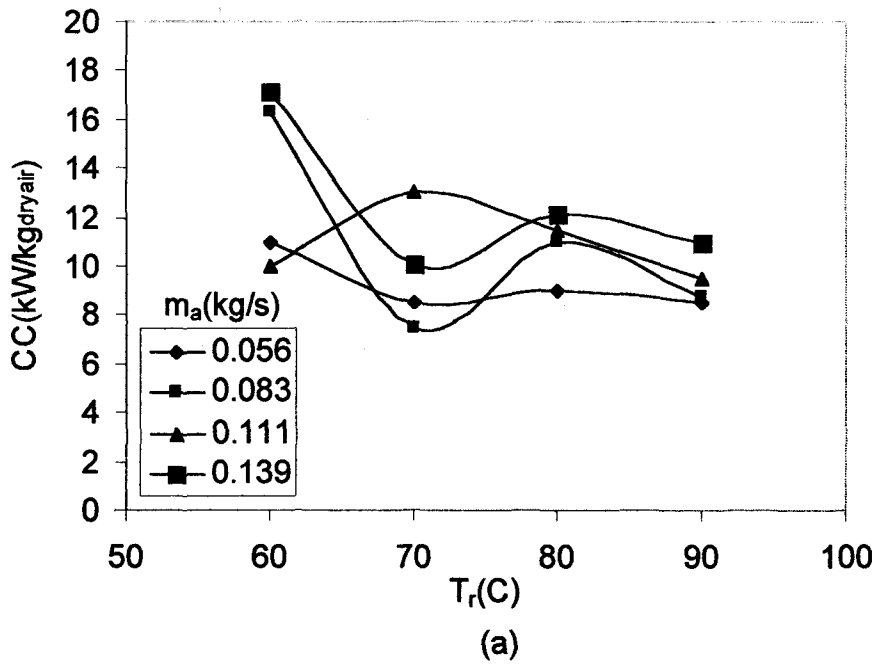


Figure 5.45 Variation of CC at  $N_{DW}=0.1$  rpm, and  $N_{RR}=5$  rpm with a)  $T_r$  for different  $m_a$ , b)  $m_a$  for different  $T_r$

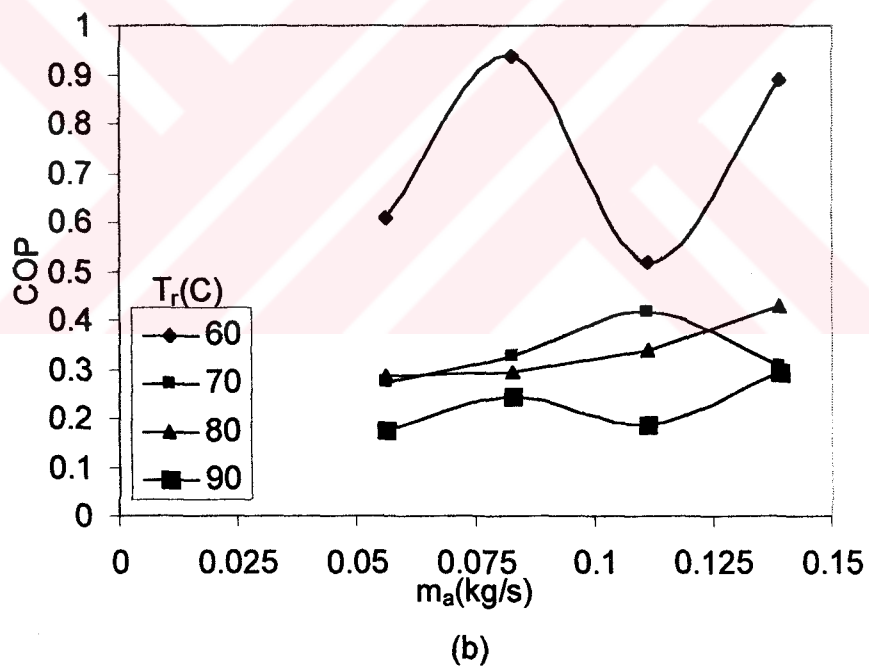
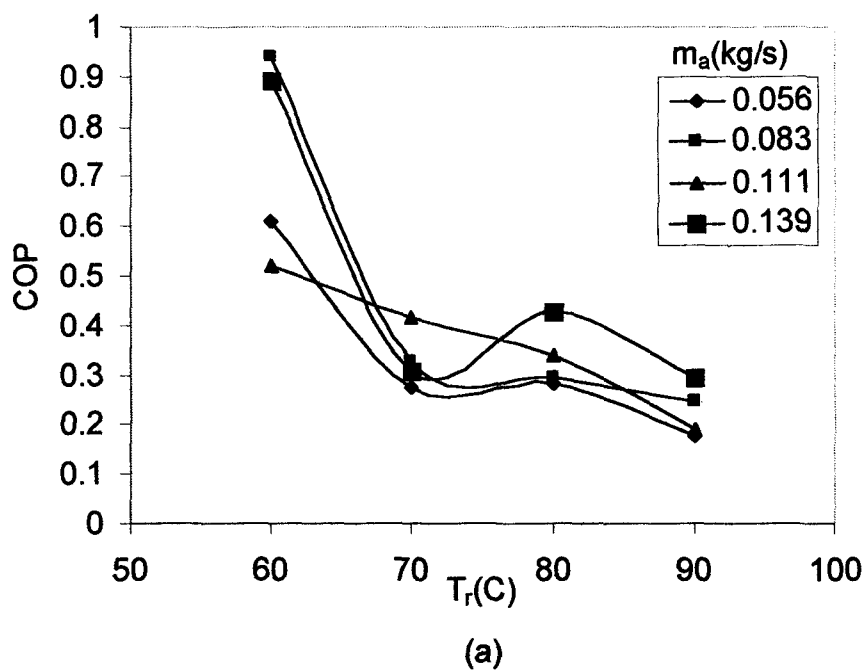


Figure 5.46 Variation of COP at  $N_{DW}=0.1$  rpm, and  $N_{RR}=5$  rpm with a)  $T_r$  for different  $m_a$ , b)  $m_a$  for different  $T_r$

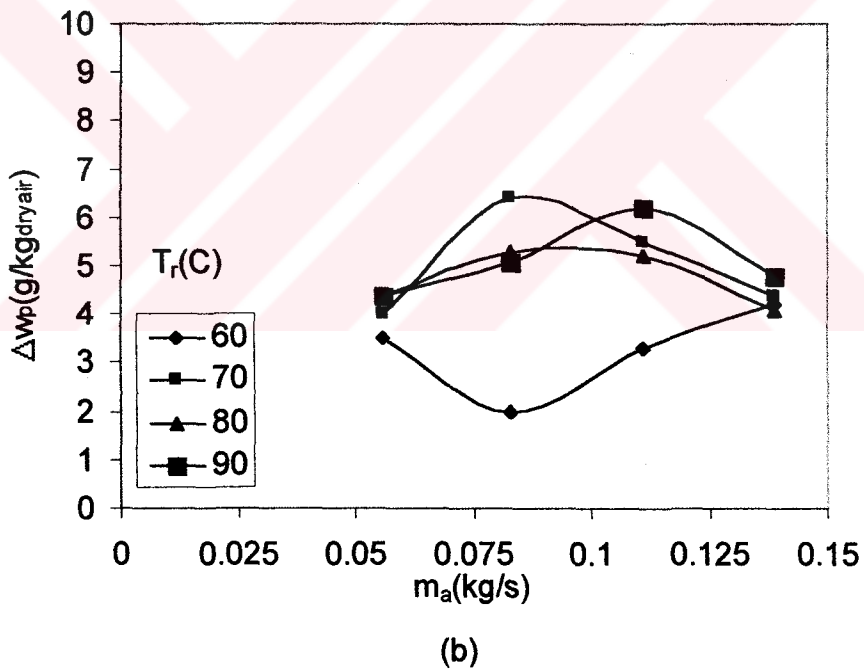
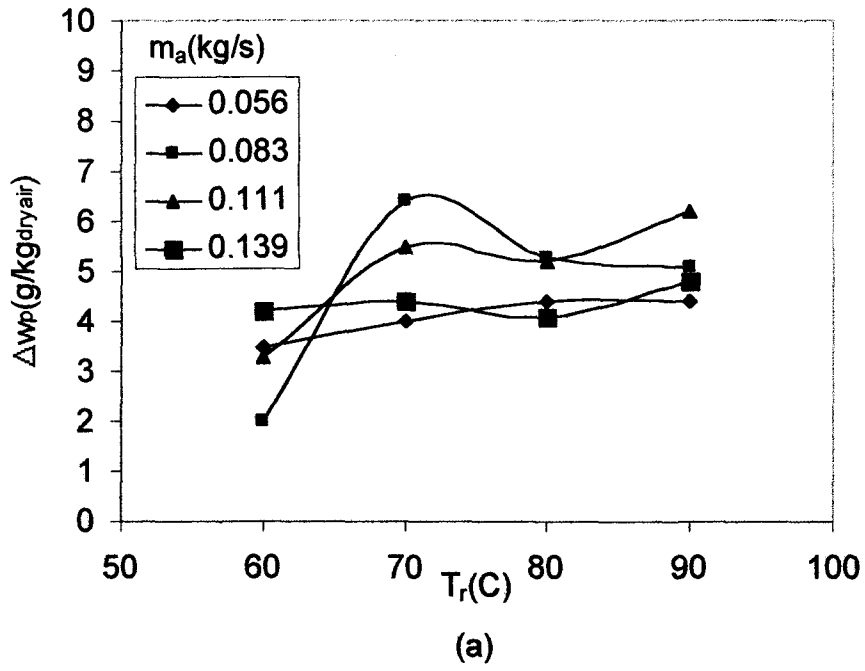
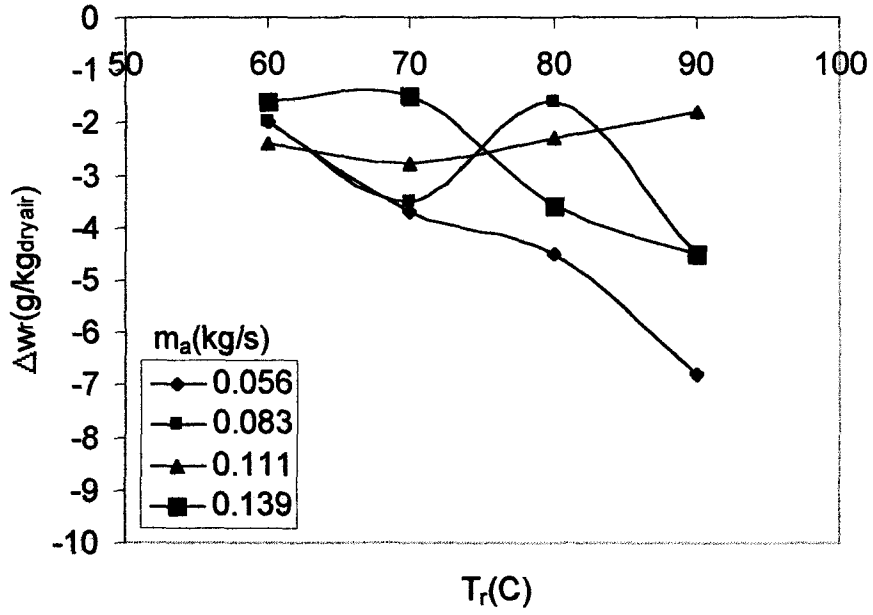
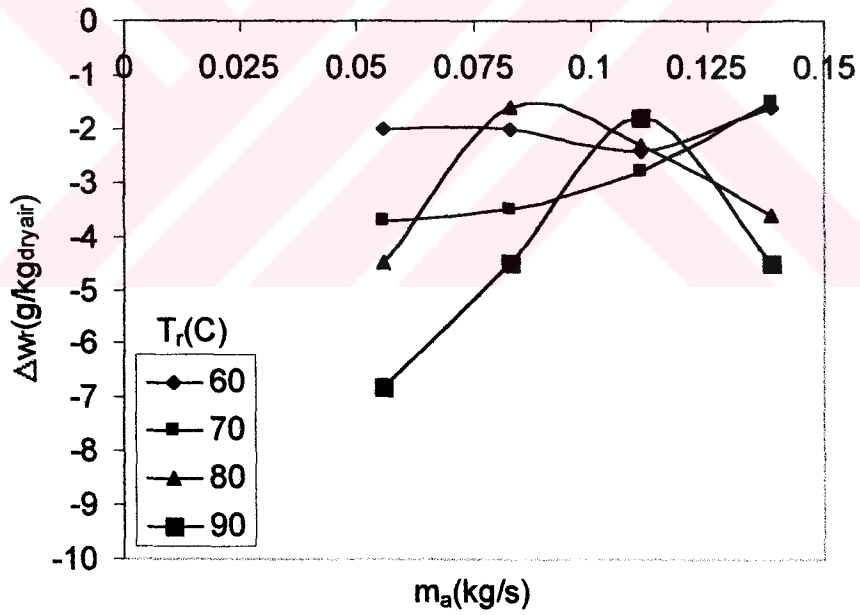


Figure 5.47 Variation of  $\Delta w_p$  at  $N_{DW}=0.1$  rpm, and  $N_{RR}=5$  rpm with a)  $T_r$  for different  $m_a$ , b)  $m_a$  for different  $T_r$



(a)



(b)

Figure 5.48 Variation of  $\Delta w_r$  at  $N_{DW}=0.1$  rpm, and  $N_{RR}=5$  rpm with a)  $T_r$  for different  $m_a$ , b)  $m_a$  for different  $T_r$

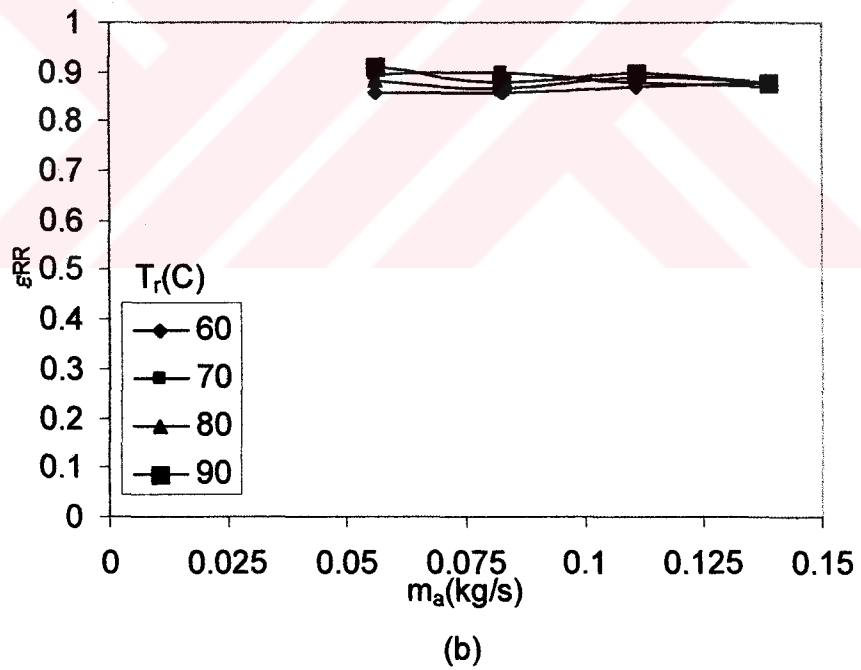
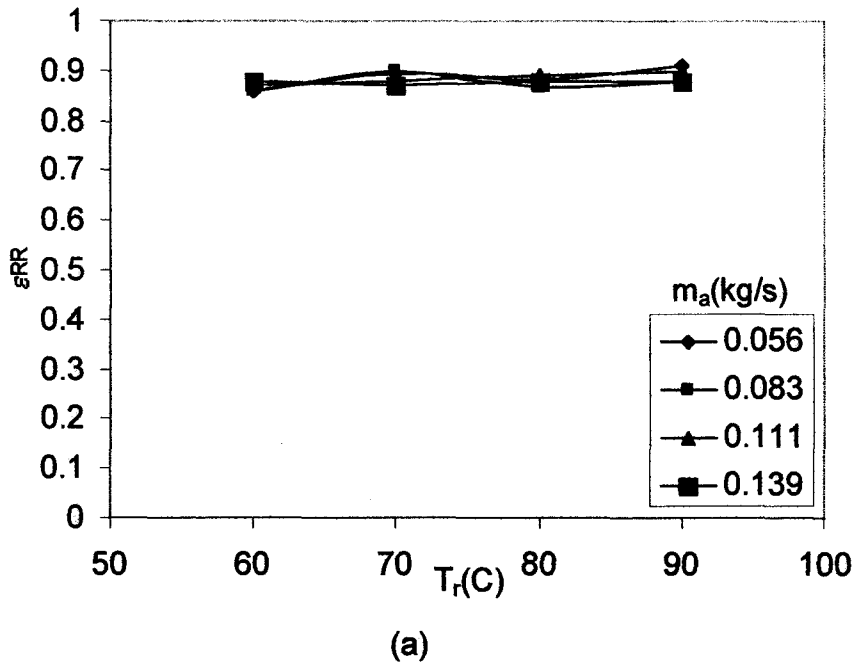
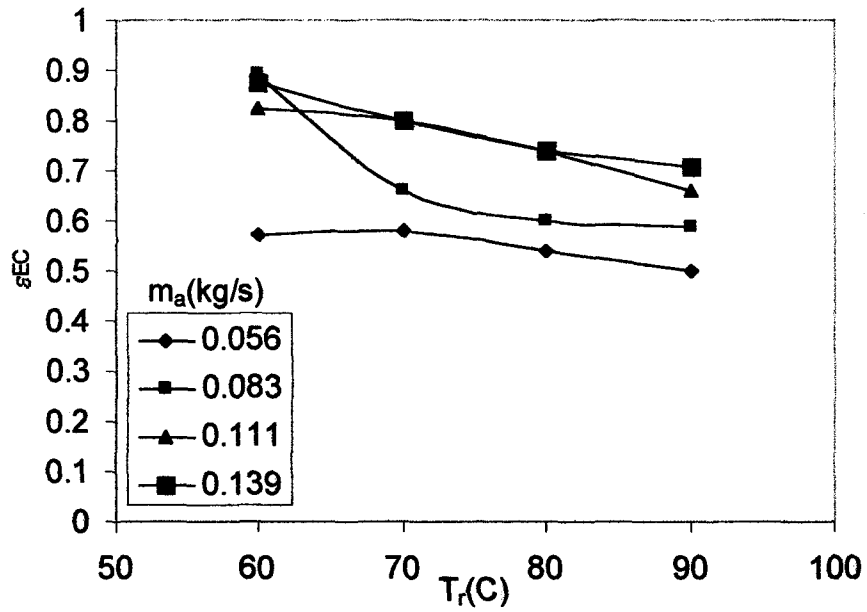
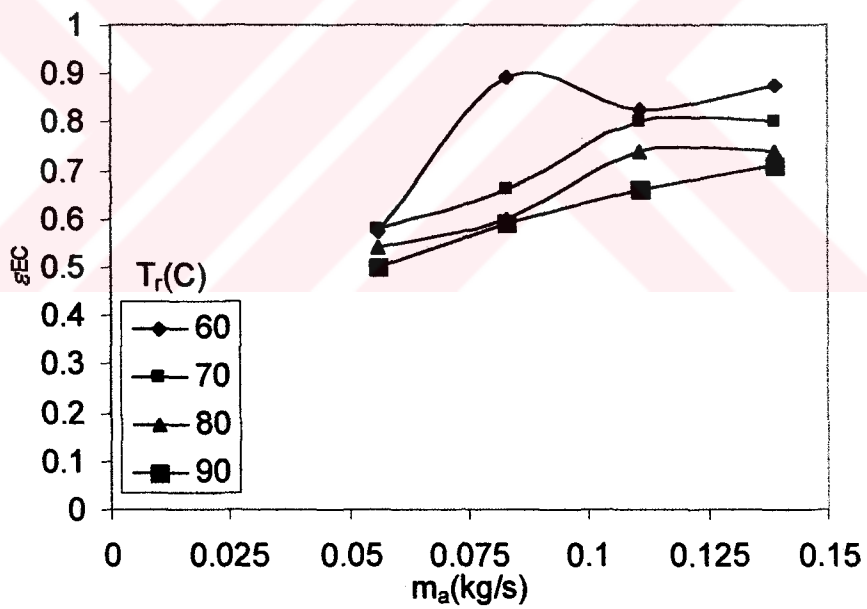


Figure 5.49 Variation of  $\epsilon_{RR}$  at  $N_{DW}=0.1$  rpm, and  $N_{RR}=5$  rpm with a)  $T_r$  for different  $m_a$ , b)  $m_a$  for different  $T_r$



(a)



(b)

Figure 5.50 Variation of  $\varepsilon_{EC}$  at  $N_{DW}=0.1$  rpm, and  $N_{RR}=5$  rpm with a)  $T_r$  for different  $m_a$ , b)  $m_a$  for different  $T_r$

## 5.6 EFFECT OF DESICCANT MATERIAL (ZEOLITE) PARTICLE SIZE ON DCS PERFORMANCE

A second set of experimental study was performed with a zeolite size,  $d_z=20\text{mm}$ . DW was reconstructed by using new sized zeolite. Therefore the constraints of the study are;  $\Delta X_{RR}=10\text{cm}$ ,  $\Delta X_{DW}=10\text{cm}$  (Table 4.1.).

In these experiments operation parameters  $N_{RR}$ ,  $N_{DW}$ ,  $T_r$  and  $m_a$  were changed in similar sequence of the first set of the experiments. The values used are;  $N_{RR}=10\text{rpm}$ ,  $N_{DW}=0.1\text{rpm}$ ,  $T_r=60\text{C}$ , and  $m_a=0.111\text{kg/s}$ . Three of them were stay constant and one of them was changed in the previously defined range as shown in Table 4.2 during the experiments. With these experiments effects of  $d_z$  on CC, COP,  $\Delta w$ ,  $\varepsilon$  and  $\Delta P$  were analyzed with different  $N_{RR}$ ,  $N_{DW}$ ,  $T_r$ , and  $m_a$ .

Effects of  $d_z$  are shown in Figures 5.51-75. Generally it can be seen that with increasing  $d_z$ , CC, COP,  $\Delta w$ ,  $\varepsilon$  and  $\Delta P$  decrease.

As it can be seen in Figures 5.51, and 5.52 there is almost no variation of CC and COP with  $N_{RR}$  for both  $d_z$  values. However, magnitudes of CC and COP of DCS with  $d_z=20\text{mm}$  are lower than those of DCS with  $d_z=10\text{mm}$ . This means that to increase CC and COP of DCS  $d_z$  must be reduced. Furthermore the influence of  $N_{DW}$  on CC and COP is given in plots of Figures 5.53, and 5.54. As an overall treatment of Figure 5.53 there is almost no dependence of CC to  $N_{DW}$  with  $d_z=20\text{mm}$  in comparison to CC variation with  $N_{DW}$  for  $d_z=10\text{mm}$ . However with  $d_z=20\text{mm}$  CC stays constant at  $9\text{kW/kg}_{\text{dryair}}$  for  $N_{DW}\leq 0.2\text{rpm}$  while for  $N_{DW}>0.2\text{rpm}$  CC decreases. Meanwhile with  $d_z=10\text{mm}$  CC stays almost constant in the range of  $N_{DW}\leq 0.2\text{rpm}$  while for  $N_{DW}>0.2\text{rpm}$  CC increases with  $N_{DW}$ . This means that there is a critical  $N_{DW}$  value which is  $0.2\text{rpm}$ . Referring to Figure 5.54 COP does not show a serious dependence on  $N_{DW}$  for  $d_z=20\text{mm}$ . However COP variation with  $N_{DW}$  for  $d_z=10\text{mm}$  is radically different from that of for  $d_z=20\text{mm}$ . Since for the range

of  $N_{DW} \leq 0.2 \text{rpm}$  COP stays constant at a value approximately 0.55 while for  $N_{DW} > 0.2 \text{rpm}$  increase in  $N_{DW}$  results an increase in COP.

In order to complete the analysis on CC and COP of DCS with the utilization of different DW of  $d_z=10\text{mm}$  and  $d_z=20\text{mm}$  the experimental data is presented as a function of  $T_r$  and  $m_a$  to understanding their influence. Referring to Figure 5.36 it seems that CC does not vary with  $T_r$  with  $d_z=20\text{mm}$  similarly COP only reduces slightly with  $T_r$  such that at  $T_r=60\text{C}$   $\text{COP}=0.2$  at  $T_r=90\text{C}$ ,  $\text{COP}=0.1$  while with  $d_z=10\text{mm}$  CC increases with  $T_r$  taking its maximum value  $\text{CC}=14\text{kW/kg}_{\text{dryair}}$  at  $T_r=70\text{C}$  for  $T_r > 70\text{C}$  CC decreases. On the other hand COP values with  $d_z=10\text{mm}$  reduces linearly with  $T_r$  such that at  $T_r=60\text{C}$   $\text{COP}=0.52$  while at  $T_r=90\text{C}$   $\text{COP}=0.2$ .

Referring Figures 5.65 and 5.66 CC and COP variation with  $m_a$  is not at considerable levels for  $d_z=20\text{mm}$  which means independence of  $m_a$  on both CC and COP. However, for  $d_z=10\text{mm}$  CC and COP have shown a dependence on  $m_a$  in a manner data points fluctuate around  $\text{CC}=14\text{kW/kg}_{\text{dryair}}$  and  $\text{COP}=0.8$  for the  $m_a$  values in the range  $0.056\text{kg/s} \leq m_a \leq 0.139\text{kg/s}$ .

In order to understand the effect of  $d_z$  on moisture removal capacity as a function of  $N_{RR}$ ,  $N_{DW}$ ,  $m_a$ ,  $T_r$  for both process and regeneration sides of DCS operation the experimental data was represented in suitable plots given in Figures 5.55-5.58, and Figures 5.66-5.70.

It is observed that  $\Delta w_p$  does not vary with  $N_{RR}$  for both  $d_z=10\text{mm}$  and  $d_z=20\text{mm}$  (Figure 5.55). However the magnitude of  $\Delta w_p$  increases with decrease in  $d_z$ . Similar behavior is also valid for  $\Delta w_r$  variation (Figure 5.56). On the other hand in comparison to  $N_{RR}$ ,  $N_{DW}$  is much more effective on  $\Delta w_p$  and  $\Delta w_r$  (Figures 5.57, and 5.58). It seems that  $\Delta w_p$  decreases with  $N_{DW}$  in the range  $N_{DW} \leq 0.25\text{rpm}$  while for  $N_{DW} \geq 0.25\text{rpm}$   $\Delta w_p$  magnitudes show an increase with both  $d_z=10\text{mm}$  and  $d_z=20\text{mm}$ .  $\Delta w_p$  values with  $d_z=10\text{mm}$  are considerable greater than those with  $d_z=20\text{mm}$  (as an example for



$N_{DW}=0.4\text{rpm}$ ,  $\Delta w_p=5.5\text{g/kg}_{\text{dryair}}$  at  $d_z=10\text{mm}$ ,  $\Delta w_p=1.6\text{g/kg}_{\text{dryair}}$  at  $d_z=20\text{mm}$ ).  $\Delta w_r$  variation with  $N_{DW}$  at  $d_z=20\text{mm}$  is severe in comparison to that of at  $d_z=10\text{mm}$ . It is also seen that increase in  $d_z$  results in an increase in  $\Delta w_r$ .

$\Delta w_p$  variation with  $T_r$  for both  $d_z=10\text{mm}$  and  $d_z=20\text{mm}$  is similar  $\Delta w_p$  increases with  $T_r$ .  $\Delta w_r$  variation with  $T_r$  is similar to  $\Delta w_p$  variation however increase in  $\Delta w_r$  is not so much with  $T_r$  (Figures 5.67, and 5.68). The dependence of both  $\Delta w_p$  and  $\Delta w_r$  on  $m_a$  seems to be seriously affected by  $d_z$ . Since  $d_z=10\text{mm}$   $\Delta w_p$  decreases with  $m_a$  for  $m_a<0.038\text{kg/s}$  while for  $m_a>0.083\text{kg/s}$   $\Delta w_p$  increases from  $\Delta w_p=2\text{g/kg}_{\text{dryair}}$  to  $\Delta w_p=4.5\text{g/kg}_{\text{dryair}}$  at  $m_a=0.139\text{kg/s}$ . However  $\Delta w_p$  increases first in  $m_a<0.083\text{kg/s}$  decreases for  $m_a>0.083\text{kg/s}$  with  $d_z=20\text{mm}$  (Figure 5.69).  $\Delta w_r$  almost stays constant with  $m_a$  for  $d_z=10\text{mm}$  with the expected desorption behavior. While for  $d_z=20\text{mm}$   $\Delta w_r$  decreases with  $m_a$  with the presence of adsorption (Figure 5.70).

In order to evaluate the  $\varepsilon_{RR}$  on be half of operating and system parameters the plots given in Figures 5.59, 5.61, 5.71, and 5.73 were formed. Analysis on these plots indicate that  $\varepsilon_{RR}$  is not seriously influenced by  $d_z$ ,  $N_{RR}$ ,  $N_{DW}$ ,  $m_a$ ,  $T_r$ . This means that  $\varepsilon_{RR}$  is only governed by design of RR as expected.

Due to the nature of DCS operation  $\varepsilon_{EC}$  is expected to be influenced by system and operating parameters. Referring to Figure 5.60  $\varepsilon_{EC}$  stays almost constant. With  $N_{RR}$  at  $d_z=10\text{mm}$  while  $\varepsilon_{EC}$  decreases with  $N_{RR}$  for  $N_{RR}\leq 10\text{rpm}$  for  $N_{RR}\geq 10\text{rpm}$   $\varepsilon_{EC}$  increases at  $d_z=20\text{mm}$

$\varepsilon_{EC}$  depends on  $N_{DW}$  in similar way for  $d_z=10\text{mm}$ ,  $d_z=20\text{mm}$  with higher  $\varepsilon_{EC}$  magnitudes at  $d_z=10\text{mm}$  (Figure 5.62).  $\varepsilon_{EC}$  decreases with  $T_r$  at  $d_z=10\text{mm}$  while  $\varepsilon_{EC}$  shows an irregular behavior with  $T_r$  at  $d_z=20\text{mm}$  (Figure 5.72).  $\varepsilon_{EC}$  generally increases with increase in  $m_a$  for both  $d_z$  values (Figure 5.74).

The amount of  $\Delta P$  through DW with use of different zeolite sizes is given as a function of  $m_a$  in Figure 5.75. As can be seen from this figure as  $d_z$  decreases magnitude of  $\Delta P$  increases for all  $m_a$  values.

All of these changes on CC, COP  $\Delta w$ , and  $\varepsilon$  due to the less amount of zeolite and less surface area with big size zeolite particles. With less amount of zeolite, heat transfer capacity of zeolite decreases. With less surface area, adsorption which is surface phenomena capacity of DW decreases.



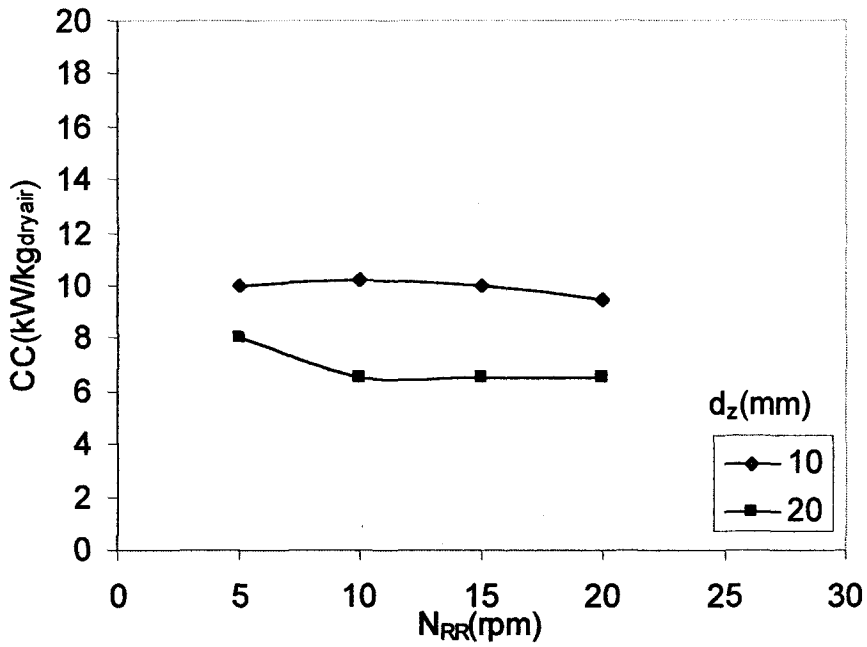


Figure 5. 51 Variation of CC with  $d_z$  at constant  $m_a=0.111$ kg/s,  
 $T_r=60$ C and  $N_{DW}=0.1$ rpm

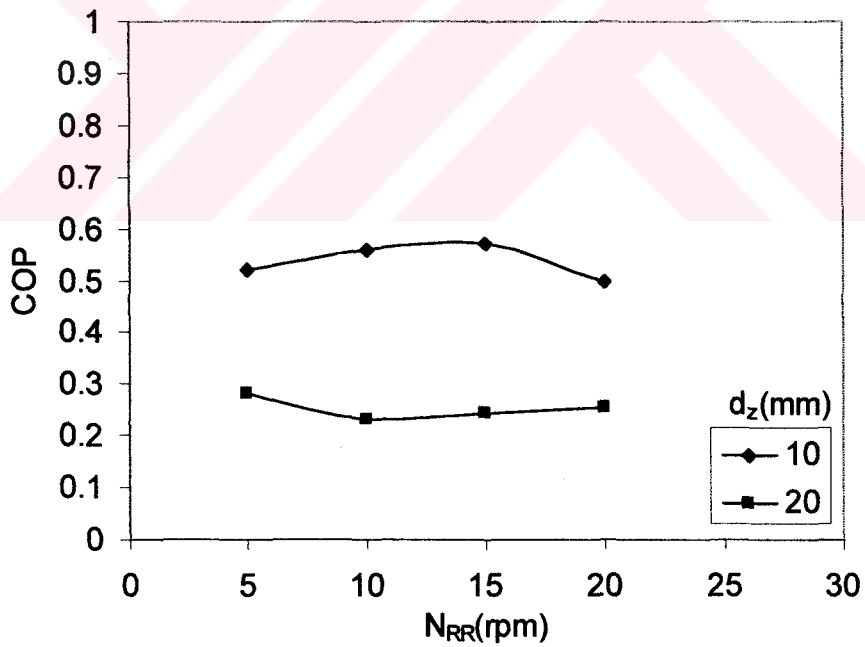


Figure 5. 52 Variation of COP with  $d_z$  at constant  $m_a=0.111$ kg/s,  
 $T_r=60$ C and  $N_{DW}=0.1$ rpm

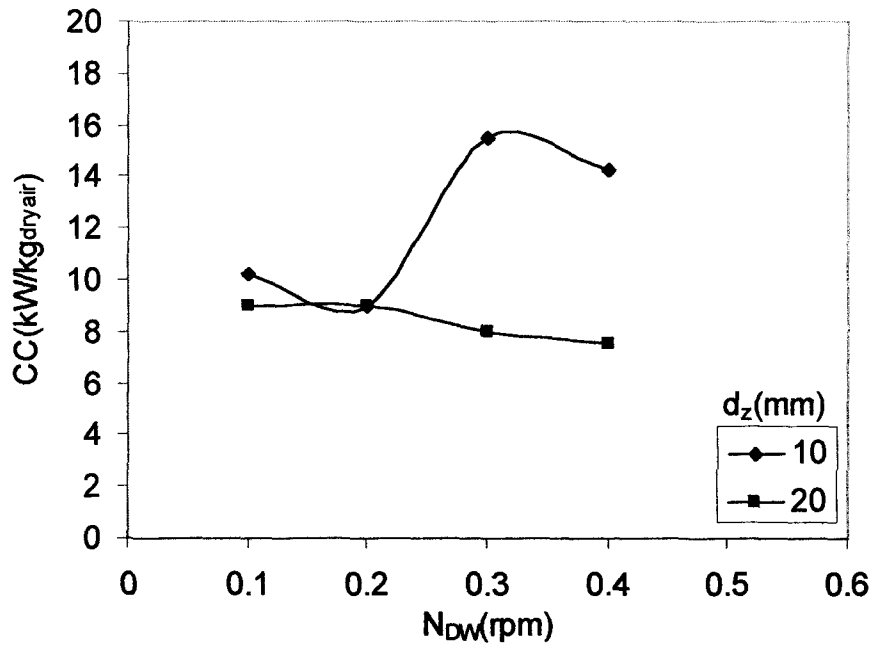


Figure 5.53 Variation of CC with  $d_z$  at constant  $m_a=0.111\text{kg/s}$ ,  $T_r=60\text{C}$  and  $N_{RR}=10\text{rpm}$

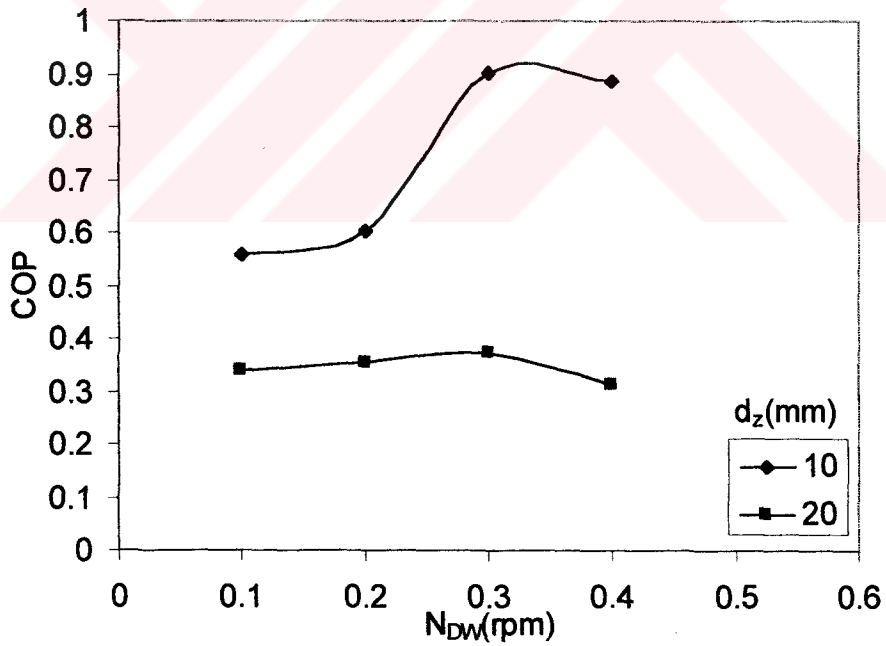


Figure 5.54 Variation of COP with  $d_z$  at constant  $m_a=0.111\text{kg/s}$ ,  $T_r=60\text{C}$  and  $N_{RR}=10\text{rpm}$

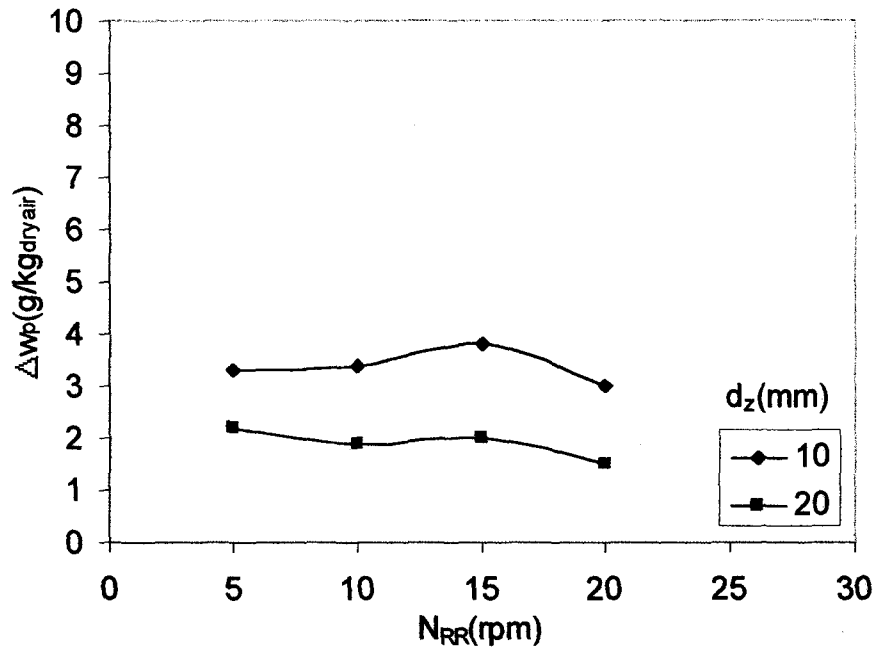


Figure 5.55 Variation of  $\Delta w_p$  with  $d_z$  at constant  $m_a = 0.111$  kg/s,  $T_r = 60^\circ\text{C}$  and  $N_{DW} = 0.1$  rpm

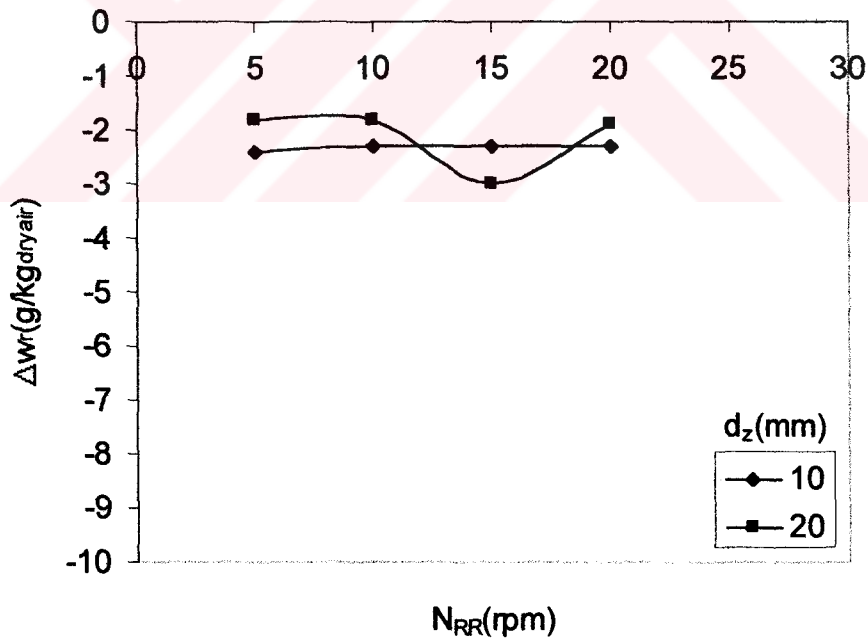


Figure 5.56 Variation of  $\Delta w_r$  with  $d_z$  at constant  $m_a = 0.111$  kg/s,  $T_r = 60^\circ\text{C}$  and  $N_{DW} = 0.1$  rpm

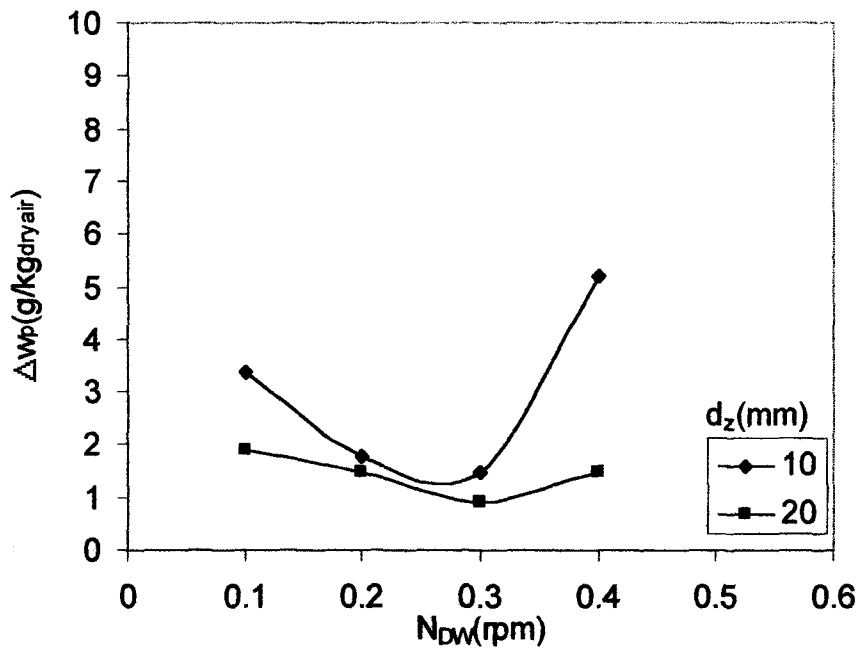


Figure 5.57 Variation of  $\Delta w_p$  with  $d_z$  at constant  $m_a = 0.111$  kg/s,  $T_r = 60$  C and  $N_{RR} = 10$  rpm

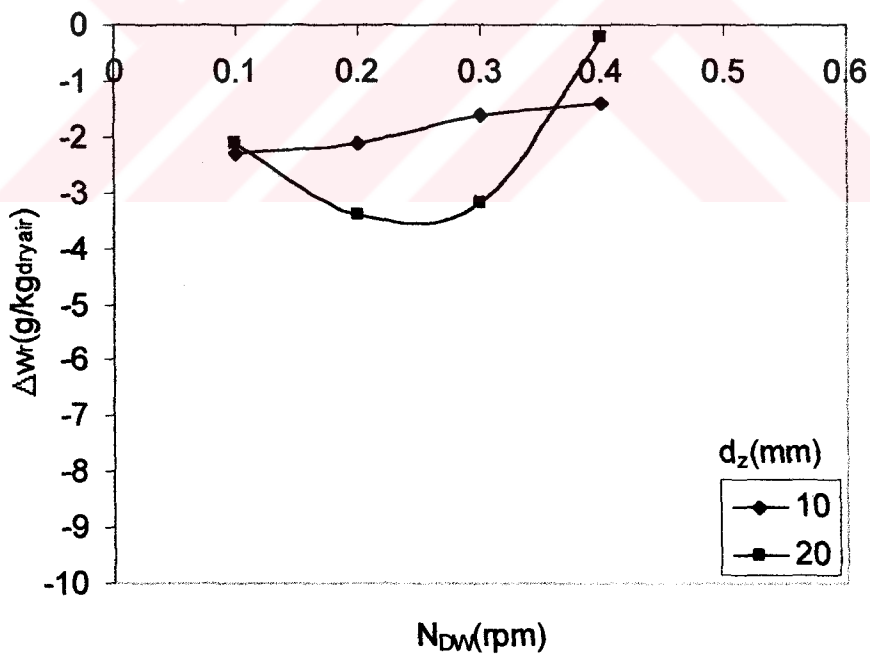


Figure 5.58 Variation of  $\Delta w_r$  with  $d_z$  at constant  $m_a = 0.111$  kg/s,  $T_r = 60$  C and  $N_{RR} = 10$  rpm

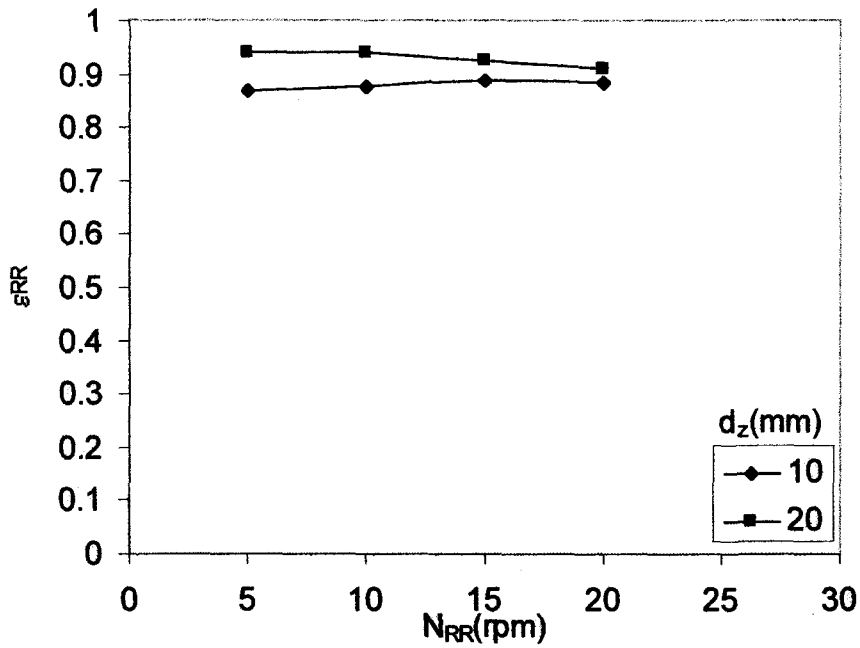


Figure 5. 59 Variation of  $\epsilon_{RR}$  with  $d_z$  at constant  $m_a=0.111\text{kg/s}$ ,  
 $T_r=60\text{C}$  and  $N_{DW}=0.1\text{rpm}$

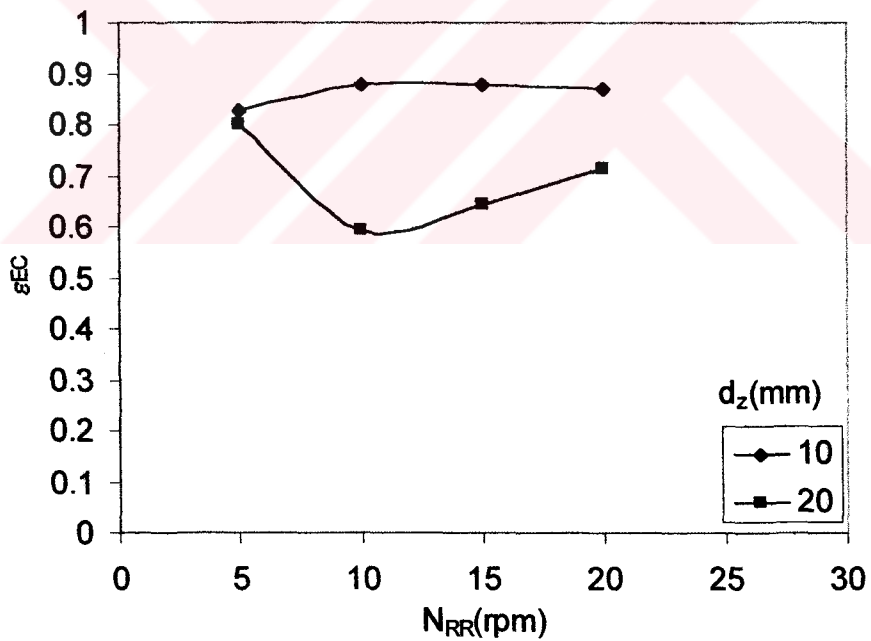


Figure 5. 60 Variation of  $\epsilon_{EC}$  with  $d_z$  at constant  $m_a=0.111\text{kg/s}$ ,  
 $T_r=60\text{C}$  and  $N_{DW}=0.1\text{rpm}$

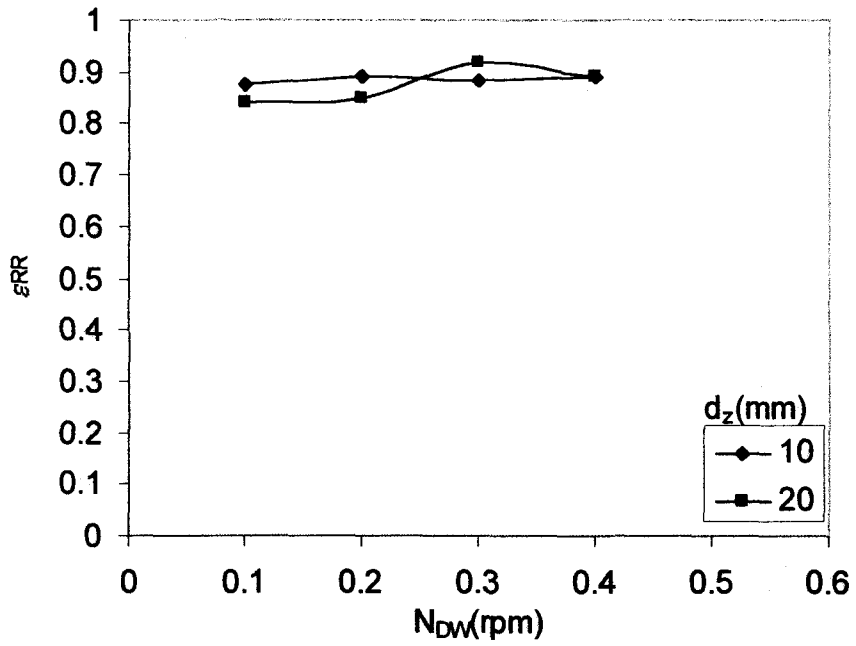


Figure 5. 61 Variation of  $\epsilon_{RR}$  with  $d_z$  at constant  $m_a=0.111\text{kg/s}$ ,  $T_r=60\text{C}$  and  $N_{RR}=10\text{rpm}$

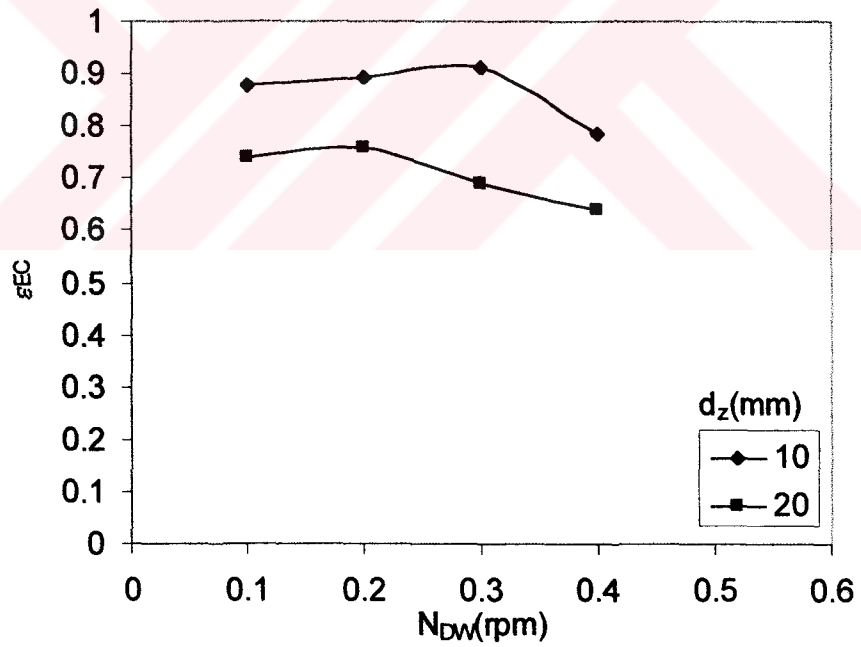


Figure 5. 62 Variation of  $\epsilon_{EC}$  with  $d_z$  at constant  $m_a=0.111\text{kg/s}$ ,  $T_r=60\text{C}$  and  $N_{RR}=10\text{rpm}$



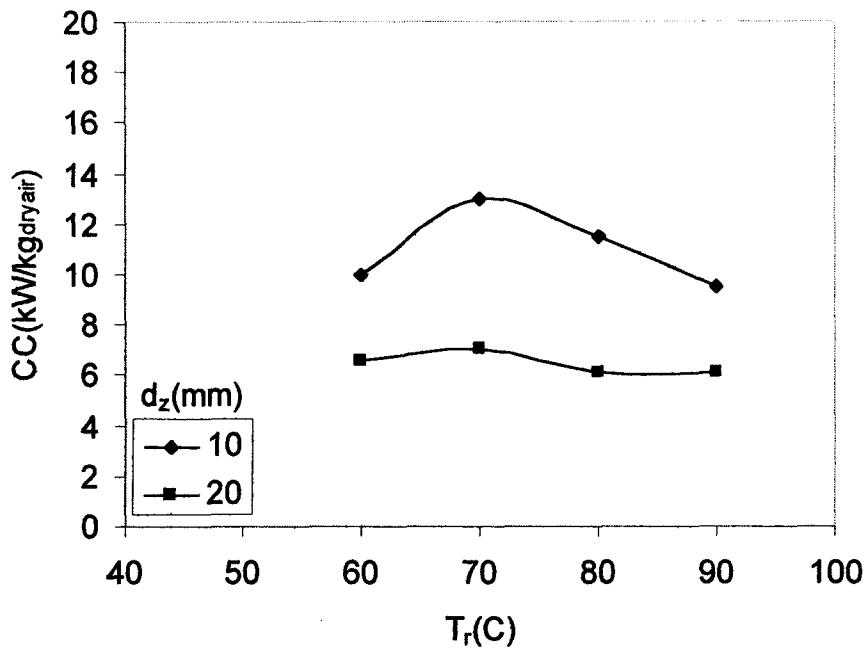


Figure 5.63 Variation of CC with  $d_z$  at constant  $N_{RR}=10$ rpm,  $N_{DW}=0.1$ rpm and  $m_a=0.111$ kg/s

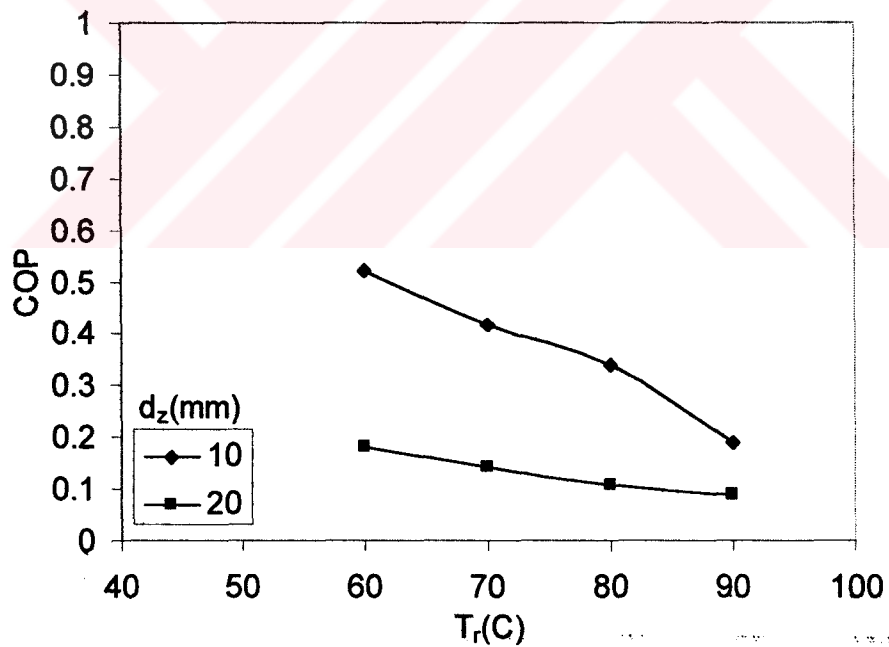


Figure 5.64 Variation of COP with  $d_z$  at constant  $N_{RR}=10$ rpm,  $N_{DW}=0.1$ rpm and  $m_a=0.111$ kg/s

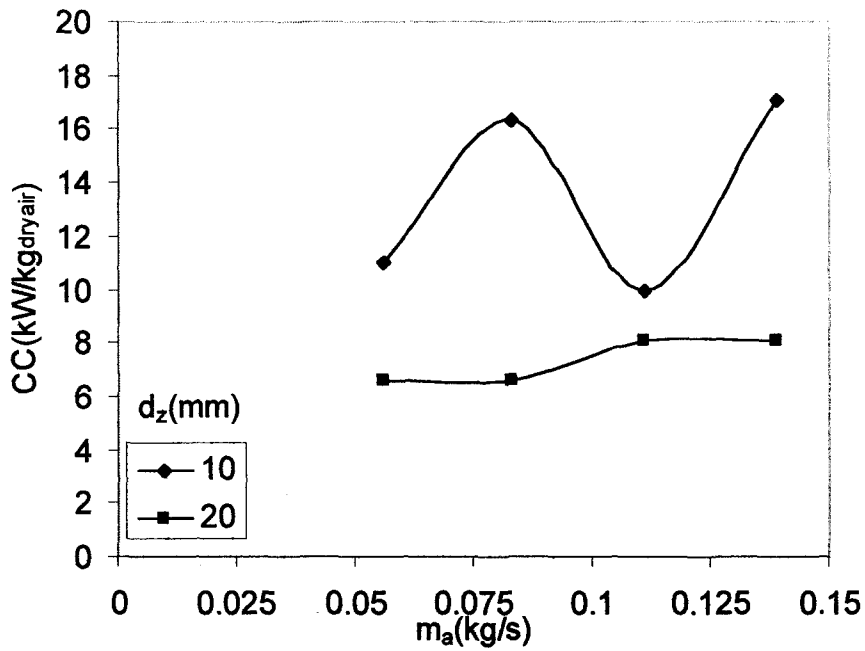


Figure 5. 65 Variation of CC with  $d_z$  at constant  $N_{RR}=10$ rpm,  
 $N_{DW}=0.1$ rpm and  $T_r=60$ C

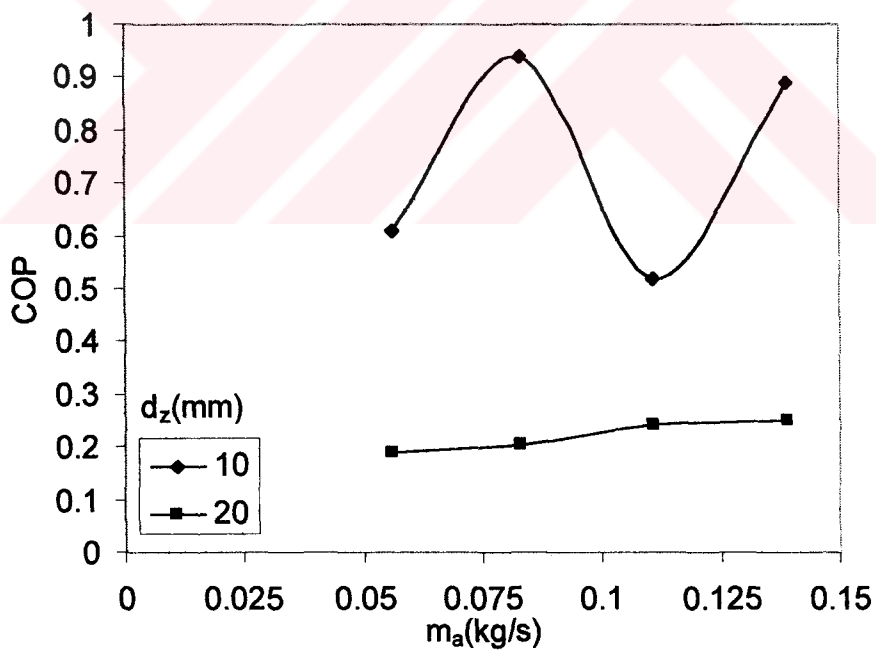


Figure 5. 66 Variation of COP with  $d_z$  at constant  $N_{RR}=10$ rpm,  
 $N_{DW}=0.1$ rpm and  $T_r=60$ C

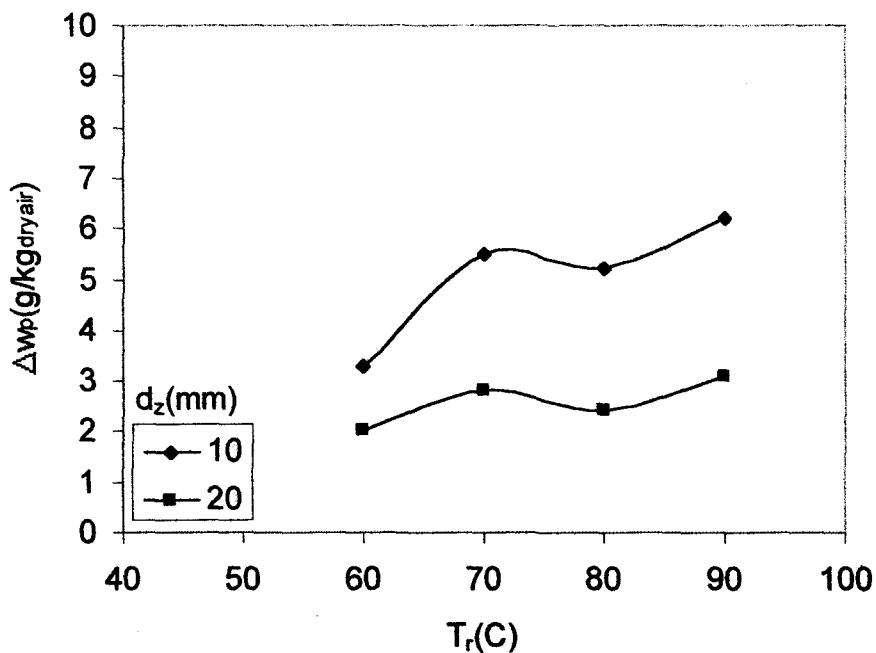


Figure 5.67 Variation of  $\Delta w_p$  with  $d_z$  at constant  $N_{RR}=10$ rpm,  $N_{DW}=0.1$ rpm and  $m_a=0.111$ kg/s

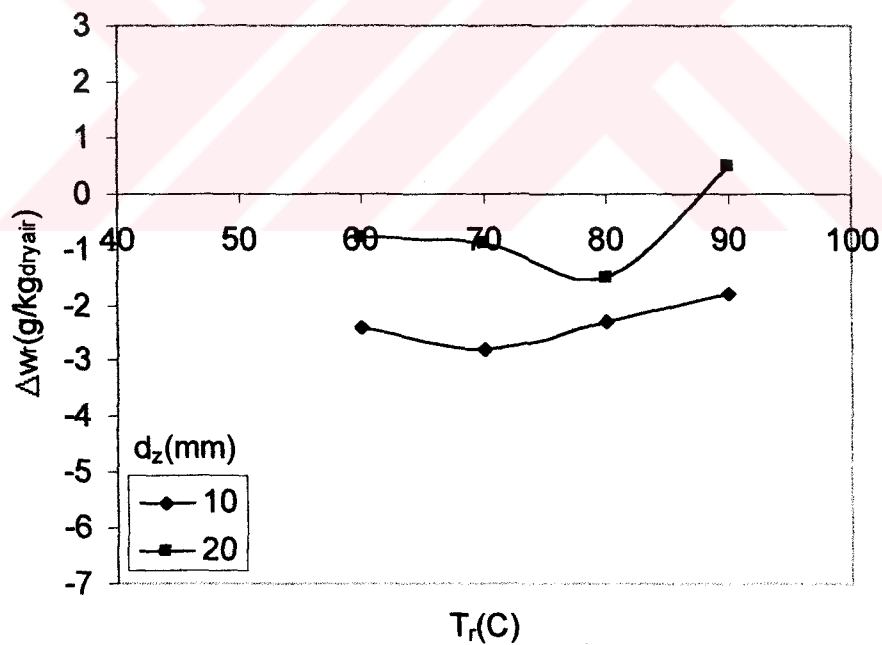


Figure 5.68 Variation of  $\Delta w_r$  with  $d_z$  at constant  $N_{RR}=10$ rpm,  $N_{DW}=0.1$ rpm and  $m_a=0.111$ kg/s

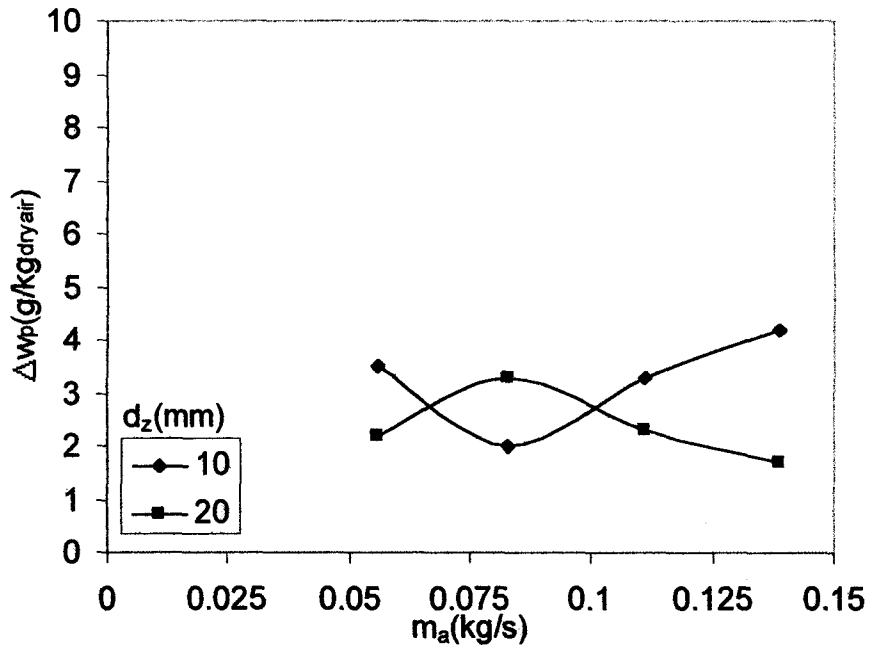


Figure 5.69 Variation of  $\Delta w_p$  with  $d_z$  at constant  $N_{RR}=10$ rpm,  $N_{DW}=0.1$ rpm and  $T_r=60$ C

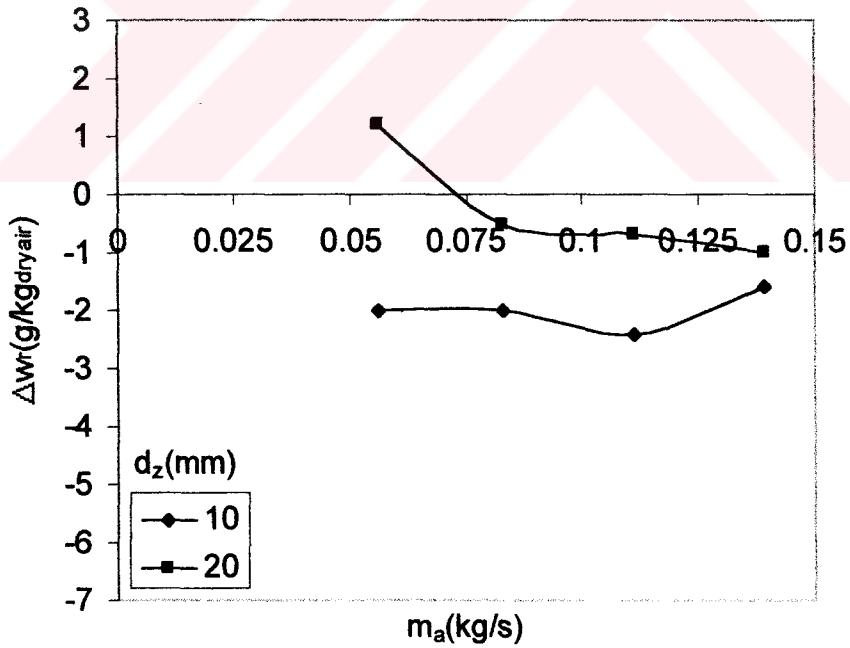


Figure 5.70 Variation of  $\Delta w_r$  with  $d_z$  at constant  $N_{RR}=10$ rpm,  $N_{DW}=0.1$ rpm and  $T_r=60$ C

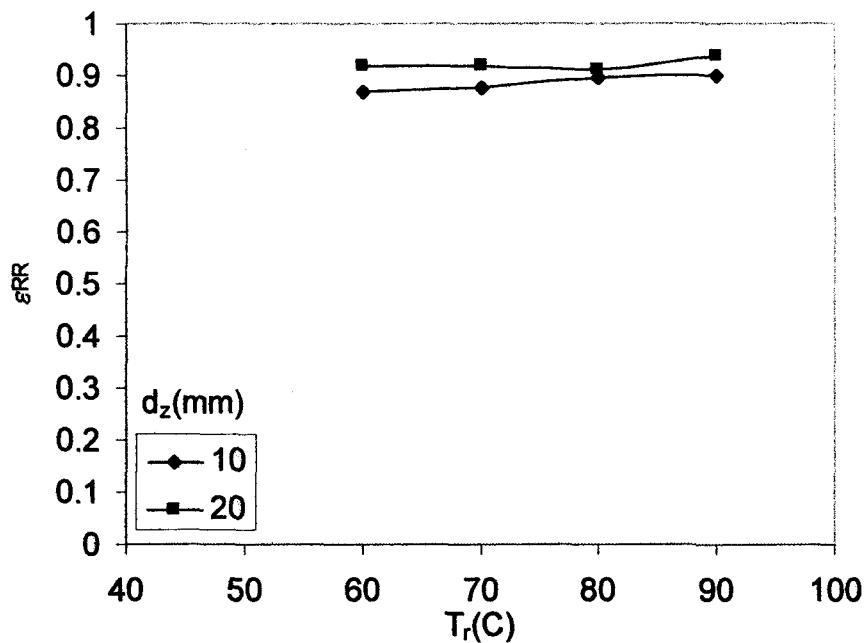


Figure 5.71 Variation of  $\epsilon_{RR}$  with  $d_z$  at constant  $N_{RR}=10\text{rpm}$ ,  $N_{DW}=0.1\text{rpm}$  and  $m_a=0.111\text{kg/s}$

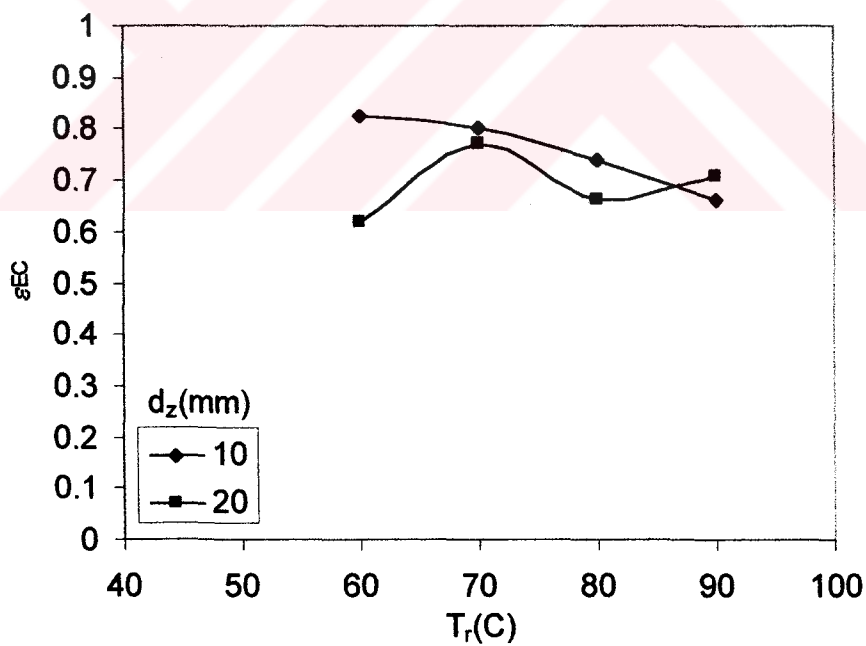


Figure 5.72 Variation of  $\epsilon_{EC}$  with  $d_z$  at constant  $N_{RR}=10\text{rpm}$ ,  $N_{DW}=0.1\text{rpm}$  and  $m_a=0.111\text{kg/s}$

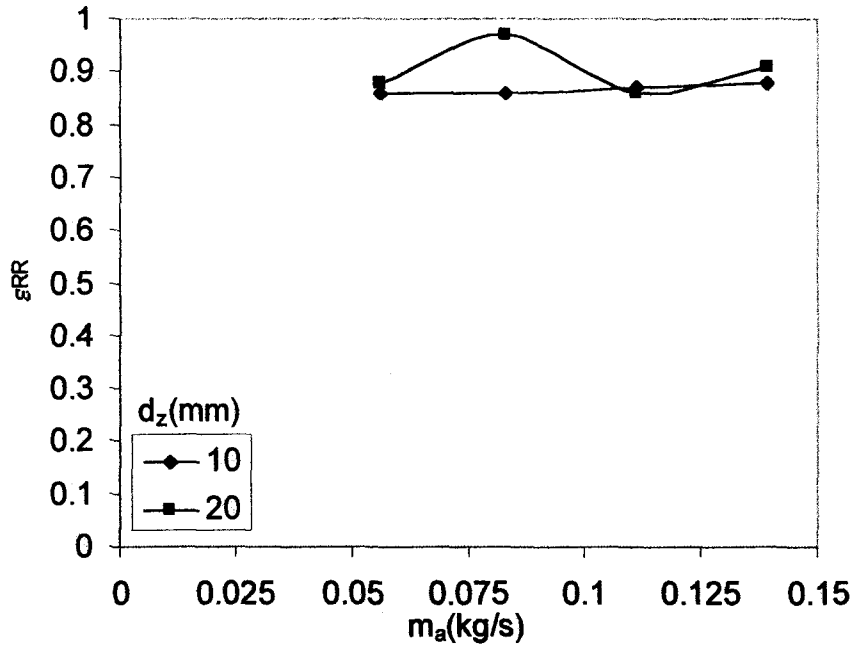


Figure 5.73 Variation of  $\epsilon_{RR}$  with  $d_z$  at constant  $N_{RR}=10$ rpm,  $N_{DW}=0.1$ rpm and  $T_r=60$ C

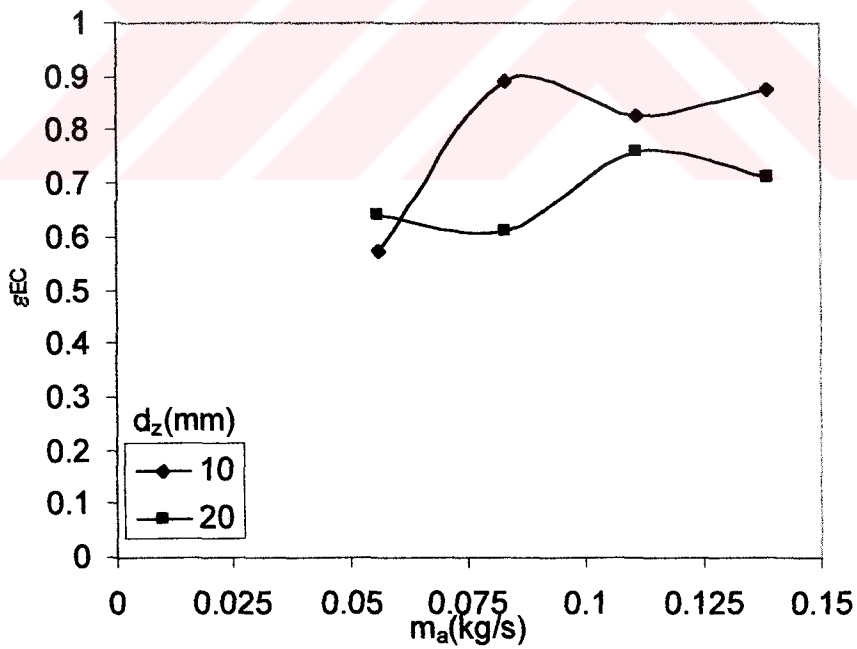


Figure 5.74 Variation of  $\epsilon_{EC}$  with  $d_z$  at constant  $N_{RR}=10$ rpm,  $N_{DW}=0.1$ rpm and  $T_r=60$ C

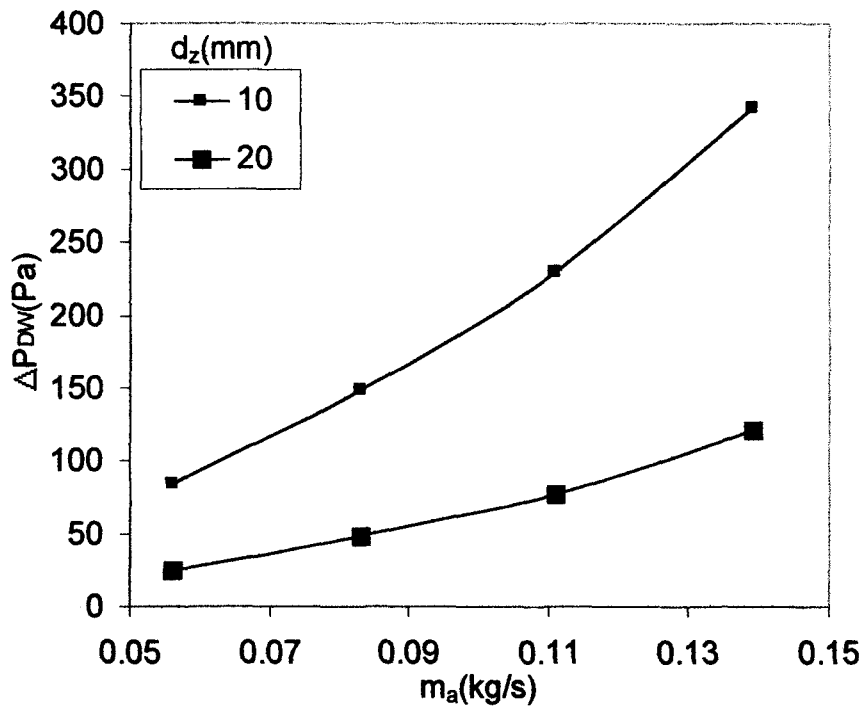


Figure 5.75 Effects of  $d_z$  as a function of  $m_a$  on  $\Delta P$  through DW with  $\Delta X_{DW} = 10$  cm and  $d_z = 10$  and 20 mm

## 5.7 EFFECTS OF DW THICKNESS ON DCS PERFORMANCE

A third set of experimental study was performed with a different  $\Delta X_{DW}$ ;  $\Delta X_{DW}=15\text{cm}$  keeping a zeolite size;  $d_z=20\text{mm}$ . Thus constraints of the study are;  $\Delta X_{RR}=10\text{cm}$ ,  $\Delta X_{DW}=15\text{cm}$  while the remaining parameters are briefly summarized in Table 4.1.

In this set of experiments; operation parameters  $N_{RR}$ ,  $N_{DW}$ ,  $T_r$  and  $m_a$  were changed in a sequence. Their constant values were;  $N_{RR}=10\text{rpm}$ ,  $N_{DW}=0.1\text{rpm}$ ,  $T_r=60\text{C}$ , and  $m_a=0.111\text{kg/s}$ . Three of them were kept constant and one of them was changed in the previously defined range as shown in Table 4.2 during the experiments. With these experiments effects of zeolite size on CC, COP,  $\Delta w$ ,  $\varepsilon$  and  $\Delta P$  were analyzed with different  $N_{RR}$ ,  $N_{DW}$ ,  $T_r$ , and  $m_a$ .

Referring to Figures 5.76-5.79 and Figures 5.88-5.91 the main performance parameters of CC and COP of DCS can be analyzed as a function of  $\Delta X_{DW}$  and operating parameters as follows:

1. Variation of CC with  $N_{RR}$  becomes significant as  $\Delta X_{DW}$  increases from 10cm to 15cm (Figure 5.76). The magnitudes of CC of DCS with  $\Delta X_{DW}=10\text{cm}$  is  $8\text{kW/kg}_{\text{dryair}}$  at  $N_{RR}=5\text{rpm}$  and decreases to  $6.5\text{kW/kg}_{\text{dryair}}$  for  $N_{RR}>5\text{rpm}$ . But the CC values of DCS are fluctuating around  $10\text{kW/kg}_{\text{dryair}}$  for the selected range of  $N_{RR}$ , with  $\Delta X_{DW} = 15\text{cm}$ .
2. Variation of CC with  $N_{DW}$  seems to be not seriously affected by  $\Delta X_{DW}$  (Figure 5.78). At  $N_{DW}=0.1\text{rpm}$ , CC values with 10cm and 15cm of  $\Delta X_{DW}$  are equal to each other as  $9\text{kW/kg}_{\text{dryair}}$ . For  $N_{DW}>0.1\text{rpm}$ , CC value with  $\Delta X_{DW} = 15\text{cm}$  get to a maximum value such as  $10.5\text{kW/kg}_{\text{dryair}}$  at  $N_{DW}=0.2\text{rpm}$ , then it starts to decrease with  $N_{DW}$ . Magnitude of CC with  $\Delta X_{DW} = 10\text{cm}$  stays constant for  $N_{DW}<0.2\text{rpm}$ , then starts to decrease with  $N_{DW}$ .



3. Variation of CC with  $T_r$  and  $m_a$  (Figures 5.88-5.90) seems to be similar in two  $\Delta X_{DW}$ . However CC magnitudes with  $\Delta X_{DW} = 15\text{cm}$  are greater than those with  $\Delta X_{DW} = 10\text{cm}$ . Magnitudes of the CC at  $T_r = 90\text{C}$  get close each other for  $\Delta X_{DW} = 10\text{cm}$  and  $\Delta X_{DW} = 15\text{cm}$ . The mean values of CC with  $\Delta X_{DW} = 10\text{cm}$  and  $\Delta X_{DW} = 15\text{cm}$  are  $6.5\text{kW/kg}_{\text{dryair}}$  and  $9.5\text{kW/kg}_{\text{dryair}}$  respectively. For the selected  $T_r = 60\text{C}$ , the values of CC with  $\Delta X_{DW} = 10\text{cm}$  and  $\Delta X_{DW} = 15\text{cm}$  increase with  $m_a$  with a small amount approximately  $\Delta\text{CC} = 1\text{kW/kg}_{\text{dryair}}$ .

Generally the magnitude of CC with  $\Delta X_{DW} = 15\text{cm}$  is greater than the CC values with  $\Delta X_{DW} = 10\text{cm}$  for different operating parameters such as  $N_{RR}$ ,  $N_{DW}$ ,  $m_a$ , and  $T_r$ .

4. COP value is not seriously affected with the thickness of the DW. It can be clearly seen in Figures 5.77, 5.79, 5.89, and 5.91. The variation of COP values are similar with the variation of the CC for  $N_{RR}$ ,  $m_a$ , and  $T_r$  and the magnitude of COP with  $\Delta X_{DW} = 15\text{cm}$  is greater than the COP with  $\Delta X_{DW} = 10\text{cm}$  with a similar behavior. However, variation of COP values with  $N_{DW}$  is not in the same behavior with the other operating parameters (Figures 5.78 and 5.79). COP values with  $\Delta X_{DW} = 10\text{cm}$  is greater than the COP values with  $\Delta X_{DW} = 15\text{cm}$ . For high values of  $N_{DW}$  and  $T_r$ , COP values of the system with both DW thickness get close each other (Figures 5.79 and 5.89).

Meanwhile COP values are greater with  $\Delta X_{DW} = 10\text{cm}$  than those with  $\Delta X_{DW} = 15\text{cm}$ . COP variation with operating parameters show similarities with different  $\Delta X_{DW}$  cases.

Variations of moisture removal capacity of DW -for different DW thickness as 10cm and 15cm are illustrated in Figures 5.80-5.83 and Figures

5.92-5.95. Moisture removal capacities of the process and regeneration sides of the DW should be considered together.

As shown in Figures 5.80 and 5.81 for  $\Delta X_{DW} = 10\text{cm}$  and for all  $N_{RR}$  adsorption in process and desorption in regeneration sides occur. Adsorption in process side and desorption in regeneration side are seen for  $N_{RR} < 10\text{rpm}$  with  $\Delta X_{DW} = 15\text{cm}$ . However only for  $\Delta X_{DW} = 15\text{cm}$  and  $N_{RR} > 10\text{rpm}$  desorption in process and adsorption in regeneration sides occur unexpectedly. The reason may be the influence of  $N_{RR}$  on  $\Delta X_{DW}$ .

As a comment on  $\Delta X_{DW}$  it can be said that increase in  $\Delta X_{DW}$  causes an adverse effect on moisture removal for both process and regeneration sides (instead of adsorption desorption or visa versa).

Referring to Figures 5.84-5.87 and Figures 5.96-5.99 the effectiveness of RR and EC can be analyzed as a function of  $\Delta X_{DW}$  and operating parameters as follows: The magnitude of  $\varepsilon_{RR}$  is not changed with varying operating parameters for  $\Delta X_{DW} = 10\text{cm}$  and  $\Delta X_{DW} = 15\text{cm}$ . It stays constant such as  $\varepsilon_{RR} = 0.9$  for  $\Delta X_{DW} = 10\text{cm}$  and  $\Delta X_{DW} = 15\text{cm}$  and for all  $N_{RR}$ ,  $N_{DW}$ ,  $m_a$ , and  $T_r$  with small deviations.

About  $\varepsilon_{EC}$ , as it can be seen in Figures 5.85 and 5.99  $\varepsilon_{EC}$  for different  $\Delta X_{DW} = 10\text{cm}$  and  $\Delta X_{DW} = 15\text{cm}$  fluctuating with  $N_{RR}$  and  $m_a$ . It is not possible to say reason for this behavior. But,  $\varepsilon_{EC}$  with  $\Delta X_{DW} = 10\text{cm}$  is greater than  $\varepsilon_{EC}$  with  $\Delta X_{DW} = 15\text{cm}$  at  $N_{DW} = 0.1\text{rpm}$ . The behavior of  $\varepsilon_{EC}$  for both DW thickness are similar for  $N_{DW} \geq 0.2\text{rpm}$ . The variation of  $\varepsilon_{EC}$  with the DW thickness is vary interesting. The  $\varepsilon_{EC}$  with  $\Delta X_{DW} = 15\text{cm}$  is greater than  $\varepsilon_{EC}$  with  $\Delta X_{DW} = 10$  for  $T_r < 85\text{C}$ , for  $T_r > 85\text{C}$  visa versa. The difference between the magnitudes of  $\varepsilon_{EC}$  with  $\Delta X_{DW} = 15\text{cm}$  and  $\Delta X_{DW} = 10\text{cm}$  is not too much for  $T_r \leq 70\text{C}$ .

Figure 5.100 shows that the pressure loss,  $\Delta P_{DW}$  through the DW is not so affected with  $\Delta X_{DW}$ , which is increased from 10cm to 15cm thickness due to the big zeolite particle size as 20mm.

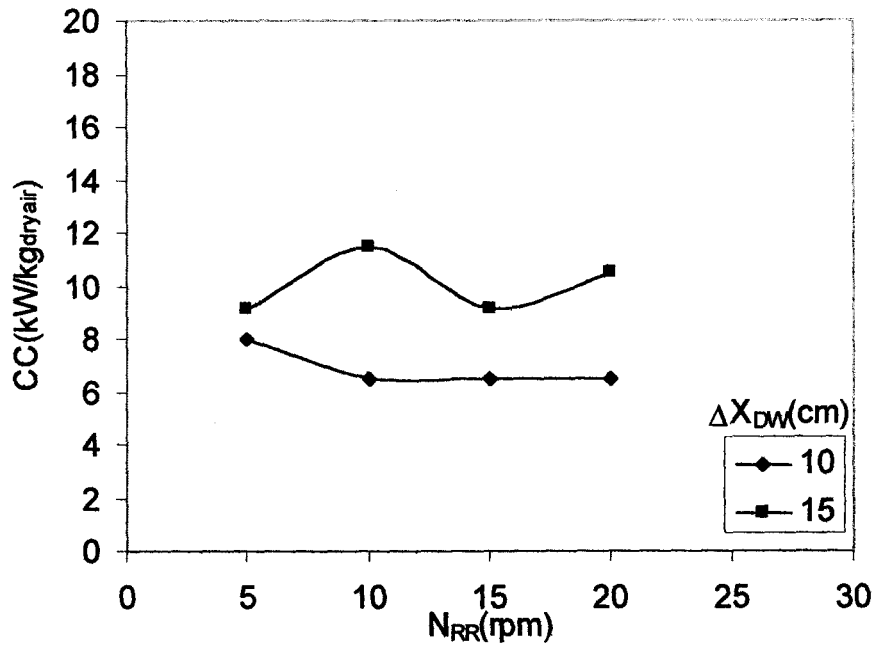


Figure 5.76 Variation of CC with  $\Delta X_{DW}$  at constant  $N_{DW}=0.1$  rpm,  $T_r=60$  C and  $m_a=0.111$  kg/s

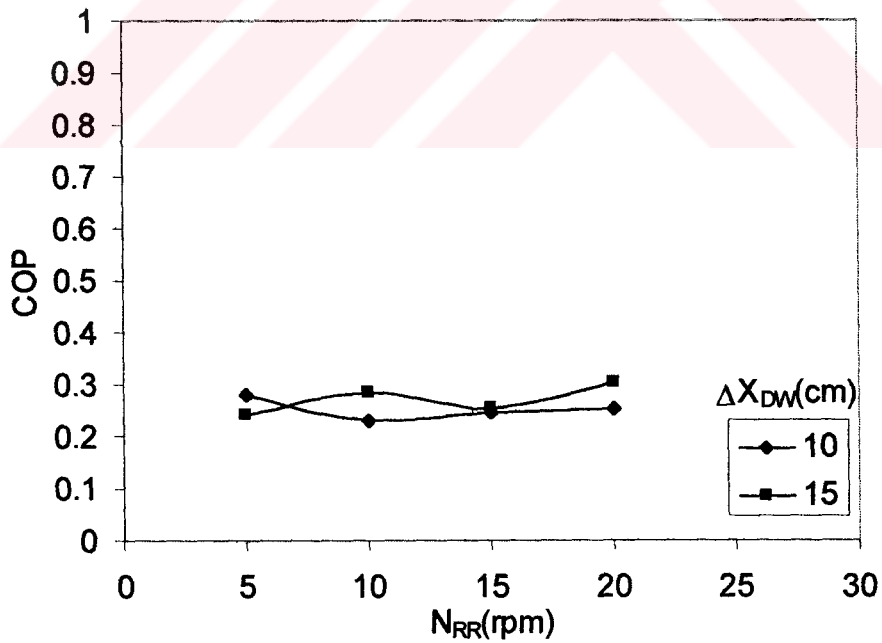


Figure 5.77 Variation of COP with  $\Delta X_{DW}$  at constant  $N_{DW}=0.1$  rpm,  $T_r=60$  C and  $m_a=0.111$  kg/s

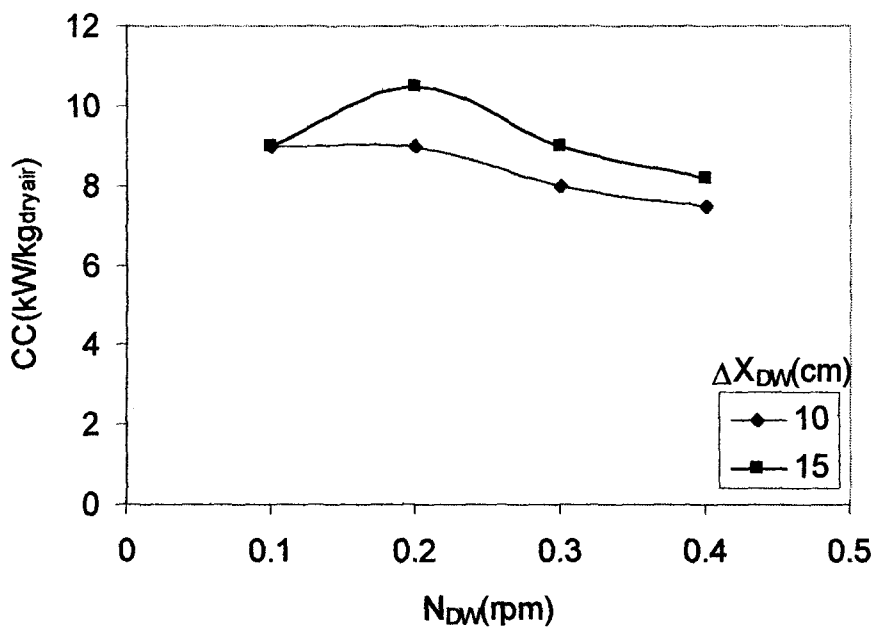


Figure 5.78 Variation of CC with  $\Delta X_{DW}$  at constant  $N_{RR}=10$ rpm,  $T_r=60$ C and  $m_a=0.111$ kg/s

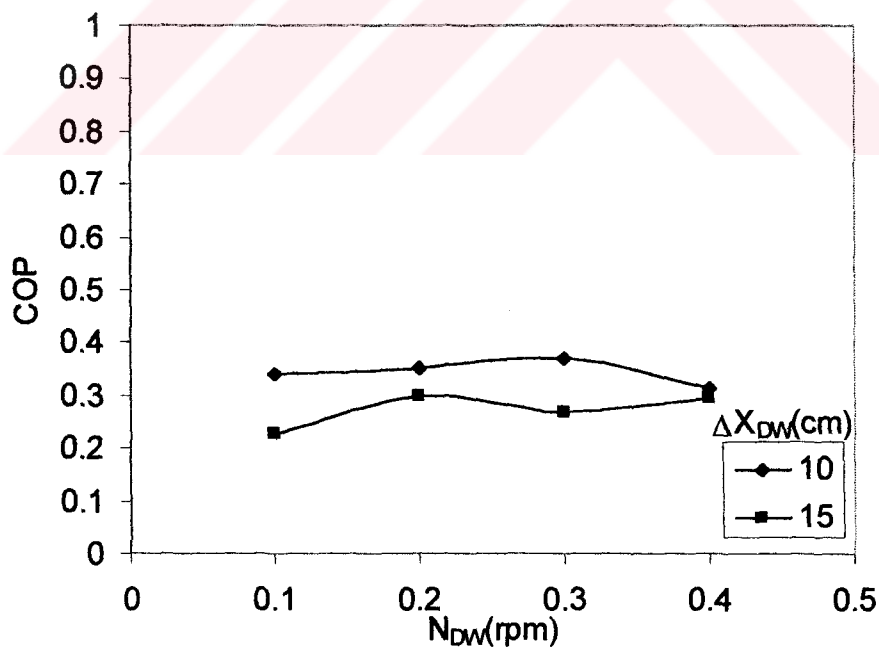


Figure 5.79 Variation of COP with  $\Delta X_{DW}$  at constant  $N_{RR}=10$ rpm,  $T_r=60$ C and  $m_a=0.111$ kg/s

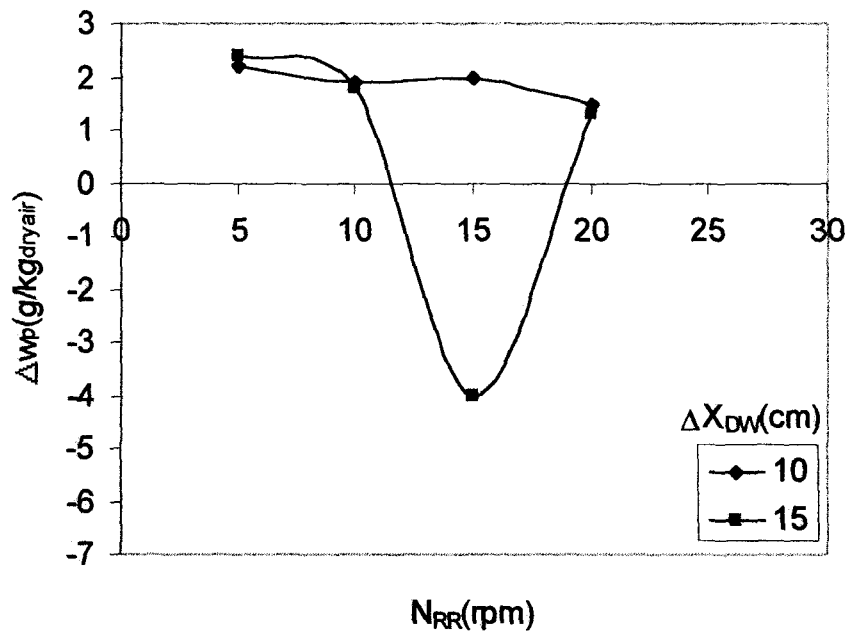


Figure 5. 80 Variation of  $\Delta w_p$  with  $\Delta X_{DW}$  at constant  $N_{DW}=0.1$  rpm,  $T_r=60$  C and  $m_a=0.111$  kg/s

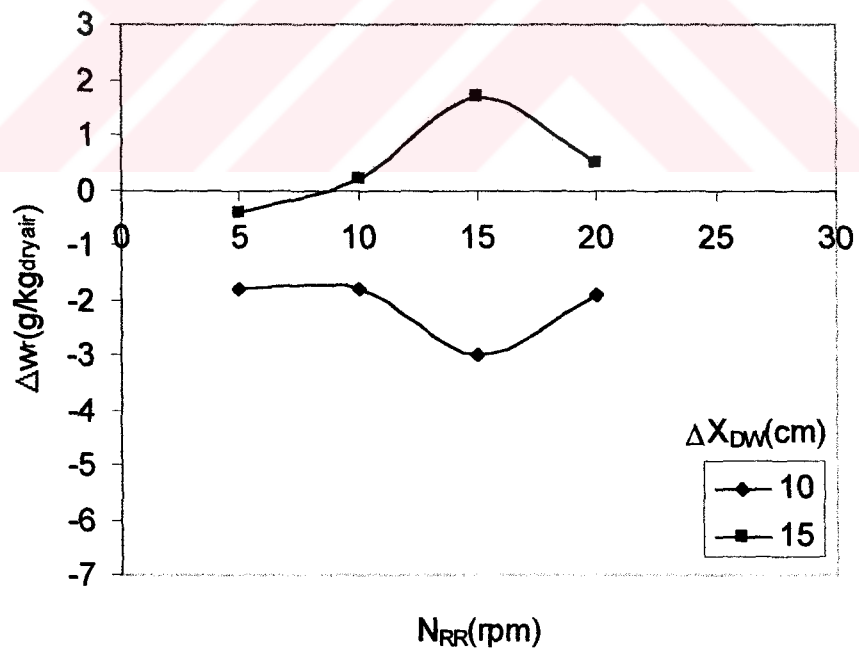


Figure 5. 81 Variation of  $\Delta w_r$  with  $\Delta X_{DW}$  at constant  $N_{DW}=0.1$  rpm,  $T_r=60$  C and  $m_a=0.111$  kg/s

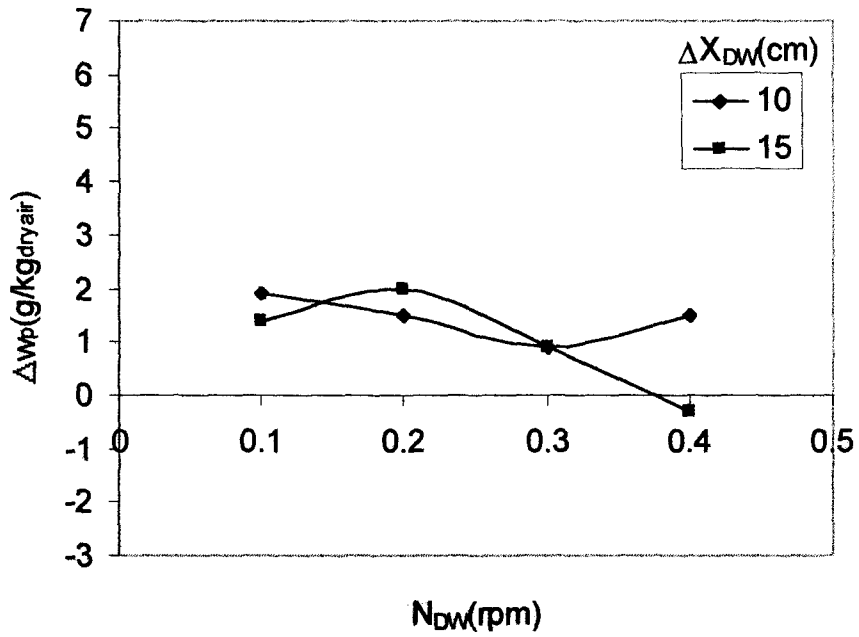


Figure 5.82 Variation of  $\Delta w_p$  with  $\Delta X_{DW}$  at constant  $N_{RR}=10$ rpm,  $T_r=60$ C and  $m_a=0.111$ kg/s

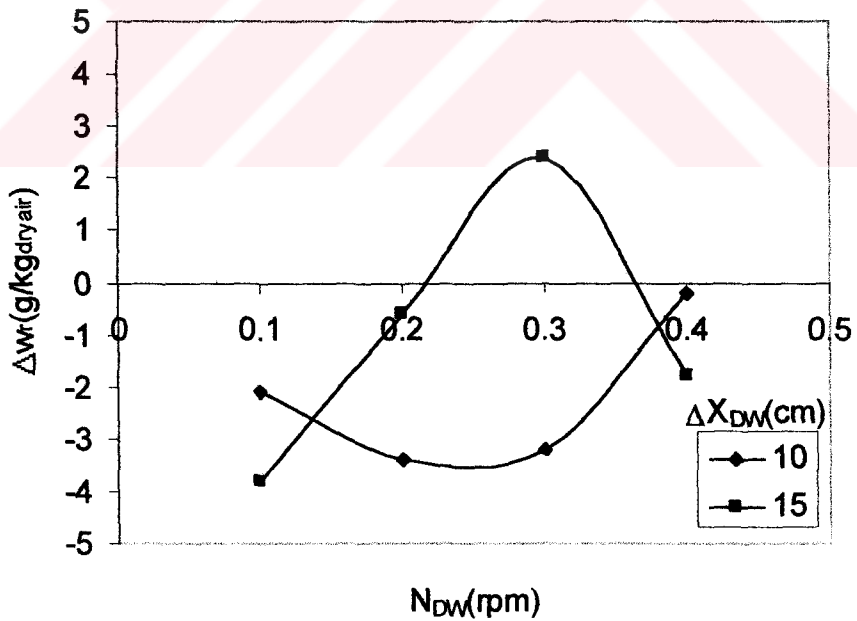


Figure 5.83 Variation of  $\Delta w_r$  with  $\Delta X_{DW}$  at constant  $N_{RR}=10$ rpm,  $T_r=60$ C and  $m_a=0.111$ kg/s

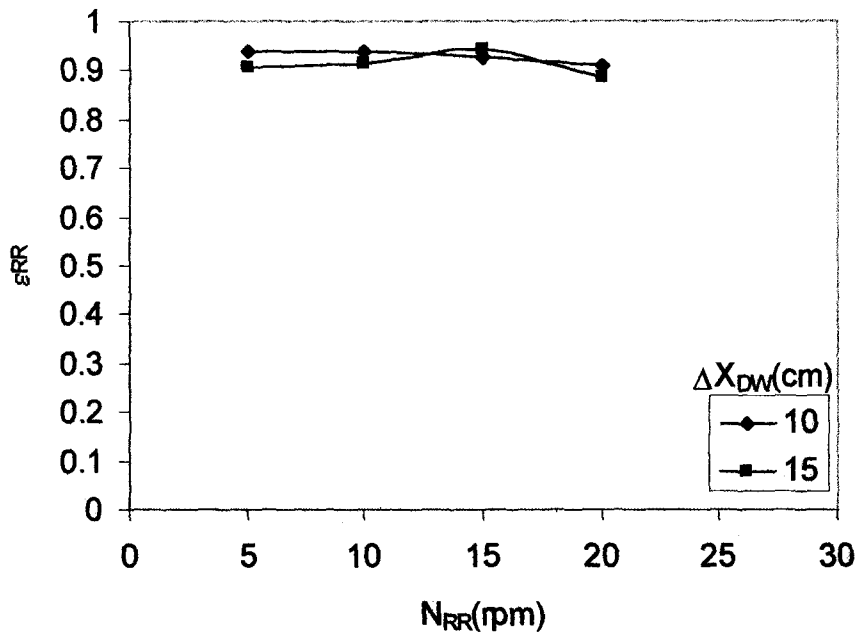


Figure 5. 84 Variation of  $\epsilon_{RR}$  with  $\Delta X_{DW}$  at constant  $N_{DW}=0.1$  rpm,  $T_r=60C$  and  $m_a=0.111$ kg/s

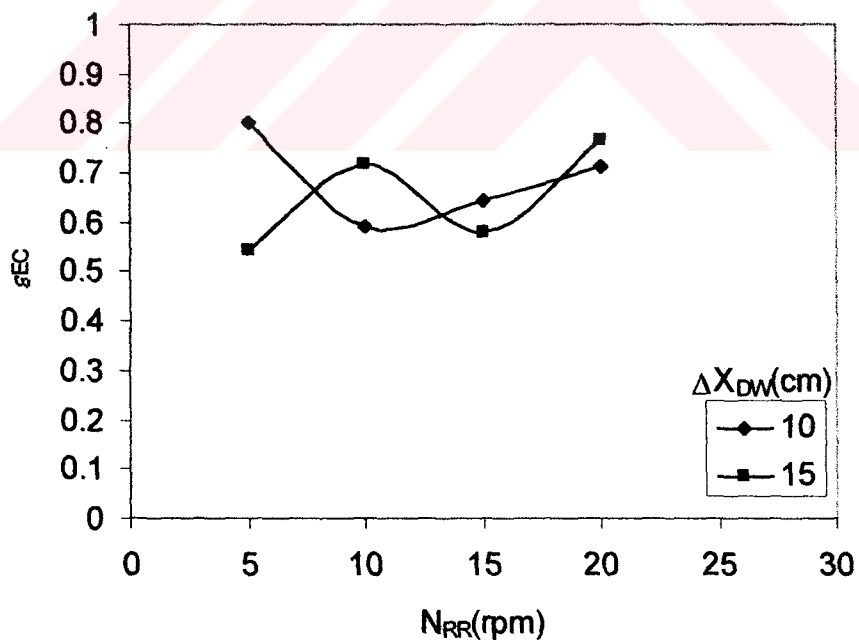


Figure 5. 85 Variation of  $\epsilon_{EC}$  with  $\Delta X_{DW}$  at constant  $N_{DW}=0.1$  rpm,  $T_r=60C$  and  $m_a=0.111$ kg/s

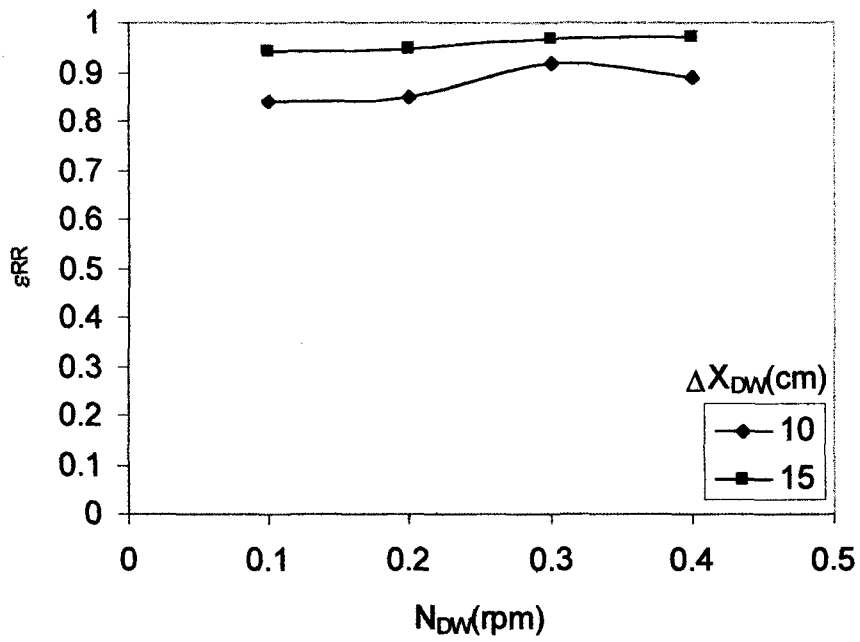


Figure 5. 86 Variation of  $\epsilon_{RR}$  with  $\Delta X_{DW}$  at constant  $N_{RR}=10$ rpm,  $T_r=60$ C and  $m_a=0.111$ kg/s

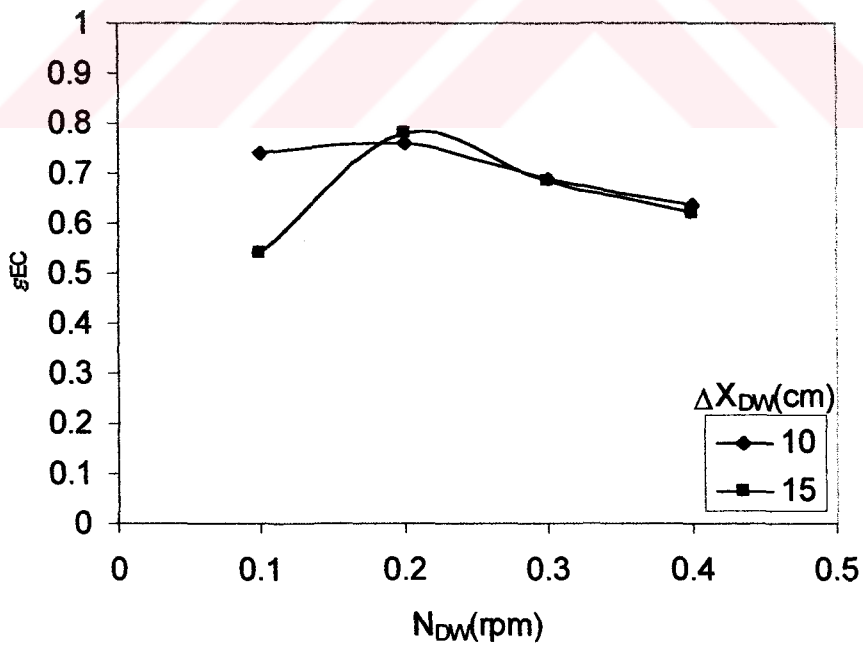


Figure 5. 87 Variation of  $\epsilon_{EC}$  with  $\Delta X_{DW}$  at constant  $N_{RR}=10$ rpm,  $T_r=60$ C and  $m_a=0.111$ kg/s



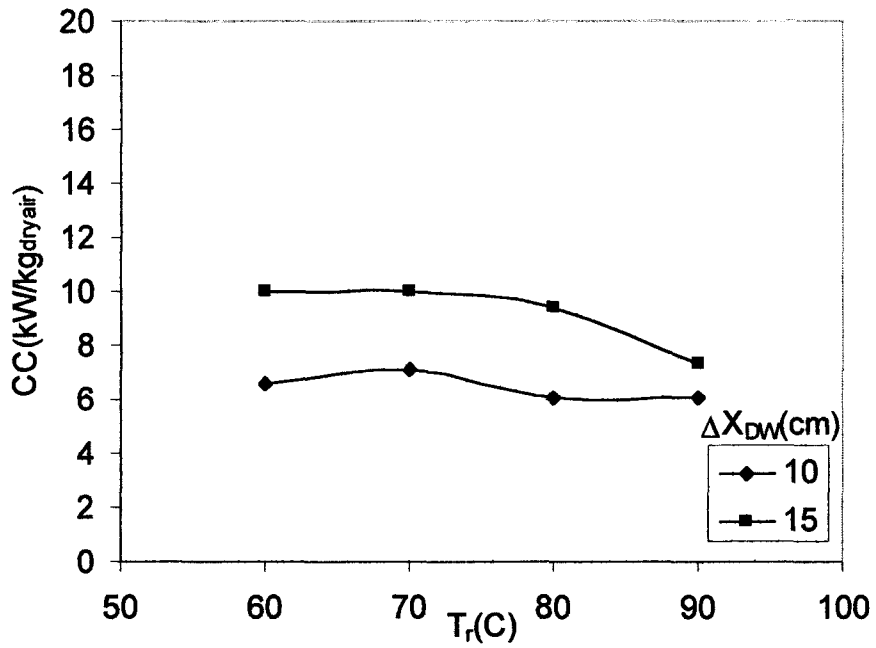


Figure 5. 88 Variation of CC with  $\Delta X_{DW}$  at constant  $N_{RR}=10$ rpm,  $N_{DW}=0.1$ rpm and  $m_a=0.111$ kg/s

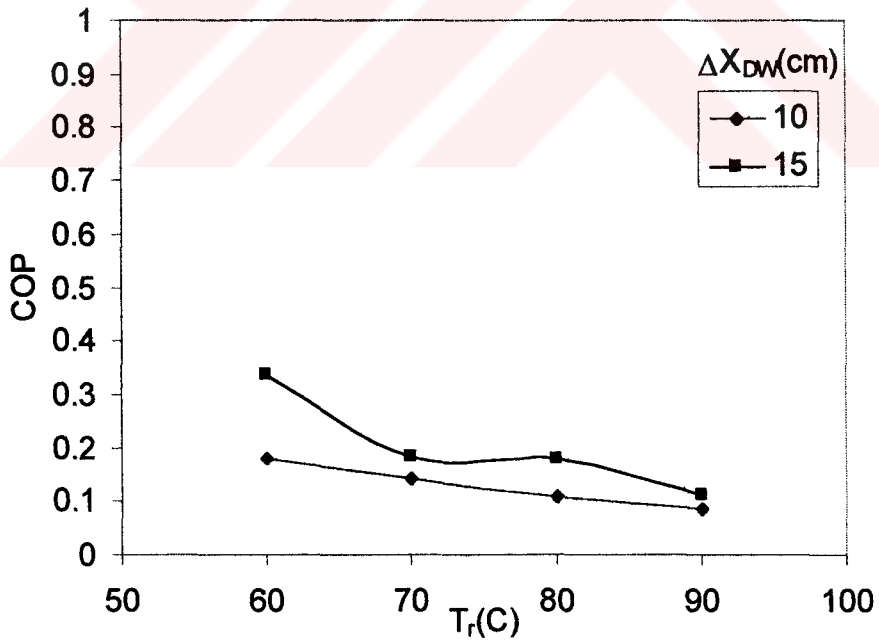


Figure 5. 89 Variation of COP with  $\Delta X_{DW}$  at constant  $N_{RR}=10$ rpm,  $N_{DW}=0.1$ rpm and  $m_a=0.111$ kg/s

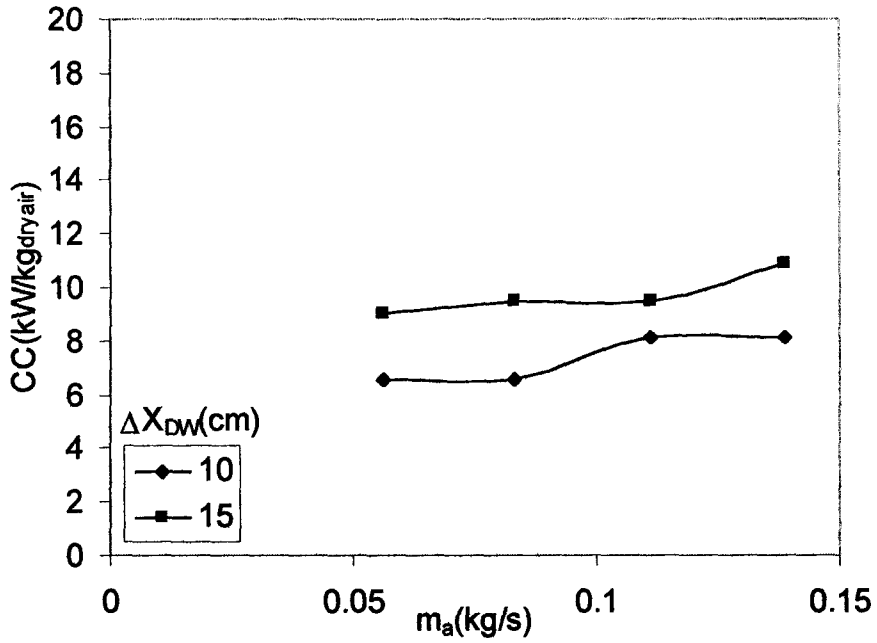


Figure 5.90 Variation of CC with  $\Delta X_{DW}$  at constant  $N_{RR}=10$ rpm,  $N_{DW}=0.1$ rpm and  $T_r=60$ C

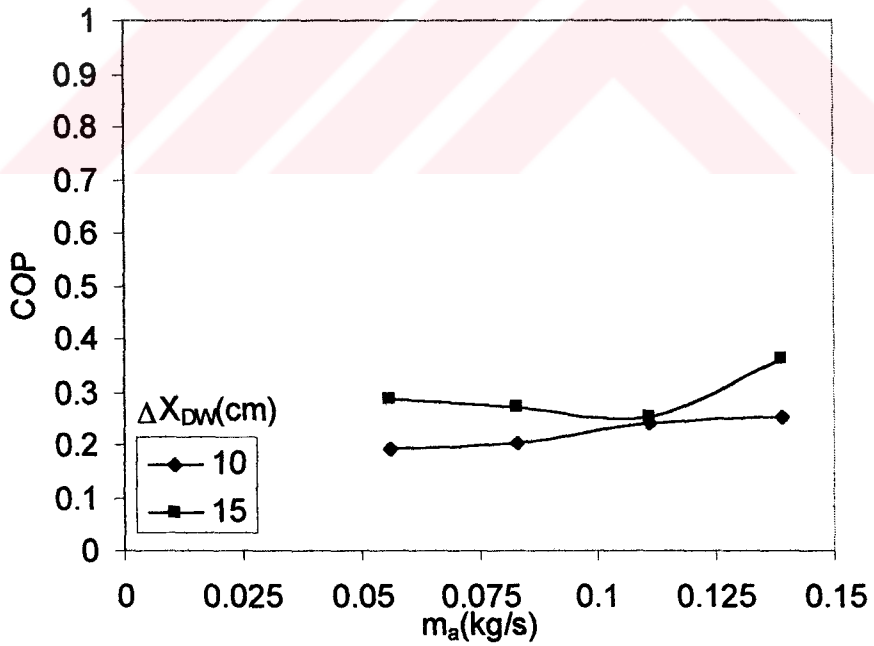


Figure 5.91 Variation of COP with  $\Delta X_{DW}$  at constant  $N_{RR}=10$ rpm,  $N_{DW}=0.1$ rpm and  $T_r=60$ C

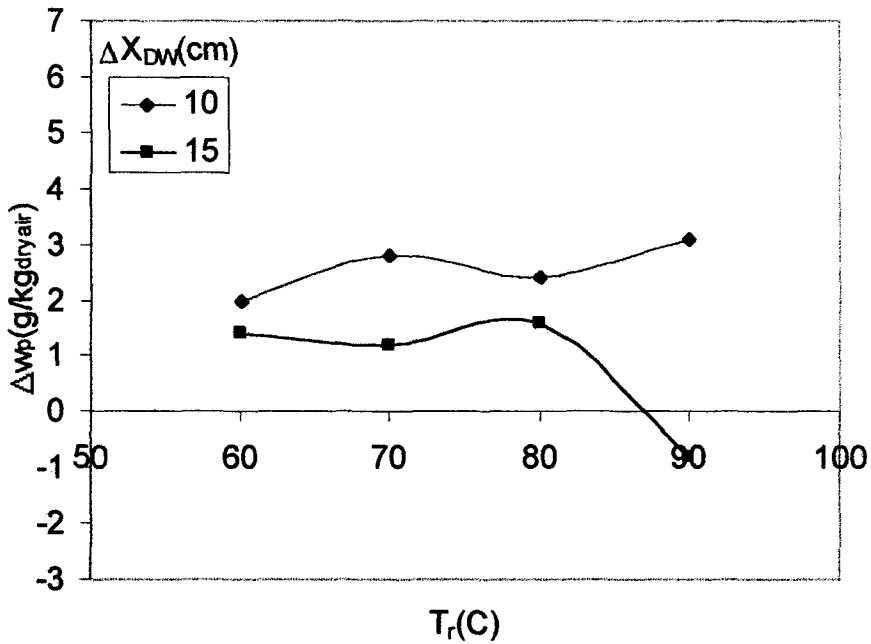


Figure 5. 92 Variation of  $\Delta w_p$  with  $\Delta X_{DW}$  at constant  $N_{RR}=10$ rpm,  $N_{DW}=0.1$ rpm and  $m_a=0.111$ kg/s

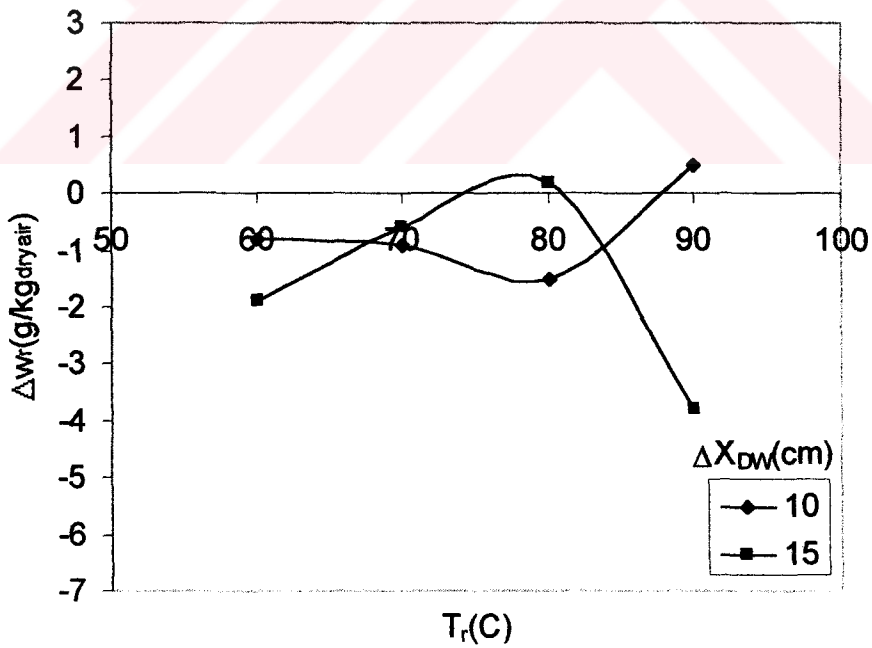


Figure 5. 93 Variation of  $\Delta w_r$  with  $\Delta X_{DW}$  at constant  $N_{RR}=10$ rpm,  $N_{DW}=0.1$ rpm and  $m_a=0.111$ kg/s

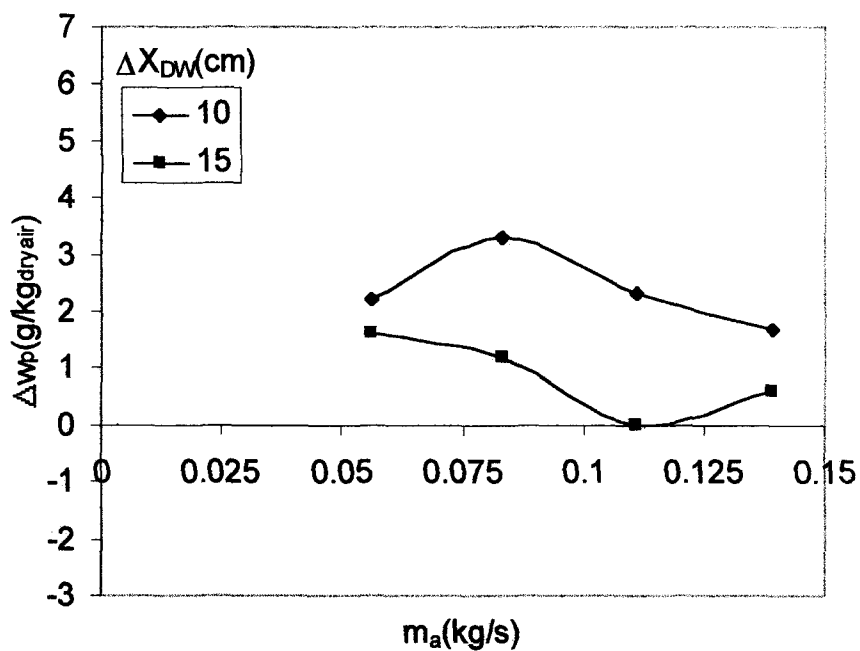


Figure 5.94 Variation of  $\Delta w_p$  with  $\Delta X_{DW}$  at constant  $N_{RR}=10$ rpm,  $N_{DW}=0.1$ rpm and  $T_r=60$ C

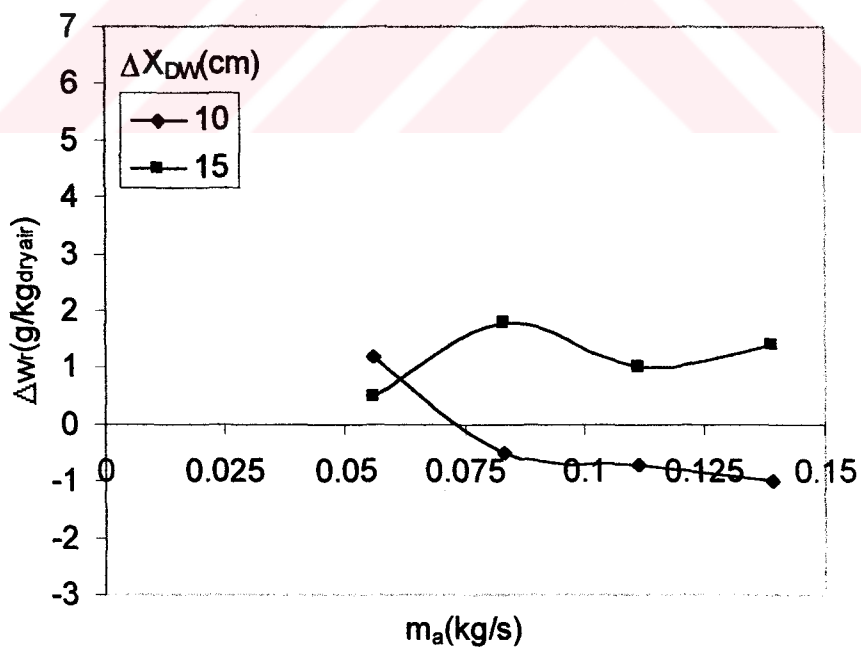


Figure 5.95 Variation of  $\Delta w_r$  with  $\Delta X_{DW}$  at constant  $N_{RR}=10$ rpm,  $N_{DW}=0.1$ rpm and  $T_r=60$ C

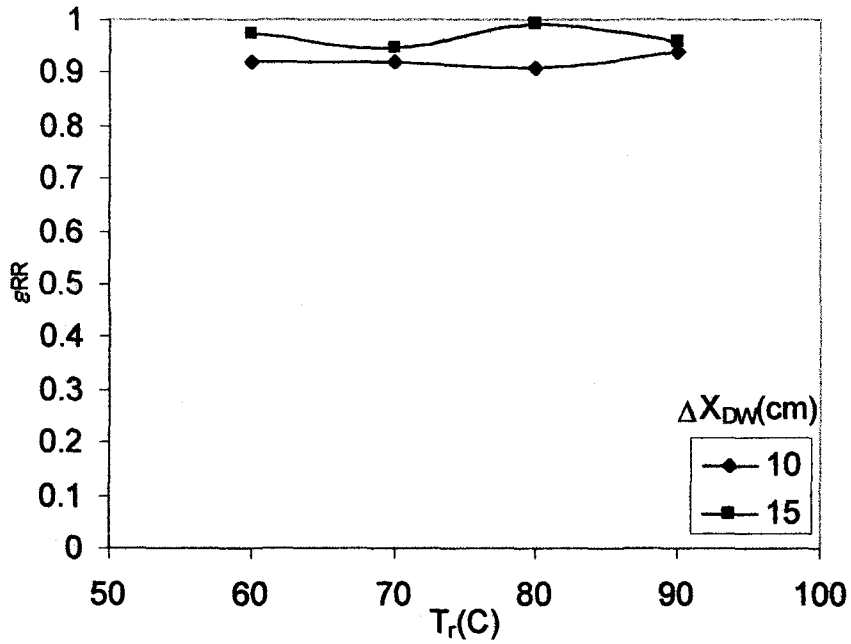


Figure 5. 96 Variation of  $\epsilon_{RR}$  with  $\Delta X_{DW}$  at constant  $N_{RR}=10$ rpm,  $N_{DW}=0.1$ rpm and  $m_a=0.111$ kg/s

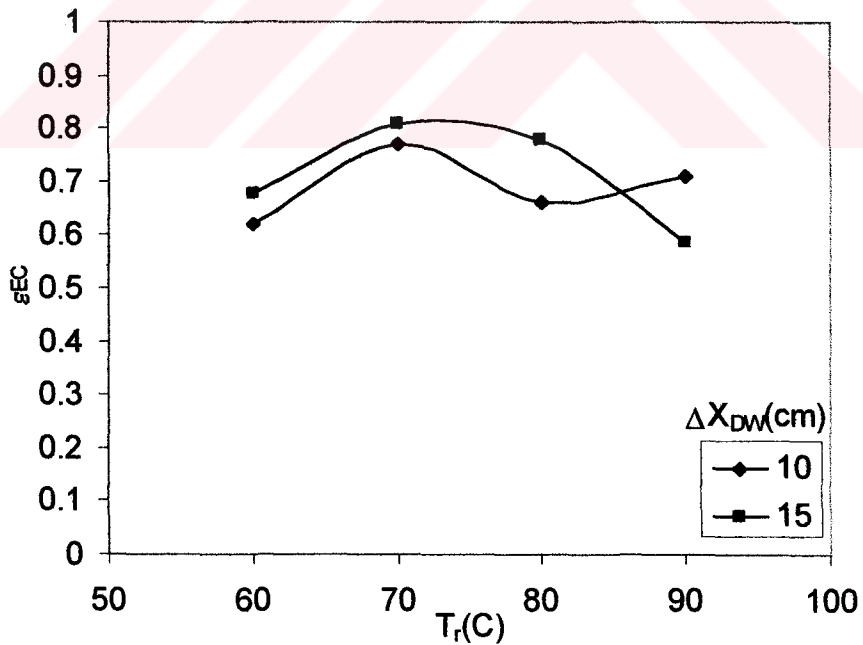


Figure 5. 97 Variation of  $\epsilon_{EC}$  with  $\Delta X_{DW}$  at constant  $N_{RR}=10$ rpm,  $N_{DW}=0.1$ rpm and  $m_a=0.111$ kg/s

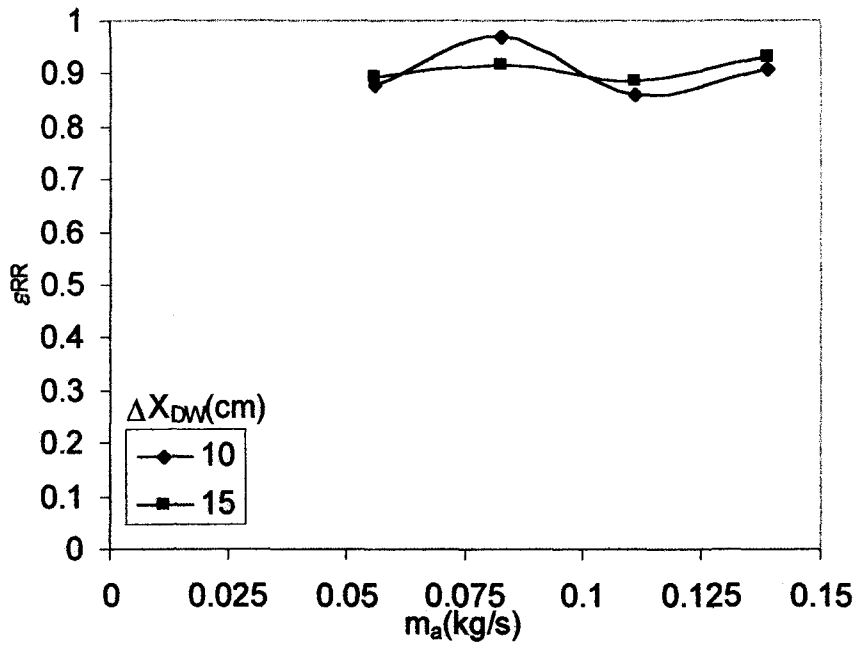


Figure 5. 98 Variation of  $\epsilon_{RR}$  with  $\Delta X_{DW}$  at constant  $N_{RR}=10$ rpm,  $N_{DW}=0.1$ rpm and  $T_r=60$ C

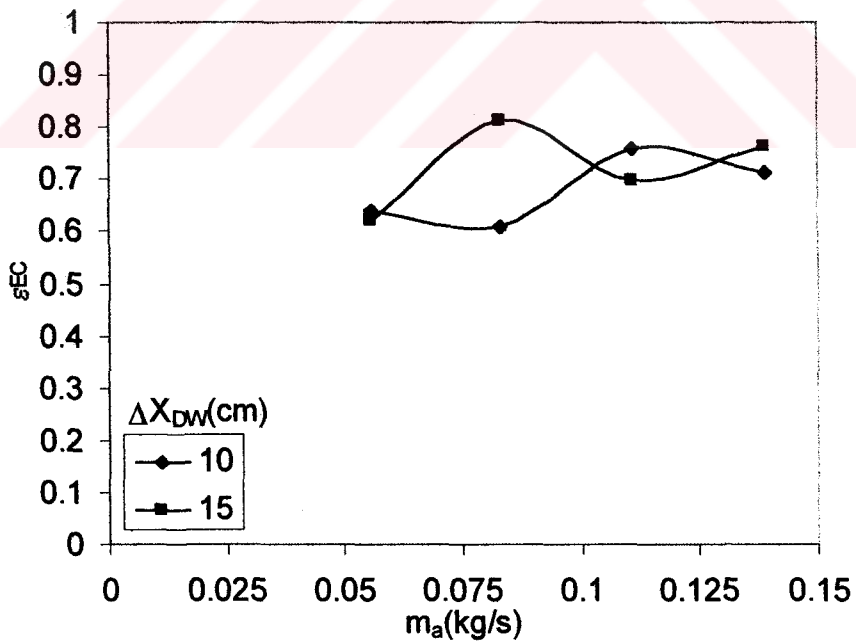


Figure 5. 99 Variation of  $\epsilon_{EC}$  with  $\Delta X_{DW}$  at constant  $N_{RR}=10$ rpm,  $N_{DW}=0.1$ rpm and  $T_r=60$ C

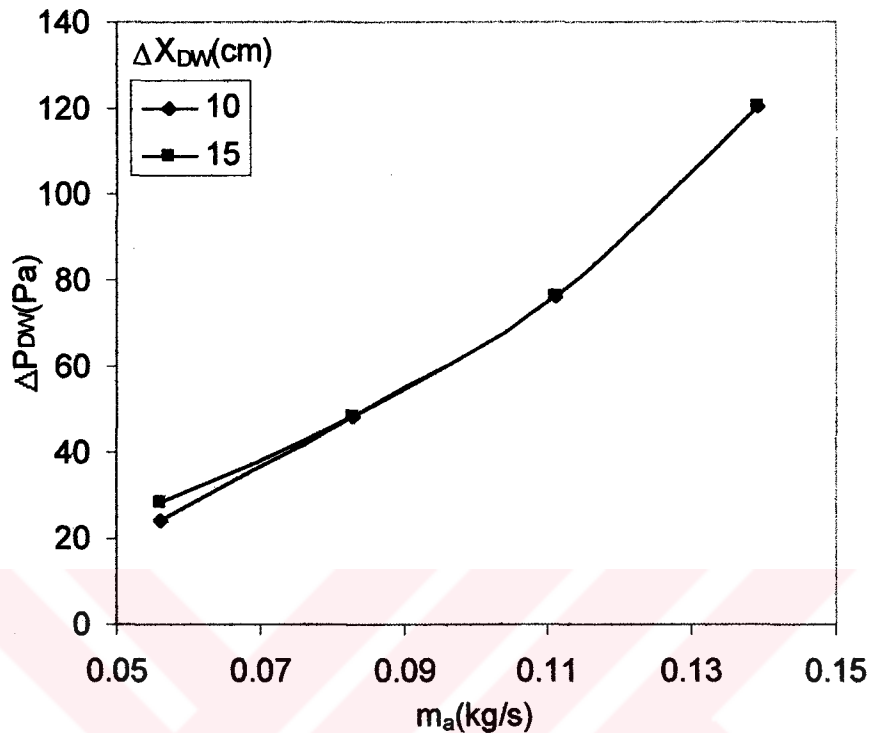


Figure 5.100 Effects of  $\Delta X_{DW}$  as a function of  $m_a$  on  $\Delta P$  through DW with  $\Delta X_{DW}=10$ cm and 15cm and  $d_z=20$ mm

## 5.8 COMPARISON WITH PREVIOUS WORKS

In this section, some experimental and theoretical results which were previously obtained on CC, COP,  $\Delta w$  and behavior of these as a function of  $T_r$ ,  $N_{DW}$ , and  $m_a$  are analyzed with respect to the experimental results of the present study.

Jalazadeh-Azar, A. A., et al experimentally obtained latent CC and COP as 0.4 and 18.7kW respectively. The face area of the DW is equally divided between the process and regeneration streams. They observed that when CC increases, COP decreases with increasing  $T_r$  in the range of  $65C < T_r < 85C$ ,  $m_a=1.42$ kg/s, and  $N_{DW}=1.33$ rpm[9].

The maximum normalized CC and COP (as 1) were obtained experimentally at  $N_{DW}=0.12\text{rpm}$  and  $N_{DW}=0.22\text{rpm}$  respectively with Virgin Silica Gel by Pesaran, A. A. and Penney, T. R. [37].

CC=10.56kW and COP=0.93 were obtained experimentally at  $N_{DW}=0.055\text{rpm}$ ,  $m_a=0.63\text{kg/s}$ , and  $T_r=70\text{C}$  by Pesaran, A. A. and Wipke, B. B. [21].

Vineyard, E. A. et al experimentally observed that latent CC and COP increase with increasing  $N_{DW}$  and latent CC increases with  $m_a$  and  $T_r$ . At  $N_{DW}=1.33\text{rpm}$ , latent CC=70 000Btu/hr and latent COP=0.375 [11].

Maximum CC and COP were 21kW and 0.55 respectively which were experimentally obtained at  $N_{DW}=20\text{rpm}$  with silica gel by Pons, M., and Kodama, A. [13]. They also observed that CC increases with increasing  $U_a$ ,  $T_r$  but COP decreases with increasing  $U_a$  and  $T_r$  in the ranges of  $0.5\text{m/s}<U_a<3.5\text{m/s}$  and  $60\text{C}<T_r<110\text{C}$ .

Löf, G. O. G. et all experimentally observed that COP=1 in the range of  $45\text{C}<T_r<70\text{C}$  with lithium chloride and COP decreases with increasing  $T_r$  when CC increases [47].

Joudi, K. A. and Mahdi, S. M. experimentally obtained maximum seasonal COP=2.8 at  $m_a=0.075\text{kg/s}$  with silica gel and they also observed that  $\Delta w$  increases with increasing  $T_r$ . COP increases with increasing  $T_r$  and  $m_p$  in the range of  $55<T_r<75\text{C}$  and  $0.025<m_p<0.075\text{kg/s}$  [48].

Outlet to inlet humidity ratio in process side decreases with increasing  $T_r$  and minimum ratio was obtained experimentally at  $N_{DW}=0.117\text{rpm}$  in the range of  $0.0\text{rpm}<N_{DW}<0.333\text{rpm}$  by Kodama A. et al [100].

Neti, S., and Wolfe, E. I. Experimentally observed that  $\Delta w$  increases with increasing  $T_r$ , but decreases with increasing  $N_{DW}$  in the ranges of  $60\text{C}<T_r<150\text{C}$ , and  $0.05\text{rpm}<N_{DW}<0.283\text{rpm}$ [102].



Nelson, J. S. et al obtained COP=2 at  $T_r=70C$  and COP decreases with increasing  $T_r$  by using silica gel as desiccant in the range of  $60C < T_r < 120C$  [57].

Dai, Y. J. et al get the results from their study that  $\Delta w$  is not changed with  $N_{DW}$  and  $\Delta X_{DW}$ ,  $\Delta w$  increases with  $T_r$  in regeneration side and decreases in process side in the ranges of  $0.0rpm < N_{DW} < 0.333rpm$  and  $75C < T_r < 125C$  [101].

Majumdar, P., and Worek, W. M. get maximum COP=1 and  $CC=13kJ/kg_{dryair}$  at  $T_r=50C$ . COP decreases with increasing  $T_r$ . CC and  $\Delta w$  does not changed rapidly with  $T_r$  in the range  $45C < T_r < 100C$  [41].

The results obtained from the study of Joudi, K. A., and Dhaidan, N. S. were COP=5 at  $T_r=60C$  and decreases with increasing  $T_r$ , but  $\Delta w$  increases with  $T_r$  in the range  $45C < T_r < 100C$  [7].

Maximum CC and COP were obtained at 0.133 and 0.2rpm of  $N_{DW}$  respectively by Pesaran, A.A. [24].

In previous studies [7, 48, 100, 102]  $\Delta w$  increases with increasing  $T_r$ . CC also increases with increasing  $T_r$  [11, 13, 47]. But COP decreases with increasing  $T_r$  [7, 13, 41, 47, 57].

Results obtained in the study as CC, COP and  $\Delta w$ , as a function  $T_r$ , like that; COP and  $\Delta w$  are in same behavior with the results of previous works. In our study CC is also decreases with increasing  $T_r$ , but increases with  $m_a$  [11, 13]. Some maximum COP's obtained in previous study are 1 at  $T_r=50C$  [41], 1.25 at  $T_r=50C$ , and 0.7 at  $T_r=65C$  [47].

As shown in Figures 5.5, and 5.7 maximum COP is 1.3 at  $m_a=0.083kg/s$ ,  $T_r=60C$ ,  $N_{RR}=20rpm$  and  $N_{DW}=0.4rpm$  (24rph). But, maximum

CC was obtained at  $T_r=60\text{C}$ ,  $m_a=0.139\text{kg/s}$ ,  $N_{RR}=5\text{rpm}$ , and  $N_{DW}=0.1\text{rpm}$  (6rph) as  $17\text{kW/kg}_{\text{dryair}}$ . Both of the highest COP and CC were obtained at  $T_{\text{db}}=35\text{C}$  and RH is 20%.

Maximum COP and CC obtained in previous studies [13, 24] at 0.133(8), 0.2(12) and 0.333(20)rpm(rph).

For  $\Delta w$  variation, as a function of  $N_{DW}$ , obtained results as shown in Figures 5.20-5.35  $\Delta w$  decreases with increasing  $N_{DW}$  and it is in the same behavior with previous studies [102].

In this study instead of one parameter all of the design and effects of operating parameters as  $N_{RR}$ ,  $N_{DW}$ ,  $m_a$ , and  $T_r$  on CC, COP of DCS,  $\Delta w_r$ ,  $\Delta w_p$ ,  $\varepsilon_{RR}$ , and  $\varepsilon_{EC}$  were investigated in the selected ranges of design, and operating parameters with the selected matrix and desiccant materials as louvered Cu plate and natural zeolite.

## 5.9 CONCLUSION

In this chapter an experimental investigation conducted with selected system parameters to evaluate the influence of operation parameter is presented.

The constructed system is an original and new contribution to the related literature, due to its design characteristics. The presented experimental study covers a wide range parameters which is a serious gap in literature.

General comments based on conducted three sets of experiments following points can be given:

On operating parameters;

1. Effects of  $N_{RR}$  is not too high on CC and COP,
2. CC decreases with increasing  $N_{DW}$ ,
3. When  $m_a$  increases, effects of  $N_{RR}$  on COP decreases,
4. At high  $T_r$  effect of  $N_{DW}$  on CC decreases,
5.  $\Delta w_p$ , and  $\Delta w_r$  decreases with increasing  $N_{DW}$ ,
6. For low  $m_a$ ,  $N_{RR}$  and  $N_{DW}$  are effective on  $\Delta w_p$ ,  $\Delta w_r$ ,
7.  $N_{RR}$ ,  $N_{DW}$ ,  $m_a$  and  $T_r$  are not effective on  $\varepsilon_{RR}$ ,
8.  $\varepsilon_{EC}$  is under the effect of  $N_{DW}$ ,
9.  $\varepsilon_{EC}$  decreases with increasing  $T_r$ ,
10. CC is not depend on  $m_a$  at high  $T_r$
11. COP decreases with increasing  $T_r$ ,
12.  $\Delta w_p$ , and  $\Delta w_r$  increase with increasing  $T_r$ ,
13.  $m_a$  and  $T_r$  are not effective on  $\varepsilon_{RR}$ ,
14.  $\varepsilon_{EC}$  decreases with increasing  $T_r$ ,
15.  $\varepsilon_{EC}$  increases with increasing  $m_a$ .

On zeolite size;

1. Small size of zeolite gives better results then big size zeolite on the CC, COP,  $\Delta w_p$ ,  $\Delta w_r$ , and  $\varepsilon_{RR}$ , for all range of the operating parameters,
2. ,  $\varepsilon_{RR}$  is high for big size of zeolite.

On thickness of DW;

1. COP variation with  $N_{DW}$  and  $\Delta w_p$ ,  $\Delta w_r$ , decreases with increasing  $\Delta X_{DW}$ ,
2. Remaining of them increase with increasing  $\Delta X_{DW}$ .

## CHAPTER 6

### SUGGESTIONS FOR FUTURE WORK

The experimental set-up designed and constructed is very flexible and it enables for doing in a wide range of experiments with so many system design and operation parameters under control for future research on the manner. Some suggestions divided into two groups as for development of set-up and study are outlined below.

#### 6.1 SUGGESTIONS FOR DEVELOPMENT OF THE EXPERIMENTAL SET-UP

The main requirements of the set-up for the future works are as:

1. The set-up should be connected to an air-conditioned space
2. For correct measurement of  $T_{wb}$  hygrometers should be used.
3. For high mass flow rate of air electrical motors of fans should be changed.
4. Axial and radial sealing should be improved to avoid mixing of process and regeneration air flow streams.

#### 6.2 SUGGESTIONS FOR FUTURE STUDY WITH VARIATION OF SYSTEM PARAMETERS

1.  $\Delta X_{RR}$  should be studied till 25 cm insteps of 5 cm.
2. Different shaped matrix material should be studied.

3. Different matrix materials should be studied.
4. Different heat transfer surface area density should be studied.
5.  $\Delta X_{DW}$  should be studied for 10, 15 and 25 cm with different zeolite sizes
6. Different type solid desiccant can be tested.
7.  $N_{RR}$  and  $N_{DW}$  ranges should be expanded.
8. Combination of solid desiccant can be studied.
9. Desiccant aging should be studied.
10. Uncertainty should be decreased.





**APPENDICES**

## APPENDIX 1

### TECHNICAL SPECIFICATIONS OF THE DRIVING UNITS FOR THE FANS

The driving units of the fans used in the set-up consisted of two AC electric motors and two AC speed control units have the following technical specifications;

#### Electric Motors

Input	: 3 $\phi$ , 400/230V, 2.7/4.6A, 50 Hz.
Power Rating	: 1.1kW
Rotational Speed	: 1410 rpm
Protection Class	: IP 55

#### AC Motor Speed Controllers

Manufacturer	: SIEMENS
Manufacturer Specification	: MICROMASTER MM110,6SE3115-2BB40
Input	: 1 AC, 230 V $\pm$ 15%, 5.2 A,
Output	: O-input V, 3 $\phi$ , 5.2A max. 0-650Hz
Power Rating	: 2.1 kVA, motor; 1.1kW
Protection Class	: IP 56
Temperature Range	: 0-50°C Duty Class II

## APPENDIX 2

### TECHNICAL SPECIFICATIONS OF THE DRIVING UNITS FOR THE RR

The driving unit of the rotary regenerator used in the set-up consisted of an AC electric motor and an AC speed control unit has the following technical specifications;

#### Electric Motor of the RR

Input	: 3 $\phi$ , 220/380V, 1.4/0.8A, 50 Hz
Power Rating	: ,25kW
Rotational Speed	: 1380
Protection Class	: IP 44

#### Gear Box

Manufacturer	: YILMAZ Redüktör
Model	: 1
Output Speed	:40rpm
Power	: 0.33hp
Speed Reduction Rate	: 34.5

#### AC Motor Speed Controller

Manufacturer	: SIEMENS
Manufacturer Specification	: MICROMASTER MM55,6SE3112-2BA40
Input	: 1 AC, 230 V $\pm$ 15%, 2.9 A,
Output	: O-input V, 3 $\phi$ , 2.9A max. 0-650Hz
Power Rating	: 1.14 kVA, motor; 0.55kW
Protection Class	: IP 56
Temperature Range	: 0-50°C Duty Class II



### APPENDIX 3

#### TECHNICAL SPECIFICATIONS OF THE DRIVING UNITS FOR DW

The driving unit of the used in the set-up consisted of an AC electric motor and an AC speed control unit, have the following technical specifications;

##### Electric Motor of the RR

Input	: 3 $\phi$ , 220/380V, ...../.....A, 50 Hz
Power Rating	:
Rotational Speed	: 1470 rpm
Protection Class	:

##### Gear Box

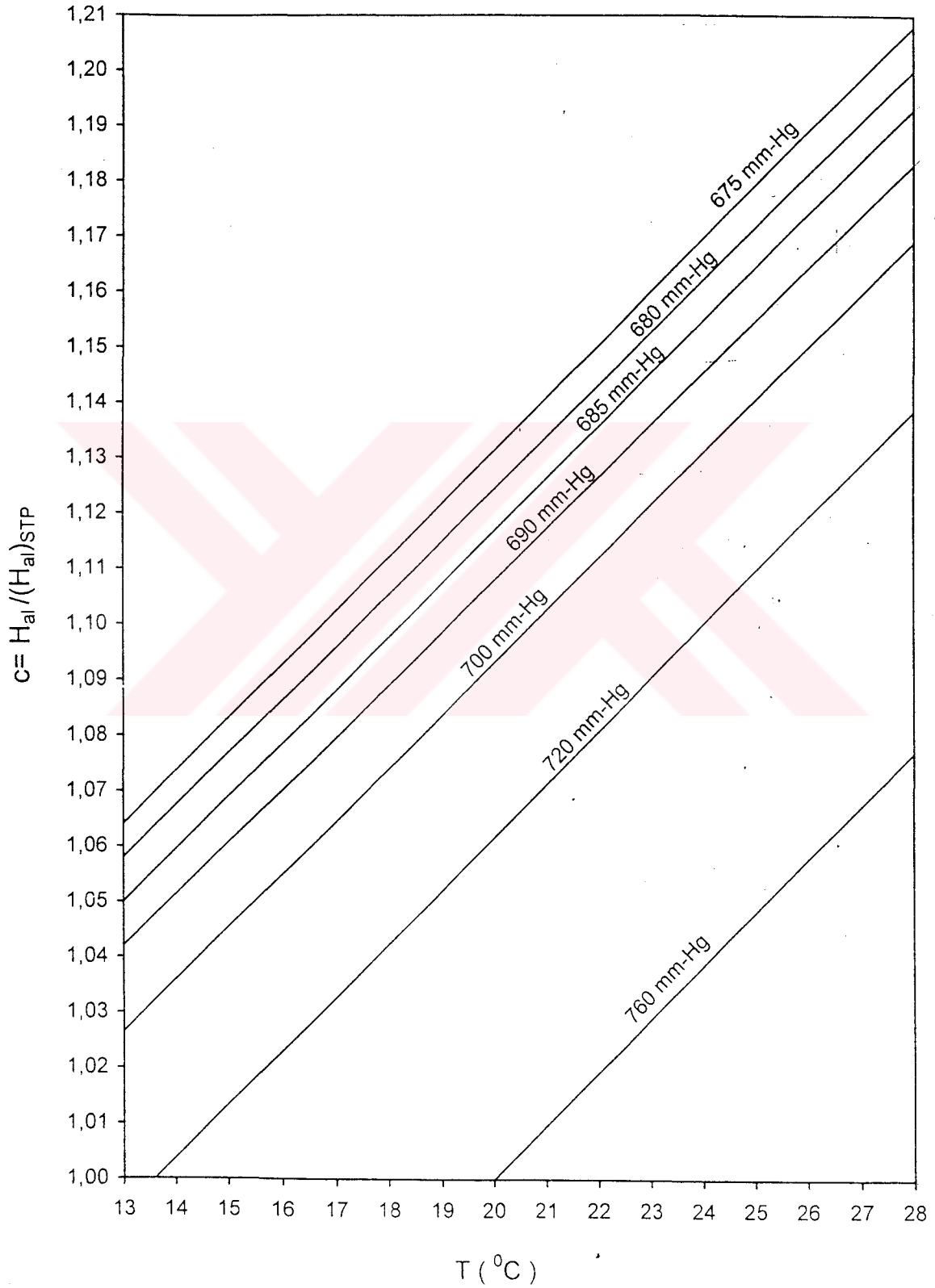
Manufacturer	:
Model	:
Output Speed	: 1.25 rpm
Power	:
Speed Reduction Rate	: 1176

##### AC Motor Speed Controllers

Manufacturer	: SIEMENS
Manufacturer Specification	: MICROMASTER MM55,6SE3112-2BA40
Input	: 1 AC, 230 V $\pm$ 15%, 2.9 A,
Output	: O-input V, 3 $\phi$ , 2.9A max. 0-650Hz
Power Rating	: 1.14 kVA, motor; 0.55kW
Protection Class	: IP 56
Temperature Range	: 0-50 $^{\circ}$ C Duty Class II

### APPENDIX 4

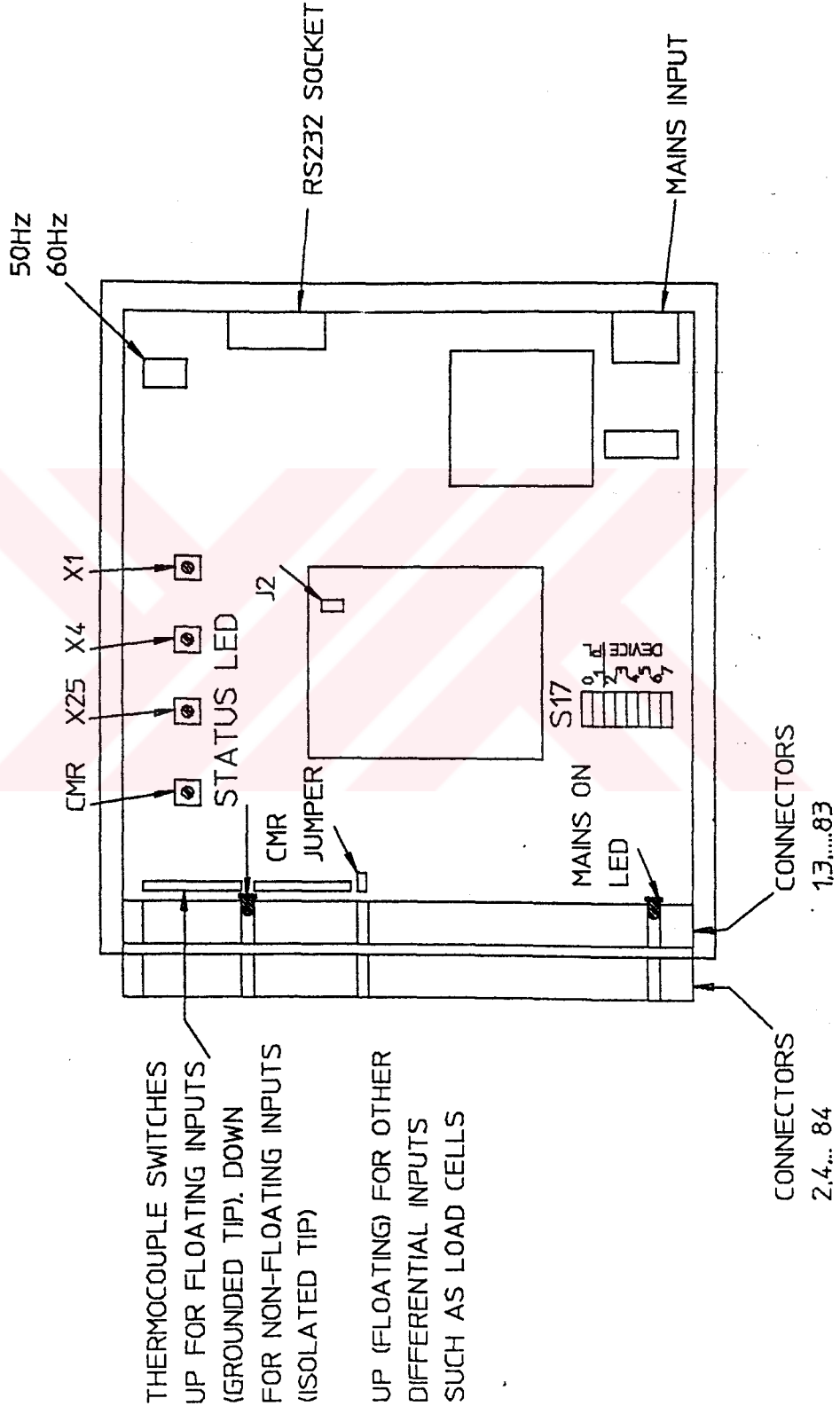
#### Correction Chart for The Head of Alcohol



APPENDIX 5

Hilton Data Logger Interface Plan View

HILTON INTERFACE PLAN VIEW.



## APPENDIX 6

- Calibrated and noted data

## DATA SHEET

Date: 03/08/2002

T <sub>lab</sub> =	31	C
P <sub>lab</sub> =	684	mmHg

	db	wb
T1db(C)=	31	21.5
T5db(C)=	31	21.5

	$\Delta P(\text{mm}_{\text{al}})$	angle	m(kg/s)
In	11	10	0.056
DW	20	30	"
Out	11	10	"
RR	18	30	"

N <sub>RR</sub> (rpm)	N <sub>DW</sub> (rpm)	T <sub>r</sub> (C)	start: 9:30
5	0.1	70	till: 9:45
10	"	"	till: 10:00
15	"	"	till: 10:15
20	"	"	till: 10:30

Date: ...../...../2002

T <sub>lab</sub> =		C
P <sub>lab</sub> =		mmHg

	db	wb
T1db(C)=		
T5db(C)=		

	$\Delta P(\text{mm}_{\text{al}})$	angle	m(kg/s)
In	11	10	0.056
DW	20	30	"
Out	11	10	"
RR	18	30	"

N <sub>RR</sub> (rpm)	N <sub>DW</sub> (rpm)	T <sub>r</sub> (C)	start: 10:30
5	0.2	70	till: 10:45
10	"	"	till: 11:00
15	"	"	till: 11:15
20	"	"	till: 11:30

Date: ...../...../2002

T <sub>lab</sub> =	31.5	C
P <sub>lab</sub> =	684	mmHg

	db	wb
T1db(C)=	32.2	21
T5db(C)=	31.5	21

	$\Delta P(\text{mm}_{\text{al}})$	angle	m(kg/s)
In	11	10	0.056
DW	20	30	"
Out	11	10	"
RR	18	30	"

N <sub>RR</sub> (rpm)	N <sub>DW</sub> (rpm)	T <sub>r</sub> (C)	start: 11:30
5	0.3	70	till: 11:45
10	"	"	till: 12:00
15	"	"	till: 12:15
20	"	"	till: 12:30

Date: ...../...../2002

T <sub>lab</sub> =		C
P <sub>lab</sub> =		mmHg

	db	wb
T1db(C)=		
T5db(C)=		

	$\Delta P(\text{mm}_{\text{al}})$	angle	m(kg/s)
In	11	10	0.056
DW	20	30	"
Out	11	10	"
RR	18	30	"

N <sub>RR</sub> (rpm)	N <sub>DW</sub> (rpm)	T <sub>r</sub> (C)	start: 12:30
5	0.4	70	till: 12:45
10	"	"	till: 13:00
15	"	"	till: 14:15
20	"	"	till: 14:30

## - Stored data with the Data Logger

14,300

1,"T2db	","øC	",150,-50,0
2,"T2wb	","øC	",150,-50,0
3,"T3db	","øC	",150,-50,0
4,"T3wb	","øC	",150,-50,0
5,"T4db	","øC	",150,-50,0
6,"T4wb	","øC	",150,-50,0
7,"T6db	","øC	",150,-50,0
8,"T6wb	","øC	",150,-50,0
9,"T7db	","øC	",150,-50,0
10,"T7wb	","øC	",150,-50,0
11,"T8db	","øC	",150,-50,0
12,"T8wb	","øC	",150,-50,0
13,"T9db	","øC	",150,-50,0
14,"T9wb	","øC	",150,-50,0

09:31:30,"03-08-2002"

4.58E+01

2.47E+01

2.85E+01

1.95E+01

2.16E+01

2.08E+01

2.68E+01

2.06E+01

3.52E+01

2.28E+01

6.87E+01

3.25E+01

3.89E+01

2.48E+01

09:36:30,"03-08-2002"

4.64E+01

2.51E+01

2.90E+01

1.97E+01

2.16E+01

2.10E+01

2.70E+01

2.07E+01

3.61E+01

2.31E+01

7.09E+01

3.30E+01

3.91E+01

2.49E+01

09:41:30,"03-08-2002"

4.80E+01

2.59E+01

2.91E+01

1.97E+01  
2.24E+01  
2.07E+01  
2.67E+01  
2.09E+01  
3.69E+01  
2.35E+01  
7.00E+01  
3.36E+01  
3.96E+01  
2.51E+01  
09:46:30,"03-08-2002"  
4.82E+01  
2.60E+01  
2.92E+01  
2.02E+01  
2.31E+01  
2.06E+01  
2.70E+01  
2.11E+01  
3.75E+01  
2.33E+01  
7.12E+01  
3.30E+01  
3.97E+01  
2.50E+01  
09:51:30,"03-08-2002"  
4.93E+01  
2.63E+01  
2.97E+01  
2.05E+01  
2.31E+01  
2.11E+01  
2.70E+01  
2.07E+01  
3.80E+01  
2.38E+01  
7.04E+01  
3.41E+01  
4.03E+01  
2.51E+01  
09:56:30,"03-08-2002"  
4.94E+01  
2.64E+01  
2.98E+01  
2.02E+01  
2.33E+01  
2.08E+01  
2.73E+01

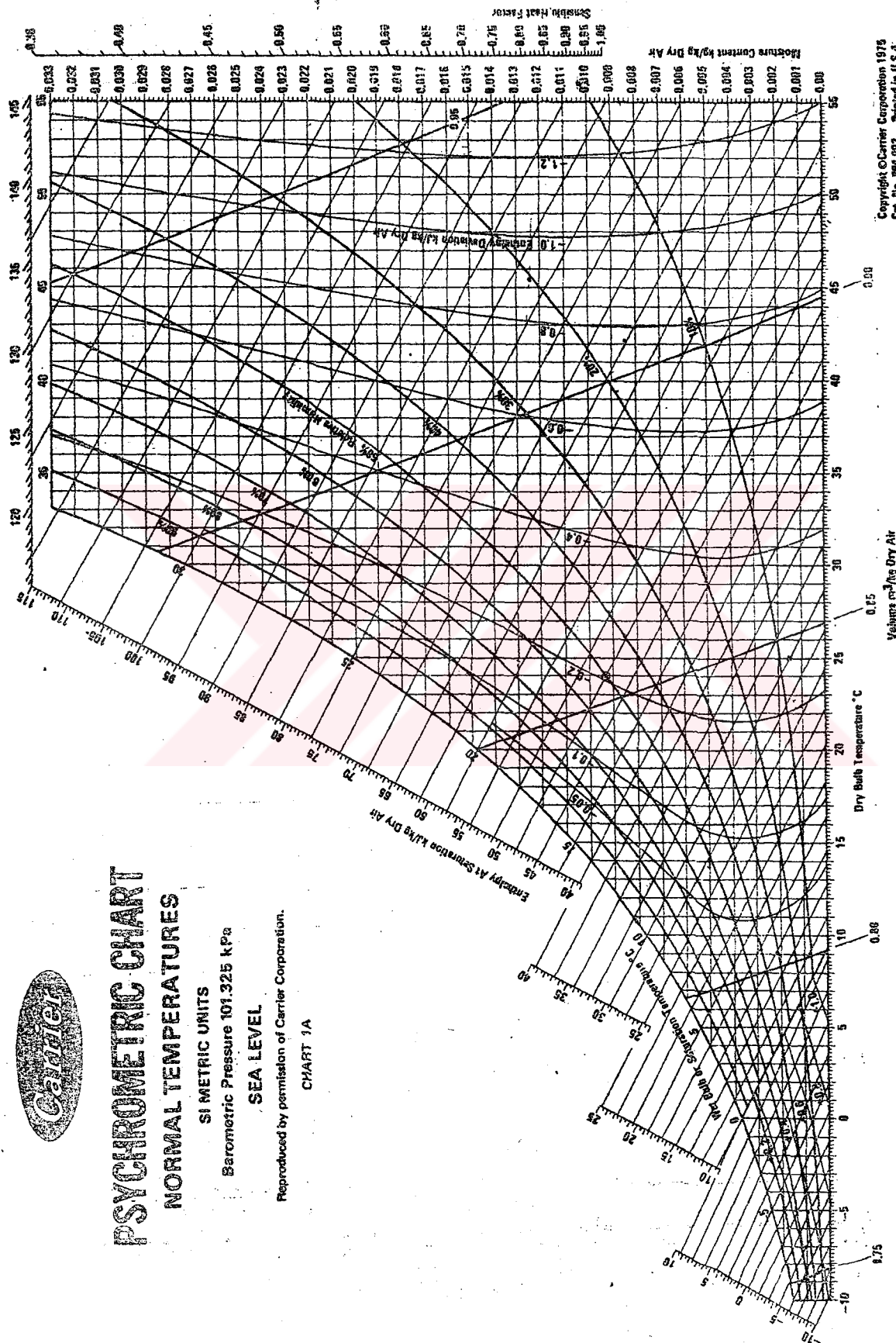
2.12E+01  
3.83E+01  
2.39E+01  
7.03E+01  
3.33E+01  
4.03E+01  
2.49E+01  
10:01:30,"03-08-2002"  
5.01E+01  
2.64E+01  
2.99E+01  
2.07E+01  
2.35E+01  
2.12E+01  
2.74E+01  
2.13E+01  
3.86E+01  
2.42E+01  
6.99E+01  
3.38E+01  
4.07E+01  
2.50E+01  
10:06:30,"03-08-2002"  
4.97E+01  
2.62E+01  
3.01E+01  
2.10E+01  
2.31E+01  
2.12E+01  
2.75E+01  
2.14E+01  
3.93E+01  
2.47E+01  
7.07E+01  
3.58E+01  
4.06E+01  
2.50E+01  
10:11:29,"03-08-2002"  
5.08E+01  
2.69E+01  
3.02E+01  
2.09E+01  
2.36E+01  
2.13E+01  
2.77E+01  
2.13E+01  
3.91E+01  
2.44E+01  
7.03E+01

3.31E+01  
4.11E+01  
2.53E+01  
10:16:30,"03-08-2002"  
5.04E+01  
2.64E+01  
3.03E+01  
2.12E+01  
2.37E+01  
2.15E+01  
2.76E+01  
2.14E+01  
3.95E+01  
2.39E+01  
5.38E+01  
2.93E+01  
4.06E+01  
2.49E+01  
10:21:29,"03-08-2002"  
5.12E+01  
2.67E+01  
3.03E+01  
2.12E+01  
2.39E+01  
2.15E+01  
2.77E+01  
2.15E+01  
3.96E+01  
2.43E+01  
6.97E+01  
3.25E+01  
4.12E+01  
2.52E+01  
10:26:29,"03-08-2002"  
5.06E+01  
2.72E+01  
3.06E+01  
2.13E+01  
2.40E+01  
2.13E+01  
2.82E+01  
2.13E+01  
3.98E+01  
2.40E+01  
7.08E+01  
3.24E+01  
4.09E+01  
2.50E+01  
10:31:29,"03-08-2002"



5.26E+01  
2.75E+01  
3.06E+01  
2.09E+01  
2.39E+01  
2.11E+01  
2.79E+01  
2.14E+01  
3.98E+01  
2.46E+01  
7.08E+01  
3.24E+01  
4.01E+01  
2.46E+01  
10:36:29,"03-08-2002"  
5.33E+01  
2.83E+01  
3.04E+01  
2.10E+01  
2.29E+01  
2.20E+01  
2.71E+01  
2.15E+01  
4.00E+01  
2.46E+01  
7.08E+01  
3.28E+01  
4.00E+01  
2.48E+01  
10:41:29,"03-08-2002"  
5.37E+01  
2.81E+01  
3.03E+01  
2.10E+01  
2.29E+01  
2.20E+01  
2.71E+01  
2.13E+01  
3.99E+01  
2.44E+01  
7.06E+01  
3.27E+01  
4.00E+01  
2.48E+01  
10:46:29,"03-08-2002"  
5.39E+01  
2.86E+01  
3.02E+01  
2.12E+01

# APPENDIX 7 Psychrometric Chart



## PSYCHROMETRIC CHART NORMAL TEMPERATURES

SI METRIC UNITS  
Barometric Pressure 101.325 kPa  
SEA LEVEL

Reproduced by permission of Carrier Corporation.

CHART 1A

Copyright © Carrier Corporation 1975  
Cat. No. 754-082 Printed in U.S.A.

Below 0° C Properties and Enthalpy Deviation Lines Are For Ice

## LIST OF REFERENCES

1. Mavroudaki, P., Beggs, C. B., Sleigh, P. A., and Halliday, S. P. (2002). The potential for solar powered single-stage desiccant cooling in southern Europe. *Applied Thermal Engineering*, **22**, 1129–1140.
2. Halliday, S. P., Beggs, C. B., and Sleigh, P. A. (2002). The use of solar desiccant cooling in the UK: a feasibility study. *Applied Thermal Engineering*, **22** 1327–1338
3. Mazzei, P., Minichiello, F., and Palma, D. (2002), Desiccant HVAC systems for commercial buildings. *Applied Thermal Engineering* **22**, 545–560
4. Dai, Y. J., Wang, R. Z., and Xu, Y. X. (2002). Study of a solar powered solid adsorption–desiccant cooling system used for grain storage. *Renewable Energy*, **25**, 417–430
5. Zhang, L.Z. and Niu, J.L. (2002). Performance comparisons of desiccant wheels for air dehumidification and enthalpy recovery. *Applied Thermal Engineering*, **22**, 1347–1367
6. Tanthapanichakoon, W., and Prawarnpit, A.( 2002). New simple mathematical model of a honeycomb rotary absorption-type dehumidifier. *Chemical Engineering Journal*, **3943** 1–5.
7. Joudi, K. A., and Dhaidan, N. S. (2001). Application of Solar Assisted Heating and Desiccant Cooling System for Domestic Building. *Energy Conversion and Management*, **42**, 995-1022.
8. Henning, H-M., Erpenbeck, T., and Santamaria, I.S. (2001).The Potential of Solar Energy Use in Desiccant Cooling Cycles. *Int. J. Of Refrigeration*, **24**, 220-229.
9. Jalalzadeh-Azar, A. A., Steele, W. G., and Hodge, B. K. (2000). Performance Characteristics of a Commercially Available Gas-Fired Desiccant System. *ASHRAE Transactions*, pp. 95-104.
10. Jalalzadeh-Azar, A. A., (2000) Consideration of transient response and

energy cost in performance evaluation of a desiccant dehumidification systems. *ASHRAE Transactions*, **106**, No: 2, 95-104.

11. Vineyard, E. A., Sand, J. R., and Durfee, D. J. (2000). Parametric Analysis of Variables That Affect the Performance of a Desiccant Dehumidification System. *ASHRAE Transactions*, pp. 87-94.
12. Pons, M., and Kodama, A. (2000). Entropic Analysis of Adsorption Open Cycles for Air Conditioning Part 1: First and Second Law Analyses. *International of Energy Research*, **24**, 251-262.
13. Pons, M., and Kodama, A. (2000). Entropic Analysis of Adsorption Open Cycles for Air Conditioning Part 2: Interpretation of Experimental Data. *International of Energy Research*, **24**, 263-278.
14. Harriman, L. G., Czachorski, M., Witte, M. J., and Kosar, D. R. (1999). Evaluating Active Desiccant Systems for Ventilating Commercial Buildings. *Ashrae Journal*, pp. 28-37.
15. Techajunta, S., Chirattananon, S., and Exell R. H. B. (1999). Experiments in a Solar Simulator on Solid Desiccant Regeneration and Air Dehumidification for Air Conditioning in a Tropic Humid Climate. *Renewable Energy*, **17**, 549-568.
16. Davanagere, B. S., Sherif, S. A., and Goswami, D. Y. (1999). A Feasibility Study of a Solar Desiccant Air Conditioning System-Part I: Psychrometrics and Analysis of the Conditioned Zone. *International of Energy Research*, **23**, 7-21.
17. Davanagere, B. S., Sherif, S. A., and Goswami, D. Y. (1999). A Feasibility Study of a Solar Desiccant Air Conditioning System-Part II: Transient Simulation and Economics. *International of Energy Research*, **23**, 103-116.
18. Belding, W. A., Delmas, M. P. F., and Holeman, W. D. (1996). Desiccant Aging and Its Effects on Desiccant Cooling System Performance. *Applied Thermal Engineering*, **16**, No: 5, 447-459.
19. Zhang, H-F., and Yu, J-D. (1996). The Research and Development of the Key Components for *Desiccant Cooling System*. *WREC*, pp. 653-656.
20. Jalalzadeh-Azar, A. A., Hodge, B. K. and Steele, W. G. (1996).

Thermodynamic Assessment of Desiccant Systems with Targeted and Relaxed Humidity Control Schemes. *ASHRAE Transactions*, **104**, No: 2, 313-319.

21. Pesaran A. A. And Wipke, K. (1994). The Use of Unglazed Solar Collectors for Desiccant Cooling. *Solar Energy*, **52**, 419-427.
22. Dupont, M., Celestine, B., Nguyen, P. H., Merigoux, J., and Brandon, B. (1994). Desiccant Solar Air Conditioning in Tropical Climates: 1-Dynamic Experimental and Numerical Studies of Silicagel and Activated Alumina. *Solar Energy*, **52**, No 6, 509-517.
23. Shelpuk, B. (1993). The Technical Challenges for Solid Desiccant cooling. *Heat Recovery Systems & CHP*, **13**, No: 4, 321-328.
24. Pesaran, A. A., (1993). Desiccant Degradation in Desiccant Cooling Systems: A System Study. *Journal of Solar Energy Engineering*, **115**, 237-241.
25. Pesaran, A. A. (1993). Desiccant Degradation in Desiccant Cooling Systems: An Experimental Study. *Journal of Solar Energy Engineering*, **115**, 213-219.
26. Collier, R. K., Kohen, B. M, and Slosberg, R. B. (1992). Desiccant Cooling Properties and Their Effects on the Performance of Desiccant Cooling Systems. *Desiccant Cooling and Dehumidification*, pp. 82-87.
27. Majumdar, P., and Sarwar, M. K. (1992). Performance of a Wet Desiccant Bed with Inert Materials. *Solar Engineering*, **1**, 253-261.
28. Van den Bulck, E., Mitchell, J. W., and Klein, S. A. (1992). The Design of Dehumidifiers for Use in Desiccant Cooling and Dehumidification Systems. *ASME*, pp.1-9.
29. Matsuki, K., and Saito, Y. (1992). Desiccant Cooling R&D in Japan. *Desiccant Cooling and Dehumidification*, pp. 134-143.
30. Warren, M., L., and Wahlig, M. (1991). Analysis and Comparison of Active Solar Desiccant and Absorption Cooling Systems: Part I- Model Description. *Transactions of the ASME Journal of Solar Energy Engineering*, **113**, 25-30.
31. Warren, M., L., and Wahlig, M. (1991). Analysis and Comparison of Active Solar Desiccant and Absorption Cooling Systems: Part II-

- Annual Simulation Results. *Transactions of the ASME Journal of Solar Energy Engineering*, **113**, 31-35.
32. Collier, R. K., and Cohen, B. M. (1991). An Analytical Examination of Methods for Improving the Performance of Desiccant Cooling Systems. *Transactions of the ASME Journal of Solar Energy Engineering*, **113**, 157-163.
  33. Farooq, S., and Ruthven, D. M. (1991). Numerical Simulation of a Desiccant Bed for Solar Air Conditioning Applications. *Transactions of the ASME Journal of Solar Energy Engineering*, **113**, 80-88.
  34. Bending, W. A., Worek, W. M., Novosel, D., and Holeman, W. D. (1991). Desiccant Development and Gas-Fired Desiccant Cooling Systems. *ASHRAE Transactions*, pp. 587-594
  35. Meckler, G. (1991). Comparative Energy Analysis of Gas-Energized Desiccant Cold-Air Unit. *ASHRAE Transactions*, pp. 637-641.
  36. Marciniak, T. J., Koopman, R. N., and Kosar, D. R. (1991). Gas-Fired Desiccant Dehumidification System in a Quick-Service Restaurant. *ASHRAE Transactions*, pp. 657-666.
  37. Pesaran, A. A., and Penney, T. R. (1991). Impact of Desiccant Degradation on Desiccant Cooling System Performance. *ASHRAE Transactions*, pp. 595-601..
  38. Worek, W. M., Zheng, W., Belding, W. A., Novosel, D., and Holeman, W. D., (1991). Simulation of Advanced Gas-Fired Desiccant Cooling Systems. *ASHRAE Transactions*, pp. 609-614.
  39. Ko, Y. J., Charoensupaya, D., and Lavan, Z. (1990). Open-Cycle Desiccant Cooling System with Staged Regeneration. *Int. Heat Transfer Conferences*, Israel, pp. 121-126.
  40. Collier, R. K., Novosel, Jr. D., and Worek, W. M. (1990). Performance Analysis of Open-Cycle Desiccant Cooling Systems. *ASHRAE Transactions*, pp. 1262-1268.
  41. Majumdar, P., and Worek, W. M. (1989). Performance of An Open-Cycle Desiccant Cooling System Using Advanced Desiccant Matrices. *Heat Recovery Systems & CHP*, **4**, No: 4, 299-311.
  42. Parson, B. K., Pesaran, A. A., Bharathan, D., and Shelpuk, B. (1989). Improving Gas-Fired Heat Pump Capacity and Performance by Adding

- a Desiccant Dehumidification Subsystem. *ASHRAE Transactions*, pp. 835-844.
43. Kang, T. S., and Maclaine-cross, I. L. (1989). High Performance, Solid Desiccant, Open Cooling Cycles. *Transactions of the ASME Journal of Solar Energy Engineering*, **111**, 176-183.
  44. Dolan, W. H. (1989). Desiccant Cooling Systems- A New HVAC Opportunity. *Energy Engineering*, **86**, No. 4, 6-9.
  45. Cohen, B. M., and Slosberg, R. B. (1989). Application of Gas-Fired Desiccant Cooling Systems. *Energy Engineering*, **86**, No. 4, 10-25.
  46. Charoensupaya, D., and Worek, W. M. (1988). Parametric Study of an Open-Cycle Adiabatic, Solid, Desiccant Cooling System. *Energy*, **13**, No. 9, 739-747.
  47. Löf, G. O. G., Cler, G., and Brisbane, T. (1988). Performance of a Solar Desiccant Cooling System. *Transactions of the ASME Journal of Solar Energy Engineering*, **110**, 165-171.
  48. Joudi, K. A., and Madhi, S. M. (1987). An Experimental Investigation into a Solar Assisted Desiccant-Evaporative Air-Conditioning System. *Solar Energy*, **39**, No. 2, 97-107.
  49. Van den Bulck, E., Mitchell, J. W., and Klein, S. A. (1986). The Use of Dehumidifiers in Desiccant Cooling and Dehumidification Systems. *Transactions of the ASME Journal of Heat Transfer*, **108**, 684-692.
  50. Calton, D. S. (1985). Application of a Desiccant Cooling System to Supermarkets. *ASHRAE Transactions*, pp. 441-445.
  51. Manley, D. L., Bowlen, K. L., and Cohen, B. M. (1985). Evaluation of Gas-Fired Desiccant-Based Space Conditioning for Supermarkets. *ASHRAE Transactions*, pp. 447-456.
  52. Burns, P. R., Mitchell, J. W., and Beckman, W. A. (1985). Hybrid Desiccant Cooling Systems in Supermarket Applications. *ASHRAE Transactions*, pp. 457-467.
  53. Sheridan, J. C., and Mitchell, J. W. (1985). A Hybrid Solar Desiccant Cooling System. *Solar Energy*, **34**, No. 2, 187-193.
  54. Maclaine-cross, I. L. (1985). High-Performance Adiabatic Desiccant Open-Cooling Cycles. *Transactions of the ASME Journal of Solar Energy Engineering*, **107**, 102-104.

55. Epstein, M., Grolmes, M., Davidson, K., and Kosar, D. (1985). Desiccant Cooling System Performance: A Simple Approach. *Transactions of the ASME Journal of Solar Energy Engineering*, **107**, 21-28.
56. Schultz, K. J., Mitchell, J. W., and Beckman, W. A. (1982). The Performance of Desiccant Dehumidifier Air-Conditioning Systems Using Cooled Dehumidifier. *AS-ISES*, pp. 1-7.
57. Nelson, J. S., Beckman, W. A., Mitchell, J. W., and Close, D. J. (1978). "Simulations of the Performance of Open Cycle Desiccant Systems Using Solar Energy. *Solar Energy*, **21**, 273-278.
58. Meckler, G. (1992). Efficient Integration of Desiccant Cooling in Commercial Hvac Systems. *Desiccant Cooling and Dehumidification*, pp. 40-46.
59. Simonson, C. J., Shang, W., and Besant, R. W. (2000). Part-Load Performance of Energy Wheels: Part I- Wheel Speed Control. *ASHRAE Transactions*, pp. 286-300.
60. Simonson, C. J., Shang, W., and Besant, R. W. (2000). Part-Load Performance of Energy Wheels: Part II- Bypass Control and Correlations. *ASHRAE Transactions*, pp. 301-310.
61. Shah, R.K. and Skiepko, T. (1999). Influence of leakage distribution on the thermal performance of a rotary regenerator. *Applied Thermal Engineering*, **19**, 685-705.
62. Willmott, A. J., and Knight, D. P. (1993). Improved Collocation Methods for Thermal Regenerator Simulations. *Int. J. Heat Mass Transfer*, **36**, No. 6, 1663-1670.
63. Sunden, B., and Karlsson, I. (1991). Enhancement of Heat Transfer in Rotary Heat Exchangers by Streamwise-Corrugated Flow Channels. *Experimental Thermal and Fluid Science*, **4**, 305-316.
64. Baclic, B. S., and Dragutinovic, G. D. (1991). Asymmetric-Unbalanced Counterflow Thermal Regenerator Problem: Solution by the Galerkin Method and Meaning of Dimensionless Parameters. *Int. J. Heat Mass Transfer*, **34**, No. 2, 483-498.
65. Keiji, K., Sakai, I., and Hijikata, K. (1991). Heat Transfer Characteristics of Rotating Ceramic Regenerators-Numerical Solution Using a Hybrid



- Finite Difference/Laplace Transform Scheme. *Transactions of the ASME*, pp. 1-11.
66. Worsøpe-Schmidt, P. (1991). Effect of Fresh Air Purging on the Efficiency of Energy Recovery from Exhaust Air in Rotary Regenerators. *Rev. Int. Froid*, **14**, 233-239.3
67. Kawasaki, K., Matsuhisa, T., Sakai, I. and Hijikata, K. (1991). Heat Transfer Characteristics of Rotating Ceramic Regenerators-Numerical Solution Using a Hybrid finite Difference/Laplace Transform Scheme. *ASME*, pp.1-11.
68. Romie, F. E. (1990). A Table of Regenerator Effectiveness. *Transactions of the ASME Journal of Heat Transfer*, **112**, 497-499.
69. Chakravarty, M., and Kayal, T. (1990). Experimental Studies of a Hybrid Heat Wheel. *Energy*, **15**, No. 11, 1065-1068.
70. Romie, F. E. (1990). Response of Rotary Regenerators to Step Changes in Mass Rates. *Transactions of the ASME Journal of Heat Transfer*, **112**, 43-48.
71. Huettner, W., and Niggemann, M. (1989). Analytical and Numerical Treatment of the Transient Behavior of Rotating Counterflow Regenerators. *Transactions of the ASME Journal of Engineering for Gas Turbines and Power*, **111**, 138-145.
72. Parsons, B. K., Pesaran, A. A., Bharathan, D., and Shelpuk, B. (1989). Improving Gas-Fired Heat Pump Capacity and Performance by Adding a Desiccant Dehumidification Subsystem. *ASHRAE Transactions*, Part ....., pp. 835-844.
73. Romie, F. E., and Baclic, B. S. (1988). Methods for Rapid Calculation of the Operation of Asymmetric Counterflow Regenerators. *Transactions of the ASME Journal of Heat Transfer*, **110**, 785-788.
74. Skiepkó, T. (1988). The Effect of Matrix Longitudinal Heat Conduction on the Temperature Fields in the Rotary Heat Exchanger. *Int. J. Heat Mass Transfer*, **31**, No. 11, 2227-2238.
75. Atthey, D. R. (1988). An Approximate Thermal Analysis for a Regenerative Heat Exchanger. *Int. J. Heat Mass Transfer*, **31**, No. 7, 1431-1441.

76. Shah, R. K. (1988). Counterflow Rotary Regenerator Thermal Design Procedure. *Heat Transfer Equipment Design*, pp. 267-296.
77. Romie, F. E. (1988). Transient Response of Rotary Regenerators. *Transactions of the ASME Journal of Heat Transfer*, **110**, 836-840.
78. Hill, A., and Willmott, A. J. (1987). A Robust Method for Regenerative Heat Exchanger Calculations. *Int. J. Heat Mass Transfer*, **30**, No. 2, 241-249.
79. Romie, F. E. (1987). Effect of the Thermal Capacitance of Contained Fluid on Performance of Symmetric Regenerators. *Transactions of the ASME Journal of Heat Transfer*, **109**, 563-558.
80. Romie, F. E. (1987). Two Functions Used in the Analysis of Crossflow Exchanger, Regenerators, and Related Equipment. *Transactions of the ASME Journal of Heat Transfer*, **109**, 518-520.
81. Baclic, B. S. (1985). The Application of the Galerkin Method to the Solution of the Symmetric and Balanced Counterflow Regenerator Problem. *Transactions of the ASME Journal of Heat Transfer*, **107**, 214-221.
82. Brandemuehl, M. J., and Banks, P. J. (1984). Rotary Heat Exchangers with Time Varying or Nonuniform Inlet Temperature. *Transactions of the ASME Journal of Heat Transfer*, **106**, 750-758.
83. Romie, F. E. (1984). Transient Response of the Counterflow Heat Exchanger. *Transactions of the ASME Journal of Heat Transfer*, **106**, 620-626.
84. Romie, F. E. (1983). Transient Response of Gas-to-Gas Counterflow Heat Exchangers with Neither Gas Mixed. *Transactions of the ASME Journal of Heat Transfer*, **105**, 563-570.
85. Banks, P. J. (1982). Effect of Fluid Carryover on Regenerator Performance. *Transactions of the ASME Journal of Heat Transfer*, **104**, 215-217.
86. Younis, M., and Shoukry, M. (1981). Regenerative Rotary Heat Exchanger for Heat Recovery in Residential Ventilation. *Energy Research*, **7**, 315-325.

87. Chawla, O. P., and Khandwawala, A. I. (1981). Thermal Performance of Regenerators and Waste Heat Recovery. *Int. J. Heat Mass Transfer*, **24**, No. 11, 1793-1800.
88. Maclaine-Cross, I. L., and Ambrose, C. W. (1980). Predicted and Measured Pressure Drop in Parallel Plate Rotary Regenerators. *Journal of Fluids Engineering*, **102**, 59-63.
89. Willmott, A. J., and Duggan, R. C. (1980). Refined Closed Methods for the Contra-Flow Thermal Regenerator Problem. *Int. J. Heat Mass Transfer*, **23**, 655-662.
90. Willmott, A. J., and Burns, A. (1979). The Recuperator Analogy for the Transient Performance of Thermal Regenerators. *Int. J. Heat Mass Transfer*, **22**, 1107-1115.
91. Romie, F. E. (1979). Periodic Thermal Storage: The Regenerator. *Transactions of the ASME Journal of Heat Transfer*, **101**, 726-731.
92. Willmott, A. J., and Burns, A. (1977). Transient Response of Periodic-Flow Regenerators. *Int. J. Heat Mass Transfer*, **20**, 753-761.
93. Razeelos, P., and Benjamin, M. K. (1977). Computer Model of Thermal Regenerators with Variable Mass Flow Rates. *Int. J. Heat Mass Transfer*, **21**, 735-743.
94. Fisher, D. R., Gawley, H. N., and Chant, R. E. (1974). Performance Testing of Rotary Air-to-air Heat Exchangers. *ASHRAE Transactions*, pp. 322-327.
95. Dunkle, R. V., Maclaine-Cross, I. L., and Grad, B. E., and Aust, I. E. (1970). Theory and Design of Rotary Regenerators for Air Conditioning. *Mechanical & Chemical Engineering Transactions*, pp.1-6.
96. Willmott, A. J. (1968). Simulation of Thermal Regenerator Under Conditions of Variable Mass Flow. *Int. J. Heat Mass Transfer*, **11**, 1105-1116.
97. Willmott, A. J. (1964). Digital Computer Simulation of a Thermal Regenerator. *Int. J. Heat Mass Transfer*, **7**, 1291-1302.
98. Rohsenow, W. M., Hartnett, J. P., and Ganic, E. N., "Handbook of Heat Transfer Application", Part 3 Compact Heat Exchangers pp. 177-307.

99. Burns, A., and Willmott, A. J., "Transient Performance of Periodic Flow Regenerators", *Int. J. Heat Mass Transfer*, **21**, 623-627
100. Kodama, A., Hirayama, T., Goto, M., Hirose, T., and Critoph, R. E. (2001). The Use of Psychrometric Charts for the Optimization of a Thermal Swing Desiccant Wheel. *Applied Thermal Engineering*, **21**, 1657-1674.
101. Dai, Y. J., Wang, R. Z., and Zhang, H. F. (2001). Parameter Analysis to Improve Rotary Desiccant Dehumidification Using a Mathematical Model. *Int. J. Therm. Sci.* **40**, 400-408.
102. Neti, S., and Wolfe, E. I. (2000). Measurements of Effectiveness in a Silica Gel Rotary Exchanger. *Applied Thermal Engineering*, **20**, 309-322.
103. Simonson, C. J. and Besant, R. W. (1997). Heat and Moisture Transfer in Desiccant Coated Rotary Exchangers: Part I- Numerical Model. *HVAC&R.RESEARCH*, **3**, No: 4 325-349.
104. Simonson, C. J. and Besant, R. W. (1997). Heat and Moisture Transfer in Desiccant Coated Rotary Exchangers: Part II- Validation and Sensitivity studies. *HVAC&R.RESEARCH*, **3**, No: 4 350-368.
105. Zheng, W., Worek, W. M., and Novosel, D. (1995). Effect of Operating Conditions on Optimal Performance of Rotary Dehumidifiers. *Transactions of the ASME Journal of Energy Resources Technology*, **117**, 62-66.
106. Banks, N. J. (1992). Utilization of Condenser Heat for Desiccant Dehumidifiers in Supermarket Applications. *Desiccant Cooling and Dehumidification*, pp. 21-26.
107. Pearson, J., and Thompson, K. (1991). Gas-Fired Dehumidification. *Energy World*, pp. 15-18.
108. Schultz, K. J., and Mitchell, J. W. (1989). Comparison of the DESSIM Model with a Finite Difference Solution for Rotary Desiccant Dehumidifiers. *Transactions of the ASME Journal of Solar energy Engineering*, **111**, 286-291.
109. Van den Bulck, E., Klein, S. A., and Mitchell, J. W. (1988). Second Law Analysis of Solid Desiccant Rotary Dehumidifiers. *Transactions of the ASME Journal of Solar energy Engineering*, **110**, 2-9.

110. Pesaran, A. A., and Mills, A. (1987). Moisture Transport in Silica Gel Packed Beds-I. Theoretical Study. *Int. J. Heat Mass Transfer*, **30**, No. 6, 1037-1049.
111. Pesaran, A. A., and Mills, A. (1987). Moisture Transport in Silica Gel Packed Beds-II. Experimental Study. *Int. J. Heat Mass Transfer*, **30**, No. 6, 1037-1049.
112. Van den Bulck, E., Mitchell, J. W., and Klein, S. A. (1984). The Design of Dehumidifiers for Use in Desiccant Cooling and Dehumidification Systems. *Transactions of the ASME*, pp. 1-9.
113. Jurinak, J. J., and Mitchell, J. W. (1984). Effect of Matrix Properties on the Performanse of a Counterflow Rotary Dehumidifier. *Transactions of the ASME Journal of Heat Transfer*, **106**, 638-645.
114. Jurinak, J. J., and Mitchell, J. W. (1984). Recirculation of Purged Flow in an Adiabatic Counterflow Rotary Dehumidifier. *Transactions of the ASME Journal of Heat Transfer*, **106**, 369-375.
115. Schultz, K. J., Mitchell, J. W., and Beckman, W. A. (1982). The Performance of Desiccant Dehumidifier Air-Conditioning Systems Using Cooled Dehumidifier. *AS-ISES*, Houston, pp. 1-7.
116. Jekel, T. B., Mitchell, J. W., and Kleln, S. A. (1993). Equilibrium Performance of Desiccant Dehumidifiers. *ASES Conference*, Washington.
117. Borde, I., Korin, E. and Eliasy, R. (1991). Studies of Air Drying by a Two-Component Solid Desiccant Material in a Rotary Packed Bed Dehumidifier. *Drying*, pp. 207-216.
118. Rau, J. J., Klein, S. A., and Mitchell, J. W. (1991). Characteristics of Lithium Chloride in Rotary Heat and Mass Exchangers. *Int. J. Heat Mass Transfer*, **34**, No. 11, 2703-2713.
119. Kravchik, T., Korin, E., and Borde, I. (1990). Influence of Material Properties and Heat Removal on Mass and Heat Transfer in Solid Desiccant Dehumidifier. *Chem. Eng. Process.*, **27**, 19-25.
120. Van den Bulck, E., Mitchell, J. W., and Klein, S. A. (1985). Design Theory for Rotary Heat and Mass Exchangers-I. Wave Analysis of Rotary Heat and Mass Exchangers with Infinite Transfer Coefficients. *Int. J. Heat Mass Transfer*, **28**, No. 8, 1575-1585.

121. Van den Bulck, E., Mitchell, J. W., and Klein, S. A. (1985). Design Theory for Rotary Heat and Mass Exchangers-II. Effectiveness-Number-of-Transfer-Units Method for Rotary Heat and Mass Exchangers. *Int. J. Heat Mass Transfer*, **28**, No. 8, 1587-1595.
122. Banks, P. J. (1985). Prediction of Heat and Mass Regenerator Performance Using Nonlinear Analogy Method: Part 1- Basis. *Transactions of the ASME Journal of Heat Transfer*, **107**, 222-229.
123. Banks, P. J. (1985). Prediction of Heat and Mass Regenerator Performance Using Nonlinear Analogy Method: Part 2- Comparison of Methods. *Transactions of the ASME Journal of Heat Transfer*, **107**, 230-238.
124. Van Leersum, J. G., and Ambrose, C. W. (1981). Comparissons Between Experiments and a Theoretical Model of Heat and Mass Transfer in Rotary Regenerators with Nonsorbing Matrices. *Trasactions of the ASME Journal of Heat Transfer*, **103**, 189-194.
125. Holmberg, R. B. (1979). Combined Heat and Mass Transfer in Regenerators with Hygroscopic Rotor Materials. *Transactions of the ASME Journal of Heat Transfer*, **101**, 205-210.
126. Holmberg, R. B. (1977). Heat and Mass Transfer in Rotary Heat Exchangers with Nonhygroscopic Rotor Materials. *Transactions of the ASME Journal of Heat Transfer*, **99**, 196-202.
127. Leonardo Goldstein, Jr., and Sparrow, E. M. (1977). Heat/Mass Transfer Characteristics for Flow in a Corrugated Wall Channel. *Transactions of the ASME Journal of Heat Transfer*, **99**, 187-195.
128. Maclaine-Cross, I. L., and Banks, P. J. (1972). Coupled Heat and Mass Transfer in Regenerators-Prediction Using An Analogy with Heat Transfer. *Int. J. Heat Mass Transfer*, **15**, 1225-1242.
129. Bending, W. A., Delmas, M. P. F., and Holeman, W. D. (1996). Desiccant Aging and Its effects on Desiccant Cooling System Performance. *Applied Thermal Engineering*, **16**, No. 5, 447-459.
130. Shen, C. M., and Worek, W. M. (1994). Cosorption Characteristics of Solid Adsorbents. *Int. J. Heat Mass Transfer*, **37**, No. 14, 2123-2129.

131. Pesaran, A. A. (1993). Desiccant Degradation in Desiccant Cooling Systems: An Experimental Study. *Transactions of the ASME Journal of Solar Energy Engineering*, **115**, 212-219.
132. Pesaran, A. A. (1993). Desiccant Degradation in Desiccant Cooling Systems: A System Study. *Transactions of the ASME Journal of Solar Energy Engineering*, **115**, 237-241.
133. Shelpuk, B. (1993). The Technical Challenges for Slid Desiccant Cooling. *Heat Recovery Systems & CHP*, **13**, No. 4, 321-328.
134. Collier, R. K., Cohen, B. M., and Slosberg, R B. (1992). Desiccant Properties and Their Effects on the Performance of Desiccant Cooling Systems. *Desiccant Cooling and Dehumidification*, pp. 75-81.
135. Czanderna, A. W. (1992). Polymers as Advanced Materialis for Desiccant Applications: 1-Commercially Available Polymers. *Desiccant Cooling and Dehumidification*, pp. 88-97.
136. Pesaran, A. A., and Mills, A. F. (1992). Moisture Transport in Silica Gel Packed Beds-1. Theoretical Study. *Desiccant Cooling and Dehumidification*, pp. 98-109.
137. Pesaran, A. A., and Mills, A. F. (1992). Moisture Transport in Silica Gel Packed Beds-2. Experimental Study. *Desiccant Cooling and Dehumidification*, pp. 110-117.
138. Schwarz, J., Kellr, C., and Soltes, J. (1991). Adsorption Cycles with the Working Fluid Zeolite/Water. *ASHRAE Transactions*, Part 1, pp. 569-577.
139. Anderson, D. R., and Pesaran, A. A. (1991). Innovative Solid Desiccant Substrates for Desiccant Dehumidifiers. *ASHRAE Transactions*, Part 1, pp. 578-586.
140. Belding, W. A., Worek, W. M., and Holeman, W. D. (1991). Desiccant Development for Gas-Fired Desiccant Cooling Systems. *ASHRAE Transactions*, Part 1, pp. 587-594.
141. Pesaran, A. A., and Penney, T. R. (1991). Impact of Desiccant Degradation on Desiccant Cooling System Performance. *ASHRAE Transactions*, Part 1, pp. 595-601.
142. Ülkü, S. (1991). Heat and Mass Transfer in Adsorbent Beds. *Convective Heat and Mass Transfer in Porous Media*, pp. 695-724.

143. Pesaran, A. A., and Bingham, C. E. (1989). Testing of Novel Desiccant Materials and Dehumidifier Matrices for Desiccant Cooling Applications. *ASHRAE Transactions, Part 2*, **95**, 1109-1115.
145. Riekert, L. (1989). Transport of Mass and Heat in Porous Adsorbents. *Chem. Eng. Process.*, **26**, 59-62.
146. Collier, R. K. (1989). Desiccant Properties and Their Effect on Cooling System Performance. *ASHRAE Transactions, Part 2*, **95**, 823-827.
147. Ülkü, A. S. (1989). Adsorption in Energy Storage. *Energy Storage Systems*, pp. 487-507.
148. Yücel, H., and Çulfaz, A. (1988). Characterization of Clinoptilolites of Western Anatolia. *Occurrence, Properties and Utilization of Natural Zeolites*, pp. 99-108.
149. Yücel, H. (1987). Zeolitler ve Uygulama Alanları. *III. Ulusal Kil Sempozyumu, 21-27 Eylül 1987, Bildiriler*, pp. 391-402.
150. Yörükoğulları, E. (1987). Isı Depolama Malzemesi Olarak Doğal Zeolitler. *III. Ulusal Kil Sempozyumu, 21-27 Eylül 1987, Bildiriler*, pp. 4023-409.
151. Ülkü, S. (1986). Solar Adsorption Heat Pumps. *Solar Energy Utilization Fundamentals and Application*, İzmir, pp. 236-247.
152. Yücel, H., and Çulfaz, A. (1985). Yerel ve Doğal Klinoptilolit Zeolitinin Fiziksel ve Kimyasal Özellikleri. *Doğa Bilim Dergisi, Seri B, Cilt. 9, Sayı. 3*, pp. 289-296.
153. Yücel, H., ..... Adsorpsiyon Temel İşlemi ve Uygulamaları. *Araştırma-İnceleme*, pp. 5-14.
154. Aimiwu, V. O. (1992). Evaporative Cooling of Water in Hot Arid Regions. *Energy Convers. Mgmt.*, **33**, No. 1, 69-74.
155. Singh, S. P., Sawhley, R. L., Bansal, N. K., and Sodha, M. S. (1987). Sizing of an Evaporative Cooler for Thermal Comfort Inside a Room", *Housing Science*, **11**, No. 2, 141-148.
156. Watt, J. R. (1987). Nationwide Evaporative Cooling is Here! *ASHRAE Transactions*, pp. 1237-1251.
157. Buglayev, V. T., Vasil'yv, F. V., and Strebkov, A. S. (1985). Experimental Investigation of Heat Transfer in Evaporative Cooling of



- Air Flows with Fine Droplets. *Heat Transfer-Soviet Research*, 17, No. 5, 7-103.
158. Srivastava, A., and Tiwari, G. N. (1984). Experimental Validation of a Thermal Model of an Evaporative Cooling System. *Energy Convers. Mgmt.*, 24, No. 4, 305-311.
  159. Çengel, Y. (1998). *Heat Transfer, A Practical Approach*. McGraw Hill.
  160. Hickman, M. J. (1970). *Measurement of Humidity* Her Majesty's Stationary Office, London.
  161. Ower, E., and Pankhurst, R. C. (1966). *The Measurement of Air Flow*. Pergamon Press, Oxford.
  162. Baker, H. D., Ryder, E. A., and Baker, N. H. (1963). *Temperature Measurement in Engineering*. John Wiley & Sons, New York.
  163. Baker, R. C. (1989). *An Introductory Guide to Flow Measurement*. Mechanical Engineering Publication Limited, London.
  164. Clark, W. J. (1965). *Flow Measurement by Square-edged Orifice Plate Using Corner Tappings*. Pergamon Press, Oxford.
  165. Douglas, J. F., Gasiorek, J. M., and Swaffield, J. A. (1985). *Fluid Mechanics*. Longman Scientific & Technical, Avon.
  166. McQuiston, F. C., and Parker, J. D., (1994) *Heating, Ventilating, and Air Conditioning Analysis and Design* John Wiley and Sons, Inc., New York.
  167. Holman, J. P., (1981). "*Heat Transfer*", McGraw Hill.
  168. Kays, W. M., and London, A. L., (1958). "*Compact Heat Exchangers*", McGraw-Hill Book Company, Inc. New York.
  169. BS 1041, Parts 1, (1943). "*British Standard Code for Temperature Measurement*", British Standard Institution.
  170. BS 1042, Parts 1, (1964). *British Standard Methods for Measurement of Fluid Flow in Pipes, Orifice Plates, Nozzles and Venturi Tubes*. British Standard Institution.
  171. BS 1042, Parts 2A, (1973). *British Standard Methods for Measurement of Fluid Flow in Pipes, Pitot Tubes*. British Standard Institution.
  172. BS 1042, Parts 3, (1965). *British Standard Methods for Measurement of Fluid Flow in Pipes, Guides to the Effects of Departure from the Methods in Part 1*. British Standard Institution.

173. BS 4937, Parts 4, (1973). *British Standard International Thermocouple Reference Tables*. British Standard Institution.
174. ASHRAE Standard 35-1983, (1983). *Method of Testing Desiccants for Refrigeration Drying*. ASHRAE Standard.
175. ASHRAE Standard 84-78, (1978). *Method of Testing Air-to-Air Heat Exchangers*. ASHRAE Standard.
176. ASHRAE Standard 41.5-75, (1975). *Standard measurement Guide Engineering Analysis of Experimental Data*. ASHRAE Standard.
177. ASHRAE Standard 41.1-74, (1974). *Standard measurement Guide: Section on Temperature Measurements*. ASHRAE Standard.
178. Tarakçı, M. (1991). *Design, Construction and Performance Analysis of a Rotary Type Regenerative Heat Exchanger*. Ms Thesis, Middle East Technical University, Ankara.
179. Sönmez, M. (1986). *Modelling and Optimization of a Rotary Regenerative Type Waste-Heat Heat Exchanger*. Ms Thesis, Middle East Technical University, Ankara.
180. Solak, A. S. (1992). *An Analytical Modeling and Numerical Simulation of a Rotary Type Regenerative Heat and Humidity Exchanger*. Ms Thesis, Middle East Technical University, Ankara.
181. Çimtay, Y. (1992). *Havadan Havaya Enerji Geri Kazanım Sistemlerinin İncelenmesi*. Lisans Üstü Tezi, Yıldız Üniversitesi, İstanbul.
182. Candar, L. (1995). *Döner Reküperatif Isı Eşanjörü Geliştirilmesi ve Denenmesi*. Yüksek Lisans Tezi, Çukurova Üniversitesi, Adana.
183. Ünal, Ş. (1996). *Döner Tip Rejeneratörlerin Etkinliğinin Nümerik Olarak Hesaplanması*. Doktora Tezi, Çukurova Üniversitesi, Adana.
184. Doğruyol, E. (1997). *Döner Rejeneratif Isı Eşanjöründe Devir Sayısına Bağlı Olarak Verimin Ölçülmesi*. Yüksek Lisans Tezi, Çukurova Üniversitesi, Adana.
185. Varol, Y. (1991). *Rejeneratif Isı Değiştirgeçleri Yardımıyla Enerji Geri Kazanımı*. Yüksek Lisans Tezi, Fırat Üniversitesi, Elazığ.
186. Srivastava, N.C., and Eames, I. W., (1998). A Review of Adsorbents and Adsorbates in Solid-Vapour Adsorption Heat Pump Systems. *Applied Thermal Engineering* ., **18**, 707-714.

## **CURRICULUM VITAE**

The author was born in Gaziantep in 1965. He has finished the high-school in Gaziantep in 1982 and entered the Mechanical Engineering Department of M.E.T.U in 1982. He has been graduated as a Mechanical Engineer in 1988. He started to work as a research assistant in the same department while has continued the M. Sc. program. He received his M. Sc. degree in Mechanical Engineering in 1991.

He has been married and has a son and a daughter.

